UNIVERSITÀ DEGLI STUDI DI CAGLIARI
Facoltà di Scienze Matematiche Fisiche e Naturali
Dipartimento di Fisica

COMBINED CONTINUUM/ATOMISTIC MODELING OF ELASTICITY IN NANOSTRUCTURED MATERIALS

PIER LUCA PALLA

Phd thesis FIS/03

November 2009

Relatore: Prof.
LUCIANO COLOMBO

Correlatore: Dott.
STEFANO GIORDANO

Pier Luca Palla: *Combined continuum/atomistic modeling of elasticity in nanostructured materials,* Phd thesis FIS/03 , © November 2009

Dedicated to
Pierluigi, Daniela and Loredana

ABSTRACT

In this thesis, we provide a picture on the elastic behavior of nanostructured systems. In particular, we focus on the effective nonlinear elasticity of nanocomposites. We adopt both continuum theory and atomistic simulations point of view, merging the two approaches in a sequential multiscale modeling. Several new developments in the field of continuum elasticity theory are considered. These methods are then applied down to the nanoscale in order to analyze the onset of atomistic effects in nanocomposite systems. A universal scaling law is provided, governing the overall elastic behavior in the range below 10 nm. Furthermore, interface elastic phenomena in embedded nanostructures are described by means of an atomistically-informed continuum model and verified through large scale atomistic simulations containing up to 10^7 atoms. Moreover, a new constitutive force field scheme is developed with applications in the field of nonlinear elasticity of complex systems.

SOMMARIO

In questo lavoro è stato studiato il comportamento elastico di sistemi nanostrutturati ed in particolare l'elasticità non lineare dei mezzi compositi. A tal fine, sono state applicate sia la teoria del continuo che le simulazioni atomistiche. Inoltre, i due approcci sono stati integrati in descrizioni multiscala afferenti alla classe dei metodi sequenziali. Nell'ambito della teoria del continuo elastico sono stati ottenuti una serie di nuovi sviluppi analitici, in seguito applicati all'interpretazione dei risultati delle simulazioni atomistiche di sistemi nano-strutturati. In questo modo sono stati identificati e descritti per mezzo di una opportuna legge di scala gli effetti di taglia dovuti alla natura discreta della struttura atomica dei materiali. Inoltre, simili fenomeni di scala, dovuti in questo caso alla presenza di interfaccie strutturate, sono stati descritti per mezzo di un modello del continuo che implementa efficacemente questi effetti atomistici. In fine, è stato sviluppato un nuovo campo di forze applicabile allo studio computazionale dell'elasticità non lineare di sistemi complessi.

PUBLICATIONS

Some ideas and figures have appeared previously in the following publications:

1. **Pier Luca Palla**, Mariella Ippolito, Stefano Giordano, Alessandro Mattoni and Luciano Colombo: *Atomistic approach to nanomechanics: Concepts, methods, and (some) applications*, in The Nanomechanics in Italy, Research Signpost, Kerala (2007): 75107 ISBN: 9788130802374. Editor: Nicola Maria Pugno. (Citation [132]).

2. **Pier Luca Palla**, Stefano Giordano, and Luciano Colombo: *Interfacial elastic properties between a-Si and c-Si*. Physical Review B 78, 012105 (2008). (Citation [174]).

3. Stefano Giordano, **Pier Luca Palla**, and Luciano Colombo: *Nonlinear elastic Landau coefficients in heterogeneous materials*. Europhysics Letters (EPL) 83, 66003 (2008).(Citation [87]).

4. Stefano Giordano and **Pier Luca Palla**: *Dielectric behavior of anisotropic inhomogeneities: interior and exterior point Eshelby tensors*. Journal of Physics A: Mathematical and Theoretical 41 (2008) 415205. (Citation [61]).

5. Stefano Giordano, **Pier Luca Palla**, and Luciano Colombo: *Effective permittivity of materials containing graded ellipsoidal inclusions*. The European Physical Journal B 66, 29-35 (2008). (Citation [62]).

6. Stefano Giordano, **Pier Luca Palla**, and Luciano Colombo: *Nonlinear elasticity of composite materials*. The European Physical Journal B 68, 89-101 (2009). (Citation [125]).

7. **Pier Luca Palla**, Stefano Giordano, and Luciano Colombo: *The role of interface elasticity in nanostructured silicon*. Physical Review B 80, 054105 (2009). Selected for the August, 24 2009 issue of Virtual Journal of Nanoscale Science & technology. (Citation [86]).

8. Emiliano Cadelano, **Pier Luca Palla**, Stefano Giordano, and Luciano Colombo: *Nonlinear Elasticity of Monolayer Graphene*. Physical Review Letters 102, 235502 (2009). Selected for the June, 22 2009 issue of Virtual Journal of Nanoscale Science & technology.(Citation [201]).

or will be reported in the following papers in preparation:

1. **Pier Luca Palla**, Stefano Giordano, and Luciano Colombo: *An atomistic approach to nano-elasticity based on constitutive force fields*. In preparation.

2. Stefano Giordano, **Pier Luca Palla**, Emiliano Cadelano, Michele Brun, and Luciano Colombo: *On the behavior of elastic nano-inhomogeneities with size and shape different from their hosting cavities*. In preparation.

CONTENTS

INTRODUCTION

During the last decade, the emphasis of the material science community has been focused on the study of the behavior of the matter at the atomic- or nano-scale. The proliferation of the theoretical and experimental approaches to the research and development on this subject has led to the coining of the phrase *nano-technology* [1]. This term generally implies the investigation and technological application of the properties of matter at length scales of one thousand nanometers or smaller. Nowadays, we have acquired new tools and techniques to synthesize nanoscale objects and characterize their many specific properties. The high-resolution electron microscopes that are available today enable the visualization of aggregates of few atoms. Thus, we have now the technology to detect single molecules, bacteria or virus particles. Synthesis of advanced materials provides the technology to tailor-design systems as small as molecules. Furthermore, the manipulation of these nano-systems is possible using scanning probe techniques.

A promising route for modern materials science: the nano-technologies

Advances in the synthesis of nanoscale materials have stimulated research activities in science and engineering devoted entirely to these materials and their applications. This is due in large part to the combination of their expected structural perfection, small size, low density, high stiffness, high strength and excellent electronic properties. As a result, nanoscale materials may find use in a wide range of applications. In fact, there is universal agreement upon the overall potential that, in particular, nano-mechanics has for the betterment of modern industry. Nano-composites, nano-alloys and nano-grained/-graded materials or nano-electro mechanical systems enter yet in most present-day consumer products, as well as in front-end technologies like automated manufacturing, environmental monitoring, automotive, aerospace, ITC technologies or even in leading-edge developments in energy-, life- or materials-science. Several low-dimensional nanostructures, including quantum dots (QDs) (nanocrystals or nanoparticles of arbitrary diameter containing about 10 to 100 atoms) or carbon nanotubes (one-dimensional structures) have been demonstrated to be efficient field emitters and are currently being incorporated in several applications, including flat panel display for television sets or computers. QDs heterostructures are also promising materials for solar photovoltaics (PVs).

Protective coatings is another area that has greatly benefited from nano-mechanics. These coatings have a wide range of applicability, examples being gears and bearings in the automotive industry. In all these applications, the goal has been to replace or augment previously known super hard materials such as diamond in designing tribological parts that use nanoceramic-type coatings to reduce friction and wear. Extending the lifetime of these parts is crucial, and will lead to a massive reduction in maintenance costs for these components. A further research topic is the development of nanoelectromechanical systems (NEMS). For example, the storage capacity of computer hard drives has been increased by orders of magnitude, thanks to magnetic materials whose thickness is on the order of nanometers. Medicine is another key area in which NEMS devices have made, and will make, large contributions. Here, nanotechnology can be used to dynamically image

living biological systems, such that the real-time study of bacteria and diseases can be performed.

Advanced structural materials: the nano-composites

In the field of nano-sciences a role of paramount importance is carried out by *nano-composite systems* [2]. Generally speaking, composite materials (also referred as composites) are inhomogeneous engineered media made by two or more homogeneous constituent materials with significantly different physical properties which remain separate and distinct within the finished structure. A key to the success of such materials is their tailored mechanical or optoelectronic behavior. In fact, a relatively inexpensive way to obtain macroscopically desired responses is to enhance a base material's properties by the addition of microscopic matter, i.e. to manipulate their inner structure. The macroscopic characteristics of modified base materials are the aggregate response of an assemblage of different "pure" components, for example several particles or fibers embedded in a binding matrix. In structural engineering applications, the classical choice is a harder particulate phase that serves as a stiffening agent for a ductile, easy to form, base matrix material. In photovoltaics applications, the incorporation of QDs (e.g InAs/InGaAs/GaAs QDs) into existing (e.g. InGaP/GaAs/Ge) solar cells will result in new devices with higher efficiency and render solar energy more cost competitive. A further meaningful application of nanocomposites is in the field of lasers technology. For example, by capping InAs quantum dots with an InGaAs strain-reducing layer, the photoluminescence peak of InAs quantum dots can be controlled by changing the indium composition of the InGaAs strain-reducing layer.

Composites at the macro-scale

As a matter of fact, *macroscopic composites*, i.e. composites where the inhomogeneity shows up at the macro-scale (rather than at the nano-scale), are not a recent development. Thus, macro- or micro-scale inhomogeneities are encountered in metal matrix composites, concrete, etc. Accordingly, not even the analysis of such heterogeneous materials can be considered as a recent topic. In this field, *continuum mechanics* has been largely applied to describe and modeling the morphology of microscopic composite materials and estimating their effective mechanical properties. Such a theory is based on the approximation of *continuum medium*: it means that the full set of pointlike atomic masses distributed within a solid body is replaced by a continuum distribution of mass. This approximation can be easily applied to macroscopic composites since the spatial wavelength of the main fields, describing their mechanical behavior, is typically larger than the interatomic distance. Within the last 150 years, estimates on the effective mechanical responses of composites have been made under a variety of assumptions on the internal fields within the microstructure. Works dating back at least to Maxwell [3, 4] and Lord Rayleigh [5] (published in 1867, 1873 and 1892, respectively) have dealt with determining overall macroscopic electric transport phenomena of materials consisting of a matrix and distributions of spherical particles. Voigt [6] (published in 1889) is usually credited with the first analysis of the effective mechanical properties of the microheterogeneous solids, with a complementary contribution given later by Reuss [7]. Within the last 50 years improved estimates have been pursued. For example, the dilute family methods assume that there is no particle interaction. With this assumption one requires only the solution to a single ellipsoidal particle in an unbounded domain. This is the primary use of the elegant Eshelby [8] formalism, based on eigenstrain concepts, which is used to determine the solution to the

The continuum approach

problem of a single inclusion embedded in an infinite matrix of material under uniform exterior loading. Also the studies of *heterogeneous materials with nonlinear constitutive behavior* go back to the early years of the century, more precisely to at least Taylor. In 1938 he studied the mechanics of polycrystals [9], and in the subsequent works by Bishop and Hill [10, 11] and by Drucker [12] they investigated the behavior of ideally plastic polycrystals and composite materials. Over the past decades or so, also numerical simulations of nonlinear materials with periodic microstructures have been carried out (see, for example [13, 14, 15]), as well as materials with more general microstructures [16, 17, 18]. A large review of such investigations can be found in the excellent work of Ponte Castañeda and Suquet [19].

From macro- to nano-scale

All the continuum-based models are appropriate for microscopic as well as macroscopic length scales, but can no longer provide all the possible insight into materials properties at the smallest length scales, namely, into the mechanics of modern nano-composites. In fact, it has been cleared that these approaches are based on the assumption that the relevant fields that describe the state of a material vary slowly on the atomic scale. Otherwise, continuum models that represent macroscopic behavior of a material by averaging the material's properties at the smaller length scales, can lose their meaning. For example, to describe properties of a material with defects, continuum theories a fortiori break down in the vicinity of the defects, or, more generally, any other entity that possesses structure on the atomic scales. In these cases, it is therefore clear that continuum theories must be "enriched" by incorporation of additional atomistic informations, and hence avert their breakdown. This is the realm of condensed matter theories such as the density functional theory (DFT) and its variants, as well as the ab initio (CP, i.e. Car-Parrinello) or model-potential (MP) molecular dynamics (MD).

Atomistic approaches

DFT nowadays represents the standard model for full-quantum, parameter-free prediction of ground-state materials properties. They can be computed in any arbitrary atomistic state of aggregation, chemical composition, degree of crystalline order or disorder, as well as under any arbitrary condition of temperature, pressure, stress, or application of external perturbing fields. While more fundamental and superior than continuum models, DFT applications are severly limited by their computational workload which can possibly be overwhelming. Accordingly, the straightforward application of DFT to nano-composite systems often results into a daunting effort. In fact, the mechanical behavior of these heterogeneous materials is largely influenced not only by the atomistic details of each inner nano-structures, but also by the (possibly disordered) complex macroscopic distribution of such inhomogeneities. In other words, to properly treat the nanocomposites mechanics, we need to take into account the atomistic description of the nano-sized inclusions as much as their actual distribution that spreads over the meso- or macro-scale. The last aspect results in the need of considering the effective response of systems involving millions of atoms, largely out of the capability of DFT-based techniques. To a less extent, similar limitations hold for the CPMD simulations. This method, pioneered by Car and Parrinello, is based on the Hellmann-Feynman theorem, which greatly simplifies the task of computing the physical forces on the particles. Even with such a simplification, the CPMD scheme is only limited to systems containing up to few thousands

atoms. Alternatively, the tight-binding molecular dynamics (TBMD) can be adopted, where the covalent bonding is incorporated into the computation from its underlying electronic structure which, in turn, is solved by a semi-emprical quantum scheme. In a TBMD simulation, electronic calculations require a few atomic orbitals for each atom, hence allowing a comparatively larger number of atoms (up to several thousands) to be used. Unfortunately, because of its semi-empirical formulation, TBMD has reduced chemical transferability and, therefore, it can be hardly adopted as a universal computational tools for nanotechnology. Under this respect, model-potential MD could offer a wider perspective, despite its validity can only be proved heuristically. The increasing popularity of MD methods is due just to the fact that highly efficient simulation techniques have been developed in order to treat simultaneously up to millions of atoms.

The multiscale approaches

In any case, the straightforward application of the atomistic models, as much as of a pure continuum approach, are not feasible for a complete description of the mechanics of nano-composites. On the contrary, atomistic and continuum models must reinforce each other in some suitable hierarchical combination. This key idea has generated the modern and fascinating concept of *multiscale modeling of materials* [20, 2]. Extensive discussions and overviews pertaining to this subject are given for example in [21] and [22]. Generally speaking, there are two types of multiscale approach for modeling various physical phenomena that occur in materials containing several disparate length scales. These approaches are either *parallel or sequential methods*, in the sense described below.

parallel methods...

The first method is not as well-developed as the sequential approach, because it requires very significant computing power which, up until very recently, was not available. In this method, different computational methods, ranging from those for atomic scales to continuum scales, are coupled for a simultaneous attack on a given problem. The reason for this coupling is that many physical phenomena are in fact inherently multiscale; that is, one must know what is happening simultaneously in different regions and scales of the system in order to understand and predict its macroscopic behavior. A good example is fracture propagation in solid materials. The atoms that constitute the material interact with each other, and nucleation of a crack and its propagation are due to what happens at this length scale, namely, breaking of the bonds between the atoms. As the nucleated crack starts to propagate, complex phenomena, such as plastic deformation, happen at a larger length scale which includes the tip of the propagating fracture. At still larger length scales, which include the region far from the tip of the crack, the material behaves as a continuum which may be described by the classical continuum mechanics.

...and sequential methods

The Sequential Multiscale Approach has been developed and used much more extensively than the parallel multiscale modeling. In this method, beginning with the smallest length scales of the problem, the results of a series of computations are used as the input to the next one performed, hierarchically, at a larger length scale. Hence, the essential idea is to pass informations from finer to coarser scales. A beautiful example of implementation of this strategy is the pioneering work of Clementi [23]. In 1988, he used accurate quantum-mechanical computations in order to evaluate the interaction of several water molecules, from which he developed an accurate empirical interatomic

potential that involved two-, three-, and four-body interactions. The potential was then utilized in a MD simulation for evaluating the viscosity of water. Subsequently, motion of water in a channel with or without obstacles was studied, using as input the viscosity that had been computed in the previous step. The resulting understanding was then employed in a fluid dynamics computation for predicting tidal circulations obtaining a first example of *Atomistically-Informed Continuum Model*.

Another example of sequential multiscale modeling is provided by work of Zepeda-Ruiz et al. [24]. Their goal was designing experimental protocols toward the development of engineering strategies for strain relaxation of semiconductor films which are grown heteroepitaxially on semiconductor substrates. The strain, caused by the lattice mismatch between the film and substrate, generates defects in the material. By controlling such effect the optimal design of the optoelectronic properties of the film can be obtained. Using a multiscale approach, Zepeda-Ruiz et al. studied layer-by-layer semiconductor heteroepitaxy, such as InAs on GaAs(110) and InAs on GaAs(111). The continuum theory provided a parameterization scheme for the atomistic simulations. A Keating-type potential [25], which contains the contributions of the stretching and bond-bending forces, was utilized for representing the interatomic interactions, and total energy minimization was used for determining the most stable configuration. A major conclusion of this work was that the continuum theory of elasticity can be accurate all the way down to the monolayer thickness, which is the finest possible length scale for the theory in the context of layer-by-layer expitaxial growth. In addition, the theory was shown, in conjunction with the atomistic simulations, to provide quantitative predictions for various properties of interest. Indeed, even the linear isotropic elasticity was capable of fitting the results of the atomistic simulations.

The present thesis

In this thesis, we have worked on the elastic behavior of nanocomposites by combining the continuum approach, namely the elasticity theory, with large scale atomistic simulations based on MP molecular dynamics. As discussed in the following, the philosophy of our approach can be framed within the sequential multiscale scheme above defined.

Mainly, we have faced the linear and nonlinear elastic behavior of embedded nanostructures with the aim of investigating the breakdown of the corresponding continuum theory predictions due to the onset of scale-effects. In other words, our goal is the characterization of the elastic behavior of these heterogeneous structures as the size of the inclusion changes; the continuum theory is inherently scale independent and, therefore, such a dependence must be related to the actual discrete distribution of the atoms within the solid body.

Continuum-based investigations

As first step, in the context of the continuum elasticity theory, we have developed a couple of original generalizations of the existing results on the elastic behavior of a single inhomogeneity embedded in a matrix with different elastic properties (Eshelby theory). Such generalizations are intended to describe, within the continuum formalism, some typical features or phenomena occurring in the atom resolved systems. One of the main features of the heterogeneous systems at the nanoscale is the presence of a structured interface between different

media. Typically, this feature is not introduced in the macroscopic continuum framework since the interface is assumed devoid of any specific mechanical response (perfect interface approximation). Thus, we have considered the case of a prestressed (or prestrained) single inclusion, i.e. an embedded inhomogeneities that exhibits a state of deformation also in absence of any external load. As we have verified by means of a series of atomistic simulations, such an effect can be induced at the atomic level by the possible lattice mismatch at the interface between the inclusion and the surrounding matrix. In the continuum model, we have introduced this prestressed state by considering a size (and possibly a shape) of the inclusion different from the corresponding hosting hole in the matrix. Moreover, a inherent character of the atomistic systems is the nonlinearity of their mechanical response induced by the complexity of the atomic interactions. This consideration leads us to consider the effect of nonlinear constitutive equations for the media involved in the heterogeneous structure. Thus, Eshelby theory has been generalized to such a case.

The atomistic approach

As for the atomistic approach, we have firstly considered some basic concepts in the microscopic theory of elasticity. More precisely, we have investigated the relation between the atomic interaction and the resulting macroscopic elastic behavior of the overall material. In other words, we have correlate the elastic properties of a medium with the details of the interatomic potential (taking into account both two-body and three body interactions) establishing the minimum level of complexity that any microscopic dynamical model must exploit in order to obtain results consistent with the continuum theory. Furthermore, we have analyzed the identification of the elastic fields defined, at the macroscopic level, within the continuum elasticity theory (classic fields) with suitable quantities achievable in MD simulations (ensemble averages of dynamical variables). Interesting enough, we have verified that the standard dynamical variable for the stress field, the so-called virial stress, does not allow for a correct evaluation of the Cauchy stress in the nonlinear formulation of the elasticity theory adopted in the present work (physical nonlinearity).

As a first computational analysis, we have considered some paradigmatic configurations of inhomogeneous (Silicon-based) systems, namely, a planar interface between two elastically different media and an atomistic model of a single inclusion embedded in a matrix. As for the first system, the continuity conditions for the elastic field across the interface have been derived and applied to the atomistic system. Furthermore, by means of large scale simulations (up to 10^7 atoms in the simulation cell for a maximum size of the sample as large as 400 nm) based on a high efficient parallel software[1] we have applied our continuum results for the elastic behavior of prestressed inclusions to the atomistic model of an embedded inclusion. A good capability of such a continuum model to mimic the observed interface induced scale-effects has been verified. We note that this continuum model can be considered as a first example of atomistically-informed continuum model where the interface-induced atomistic features are introduced by considering a a size of the inclusion different from the corresponding hosting hole in the matrix.

1 The "CMPTool" HPC code developed by the CASPUR (Rome, Italy) computing center staff and improved by the present author.

In the above described computational works, we have modeled the atomistic interaction through *realistic interatomic potentials*, i.e. by means of model-potential intended to reproduce any possible thermodynamic and structural properties of the specific elements under consideration (namely the Stillinger-Weber [26] and Tersoff [27] potentials parametrized for Si-based systems). The performed investigations on the elastic behavior of nano-structured systems have shown that different atomistic effects are possible: bulk disorder, interface effects, relaxation induced prestrains. These effects strongly depend on the details of the atomic structure and of the considered interaction. In order to better understand the general rules underlying the onset of the atomistic effects in nanocomposites, we have developed a versatile model system, based on a new class of *constitutive force fields*, that allow us to control these features by tuning the structural and elastic properties of the medium. The key idea of such an *Atomistic Virtual Laboratory* is based on the development of a coarse graining procedure of the physical information that allows for the reduction of the otherwise over-rich interatomic potentials nowadays available into a new force field optimized to describe the elastic behaviors of complex nano-systems. The above force field is quite dissimilar to ordinary interatomic potentials for molecular dynamics simulation: in fact, it is intended as general-purpose functional form (containing a given set of material-specific parameters), exploiting a fully-atomistic coding of elastic features, i.e. able to mimic any observed elastic behavior at any order of nonlinearity.

An Atomistic Virtual Laboratory for Nano-elasticity based on a novel constitutive force field

The implementation of the constitutive force field in a parallel computing tool, and the application of this *Atomistic Virtual Laboratory* to the investigation of the elastic response of a single, as much as of a dispersion of nonlinear inclusions have provided a series of results on the onset of both linear and nonlinear size-effects in nanocomposites. In particular, a full characterization of the scaling laws governing such effects has been derived.

Outline

The Thesis is organized as follows:

- In Part I we treat the continuum approach to composites materials:
  - In Chapter 1, a brief outline of the main concepts and of the formalism of continuum elasticity theory is reported. In particular, we present a discussion of the elasticity formalism in two-dimensional systems.
  - Chapter 2 is addressed to the description of two novel generalizations of the Eshelby theory. The first one considers the elastic behavior of prestressed inclusions while the second solves the case of a nonlinear inclusion.
  - In Chapter 3, the effective behavior of a dispersion of nonlinear inhomogeneities (nanocomposite) is calculated by means of an homogeneization procedure based on the nonlinear Eshelby theory.
- Part II deals with the atomistic modeling of solid mechanics:
  - Chapter 4 provides an insight into some basic concepts underlying the the atomistic approach to nanomechanics. In

particular, it contains a review of model-potentials for molecular dynamics and a discussion on the identification of the Cauchy stress field at the atomic level.

- In Chapter 5 we report some meaningful atomistic investigations on the interface elasticity of Si-based nanostructures. A planar interface between a-Si and c-Si and a single Si inclusion embedded in a matrix are considered.

- Part III is addressed to the foundation of the constitutive force field:
  - Chapter 6 supplies a detailed description of the basic idea underlying the constitutive force field and a paradigmatic implementation in the case of a planar two-dimensional triangular lattice.
  - Finally, in Chapter 7 we report the results of the atomistic investigations on the elastic behavior of nanocomposites performed through our *Atomistic Virtual Laboratory* based on the constitutive force field approach.

Part I

CONTINUUM MECHANICS

1 THE ELASTICITY THEORY

Contents

1.1 OUTLINE OF THE ELASTICITY THEORY

The classical theory of elasticity is based on the approximation of *continuum medium*, which consists in replacing the full set of pointlike atomic masses distributed within a solid body by a continuum distribution of mass. This approximation is valid when the spatial wavelength of the displacement field (describing the imposed deformation) is much greater than the interatomic distance. In this case the crystalline structure is not relevant for determining the variation of the shape of the solid body: the continuum macroscopic description is in fact sufficient to study its mechanical response. The next most important ideas of elasticity theory are the concepts of strain and the stress, both of which are easily described by means of specific mathematical objects [28, 29, 30].

A deformation relates two configurations (or states) of the material. The initial state is called the *reference configuration* and usually refers to the initial time; the other is called the *current configuration* and refers to a following time (which may be regarded conveniently as the present moment) [31, 32]. In linear elasticity the strains (typically extensions and shears) and the angles of rotation are considered small [33]. In this case we use the *infinitesimal strain tensor* (or *small strain tensor*), which is the main object introduced in order to describe all the deformation features [34, 35].

To calculate the force of interaction between volume elements situated in an arbitrary closed region (imagined to be isolated within the body) and volume elements situated outside this region, it was found advantageous to introduce the concept of the averaged force of interaction between them. This approach provides us with the definition of the *stress tensor*, which takes into consideration all the interaction forces among the volume elements of the continuum body [36, 37].

The strain in a given body can be considered as the effect of the applied stress. The relationship between the strain tensor and the stress tensor depends on the material under consideration and, therefore, it is called the *constitutive equation* [36]. The empirical Hooke law establishes a linear relation between stresses (forces inside the body) and strains (deformations of the body itself). In its general form, Hooke's law is able to describe an arbitrary inhomogeneous and anisotropic behavior of the material under consideration [34]. However, the most simple and important constitutive equation used in elasticity theory applies to materials that are homogeneous (the elastic behavior is the same at any point of the body) and isotropic (the direction of application of the stress is not relevant). The linear, homogeneous and isotropic constitutive equation is obtained and discussed in the following Section.

1.1.1 *The strain tensor definition*

Let $\vec{x}$ be the position vector of a volume element within a body in its reference (equilibrium) configuration and let $\vec{X}$ be the position of the same volume element in the current configuration. Both configurations are framed within the same cartesian coordinate system (see Fig.1). Since $\vec{X}$ is a function of $\vec{x}$, we can write

$$\vec{X} = \vec{f}(\vec{x}) = (f_1(\vec{x}), f_2(\vec{x}), f_3(\vec{x})) \tag{1.1}$$

We observe that the function $\vec{f}$, connecting the vector $\vec{X}$ to the vector $\vec{x}$, is a vector field. Of course, the relation $\vec{f}(\vec{x}) \neq \vec{f}(\vec{y})$ is verified for any pair of volume elements with $\vec{x} \neq \vec{y}$ in the reference configuration. This means that $\vec{f}$ is a biunivocal vector function and, therefore, the inverse function $\vec{f}^{-1}$ always exists. We also assume that $\vec{f}$ and $\vec{f}^{-1}$ are differentiable functions. Basically, the vector field $\vec{f}(\vec{x})$ contains all the information about the deformation driving the solid body from the reference to the current configuration. In the theory of elasticity the deformation gradient $\hat{F} = \{F_{ij},\ i,j = 1,2,3\}$

Deformation gradient

$$F_{ij} = \frac{\partial f_i}{\partial x_j} \tag{1.2}$$

is introduced. The matrix $\hat{F}$ is also referred to as the Jacobian matrix of the transformation and has two important properties: (i) it is not singular because of the invertibility of $\vec{f}$ ($\exists\ \hat{F}^{-1}$ such that $\hat{F}\hat{F}^{-1} = \hat{F}^{-1}\hat{F} = \hat{I}$); (ii) its determinant is always strictly positive ($\det F > 0$) [31]. We can better exploit the concept of deformation by introducing the displacement field $\vec{u}(\vec{x})$ as

Displacement field

$$\vec{X} = \vec{f}(\vec{x}) = \vec{x} + \vec{u}(\vec{x}) \tag{1.3}$$

The Jacobian matrix of the displacement $\hat{J} = \{J_{ij},\ \ i,j = 1,2,3\}$ (i.e., the displacement gradient) is therefore calculated as

Displacement gradient

$$J_{ij} = \frac{\partial u_i}{\partial x_j} \tag{1.4}$$

From the definitions of $\hat{F}$ and $\hat{J}$ we have $\hat{F} = \hat{I} + \hat{J}$ or $\hat{J} = \hat{F} - \hat{I}$.

In *linear* elasticity the extent of the deformations is assumed small. While this notion is rather intuitive, it can be formalized by imposing that for small deformations $\hat{F}$ is very similar to $\hat{I}$ or, equivalently, that $\hat{J}$

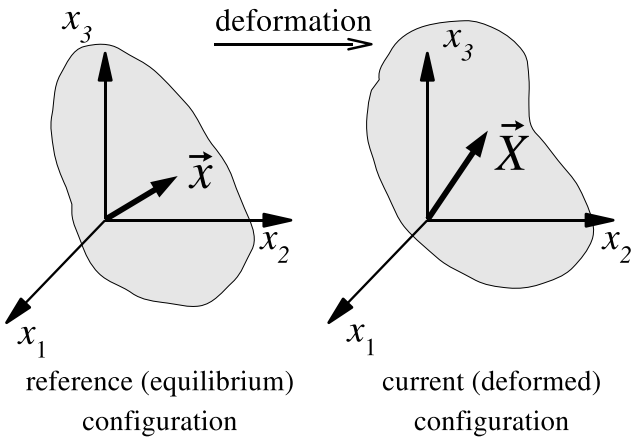

Figure 1: Reference configuration and current configuration after a deformation.

is very small. Therefore, we adopt as an operative definition of *small deformation* the relation

Small deformation condition

$$\mathrm{Tr}(\hat{J}\hat{J}^T) \ll 1 \tag{1.5}$$

i.e., a deformation will be hereafter regarded to as *small* provided that the trace of the product $\hat{J}\hat{J}^T$ is negligible. We observe that $\hat{J}$ can be written as the sum of a symmetric and a skew-symmetric (antisymmetric) part as follows

$$J_{ij} = \underbrace{\frac{1}{2}\left(\frac{\partial u_i}{\partial x_j} + \frac{\partial u_j}{\partial x_i}\right)}_{\mathrm{symmetric}} + \underbrace{\frac{1}{2}\left(\frac{\partial u_i}{\partial x_j} - \frac{\partial u_j}{\partial x_i}\right)}_{\mathrm{skew-symmetric}} = \epsilon_{ij} + \Omega_{ij} \tag{1.6}$$

Accordingly, we define the (symmetric) *infinitesimal strain tensor* (or *small strain tensor*) as

$$\epsilon_{ij} = \frac{1}{2}\left(\frac{\partial u_i}{\partial x_j} + \frac{\partial u_j}{\partial x_i}\right) \tag{1.7}$$

and the (antisymmetric) *local rotation tensor* as

$$\Omega_{ij} = \frac{1}{2}\left(\frac{\partial u_i}{\partial x_j} - \frac{\partial u_j}{\partial x_i}\right) \tag{1.8}$$

Such a decomposition [34] is useful to obtain four very important properties of the small strain tensor, which is the key quantity to determine the state of deformation of an elastic body:

- for a pure local rotation (a volume element is rotated, but not changed in shape and size) we have $\hat{J} = \hat{\Omega}$ and therefore $\hat{\epsilon} = 0$. This means that the small strain tensor does not take into account any local rotation, but only the changes of shape and size (dilatations or compression) of that element of volume [36]. Let us clarify this fundamental result. We consider a point $\vec{x}$ inside a volume element which is transformed to $\vec{x} + \vec{u}(\vec{x})$ in the current configuration. Under a pure local rotation we have: $\vec{x} + \vec{u}(\vec{x}) = \hat{R}\vec{x}$, where $\hat{R}$ is a given orthogonal rotation matrix (satisfying $\hat{R}\hat{R}^T = \hat{I}$).

The strain tensor does not take into account the local rotations

We simply obtain $\vec{u}(\vec{x}) = (\hat{R} - \hat{I})\vec{x}$ or, equivalently, $\hat{J} = \hat{R} - \hat{I}$. Since the applied deformation (i.e., the local rotation) is small by hypothesis, we observe that the difference $\hat{R} - \hat{I}$ is very small too. The product $\hat{J}\hat{J}^T$ will be therefore negligible, leading to the following expression

$$\begin{aligned} 0 &\cong \hat{J}\hat{J}^T = \left(\hat{R} - \hat{I}\right)\left(\hat{R}^T - \hat{I}\right) = \hat{R}\hat{R}^T - \hat{R} - \hat{R}^T + \hat{I} \\ &= \hat{I} - \hat{R} - \hat{R}^T + \hat{I} = -\hat{J} - \hat{J}^T \end{aligned} \tag{1.9}$$

Therefore $\hat{J} = -\hat{J}^T$ or, equivalently, $\hat{J}$ is a skew-symmetric tensor. It follows that $\hat{J} = \hat{\Omega}$ and $\hat{\epsilon} = 0$. We have verified that a pure rotation corresponds to zero strain. In addition, we remark that the local rotation of a volume element within a body cannot be correlated with any arbitrary force exerted in that region (the forces are correlated with $\hat{\epsilon}$ and not with $\hat{\Omega}$): for this reason the infinitesimal strain tensor is the only relevant object for the analysis of the deformation due to applied loads in elasticity theory.

The strain tensor components ϵ_{ii} (i=1,2,3) represent the lenght variations along the axes of the reference frame

- the infinitesimal strain tensor allows for the determination of the length variation of any vector from the reference to the current configuration. By defining $\epsilon_{\vec{n}}$ as the relative length variation in direction $\vec{n}$, it is possible to prove that [36]

$$\epsilon_{\vec{n}} = \vec{n} \cdot (\hat{\epsilon}\ \vec{n}) \tag{1.10}$$

If $\vec{n}$ is actually any unit vector of the reference frame, it is straightforward to attribute a geometrical meaning to the components ϵ_{11}, ϵ_{22}, ϵ_{33} of the strain tensor. Since $\epsilon_{\vec{e}_i} = \vec{e}_i \cdot (\hat{\epsilon}\ \vec{e}_i) = \epsilon_{ii}$, they describe the relative length variations along the three axes of the reference frame.

The strain tensor components ϵ_{ij} ($i \neq j$) represent half the variation of the right angles between the axes i and j

- the infinitesimal strain tensor allows for the determination of the angle variation between any two vectors from the reference to the current configuration. The variation of the angle defined by the two orthogonal directions $\vec{n}_1$ and $\vec{n}_2$ is given by [36]

$$\Delta\alpha_{\vec{n}_1,\vec{n}_2} = 2\vec{n}_1 \cdot (\hat{\epsilon}\ \vec{n}_2) \tag{1.11}$$

The present result is also useful for giving a direct geometrical interpretation of the components ϵ_{12}, ϵ_{23} and ϵ_{13} of the infinitesimal strain tensor. As an example, we take into consideration the component ϵ_{12} and we assume that $\vec{n}_1 = \vec{e}_1$ and $\vec{n}_2 = \vec{e}_2$. The quantity $\Delta\alpha_{\vec{n}_1,\vec{n}_2}$ represents the variation of a right angle lying on the plane (x_1, x_2). Since $\epsilon_{12} = \vec{e}_1 \cdot (\hat{\epsilon}\ \vec{e}_2)$, we easily obtain the relationship $\Delta\alpha_{\vec{n}_1,\vec{n}_2} = 2\epsilon_{12} = \frac{\partial u_1}{\partial x_2} + \frac{\partial u_2}{\partial x_1}$. In other words, ϵ_{12} is half the variation of the right angle formed by the axis x_1 and x_2. Of course, the same interpretation is valid for the other components ϵ_{23} and ϵ_{13}.

The trace $\mathrm{Tr}(\hat{\epsilon})$ of the strain tensor represent the local variations of the volumes

- knowing the $\hat{\epsilon}$ tensor field within a strained (i.e., deformed) elastic body allows us to calculate the volume change ΔV of a given region. We get $\Delta V = \int_V \mathrm{Tr}(\hat{\epsilon})d\vec{x}$, where V is the volume of the unstrained region [31].

The above discussion states that, given a displacement field $\vec{u}(\vec{x})$, the components of the infinitesimal strain tensor are easily calculated by direct differentiation. The inverse problem is much more complicated [31, 36]. Given an arbitrary infinitesimal strain tensor $\hat{e}(\vec{x})$ we could search for that displacement field $\vec{u}(\vec{x})$ generating the imposed deformation. In general, such a displacement field may not exist. There are, however, suitable conditions under which the solution of this inverse problem is actually found. These conditions are written in the very compact form

Infinitesimal strain compatibility or Beltrami Saint-Venant equations

$$\eta_{qki}\eta_{phj}\frac{\partial^2\epsilon_{ij}}{\partial x_k \partial x_h} = 0 \tag{1.12}$$

where η's are the Levi-Civita permutation symbols. Eqs.(1.12) are known as infinitesimal strain compatibility equations or Beltrami Saint-Venant equations [32]. A detailed discussion of this relation is given in the next Section.

1.1.2 *Compatibility equations*

Given a displacement field $\vec{u}(\vec{x})$, the components of the infinitesimal strain tensor, $\epsilon_{ij} = \frac{1}{2}\left(\frac{\partial u_i}{\partial x_j} + \frac{\partial u_j}{\partial x_i}\right)$, are easily calculated by direct differentiation. The inverse problem is much more complicated [31, 36]. Given an arbitrary infinitesimal strain tensor ϵ_{ij} we can search for a displacement field $\vec{u}(\vec{x})$ fulfilling the same relations. However, a displacement field satisfying these relations for the given strain may not exist. We now consider what conditions must be satisfied by the components ϵ_{ij} to ensure the existence of the displacement components. To this aim we follow the following reasoning.

We suppose to consider a given ϵ_{ij} and we also suppose that the corresponding displacement u_i exists. Therefore, some coefficients Ω_{ij} must exist (see Eq. (1.6)) such that

$$\frac{\partial u_i}{\partial x_j} = \epsilon_{ij} + \Omega_{ij} \tag{1.13}$$

The previous equations has solutions with respect to the components u_i if the irrotationality conditions is fulfilled. For an arbitrary vector field $\vec{V}$ the following property is true: if $\vec{\nabla} \times \vec{V} = 0$ (i.e. if $\frac{\partial V_k}{\partial x_h} = \frac{\partial V_h}{\partial x_k}$), then a scalar function $\mathcal{V}$ exixts such that $\vec{V} = \vec{\nabla}\mathcal{V}$ (i.e. such that $V_j = \frac{\partial \mathcal{V}}{\partial x_j}$) [31, 36]. Therefore, the following relation must be satisfied

$$\frac{\partial\left(\epsilon_{ik} + \Omega_{ik}\right)}{\partial x_h} = \frac{\partial\left(\epsilon_{ih} + \Omega_{ih}\right)}{\partial x_k} \tag{1.14}$$

or, equivalently

$$\frac{\partial \epsilon_{ik}}{\partial x_h} - \frac{\partial \epsilon_{ih}}{\partial x_k} = \frac{\partial \Omega_{ih}}{\partial x_k} - \frac{\partial \Omega_{ik}}{\partial x_h} \tag{1.15}$$

A simple calculation gives

$$\begin{aligned}\frac{\partial \Omega_{ih}}{\partial x_k} - \frac{\partial \Omega_{ik}}{\partial x_h} \quad = \quad & \frac{1}{2}\frac{\partial}{\partial x_k}\left(\frac{\partial u_i}{\partial x_h} - \frac{\partial u_h}{\partial x_i}\right) \\ & -\frac{1}{2}\frac{\partial}{\partial x_h}\left(\frac{\partial u_i}{\partial x_k} - \frac{\partial u_k}{\partial x_i}\right) = \frac{\partial \Omega_{hk}}{\partial x_i}\end{aligned} \tag{1.16}$$

Therefore, Eq.(1.15) assumes the form

$$\frac{\partial \epsilon_{ik}}{\partial x_h} - \frac{\partial \epsilon_{ih}}{\partial x_k} = \frac{\partial \Omega_{kh}}{\partial x_i} \tag{1.17}$$

The components Ω_{kh} are still unknown and they exist if the following further irrotationalty condition is satisfied

$$\frac{\partial}{\partial x_j}\left(\frac{\partial \epsilon_{ik}}{\partial x_h} - \frac{\partial \epsilon_{ih}}{\partial x_k}\right) = \frac{\partial}{\partial x_i}\left(\frac{\partial \epsilon_{jk}}{\partial x_h} - \frac{\partial \epsilon_{jh}}{\partial x_k}\right) \tag{1.18}$$

Finally, the previous relation leads to the following compatibility equation for the strain

$$\frac{\partial^2 \epsilon_{ij}}{\partial x_h \partial x_k} + \frac{\partial^2 \epsilon_{hk}}{\partial x_i \partial x_j} - \frac{\partial^2 \epsilon_{ik}}{\partial x_j \partial x_h} - \frac{\partial^2 \epsilon_{jh}}{\partial x_i \partial x_k} = 0 \tag{1.19}$$

It can be also written in the very compact form of Eq.1.12

Eq.(1.19) or Eq.(1.12) consists of six independent relations which must be necessarily satisfied by the components of the infinitesimal strain tensor

$$\begin{aligned}
\frac{\partial^2 \epsilon_{22}}{\partial x_3^2} + \frac{\partial^2 \epsilon_{33}}{\partial x_2^2} - 2\frac{\partial^2 \epsilon_{23}}{\partial x_2 \partial x_3} &= 0 \\
\frac{\partial^2 \epsilon_{33}}{\partial x_1^2} + \frac{\partial^2 \epsilon_{11}}{\partial x_3^2} - 2\frac{\partial^2 \epsilon_{31}}{\partial x_3 \partial x_1} &= 0 \\
\frac{\partial^2 \epsilon_{11}}{\partial x_2^2} + \frac{\partial^2 \epsilon_{22}}{\partial x_1^2} - 2\frac{\partial^2 \epsilon_{12}}{\partial x_1 \partial x_2} &= 0 \\
\frac{\partial^2 \epsilon_{11}}{\partial x_2 \partial x_3} + \frac{\partial^2 \epsilon_{23}}{\partial x_1^2} - \frac{\partial^2 \epsilon_{12}}{\partial x_1 \partial x_3} - \frac{\partial^2 \epsilon_{13}}{\partial x_1 \partial x_2} &= 0 \\
\frac{\partial^2 \epsilon_{22}}{\partial x_1 \partial x_3} + \frac{\partial^2 \epsilon_{13}}{\partial x_2^2} - \frac{\partial^2 \epsilon_{21}}{\partial x_2 \partial x_3} - \frac{\partial^2 \epsilon_{23}}{\partial x_2 \partial x_1} &= 0 \\
\frac{\partial^2 \epsilon_{33}}{\partial x_1 \partial x_2} + \frac{\partial^2 \epsilon_{12}}{\partial x_3^2} - \frac{\partial^2 \epsilon_{31}}{\partial x_3 \partial x_2} - \frac{\partial^2 \epsilon_{32}}{\partial x_3 \partial x_1} &= 0
\end{aligned} \tag{1.20}$$

Inspection of Eq.(1.12) reveals that they fall into two groups, the equations in each group having similar form. The first group may be obtained by taking the suffixes p and q to be equal and the secon group is obtained by taking $p \neq q$. These conditions are known as infinitesimal strain compatibility equations. They are also sufficient to ensure the existence of the displacement components. The proof here reported is due to Beltrami (1889). However, such conditions have been called Saint-Venant equations [32].

1.1.3 *The stress tensor definition*

In continuum mechanics we must consider two kinds of forces acting on a given region of a material body, namely body forces and surface forces.

Body forces

Body forces depend on the external fields acting on the elastic body. They are described by the vector field $\vec{b}(\vec{x})$, representing their volume density. The total force $d\vec{F}_V$ applied to a small volume dV centered on the point $\vec{x}$ is given by $d\vec{F}_V = \vec{b}(\vec{x})dV$. A typical example is given by the gravitational forces, proportional to the mass of the volume under consideration. In this case we can write $d\vec{F}_V = \vec{g}dm$ where $\vec{g}$ is the

gravitational acceleration and dm is the mass of the volume dV. If we define $\rho = \frac{dm}{dV}$ as the density of the body, we simply obtain $\vec{b}(\vec{x}) = \rho\vec{g}$.

Surface forces are concerned with the interaction between neighboring internal portions of deformable bodies. Although such an interaction results from the full set of interatomic forces, we can make the simplifying assumption that its overall effect can be adequately represented by a single vector field defined across the surface. *Surface forces*

In principle, it is possible to introduce more complicated forces, such as volume and surface distributions of couples. However, the elastic behavior of most materials is adequately described by body and surface forces only. More advanced formulations, based on non-classical or multipolar continuum theories, can be found elsewhere [38].

It is useful to introduce the following notation for the surface force $d\vec{F}_S$ applied to the area element dS

$$d\vec{F}_S = \vec{f}dS \tag{1.21}$$

where $\vec{f}$ assumes the meaning of a surface density of forces. The Cauchy theorem [31] states that a tensor $\hat{T}$ exists such that *Cauchy stress tensor*

$$\vec{f} = \hat{T}\vec{n} \tag{1.22}$$

where $\vec{n}$ is the external normal unit vector to the surface delimiting the portion of body subjected to the force field $\vec{f}$. The quantity $\hat{T}$ has been called the *Cauchy stress tensor* or simply the *stress tensor*. The proof of this theorem is not trivial and can be found in any standard book on continuum mechanics [36, 34]. The forces applied to the area element can be therefore written in the following form

$$d\vec{F}_S = \hat{T}\vec{n}dS \tag{1.23}$$

or, equivalently, $\frac{dF_{S,i}}{dS} = T_{ij}n_j$. We identify the stress tensor $\hat{T}$ with the opposite of a vector pressure. Typical stress values in solid mechanics range from MPa and GPa.

To better understand the physical meaning of the stress tensor we consider the cubic element of volume shown in Fig.2, corresponding to an infinitesimal portion $dV = (dl)^3$ taken in an arbitrary solid body. The six faces of the cube have been numbered as shown in Fig.2. We suppose that a stress $\hat{T}$ is applied to that region: the T_{ij} component represents the pressure applied on the j-th face along the i-th direction.

1.1.4 *The formal structure of elasticity theory*

The relationships among the mathematical objects introduced in the previous Sections represent the formal structure of the theory of elasticity (for small deformations).

The first two equations can be derived from the balance equations holding for the linear and angular momentum [30, 31, 35]. In solid mechanics the two key quantities are the linear and angular momentum densities for a continuum material system. We consider a portion V within a material body limited by the close surface S and we define: $\vec{P}$ as its total linear momentum, $\vec{F}$ as the resultant of the applied forces, $\vec{L}$ as the total angular momentum, and $\vec{M}$ as the resultant torque. The momentum balance equation of Newtonian dynamics $\frac{d\vec{P}}{dt} = \vec{F}$ for a portion V is written in the form

$$\frac{d}{dt}\int_V \rho\frac{\partial u_j}{\partial t}d\vec{x} = \int_S T_{ji}n_i dS + \int_V b_j d\vec{x} \tag{1.24}$$

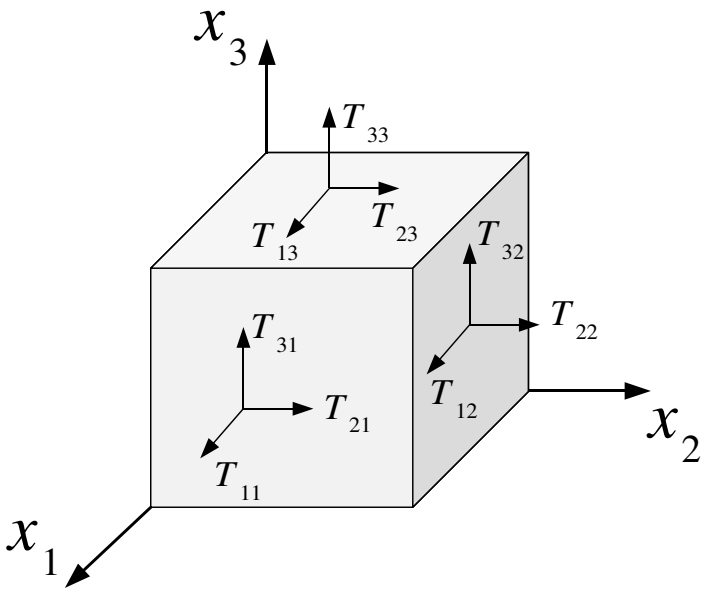

Figure 2: Geometrical representation of the stress tensor $\hat{T}$: the T_{ij} component represents the pressure applied on the j-th face of the cubic volume along the i-th direction.

where we made use of body and surface forces as described in the previous Section. The density of mass ρ is assumed to be constant and uniform under the small deformation assumption. By means of the Gauss divergence theorem, we get

$$\frac{d}{dt}\int_V \rho \frac{\partial u_j}{\partial t} d\vec{x} = \int_V \frac{\partial T_{ji}}{\partial x_i} d\vec{x} + \int_V b_j d\vec{x} \tag{1.25}$$

The linear momentum balance equation

Since the volume V is arbitrary, we easily obtain

$$\frac{\partial T_{ji}}{\partial x_i} + b_j = \rho \frac{\partial^2 u_j}{\partial t^2} \tag{1.26}$$

which represents a first important relation. We turn now to the angular momentum balance equation $\frac{d\vec{L}}{dt} = \vec{M}$ which can be written in the following form

$$\frac{d}{dt}\int_V \vec{x} \times \frac{\partial \vec{u}}{\partial t} \rho d\vec{x} = \int_S \vec{x} \times \left(\hat{T}\vec{n}\right) dS + \int_V \vec{x} \times \vec{b}\, d\vec{x} \tag{1.27}$$

As before, the surface integral can be simplified with the application of the Gauss divergence theorem

$$\int_S \vec{x} \times \left(\hat{T}\vec{n}\right) dS = \int_V \left[T_{kh} + x_h \frac{\partial T_{kp}}{\partial x_p}\right] \eta_{hkj} \vec{e}_j d\vec{x} \tag{1.28}$$

and we get

$$\int_V \left\{ x_h \left[\frac{\partial^2 u_k}{\partial t^2}\rho - \frac{\partial T_{kp}}{\partial x_p} - b_k\right] - T_{kh} \right\} \eta_{hkj} \vec{e}_j d\vec{x} = 0 \tag{1.29}$$

Because of Eq.(1.26) we obtain $\int_V T_{kh}\eta_{hkj}\vec{e}_j d\vec{x} = 0$ or, equivalently, $T_{kh}\eta_{hkj} = 0$. This leads to

The angular momentum balance equation

$$T_{ij} = T_{ji} \tag{1.30}$$

This second fundamental equation states that the stress tensor is symmetric.

Eqs.(1.7), (1.12), (1.26) and (1.30) hold for most materials regardless of their constitution and microstructure. To complete the formal structure of the theory of elasticity we need to introduce the specific constitutive equations, characterizing the elastic behavior of the material under investigation [39, 40]. They are written as

$$T_{ij} = f(\{\epsilon_{ij}\}) \tag{1.31}$$

defining, at any point of the solid, a biunivocal correspondance between stress and strain. When a perfect elastic behavior is observed, the body relaxes back to its equilibrium configuration when applied forces are removed. In other words $\hat{T} = 0$ if and only if $\hat{\epsilon} = 0$. For most materials Eq.(1.31) is linear for small deformations. The following Section is devoted to the study of the linear constitutive equations for both isotropic and anisotropic materials. The actual form of the constitutive equations cannot be determined within continuum mechanics: it is an input information of elasticity theory. Typically, it is determined experimentally [40] and formalized a posteriori [31]. We remark that in this work we only concern ourselves with fully-recoverable small deformations and point out that possible variations from a purely elastic behavior (e.g., plasticity) are treated elsewhere [41].

1.1.5 *Constitutive equations*

Because of the symmetry of $\hat{T}$, the elastic stress-strain relation is defined by six relations of the form $T_{ij} = f(\{\epsilon_{ij}\})$ which are uniquely solvable for each different component of the strain. A thermo-elastic material is one whose state of stress depends on the present strain and on the temperature (or entropy). In what follows we shall always assume that the temperature (or entropy) is constant so that, effectively, we have a pure stress-strain relationship [39].

For most materials Eq.(1.31) is linear if the strain is small [31, 33]. This corresponds to the generalized Hooke's law which has the following general form

Generalized Hooke's law

$$T_{ij} = \mathcal{C}_{ijkh}\epsilon_{kh} \tag{1.32}$$

where $\mathcal{C}_{ijkh}$ are constants (for homogeneous materials). Eq.(1.32) is of general validity, including all possible crystalline symmetries or, in other words, any kind of anisotropy. The fourth-rank tensor (with 81 components) of the elastic constants satisfies the following symmetry rules:

- Symmetry in the first pair of indices: since $T_{ij} = T_{ji}$ we have

$$\mathcal{C}_{ijkh} = \mathcal{C}_{jikh} \tag{1.33}$$

- Symmetry in the last pair of indices: since $\epsilon_{kh} = \epsilon_{hk}$ we have

$$\mathcal{C}_{ijkh} = \mathcal{C}_{ijhk} \tag{1.34}$$

- Symmetry between the first pair and the last pair of indices:

$$\mathcal{C}_{ijkh} = \mathcal{C}_{khij} \tag{1.35}$$

This result is easily proved if we suppose that an elastic energy density $U = U(\hat{\epsilon})$ exists, being dependent only on the state of strain. From the energy density we derive the constitutive relation $T_{ij} = \frac{\partial U(\hat{\epsilon})}{\partial \epsilon_{ij}}$ (just think about the case of the one-dimensional harmonic spring, where $U = \frac{1}{2}kx^2$ and $F = kx$). Drawing a comparison between the energy based constitutive relation $T_{ij} = \frac{\partial U(\hat{\epsilon})}{\partial \epsilon_{ij}}$ and Eq. (1.32) we simply obtain

$$C_{ijkh} = \frac{\partial T_{ij}}{\partial \epsilon_{kh}} = \frac{\partial^2 U(\hat{\epsilon})}{\partial \epsilon_{kh} \partial \epsilon_{ij}} \tag{1.36}$$

The symmetry of the second order derivative directly leads to Eq.(1.35).

According to the above universal symmetry properties, C_{ijkh} has at most 21 independent components. Further reductions of the number of independent elastic constants depend upon the possible crystalline symmetry of the material body [42, 39].

Stiffness and Compliance tensors

The linear relation can be written in tensor compact form $\hat{T} = \hat{C}\hat{\epsilon}$, where the elastic tensor $\hat{C}$ is called *stiffness tensor*. We also introduce the inverse relation $\hat{\epsilon} = \hat{D}\,\hat{T}$ with $\hat{D} = \hat{C}^{-1}$. The new tensor $\hat{D}$ is called *compliance tensor*.

As above said, the stiffness and the compliance tensors describe all the behaviors of all the crystal classes. We may recapitulate the number of independent parameters (elastic moduli) for the classes of various crystalline systems [39]:

Triclinic	→	21 independent components
Monoclinic	→	13 independent components
Orthorhombic	→	9 independent components
Tetragonal (C_4, S_4, C_{4h})	→	7 independent components
Tetragonal $(C_{4v}, D_{2d}, D_4, D_{4h})$	→	6 independent components
Rhombohedral (C_3, S_6)	→	7 independent components
Rhombohedral (C_{3v}, D_3, D_{3d})	→	6 independent components
Hexagonal (transverse isotropy)	→	5 independent components
Cubic	→	3 independent components

The above discussion relates, of course, to single crystals. Polycrystalline bodies whose component crystallites are sufliciently small may be regarded as isotropic bodies (since we are concerned with deformations in regions large compared with the dimensions of the crystallites). Like any isotropic body, a polycrystal has only two independent moduli of elasticity.

1.1.6 *The Voigt notation*

The above described symmetries of the stress and strain tensor and those of the stiffness tensor allow us to introduce the so called Voigt notation largely adopted in continuum mechanics. In fact , the six independent components of a symmetric 3-dimensional second-rank-

tensor can be arranged in a simpler 6-dimensional first-rank tensor by means of the following role:

$$\begin{pmatrix} T_{11} & T_{12} & T_{13} \\ T_{12} & T_{22} & T_{23} \\ T_{13} & T_{23} & T_{33} \end{pmatrix} \rightarrow \begin{pmatrix} T_{11} \\ T_{22} \\ T_{33} \\ T_{12} \\ T_{23} \\ T_{31} \end{pmatrix} \tag{1.37}$$

Consistently, the 21 independent components of the 3-dimensional fourth-rank stiffness tensors, can be arranged in a 6-dimensional symmetric second-rank tensor through the following scheme.

$$\begin{aligned} \mathcal{C}_{\alpha\beta\gamma\delta} &\rightarrow \mathcal{C}_{ij} \\ \alpha\beta(or\ \ \gamma\delta) = 11, 22, 33, 12, 23, 31 &\rightarrow i(or\ \ j) = 1, 2, 3, 4, 5, 6 \end{aligned} \tag{1.38}$$

Through the Voigt notation the constitutive equation (1.32) can be expressed in a 6-dimensional vector space by the relation $T_i = \mathcal{C}_{ij}\epsilon_j$ $(i, j = 1, ..., 6)$.

1.2 THE ISOTROPIC AND HOMOGENEOUS ELASTIC BODY

The paradigmatic system investigated by elasticity theory is the linear, isotropic and homogeneous medium. The homogeneity property implies that the elastic behavior of the medium is the same in all its points: the stiffness and the compliance tensors are constant everywhere in the medium. The isotropy property implies that the mechanical response does not depend on the direction considered: stiffness or compliance tensors are invariant under arbitrary rotations. For a linear, isotropic and homogeneous body we will prove that only two elastic moduli are independent. They are typically called Lamé coefficients and they are referred to as μ (shear modulus) and λ, respectively. Alternatively, we may use the Young modulus E and the Poisson ratio ν. A bulk modulus K can be used as well.

Let us now derive the constitutive equation for a linear, isotropic and homogeneous elastic body. Because the stress tensor $\hat{T}$ is symmetric, we can select a suitable reference frame where $\hat{T}$ is diagonal [28]. In this reference frame we refer to $\hat{T}^*$ as the diagonal representation of $\hat{T}$, where the only components different from zero are T^*_{11}, T^*_{22} and T^*_{33}. To begin we consider the case of a uniaxial traction, i.e., an elongation, along the x_1 axis, which means $T^*_{11} \neq 0$, $T^*_{22} = 0$ and $T^*_{33} = 0$. For most materials the experimental observation [29, 36] shows that the body will be elongated along the direction x_1, while it shrinks in the plane (x_2, x_3). We can formalize this response by writing the linear relations

$$\begin{aligned} \epsilon^*_{11} &= +\frac{1}{E}T^*_{11} \\ \epsilon^*_{22} &= -\frac{\nu}{E}T^*_{11} \\ \epsilon^*_{33} &= -\frac{\nu}{E}T^*_{11} \\ \epsilon^*_{12} &= \epsilon^*_{23} = \epsilon^*_{31} = 0 \end{aligned} \tag{1.39}$$

Young modulus and Poisson ratio definition

The Young modulus E describes the length variation along the direction x_1 while the Poisson ratio ν describes the contractions in the two

perpendicular directions. Of course, in these conditions we can not observe shear deformations.

When the diagonal stress $\hat{T}^*$ assumes triaxial character Eq.(1.39) can be easily generalized as

$$\begin{aligned}
\epsilon^*_{11} &= \frac{1}{E}\left[T^*_{11} - \nu\left(T^*_{22} + T^*_{33}\right)\right] \\
\epsilon^*_{22} &= \frac{1}{E}\left[T^*_{22} - \nu\left(T^*_{11} + T^*_{33}\right)\right] \\
\epsilon^*_{33} &= \frac{1}{E}\left[T^*_{33} - \nu\left(T^*_{22} + T^*_{11}\right)\right] \\
\epsilon^*_{12} &= \epsilon^*_{23} = \epsilon^*_{31} = 0
\end{aligned} \tag{1.40}$$

The constitutive relations given in Eq.(1.40) are valid only in the reference frame where the stress tensor is diagonal. We remark that Eq.(1.40) can be written in the following more compact form

$$\hat{\epsilon}^* = \frac{1}{E}\left[(1+\nu)\hat{T}^* - \nu\hat{I}\,\mathrm{Tr}\left(\hat{T}^*\right)\right] \tag{1.41}$$

If we make an arbitrary change of reference frame by means of a rotation matrix $\hat{R}$, the stress tensor $\hat{T}^*$ is transformed into $\hat{T}$ and the strain tensor $\hat{\epsilon}^*$ is transformed into $\hat{\epsilon}$ ($\hat{\epsilon} = \hat{R}^T\hat{\epsilon}^*\hat{R}$ and $\hat{T} = \hat{R}^T\hat{T}^*\hat{R}$) [28]. By means of such transformations, we obtain the isotropic constitutive equation in an arbitrary reference frame in the form

Constitutive equation in terms of the Young moduli and Poisson ratio

$$\hat{\epsilon} = \frac{1}{E}\left[(1+\nu)\hat{T} - \nu\hat{I}\,\mathrm{Tr}\left(\hat{T}\right)\right] \tag{1.42}$$

This is in fact the constitutive equation of a linear, isotropic and homogeneous elastic material. Eq.(1.42) can be inverted, thus obtaining the stress tensor in terms of the strain tensor

$$\hat{T} = \frac{E}{1+\nu}\hat{\epsilon} + \frac{\nu E}{(1+\nu)(1-2\nu)}\hat{I}\,\mathrm{Tr}\left(\hat{\epsilon}\right) \tag{1.43}$$

We now introduce the Lamé coefficients μ and λ defined by the following relations

$$\mu = \frac{E}{2(1+\nu)} \qquad \lambda = \frac{\nu E}{(1+\nu)(1-2\nu)} \tag{1.44}$$

which, inserted into Eq.(1.43), provide the constitutive equation in its most popular form

Lamé coefficients

$$\hat{T} = 2\mu\hat{\epsilon} + \lambda\hat{I}\mathrm{Tr}(\hat{\epsilon}) \tag{1.45}$$

Similarly, Eq.(1.42) can be also written in terms of the Lamé coefficients

$$\hat{\epsilon} = \frac{1}{2\mu}\hat{T} - \frac{\lambda}{2\mu(2\mu+3\lambda)}\hat{I}\mathrm{Tr}(\hat{T}) \tag{1.46}$$

In order to introduce the bulk modulus K, we consider an hydrostatic stress described by the tensor

$$\hat{T} = \begin{bmatrix} \sigma & 0 & 0 \\ 0 & \sigma & 0 \\ 0 & 0 & \sigma \end{bmatrix} \tag{1.47}$$

By means of Eq.(1.46) we easily obtain the corresponding state of strain

$$\hat{\epsilon} = \frac{1}{3}\frac{1}{\lambda + \frac{2}{3}\mu}\sigma\hat{I} \tag{1.48}$$

This simple result allows us to define the bulk modulus K as

Bulk modulus

$$K = \lambda + \frac{2}{3}\mu \tag{1.49}$$

Therefore, the stress-strain relation in hydrostatic condition can be summarized as $\hat{e} = \frac{1}{3K}\sigma\hat{I}$ where σ represents the (scalar) pressure applied to the system. The further relation $\mathrm{Tr}(\hat{e}) = \frac{\sigma}{K}$ has an important physical interpretation: it describes the local volumetric variation under the assumption of hydrostatic stress.

To conclude, we observe that the stress-strain relation (Hooke's law) for an isotropic elastic medium can be written in terms of any two independent material constants, chosen in the set λ, μ, K, E, ν. In Table 1 one can find all the possible conversions among the above defined elastic moduli. The elastic moduli E, λ, μ and K are measured in Pa while the Poisson ratio ν is dimensionless being defined as a ratio between deformations.

Table 1: Relations among the different elastic moduli.

	(λ, μ)	(K, μ)	(μ, ν)	(E, ν)	(E, μ)
λ		$K - \frac{2}{3}\mu$	$\frac{2\mu\nu}{1-2\nu}$	$\frac{\nu E}{(1+\nu)(1-2\nu)}$	$\frac{\mu(E-2\mu)}{3\mu-E}$
μ				$\frac{E}{2(1+\nu)}$	
K	$\frac{3\lambda+2\mu}{3}$		$\frac{2\mu(1+\nu)}{3(1-2\nu)}$	$\frac{E}{3(1-2\nu)}$	$\frac{E\mu}{3(3\mu-E)}$
E	$\frac{\mu(3\lambda+2\mu)}{\lambda+\mu}$	$\frac{9K\mu}{3K+\mu}$	$2(1+\nu)\mu$		
ν	$\frac{\lambda}{2(\lambda+\mu)}$	$\frac{3K-2\mu}{2(3K+\mu)}$			$\frac{E-2\mu}{2\mu}$

1.2.1 *Elasticity in a two-dimensional system*

If we deal with an elastic system defined in a two-dimensional space a different set of elastic moduli can be adopted. This is due in order to obtain the same physical interpretation of the corresponding three-dimensional coefficients. First of all, we note that in the two-dimensional case, the stress tensor components and, as a consequence, the elastic moduli are calculated as a force per unit of lenght (e.g N/m). The two-dimensional Lamè coefficients, λ^{2d} and μ^{2d}, are introduced through the relation

$$\hat{T} = 2\mu^{2d}\hat{e} + \lambda^{2d}\hat{I}\mathrm{Tr}(\hat{e}) \tag{1.50}$$

that is formaly equal to Eq.(1.45) but involves two-dimensional tensors. The bulk modulus is defined so as to represent the area variation due to

an hydrostatic strain $\epsilon_{ij} = \varepsilon\delta_{ij}$, being ε the scalar parameter governing the hydrostatic deformation

$$\frac{1}{2}\mathrm{Tr}(\hat{T}^{hydro}) = 2K^{2d}\varepsilon \tag{1.51}$$

where $\hat{T}^{hydro}$ is the stress due to the hydrostatic deformation. If we calculate the trace of the stress tensor for such a deformation by means of the equation (1.50) we obtain the relation between the two-dimensional bulk modulus K^{2d} and the two-dimensional Lamé moduli

Two-dimensional Bulk modulus

$$K^{2d} = \lambda^{2d} + \mu^{2d} \tag{1.52}$$

The Young modulus and the Poisson ratio physically corresponds to the parameters describing respectively the longitudinal and transverse deformation due to an applied uniaxial stress. In particular, if we consider a uniaxial stress applied along the direction 1 of magnitude σ: $T_{11} = \sigma$ and $T_{ij} = 0$ for $(i,j) \neq (1,1)$, we have

$$\epsilon_{11} = \frac{\sigma}{E^{2d}} \tag{1.53}$$

$$\epsilon_{22} = -\nu^{2d}\epsilon_{11} \tag{1.54}$$

These relations impliy that the constitutive equation must assumes the following form

$$\hat{T} = \frac{E^{2d}}{1+\nu^{2d}}\hat{\epsilon} + \frac{\nu^{2d}E^{2d}}{1-(\nu^{2d})^2}\mathrm{Tr}(\hat{\epsilon})\hat{I} \tag{1.55}$$

By confronting this equation with Eq.(1.50) we easily find the relation between the two-dimensional Young modulus and Poisson ratio and the corresponding Lamè coefficients

two-dimensional Young modulus and Poisson ratio

$$E^{2d} = \frac{4\mu^{2d}(\lambda^{2d}+\mu^{2d})}{\lambda^{2d}+2\mu^{2d}} \tag{1.56}$$

$$\nu^{2d} = \frac{\lambda^{2d}}{\lambda^{2d}+2\mu^{2d}} \tag{1.57}$$

By means of Eqs(1.52), (1.56) and (1.57) we can derive the conversions among all the two-dimensional elastic moduli. These relations are reported in Table 2 (two-dimensional counterpart of the Table 1).

1.2.2 *Governing equations of elasticity and border conditions*

When we are dealing with a linear, isotropic and homogeneous material the governing equations of the elasticity theory can be summed up as follows

$$\begin{cases} \frac{\partial T_{ij}}{\partial x_j} + b_i = \rho\frac{\partial^2 u_i}{\partial t^2} \\ \epsilon_{ij} = \frac{1}{2}\left(\frac{\partial u_i}{\partial x_j} + \frac{\partial u_j}{\partial x_i}\right) \\ T_{ij} = 2\mu\epsilon_{ij} + \lambda\epsilon_{kk}\delta_{ij} \end{cases} \tag{1.58}$$

From the above equations we can obtain a pure equation describing the time behavior of the displacement field during the deformation process. To this aim we begin substituting the constitutive equation into the motion equation

$$2\mu\frac{\partial\epsilon_{ij}}{\partial x_j} + \lambda\frac{\partial\epsilon_{kk}}{\partial x_i} + b_i = \rho\frac{\partial^2 u_i}{\partial t^2} \tag{1.59}$$

Table 2: Relations among the two-dimensional elastic moduli.

	(λ^{2d}, μ^{2d})	(K^{2d}, μ^{2d})	(μ^{2d}, ν^{2d})	(E^{2d}, ν^{2d})	(E^{2d}, μ^{2d})
λ^{2d}		$K^{2d} - \mu^{2d}$	$\frac{2\mu^{2d}\nu^{2d}}{1-\nu^{2d}}$	$\frac{\nu^{2d}E^{2d}}{1-(\nu^{2d})^2}$	$\frac{2\mu^{2d}(E^{2d}-2\mu^{2d})}{4\mu^{2d}-E^{2d}}$
μ^{2d}				$\frac{E^{2d}}{2(1+\nu^{2d})}$	
K^{2d}	$\lambda^{2d} + \mu^{2d}$		$\frac{\mu^{2d}(1+\nu^{2d})}{(1-\nu^{2d})}$	$\frac{E^{2d}}{2(1-\nu^{2d})}$	$\frac{E^{2d}\mu^{2d}}{4\mu^{2d}-E^{2d}}$
E^{2d}	$\frac{4\mu^{2d}(\lambda^{2d}+\mu^{2d})}{\lambda^{2d}+2\mu^{2d}}$	$\frac{4K^{2d}\mu^{2d}}{K^{2d}+\mu^{2d}}$	$2\mu^{2d}(1+\nu^{2d})$		
ν^{2d}	$\frac{\lambda^{2d}}{(\lambda^{2d}+2\mu^{2d})}$	$\frac{K^{2d}-\mu^{2d}}{K^{2d}+\mu^{2d}}$			$\frac{E^{2d}-2\mu^{2d}}{2\mu^{2d}}$

Now, we can substitute the definition of the strain tensor into the previous Eq. (1.59), by obtaining

$$(\mu+\lambda)\frac{\partial^2 u_j}{\partial x_i \partial x_j}+\mu\frac{\partial^2 u_i}{\partial x_j \partial x_j}+b_i=\rho\frac{\partial^2 u_i}{\partial t^2} \tag{1.60}$$

Lamé or Navier equation

We have obtained an equation of motion where the displacement field is the single unknown, which have been called Lamé or Navier equation [31, 36]. It can be also written in vector notation as

$$(\lambda+\mu)\,\vec{\nabla}\left(\vec{\nabla}\cdot\vec{u}\right)+\mu\vec{\nabla}^2\vec{u}+\vec{b}=\rho\frac{\partial^2\vec{u}}{\partial t^2} \tag{1.61}$$

Such a motion equation for a isotropic elastic body can be also written in a different form by utilizing the general property $\vec{\nabla}\times\left(\vec{\nabla}\times\vec{u}\right)=\vec{\nabla}\left(\vec{\nabla}\cdot\vec{u}\right)-\vec{\nabla}^2\vec{u}$, which holds for the differential operators. The result is

$$(\lambda+\mu)\,\vec{\nabla}\times\left(\vec{\nabla}\times\vec{u}\right)+(\lambda+2\mu)\vec{\nabla}^2\vec{u}+\vec{b}=\rho\frac{\partial^2\vec{u}}{\partial t^2} \tag{1.62}$$

Both Eq. (1.61) and Eq. (1.62) are partial differential equations of the second order with a vector field $\vec{u}\,(\vec{r})$ as unknown. In order to find a solution of Eq. (1.61) or Eq. (1.62) we must impose some boundary conditions depending on the physical problem under consideration [34, 35]. From the mathematical point of view some different forms of the boundary conditions can be taken into consideration. We consider a body with an external surface S. A first type of boundary condition fixes the values of the displacement field on this surface at any time. It means that $\vec{u}=\vec{g}(\vec{x},t)$ for any $\vec{x}\in S$ and for any t in a given interval. When the entire external surface is described by these conditions we say that we are solving an elastic problem of the first kind, subjected to the Dirichlet conditions. A second kind of boundary conditions fixes the stress applied on the external surface. It means that $T_{ij}n_j=f_i(\vec{x},t)$ for any $\vec{x}\in S$ and for any t in a given interval. When the entire external surface is described by these conditions we say that we are solving an elastic problem of the second kind, subjected to the Neumann conditions. Finally, a third case can be defined by dividing the surface S in two parts and by applying the Dirichlet conditions to the first part and the Neumann conditions to the second part. In this case we say that we are solving an elastic problem of the third kind, subjected to mixed boundary conditions. These problems can be considered with a time dependent behavior of all the elastic fields (dynamics theory leading, in particular, to the propagation of elastic waves [43]) or under static condition, leading to the analysis of the equilibrium of an elastic solid body [44]. One of the most largely applied approach for solving these problems is based on the use of the Green functions which are well known in closed form both for static problems (static Green function) and for dynamic ones (dynamic Green function) [43, 45].

Boundary conditions

It is important to observe that the governing equations for the elasticity theory as stated in Eq.(1.58) are useful to obtain the final relations (Eq. (1.61) and Eq. (1.62)) in terms of the displacement. Alternatively, for many static problems, it is useful to use pure equations in terms of

the stress tensor. To obtain them, insted of the system stated in Eq.(1.58), we start with the following one

$$\begin{cases} \frac{\partial T_{ij}}{\partial x_j} + b_i & = & 0 \\ \eta_{qki}\eta_{phj}\frac{\partial 2\epsilon_{ij}}{\partial x_k \partial x_h} & = & 0 \\ \epsilon_{ij} & = & \frac{1}{2\mu}T_{ij} - \frac{\lambda}{2\mu(2\mu+3\lambda)}T_{kk}\delta_{ij} \end{cases} \tag{1.63}$$

formed by the static version of the linear momentum principle, the compatibility conditions for the strain and the constitutive equation (in its inverse form). By substituting the constitutive relation in the compatibility equations for the strain we obtain a system where the stress tensor appears as the unknown

$$\begin{cases} \frac{\partial T_{ij}}{\partial x_j} + b_i & = & \rho\frac{\partial^2 u_i}{\partial t^2} \\ \nabla^2 T_{ik} + \frac{1}{1+\nu}\frac{\partial 2 T_{jj}}{\partial x_i \partial x_k} & = & -\frac{\nu}{1-\nu}\delta_{ik}\frac{\partial b_j}{\partial x_j} - \left(\frac{\partial b_i}{\partial x_k} + \frac{\partial b_k}{\partial x_i}\right) \end{cases} \tag{1.64}$$

Beltrami-Michell compatibility equation

The second equation of this system is referred to as the Beltrami-Michell compatibility equation for the stress tensor (in static regime) [29]. This formulation of the governing equations of the elasticity theory is the most convenient set to be used in the solution of the second boundary-value problem, subjected to the Neumann conditions.

The formulations described in the present section concern three-dimensional problems of the elasticity theory. In many cases of great practical interest the setting of a given problem can be considerably simplified. For example, many elastic systems can described by means of two-dimensional equations, which can be solved with a series of very efficient specific methodologies. In the following sections we will consider three particular problems which can be described by two-dimensional equations:

- plane strain condition
- plane stress condition
- anti-plane shear condition

We first introduce the *plane strain border condition*, which consider to be a displacement field described by $u_1(x_1, x_2, x_3)$, $u_2(x_1, x_2, x_3)$ and $u_3(x_1, x_2, x_3)$. A state of plane strain is said to exist in a body if the displacement components take the form $u_1 = u_1(x_1, x_2)$, $u_2 = u_2(x_1, x_2)$ and $u_3 = 0$. In other words, these conditions are fulfilled if the displacement vector belongs to the plane x_1, x_2 and it does not depend on the coordinate x_3. Of course, the definition of the plane strain conditions can be generalized to any arbitrarily-oriented plane. It is easy to prove that the plane strain conditions impose the following relations on the strain tensor: $\epsilon_{33} = 0$, $\epsilon_{13} = 0$ and $\epsilon_{23} = 0$. The constitutive equations given in Eq.(1.43) take (in the Voigt notation) the following simplified form

$$\begin{bmatrix} T_{11} \\ T_{22} \\ T_{12} \end{bmatrix} = \frac{E}{(1+\nu)(1-2\nu)} \begin{bmatrix} 1-\nu & \nu & 0 \\ \nu & 1-\nu & 0 \\ 0 & 0 & 1-2\nu \end{bmatrix} \begin{bmatrix} \epsilon_{11} \\ \epsilon_{22} \\ \epsilon_{12} \end{bmatrix} \tag{1.65}$$

Constitutive equations under plane strain boundary conditions

The inverse constitutive equation is therefore given by

$$\begin{bmatrix} \epsilon_{11} \\ \epsilon_{22} \\ \epsilon_{12} \end{bmatrix} = \frac{1}{E} \begin{bmatrix} 1-\nu^2 & -\nu(1+\nu) & 0 \\ -\nu(1+\nu) & 1-\nu^2 & 0 \\ 0 & 0 & 1+\nu \end{bmatrix} \begin{bmatrix} T_{11} \\ T_{22} \\ T_{12} \end{bmatrix} \tag{1.66}$$

The relation $T_{33} = \frac{E}{1+\nu}\frac{\nu}{1-2\nu}(\epsilon_{11}+\epsilon_{22})$ is not included in the previous sets, but it is still valid and it can be useful for some applications.

We now introduce the *plane stress border condition*. A state of plane stress is said to exist when the stress tensor satisfies the property $\hat{T}\vec{n} = 0$ for a given unit vector $\vec{n}$, in any point of the material. We consider $\vec{n}$ parallel to the x_3 axis. It follows that $T_{33} = 0$, $T_{13} = 0$ and $T_{23} = 0$. Moreover we suppose that $T_{11} = T_{11}(x_1, x_2)$, $T_{22} = T_{22}(x_1, x_2)$ and $T_{12} = T_{12}(x_1, x_2)$. With these assumptions the constitutive relation given in Eq.(1.42) can be simplified as follows

Constitutive equations under plane stress boundary conditions

$$\begin{bmatrix} \epsilon_{11} \\ \epsilon_{22} \\ \epsilon_{12} \end{bmatrix} = \frac{1}{E}\begin{bmatrix} 1 & -\nu & 0 \\ -\nu & 1 & 0 \\ 0 & 0 & 1+\nu \end{bmatrix}\begin{bmatrix} T_{11} \\ T_{22} \\ T_{12} \end{bmatrix} \tag{1.67}$$

They can also be inverted as follows

$$\begin{bmatrix} T_{11} \\ T_{22} \\ T_{12} \end{bmatrix} = \frac{E}{1-\nu^2}\begin{bmatrix} 1 & \nu & 0 \\ \nu & 1 & 0 \\ 0 & 0 & 1-\nu \end{bmatrix}\begin{bmatrix} \epsilon_{11} \\ \epsilon_{22} \\ \epsilon_{12} \end{bmatrix} \tag{1.68}$$

As above, the relation $\epsilon_{33} = -\frac{\nu}{E}(T_{22}+T_{11})$ is not included in the previous sets, but it too is still valid and it can be useful for some applications.

It is important to observe that a simple formal substitution transforms Eqs.(1.67) and (1.68) for plane stress conditions into the corresponding Eqs.(1.65) and (1.66) for plane strain condition. In fact, if we consider in Eqs.(1.67) and (1.68) the change of variables $E \to \frac{E}{1-\nu^2}$ and $\nu \to \frac{\nu}{1-\nu}$ we obtain Eqs.(1.65) and (1.66) exactly . This property is very useful in many practical applications.

Anti-plane shear boundary condition

The *anti-plane shear boundary condition* imposes a displacement field with the following form $\vec{u} = (0, 0, u_3(x_1, x_2, t))$. It means that each point of the body can move only along a line parallel to the x_3 axis. The term anti-plane means that the motion occour in lines perpendicular to the (x_1, x_2) plane. The simple calculation of the strain tensor leads to the results $\epsilon_{13} = \frac{1}{2}\frac{\partial u_3}{\partial x_1}$ and $\epsilon_{23} = \frac{1}{2}\frac{\partial u_3}{\partial x_2}$. The other components of the strain are zero. The corresponding stress tensor can be obtained by means of the constitutive relation, obtaining $T_{13} = \mu\frac{\partial u_3}{\partial x_1}$ and $T_{23} = \mu\frac{\partial u_3}{\partial x_2}$. Therefore, only two shear components of the stress are present in this system. We also suppose that the body forces fulfill the additional conditions $b_1 = 0, b_2 = 0$ and $b_3 = b_3(x_1, x_2, t)$. Under these conditions, it is easy to observe that only the third component of the linear momentum principle is meaningful

$$\frac{\partial T_{13}}{\partial x_1} + \frac{\partial T_{23}}{\partial x_2} + b_3 = \rho\frac{\partial^2 u_3}{\partial t^2} \tag{1.69}$$

Two-dimensional D'Alambert equation

By considering the above described components of the stress tensor, we obtain

$$\mu\nabla^2 u_3 + b_3 = \rho\frac{\partial^2 u_3}{\partial t^2} \tag{1.70}$$

which is a second order partial differential equation in the unknown displacement component u_3. In order to solve this kind of equation we must take into account the boundary conditions on the external surface of the body. Of course, under the anti-plane shear condition the shape

of the body is an arbitrary cylinder aligned along the x_3 axis. Therefore, the boundary conditions will be applied to a closed line γ on the (x_1, x_2) plane. For a mixed problem, on a first part of the border γ_1 we take into consideration the Dirichlet condition $u_3 = v_3(x_1, x_2, t)$ for any point belonging to γ_1. On the second part γ_2 of the closed line ($\gamma = \gamma_1 \cup \gamma_2$) we must impose the applied stress. Since $\hat{T}\vec{n} = (0, 0, n_1 T_{13} + n_2 T_{23})$ we have $(\hat{T}\vec{n})_3 = \mu n_1 \frac{\partial u_3}{\partial x_1} + \mu n_2 \frac{\partial u_3}{\partial x_2} = \mu \vec{n} \cdot \vec{\nabla} u_3 = \mu \frac{\partial u_3}{\partial n}$. So, we consider the Neumann condition $\mu \frac{\partial u_3}{\partial n} = f_3(x_1, x_2, t)$ on γ_2. In the case of a static elastic regime without body forces applied to the system, Eq.(1.70) can be simplified to the two-dimensional Laplace equation $\nabla^2 u_3 = 0$. Therefore, a body in elastic equilibrium under anti-plane shear conditions is analogous, from the mathematical point of view, to a two-dimensional electrostatic system without free charge distributed in the space.

Two-dimensional Laplace equation

1.2.3 *Two-dimensional elastic moduli under plane border conditions*

As shown in the previous section, under the described plane bondary conditions the three-dimensional fourth rank stress and strain tensors can be reduced to two-dimensional tensor (or, in the Voigt notation, we can simplify the six-dimensional second rank tensors with two three-dimensional tensors). Therefore, we can describe the elasticity of such systems with the same formalism adopted in the actual two-dimensional case of Section 1.2.1, i.e. through the two-dimensional parameters above defined. Nevertheless, in this case these parameters are again expressed as a force per unit of area.

The relations between the two-dimensional moduli and the corresponding three-dimensional parameters depend on the adopted boundary condition. If we assume the plane strain boundary condition the constitutive equation in terms of the three-dimensional moduli is reported in Eq.(1.65) and it can be expressed in the following form

Two-dimensional moduli for a three-dimensional system under plane strain boundary conditions

$$\hat{T} = \frac{E}{1+\nu}\hat{e} + \frac{\nu E}{(1+\nu)(1-2\nu)}\hat{I}\mathrm{Tr}(\hat{e}) \tag{1.71}$$

where $\hat{T}$ and $\hat{e}$ are represented by two-dimensional tensors. By comparing this equation with Eq.(1.55) we obtain

$$\frac{E^{2d}}{1+\nu^{2d}} = \frac{E}{1+\nu} \tag{1.72}$$

$$\frac{\nu^{2d} E^{2d}}{1-(\nu^{2d})^2} = \frac{\nu E}{(1+\nu)(1-2\nu)} \tag{1.73}$$

and, therefore, the following conversion formulas

$$E^{2d} = \frac{E}{1-\nu^2} \tag{1.74}$$

$$\nu 2d = \frac{\nu}{1-\nu} \tag{1.75}$$

By means of Eqs.(1.74) and (1.72) and by confronting the results in Table 1 and Table 2, we can see that the Lamé coefficients assumes the same value of the three-dimensional case, i.e.

$$\mu^{2d} = \mu \tag{1.76}$$

$$\lambda^{2d} = \lambda \tag{1.77}$$

Finaly, the above results allows us to obtain the conversion formula for the bulk modulus

$$K^{2d} = K + \frac{1}{3}\mu \tag{1.78}$$

Two-dimensional moduli for a three-dimensional system under plane stress boundary conditions

On the other hand, if we adopt the plane stress boundary condition, the constitutive equation is reported in Eq.(1.68), i.e.

$$\hat{T} = \frac{E}{1+\nu}\hat{\epsilon} + \frac{\nu E}{1-\nu^2}\hat{I}\mathrm{Tr}(\hat{\epsilon}) \tag{1.79}$$

where $\hat{T}$ and $\hat{\epsilon}$ are two-dimensional tensors. By means of Eq.(1.55), we easily verify that

$$E^{2d} = E \tag{1.80}$$

$$\nu 2d = \nu \tag{1.81}$$

and, by confronting once again Table 1 and Table 2, we get

$$\mu^{2d} = \mu \tag{1.82}$$

$$\lambda^{2d} = \frac{2\lambda\mu}{\lambda+2\mu} \tag{1.83}$$

and

$$K^{2d} = \frac{9K\mu}{3K+4\mu} \tag{1.84}$$

This relation concludes the set of conversion equations for the two-dimensional formulation of a three-dimensional elastic system under plane stress conditions. All the derived conversion formulas are summarized in Table 3.

Table 3: Relations among two-dimensional elastic moduli and the corresponding three-dimensional coefficients under plane boundary conditions.

modulus	plane strain	plane stress
E^{2d}	$\frac{E}{1-\nu^2}$	E
ν^{2d}	$\frac{\nu}{1-\nu}$	ν
λ^{2d}	λ	$\frac{2\lambda\mu}{\lambda+2\mu}$
μ^{2d}	μ	μ
K^{2d}	$K+\frac{1}{3}\mu$	$\frac{9K\mu}{3K+4\mu}$

1.3 ELASTIC ENERGY

In general the constitutive equation of an elastic material can be derived by the strain energy function by means of the relation [36]

$$T_{ij} = \frac{\partial U(\hat{\epsilon})}{\partial \epsilon_{ij}} \tag{1.85}$$

We consider a linear elastic body described by the constitutive relation given in Eq.(1.32). It is possible to obtain the explicit form of its energy density U in terms of the strain tensor. From the relation

$$\frac{dU}{dt} = \frac{\partial U}{\partial \epsilon_{ij}} \frac{d\epsilon_{ij}}{dt} = T_{ij} \frac{d\epsilon_{ij}}{dt} \tag{1.86}$$

giving the rate of change of the energy density during a time-dependent deformation, we obtain

$$\frac{dU}{dt} = \mathcal{C}_{ijkh} \epsilon_{kh} \frac{d}{dt} \epsilon_{ij} \tag{1.87}$$

which, by using the symmetry given in Eq.(1.35), can be written as

$$\frac{dU}{dt} = \frac{1}{2} \mathcal{C}_{ijkh} \frac{d}{dt} \left(\epsilon_{ij} \epsilon_{kh} \right) \tag{1.88}$$

It follows that the energy density can be placed in the very general form

Strain energy function for linear media

$$U = \frac{1}{2} \mathcal{C}_{ijkh} \epsilon_{ij} \epsilon_{kh} \tag{1.89}$$

This expression can be further simplified when the material is linear, isotropic and homogeneous. Indeed, it assumes the very compact form [39]

$$U(\hat{\epsilon}) = \frac{1}{2} T_{ij} \epsilon_{ij} = \mu \epsilon_{ij} \epsilon_{ij} + \frac{1}{2} \lambda \epsilon_{kk} \epsilon_{ii} \tag{1.90}$$

where we have made use of the Lamé coefficients defined in a previous Section. Since $\epsilon_{kk} = \epsilon_{ii} = \mathrm{Tr}(\hat{\epsilon})$ and $\epsilon_{ij}\epsilon_{ij} = \mathrm{Tr}(\hat{\epsilon}^2)$ we obtain the final tensor form

$$U(\hat{\epsilon}) = \mu \mathrm{Tr}(\hat{\epsilon}^2) + \frac{1}{2} \lambda \left[\mathrm{Tr}(\hat{\epsilon}) \right]^2 \tag{1.91}$$

which represents the elastic energy density for an isotropic material.

For an elastic solid body at equilibrium, i.e., for $\epsilon_{ij} = 0 \ \ \forall \ i, j$, the function $U(\hat{\epsilon})$ must exhibit a minimum (i.e., the equilibrium configuration is stable). Because $U(\hat{\epsilon} = 0) = 0$, we conclude that the quadratic form defined in Eqs.(1.89) or (1.91) is positive definite. In other words, we have proved that the stiffness and the compliance tensors are always positive definite for real materials. We search for the specific conditions assuring a positive definite energy density for an isotropic material. To this aim, we apply a deformation satisfying the relation $\epsilon_{ii} = 0$, leading to $U = \mu \epsilon_{ij} \epsilon_{ij} > 0$ or, equivalently, $\mu > 0$. Moreover, if we apply an hydrostatic deformation $\epsilon_{ij} = \varepsilon \delta_{ij}$, where ε is a constant, we obtain $U = 3\varepsilon^2 (3\lambda/2 + \mu) > 0$ or, equivalently, $3\lambda + 2\mu > 0$. By means of Tab.1 we obtain the additional relations $K > 0$ and $E > 0$. Finally, by means of the expression $\nu = \frac{3K - 2\mu}{2(3K + \mu)}$ we can easily prove that $-1 < \nu < \frac{1}{2}$. It is interesting to observe that the last result admits negative values for the Poisson ratio. This point was considered controversial for a long time. In fact, standard natural materials exhibit a non negative Poisson ratio meaning that all traditional materials, when elongated in a given direction, always display a shrinking in the transverse (perpendicular) directions. However, during last decades many composite and complex materials have been realized with negative values of the Poisson ratio [46, 47, 48]. Hence, when elongated in a given direction, these materials show an unconventional extension in the transverse directions. Although intriguing, this phenomenon, as above proved, does not violate thermodynamics.

Thermodynamics bounds for the elastic coefficients

Negative Poisson ratio

2 ESHELBY THEORIES

Contents

2.1 STANDARD ESHELBY THEORY

Probably, the most important result in the extensive literature on elastic composites is the Eshelby theorem on the response of a single ellipsoidal elastic particle in an elastic space to a strain imposed at infinity. Between 1957 and 1973 Eshelby published three seminal papers [8, 49, 50] systematically studying this problem and founding that a uniform strain at infinity results in a uniform strain within the ellipsoidal inclusion. Therefore, this property was used in more detailed calculations in order to obtain the fourth-rank tensor relating these two uniform strains. This is the so-called Eshelby tensor and it depends on the geometry of the ellipsoid (i.e. on the three semi-axes length) and on the elastic properties of the homogeneous hosting matrix. The tensor entries are not simple since they involve elliptic integrals, but Eshelby was able to enumerate and explicitly evaluate all of these integrals for simple shapes like spheres, oblate and prolate spheroids, needles, and disks. Some years later, a similar property was proved also for the elastic field of an anisotropic particle embedded in an anisotropic medium [51].

The Eshelby theorem

The Eshelby solutions, in their first version, have been found within the elastostatics regime. Nevertheless, Somethe determination of the elastodynamic fields due to ellipsoidal inclusions and inhomogeneities are of fundamental interest in a wide range of problems in the mechanics of heterogeneous solids. Therefore, the dynamic Eshelby inclusion problem for an ellipsoidal inclusion in a three-dimensional isotropic medium was recently considered [52]. The dynamic Eshelby tensor has been expressed in terms of solutions of the Helmholtz equation. This approach leads to closed-form expressions in the particular cases of spheres and cylinders coinciding with those given in [53] and in [54], obtained by employing different techniques.

Generalization of the Eshelby theory to dynamic inclusion problem

Two different problems concerning the elastic fields generated by particular inclusions have been solved by L.J. Walpole [55, 56]. In the first case a rigid inclusion of ellipsoidal shape is bonded firmly at arbitrary orientation to a surrounding, unbounded, homogeneous elastic matrix of arbitrary anisotropy, and is translated infinitesimally by the action of

an externally imposed force. Walpole [55] founds out the complete solution by utilizing an approach very similar to that of Eshelby. A second problem deals with a rigid inclusion of ellipsoidal shape, bonded firmly at arbitrary orientation to a surrounding matrix of arbitrary anisotropy, and rotated infinitesimally, about an axis through its centre, by means of an externally imposed couple. Also in this case an exact solution has been found with very elegant procedures [56].

Generalizations of the Eshelby for different physical situations

Some other interesting generalization have been made to obtain the counterpart of the (elastic) Eshelby property for different physical situations. It has shown [57] how the Eshelby theory may be generalized to both poroelasticity and thermoelasticity. The resulting formulas are important for applications to analysis of poroelastic and thermoelastic composites, including but not restricted to rocks [58]. Moreover, a simple and unified explicit expression for electroelastic Eshelby tensors is presented by Yu and Huang [59]. They extended Eshelby's tensors for elastic isotropic inclusions to the piezoelectric cases. As in the uncoupled elastic cases, the resulting electroelastic Eshelby tensors are functions of the shape of the inclusion and the properties of the surrounding matrix. Furthermore, the magneto-electro-elastic Eshelby tensors that represent the stress, electric displacement, and magnetic induction in an inclusion resulting from the constraint of the surrounding matrix of piezomagnetic-piezoelectric composites have been found [60]. Finally, the Eshelby theory has been applied to the dielectric characterization of anisotropic inhomogeneities [61] and graded structures [62].

The most important aspect of the Eshelby work is that the interior points Eshelby tensor is constant for an ellipsoidal inclusion. This fact implies that an uniform strain at infinity results in a uniform strain in the ellipsoidal inclusion. In his third paper on this subject [50], Eshelby conjectured that, among all the closed surfaces, the ellipsoid alone has this convenient property. The search for a correct answer to this conjecture has produced a series of important investigations. To frame the question in more rigorous terms, we must distinguish two different versions of the conjecture. The strong Eshelby conjecture is: if the induced elastic fields inside an inclusion are uniform under a single uniform loading, the inclusion is of elliptic or ellipsoidal shape. Moreover, the weak Eshelby conjecture is: if the induced elastic fields inside an inclusion are uniform under all (any) uniform loadings, the inclusion is of elliptic or ellipsoidal shape. Of course, the strong conjecture implies the weak conjecture. The first result was found by Sendeckyj [63] who proved the strong Eshelby conjecture for a two-dimensional inclusion under plane strain or plane stress conditions. Successively [64], the strong Eshelby conjecture has been verified for the anti-plane problem. More recently [65], it has been proved the weak Eshelby conjecture for three-dimensional inclusions for isotropic materials by using the maximum principle of harmonic potentials. Finally, Liu showed [66] that the strong Eshelby conjecture is false in three and higher dimensions, by constructing explicit counterexamples.

Eshelby conjecture: strong formulation

Eshelby conjecture: weak formulation

The Eshelby result and its generalizations have been found to be immensely useful also in the analysis of composite materials, since most inclusion shapes commonly of interest can be approximated by some ellipsoid.

Homogenization approach to heterogeneous material

The investigations on the physical properties of heterogeneous materials have been focused on the search for the effective physical properties

exhibited at the macroscopic scale [67, 68]. Typically, such investigations are based on homogenization techniques. They basically contain at first the exact mathematical analysis of the mechanical behavior induced by a single inhomogeneity [45], and then proceed by considering the more general case of interacting particles [69, 70]. This approach is generally carried out in the limit of a low density defect population [71]. Such an hypothesis can be partially removed by means of different methods, such as iterated homogenizations [72] and differential schemes [73, 74]. These techniques have been applied with great accuracy both to the case of embedded inhomogeneities [75, 76, 77] and to the case of dispersed defects, such as micro-cracks in a matrix [78, 79, 80].

2.1.1 *Outline of the Eshelby theory*

The main purpose of this Section is to define the basic equations describing the elastic field inside and outside an ellipsoidal inclusion Ω embedded into a homogeneous matrix. The materials are supposed to be linear elastic, homogeneous and isotropic. We suppose to consider an infinite medium with stiffness tensor $\hat{\mathcal{C}}^{(1)}$; it means that the homogeneous solid matrix (hereafter labelled as material 1) is characterized by the relation $\hat{\mathbf{T}} = \hat{\mathcal{C}}^{(1)}\hat{\boldsymbol{\epsilon}}$ Moreover, we define an embedded ellipsoidal inclusion Ω as a region of space described by the constitutive equation $\hat{\mathbf{T}} = \hat{\mathcal{C}}^{(1)}(\hat{\boldsymbol{\epsilon}} - \hat{\boldsymbol{\epsilon}}^*)$. (see Fig.3)

The eigenstrain and the concept of inclusion

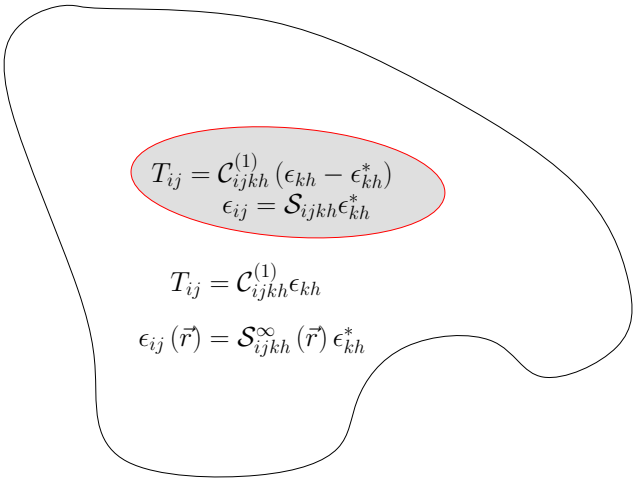

Figure 3: Scheme of an ellipsoidal inclusion

The strain $\hat{\boldsymbol{\epsilon}}^*$ is *a-priori* given and it is called eigenstrain (or stress-free strain). In other words, throughout this paper we denote as an inclusion a region containing a distribution of eigenstrains with the same moduli as the matrix. It is important to remark that the concept of inclusion is different from that of inhomogeneity. The inhomogeneity is defined as follows: we consider an infinite medium with stiffness tensor $\hat{\mathcal{C}}^{(1)}$ in $\mathfrak{R}^3\backslash\Omega$ (matrix) and $\hat{\mathcal{C}}^{(2)}$ in the ellipsoidal region Ω (inhomogeneity). We remotely load the system with a uniform strain $\hat{\boldsymbol{\epsilon}}^{\infty}$ or, equivalently, with the uniform stress $\hat{\mathbf{T}}^{\infty} = \hat{\mathcal{C}}^{(1)}\hat{\boldsymbol{\epsilon}}^{\infty}$. This configuration can be analyzed by means of the Eshelby equivalence principle as discussed in a following

The concept if inhomogeneity

Sections. For an isotropic matrix the stiffness tensor can be represented as

$$\mathcal{C}^{(1)}_{ijkh} = \left(K_1 - \frac{2}{3}\mu_1\right)\delta_{ij}\delta_{kh} + \mu_1\left(\delta_{ik}\delta_{jh} + \delta_{ih}\delta_{jk}\right) \tag{2.1}$$

where the elastic moduli are named K_1 (bulk modulus) and μ_1 (shear modulus). The bulk and the shear moduli can be replaced when needed by the Young modulus $E_1 = \frac{9K_1\mu_1}{\mu_1+3K_1}$ and the Poisson ratio $\nu_1 = \frac{3k_1-2\mu_1}{2(\mu_1+3k_1)}$. The displacement u_i induced by the presence of the inclusion (i.e. of the equivalent eigenstrain $\hat{\epsilon}^*$) can be evaluated in term of the so-called harmonic potential $\Phi(\vec{r})$ and biharmonic potential $\Psi(\vec{r})$ [8, 49]:

Inclusion displacement field as a function of the harmonic and biharmonic potentials

$$u_i(\vec{r}) = \epsilon^*_{kh}\left[\frac{1}{8\pi(1-\nu_1)}\Psi_{,ikh} - \frac{\delta_{ih}}{4\pi}\Phi_{,k} - \frac{\delta_{ik}}{4\pi}\Phi_{,h} - \frac{\nu_1}{1-\nu_1}\frac{\delta_{kh}}{4\pi}\Phi_{,i}\right] \tag{2.2}$$

where $\vec{r} = (x_1, x_2, x_3)$ is the position vector. Hereafter we write the symbol $f_{,i} = \frac{\partial f}{\partial x_i}$ and we extend this notation to higher order derivatives. Eq. (2.2) is valid anywhere. The harmonic potential is defined, as well known, by the Poisson equation $\nabla^2\Phi = -4\pi$ if $\vec{r} \in \Omega$, 0 if $\vec{r} \notin \Omega$ and the integral form of its solution is $\Phi(\vec{r}) = \int_\Omega \frac{1}{\|\vec{r}-\vec{x}\|}d\vec{x}$ where the symbol $\|\cdot\|$ indicates the standard Euclidean norm. Similarly, the biharmonic potential is defined by means of the biharmonic equation $\nabla^4\Psi = -8\pi$ if $\vec{r} \in \Omega$, 0 if $\vec{r} \notin \Omega$ and the standard integral representation is $\Psi(\vec{r}) = \int_\Omega \|\vec{r}-\vec{x}\|\,d\vec{x}$ [8, 45]. Such harmonic and biharmonic potentials only contain geometrical information about the embedded ellipsoid (i.e. the semi-axes lenghts b_1, b_2 and b_3). It is worthwhile recalling some explicit expressions providing the above potentials or their derivative as used to determine the elastic fields [45]:

$$\begin{cases} \Phi(\vec{r}) = \pi b_1 b_2 b_3 \int_{\eta(\vec{r})}^{+\infty} \frac{1-f(\vec{r},s)}{R(s)}ds \\ \Psi_{,i}(\vec{r}) = \pi b_1 b_2 b_3 x_i \int_{\eta(\vec{r})}^{+\infty} \frac{1-f(\vec{r},s)}{R(s)}\frac{s}{b_i^2+s}ds \end{cases} \tag{2.3}$$

where $f(\vec{r},s)$, $\eta(\vec{r})$ and $R(s)$ are defined as follows:

$$\begin{cases} f(\vec{r},s) = \frac{x_1^2}{b_1^2+s} + \frac{x_2^2}{b_2^2+s} + \frac{x_3^2}{b_3^2+s} \\ \eta(\vec{r}): \quad f(\vec{r},\eta(\vec{r})) = 1 \\ R(s) = \sqrt{(b_1^2+s)(b_2^2+s)(b_3^2+s)} \end{cases} \tag{2.4}$$

The quantity $\eta(\vec{r})$ is defined in implicit form and it is considered as the largest positive root of the equation $f(\vec{r},\eta(\vec{r})) = 1$. The integrals defined in Eq. (2.3) are used for the external region assuming $\eta(\vec{r})$ given in Eq. (2.4) and for the internal region assuming $\eta(\vec{r}) = 0$. We summarize the solution of the problem in terms of the gradient of the displacement and of strain tensor. The gradient of the displacement is given by $J_{ij} = u_{i,j}$ and the strain is defined as $\epsilon_{ij} = \frac{1}{2}(u_{i,j} + u_{j,i})$. They can be evaluated accordingly to the relations

$$J_{ij} = \frac{\partial u_i}{\partial x_j} = \mathcal{D}_{ijkh}(\vec{r})\,\epsilon^*_{kh} \tag{2.5}$$

$$\epsilon_{ij} = \frac{1}{2}\left(\frac{\partial u_i}{\partial x_j} + \frac{\partial u_j}{\partial x_i}\right) = \mathcal{S}_{ijkh}(\vec{r})\,\epsilon^*_{kh} \tag{2.6}$$

where $\mathcal{S}_{ijkh}(\vec{r})$ is the Eshelby tensor and $\mathcal{D}_{ijkh}(\vec{r})$ is a new tensor useful to determine the gradient of the displacement over the whole space. We observe that $\mathcal{S}_{ijkh}$ is the symmetrization of the tensor $\mathcal{D}_{ijkh}$ with respect to the first couple of indexes: $\mathcal{S}_{ijkh} = \frac{1}{2}\left(\mathcal{D}_{ijkh} + \mathcal{D}_{jikh}\right)$. The generic forms of such tensors, which is correct both inside the inclusion and outside it, can be written by means of the elastic potentials as follows

The Eshelby tensor

$$\begin{aligned}
\mathcal{S}_{ijkh}(\vec{r}) &= \frac{1}{8\pi(1-\nu_1)}\Psi_{,ijkh} - \frac{\nu_1}{1-\nu_1}\frac{\delta_{kh}}{4\pi}\Phi_{,ij} + \\
&- \frac{1}{8\pi}\left(\delta_{ih}\Phi_{,jk} + \delta_{ik}\Phi_{,jh} + \delta_{jh}\Phi_{,ik} + \delta_{jk}\Phi_{,ih}\right) \quad (2.7)\\
\mathcal{D}_{ijkh}(\vec{r}) &= \frac{1}{8\pi(1-\nu_1)}\Psi_{,ijkh} - \frac{\nu_1}{1-\nu_1}\frac{\delta_{kh}}{4\pi}\Phi_{,ij} + \\
&- \frac{1}{4\pi}\left(\delta_{ih}\Phi_{,kj} + \delta_{ik}\Phi_{,hj}\right) \quad (2.8)
\end{aligned}$$

The notation adopted for the tensors is different for the *internal* points and for *external* ones:

$$\begin{aligned}
&\mathcal{S}_{ijkh}(\vec{r}) = \mathcal{S}_{ijkh} \qquad \mathcal{D}_{ijkh}(\vec{r}) = \mathcal{D}_{ijkh} \qquad \text{if } \vec{r} \in \Omega\\
&\mathcal{S}_{ijkh}(\vec{r}) = \mathcal{S}^{\infty}_{ijkh}(\vec{r}) \quad \mathcal{D}_{ijkh}(\vec{r}) = \mathcal{D}^{\infty}_{ijkh}(\vec{r}) \quad \text{if } \vec{r} \notin \Omega
\end{aligned} \quad (2.9)$$

Taking a different notation for the *internal* and the *external* region is particularly efficient in order to remind that the internal tensors are constant and, therefore, the internal stress, strain and gradient of displacement are uniform tensor fields. By defining the depolarization factors of the first kind as

Depolarization factors

$$\Gamma_i = \frac{b_1 b_2 b_3}{2}\int_0^{+\infty} \frac{ds}{\left(b_i^2 + s\right)R(s)}ds \quad (2.10)$$

and the depolarization factors of the second kind

$$\Theta_{ij} = \frac{b_1 b_2 b_3}{2}\int_0^{+\infty} \frac{sds}{(b_i^2 + s)(b_j^2 + s)R(s)}ds \quad (2.11)$$

we obtain the explicit expressions for the derivatives of the elastic potentials within the region Ω

$$\begin{aligned}
\Phi_{,ij} &= -4\pi\delta_{ij}\Gamma_i \quad (2.12)\\
\Psi_{,ijkh} &= -4\pi\left(\delta_{ij}\delta_{kh}\Theta_{ki} + \delta_{ik}\delta_{jh}\Theta_{hi} + \delta_{ih}\delta_{jk}\Theta_{ji}\right) \quad (2.13)
\end{aligned}$$

Therefore, the internal tensors assume the explicit forms

$$\begin{aligned}
\mathcal{D}_{ijkh} &= -\frac{1}{2(1-\nu_1)}\left(\delta_{ij}\delta_{kh}\Theta_{ki} + \delta_{ik}\delta_{jh}\Theta_{hi} + \delta_{ih}\delta_{jk}\Theta_{ji}\right)\\
&\quad + \frac{\nu_1}{1-\nu_1}\delta_{kh}\delta_{ij}\Gamma_i + \delta_{ih}\delta_{kj}\Gamma_k + \delta_{ik}\delta_{hj}\Gamma_h \quad (2.14)\\
\mathcal{S}_{ijkh} &= \frac{1}{2}\left(\mathcal{D}_{ijkh} + \mathcal{D}_{jikh}\right) \quad (2.15)
\end{aligned}$$

2.1.2 *Eshelby equivalence principle*

In the previous section, we have described the Eshelby solution for the ellipsoidal inclusion problem (see Fig. 3). This configuration is composed by a matrix made of an homogeneous isotropic elastic medium

(material 1) characterized by the stiffness tensor $\mathcal{C}^{(1)}_{ijkh}$ and by a standard constitutive relation $\hat{T} = \hat{\mathcal{C}}^{(1)}\hat{\epsilon}$. Into this infinite matrix we suppose to identify an ellipsoidal region Ω with the same stiffness tensor of the matrix but with an elastic behavior described by $T_{ij} = \mathcal{C}^{(1)}_{ijkh}\left(\epsilon_{kh} - \epsilon^{*}_{kh}\right)$ involving the eigenstrain $\hat{\epsilon}^{*}$. In this Section, the solution of the inclusion problem will be applied in order to solve the inhomogeneity configuration (see Fig. 4) where the elastic behavior of the region Ω is described by a standard consitutive equation with a stiffness tensor $\mathcal{C}^{(2)}_{ijkh}$ different from the matrix. To this aim, we will describe the so-called Eshelby equivalence principle.

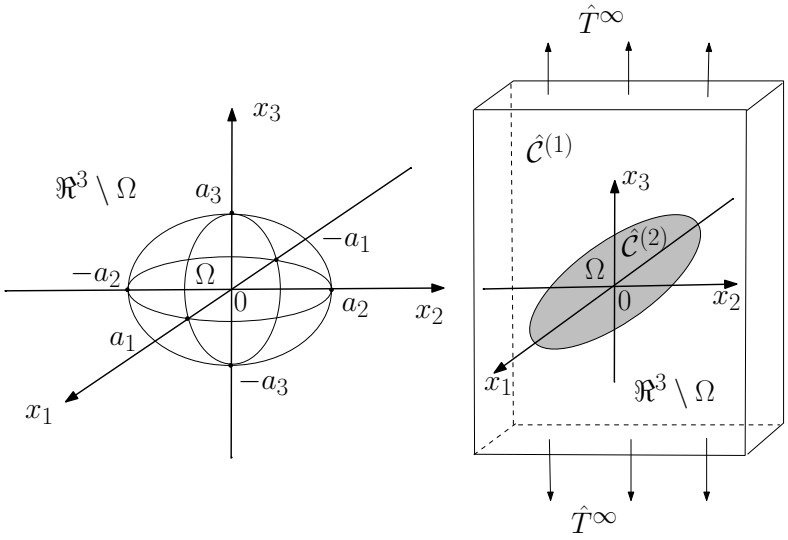

Figure 4: Scheme of an ellipsoidal inhomogeneity.

We suppose to submit the overall inhomogeneity configuration to a remote load so that the asymptotic strain field, ϵ^{∞}_{ij}, is uniform. As a consequence, the corresponding asymptotic stress field, T^{∞}_{ij}, results to be uniform and related to the remotely applied strain by the constitutive relation of the medium 1, i.e. $T^{\infty}_{ij} = \mathcal{C}^{(1)}_{ijkh}\epsilon^{\infty}_{kh}$. According to *Eshelby equivalence principle*, this configuration can be obtained by superimposing the solutions of two different problems (see Fig. 5).

Eshelby equivalence principle

The first one, *problem A*, corresponds to the application of the remote uniform load to a simple homogeneous elastic system with stiffness tensor $\mathcal{C}^{(1)}_{ijkh}$. The second configuration, *problem B*, corresponds to an inclusion, with a suitable eigenstrain $\hat{\epsilon}^{*}$, placed into the matrix. In this case the overall system is not subjected to any remote load. At this stage of the derivation we must derive the value of the eigenstrain that allows for a complete equivalence of the superimposition $A + B$ with the inhomogeneity problem. Before proceeding with such a derivation, is useful to fix some further notation. In the following we will indicate the strain and stress fields into the region Ω with ϵ^{in}_{ij} and T^{in}_{ij} for the total (or inhomogeneity) problem, with $\epsilon^{A,in}_{ij}$ and $T^{A,in}_{ij}$ for the problem A and with $\epsilon^{B,in}_{ij}$ and $T^{B,in}_{ij}$ for the problem B. Moreover, the corresponding external stress fields will be indicated with ϵ^{out}_{ij}, T^{out}_{ij}, $\epsilon^{A,out}_{ij}$, $T^{A,out}_{ij}$, $\epsilon^{B,out}_{ij}$ and $T^{B,out}_{ij}$.

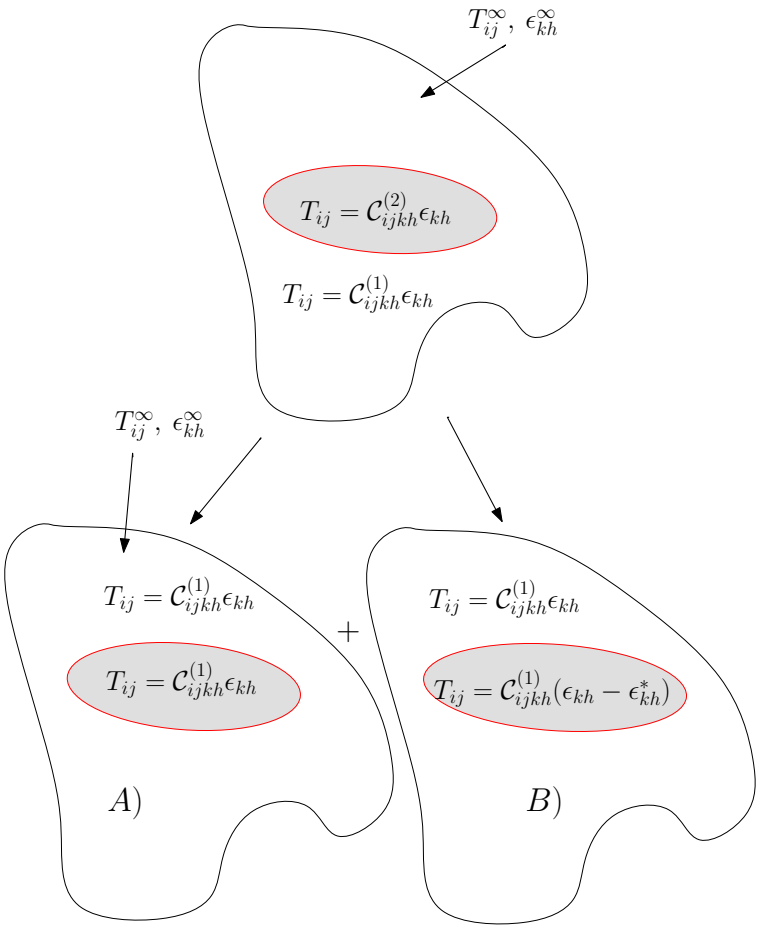

Figure 5: Scheme of the Eshelby equivalence principle. The inhomogeneity problem is obtained as the superimposition of the a configuration where an homogeneous medium is subjected to a remote load (problem A) with the inclusion configuration (problem B).

In terms of the above stated formalism, and by means of the results reported in the previous Section, we can find the solution of the problem A

$$\begin{aligned} \epsilon_{ij}^{A,in} &= \epsilon_{ij}^{\infty} \\ \epsilon_{ij}^{A,out} &= \epsilon_{ij}^{\infty} \\ T_{ij}^{A,in} &= T_{ij}^{\infty} \\ T_{ij}^{A,out} &= T_{ij}^{\infty} \end{aligned} \tag{2.16}$$

and the solution of the problem B

$$\begin{aligned} \epsilon_{ij}^{B,in} &= \mathcal{S}_{ijkh}\epsilon_{kh}^{*} \\ \epsilon_{ij}^{B,out}(\vec{r}) &= \mathcal{S}_{ijkh}^{\infty}(\vec{r})\epsilon_{kh}^{*} \\ T_{ij}^{B,in} &= \mathcal{C}_{ijkh}^{(1)}\left(\epsilon_{kh}^{B,in} - \epsilon_{kh}^{*}\right) \\ T_{ij}^{B,out}(\vec{r}) &= \mathcal{C}_{ijkh}^{(1)}\mathcal{S}_{khnm}^{\infty}(\vec{r})\epsilon_{nm}^{*} \end{aligned} \tag{2.17}$$

Regarding the total problem, we have the following boundary conditions

$$\begin{array}{lcll} u^{in}(\vec{r}) & = & u^{out}(\vec{r}) & \text{if } \vec{r} \in \Gamma \\ \hat{T}^{in}(\vec{r})\vec{n} & = & \hat{T}^{out}(\vec{r})\vec{n} & \text{if } \vec{r} \in \Gamma \\ T^{in}_{ij} & = & \mathcal{C}^{(2)}_{ijkh}\epsilon^{in}_{kh} & \text{in } \Omega \\ T^{out}_{ij} & = & \mathcal{C}^{(1)}_{ijkh}\epsilon^{out}_{kh} & \text{in } \mathfrak{R}^3 - \Omega \\ \epsilon^{out}_{ij}(\vec{r}) & \to & \epsilon^{\infty}_{ij} & \text{if } |\vec{r}| \to \infty \\ T^{out}_{ij}(\vec{r}) & \to & T^{\infty}_{ij} & \text{if } |\vec{r}| \to \infty \end{array} \tag{2.18}$$

being $u^{in}(\vec{r})$ and $u^{out}(\vec{r})$ the displacement fields inside and outside Ω and Γ stands for the boundary of Ω The continuity of the displacement fields at the interface between inhomogeneity and matrix (boundary Γ) corresponds to the assumption that the two pieces are perfectly glued.

By superimposing the solutions of the problems A and B we get the following equation

$$\begin{aligned} \epsilon^{in} &= \epsilon^{A,in} + \epsilon^{B,in} = \epsilon^{\infty} + \mathcal{S}\epsilon^{*} \\ T^{in} &= T^{A,in} + T^{B,in} = \mathcal{C}^{(1)}\epsilon^{\infty} + \mathcal{C}^{(1)}\left(\epsilon^{B,in} - \epsilon^{*}\right) \\ &= \mathcal{C}^{(1)}\epsilon^{\infty} + \mathcal{C}^{(1)}\left(\mathcal{S}\epsilon^{*} - \epsilon^{*}\right) \end{aligned} \tag{2.19}$$

Moreover, we can note that into the inhomogeneity the constitutive relation $T^{in} = \mathcal{C}^{(2)}\epsilon^{in}$ holds. Therefore, the value of the eigenstrain, ϵ^{*} that allows for the complete equivalence of $A + B$ problem with the required inhomogeneity solution, can be derived by solving the following equation

$$\underbrace{\mathcal{C}^{(1)}\epsilon^{\infty} + \mathcal{C}^{(1)}\left(\mathcal{S}\epsilon^{*} - \epsilon^{*}\right)}_{T^{in}} = \mathcal{C}^{(2)}\underbrace{\left(\epsilon^{\infty} + \mathcal{S}\epsilon^{*}\right)}_{\epsilon^{in}} \tag{2.20}$$

obtaining

$$\epsilon^{*} = \left[\left(I - \left(\mathcal{C}^{(1)}\right)^{-1}\mathcal{C}^{(2)}\right)^{-1} - \mathcal{S}\right]^{-1}\epsilon^{\infty} \tag{2.21}$$

By means of Eqs.(2.19) and (2.20) we find also

$$\mathcal{C}^{(2)}\epsilon^{d} = \mathcal{C}^{(1)}\left(\epsilon^{in} - \epsilon^{*}\right) \tag{2.22}$$

Finaly, by exploiting the result in Eq.(2.21), and solving the last equation the internal strain ϵ^{in} is found

$$\epsilon^{in} = \left[I - \mathcal{S}\left(I - \left(\mathcal{C}^{(1)}\right)^{-1}\mathcal{C}^{(2)}\right)\right]^{-1}\epsilon^{\infty} \tag{2.23}$$

and

$$T^{in} = \mathcal{C}^{(2)}\left[I - \mathcal{S}\left(I - \left(\mathcal{C}^{(1)}\right)^{-1}\mathcal{C}^{(2)}\right)\right]^{-1}\epsilon^{\infty} \tag{2.24}$$

Moreover, the solution for the external fields can be obtained by superimposing the corresponding solutions for the problem A and B

$$\begin{aligned} \epsilon^{out}_{ij}(\vec{r}) &= \epsilon^{A,out}_{ij}(\vec{r}) + \epsilon^{B,out}_{ij}(\vec{r}) = \epsilon^{\infty}_{ij} + \mathcal{S}^{\infty}_{ijkh}(\vec{r})\epsilon^{*}_{kh} \\ T^{out}_{ij}(\vec{r}) &= T^{A,out}_{ij}(\vec{r}) + T^{B,out}_{ij}(\vec{r}) = \mathcal{C}^{(1)}_{ijkh}\left[\epsilon^{\infty}_{kh} + \mathcal{S}^{\infty}_{khnm}(\vec{r})\epsilon^{*}_{nm}\right] \end{aligned} \tag{2.25}$$

These equations, together with the eigenstrain given in Eq.(2.21) supplies us the complete solution for the external fields.

2.2 GENERALIZED ESHELBY THEORY FOR PRESTRESSED INCLUSIONS

In this Section we consider a generalization of the Eshelby theory, concerning the elastic behavior of prestrained or prestressed inhomogeneities. The theory, in its original version, deals with a configuration where both the ellipsoidal particle and the surrounding matrix are in elastostatic equilibrium if no external loads are applied to the system. Here, we consider slightly different shapes and sizes for the particle and the hosting cavity (whose surfaces are firmly bonded together) and, therefore, we observe a given state of strain (or stress) even without externally applied loads. In particular, we develop a mathematical procedure able to quantify the prestrains (or prestresses) induced by the differences between the particle and the cavity. It means that we analyze the deformations necessary to create the perfect bonding between the external surface of the particle and the internal surface of the cavity. Moreover, we determine the uniform elastic field induced in an arbitrarily prestrained particle subjected to arbitrary remote loadings.

Prestressed Eshelby configuration

Typical examples of prestressed systems are represented by semiconductor quantum dots or quantum wires, embedded in a matrix with different properties. In fact, the mechanical behavior of nanostructured materials is strongly affected by interface features, occurring at the boundary between phases characterized by different elastic constitutive equations or crystalline structures. In particular, the embedding of a given nanoinclusion in a hosting homogeneous matrix is deeply influenced by the lattice mismatch. In fact, both the inclusion and the matrix accomplish an elastic relaxation to accommodate these mismatches and, therefore, they admit a state of deformation even if no external load is applied. For example, in Fig.6 one can find the atomistic structure

Actual prestressed systems

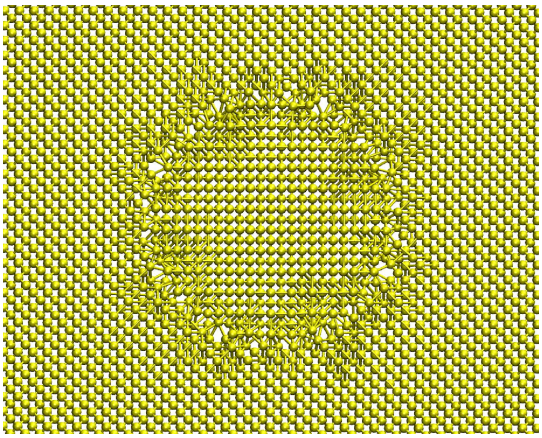

Figure 6: Example of an atomistically resolved prestrained cylindrical inhomogeneity.

of an interface between a matrix and a cylindrical inhomogeneity: the effects of the lattice mismatch and of the different radius of cylinder and cavity are evident in the region close to the interface.

First of all we will analyze inhomogeneities with circular symmetry, namely cylinders and spheres of radius R_2, embedded in a matrix with a cavity of different radius R_1. The radius difference is considered very small, thus allowing for the application of the infinitesiaml theory of elasticity [39, 31]. It is important to remark that this configuration corresponds to a continuum dislocation distributed over the (cylindrical

Equivalence with the Volterra dislocation

or spherical) interface between the materials [81, 82]. It must be considered as a Volterra dislocation with constant Burger vector of modulus $R_1 - R_2$ and radial direction (referred to as $\vec{n}$). More specifically, if we start from a situation with $R_1 = R_2$ and we consider such a dislocation of the inhomogeneity with Burger vector $\vec{b} = (R_1 - R_2)\vec{n}$, we obtain the final configuration corresponding to the prestrained inhomogeneity. In this work we approach this problem with the theory of the inhomogeneities, based on the Eshelby tensor. The solution through the dislocation theory is much more complicated since we are dealing with a heterogeneous structure. The same problem is solved for an ellipsoidal inhomogeneity embedded in a different ellipsoidal cavity of the matrix. Also in this case there is a direct correspondence with the dislocation theory. In particular, the elastic fields can be attributed to a Somigliana dislocation distributed over the interface. In such a case the Burger vector connects a point of the inhomogeneity surface (in elastostatic equilibrium) with the corresponding point of the cavity surface in the matrix.

2.2.1 *Spherical or cylindrical inclusions*

The first step in considering inhomogeneities with shape and size slightly different from the hosting cavity is given by the analysis of spherical or cylindrical particles embedded in similar cavities with different radius. A following Section will deal with the most general case of an ellipsoidal particle embedded in a different ellipsoidal cavity. More precisely, in this Section, we consider a (spherical or cylindrical) particle of radius R_2 and stiffness $\hat{\mathcal{C}}^{(2)}$ which must be enclosed in the (spherical or cylindrical) cavity of radius R_1 in a matrix with stiffness $\hat{\mathcal{C}}^{(1)}$. We suppose a perfect gluing of the spherical or cylindrical surfaces obtained by means of radial deformations of both bodies. We also suppose that a system of forces remotely applied generates an uniform stress in a homogeneous matrix $\hat{\mathcal{C}}^{(1)}$ (without the inhomogeneity). The corresponding elastic state is fully described by the following fields: linear displacement $u_i^\infty(\vec{y})$, constant strain $\epsilon_{kh}^\infty = \frac{1}{2}\left(\frac{\partial u_k^\infty}{\partial y_h} + \frac{\partial u_h^\infty}{\partial y_k}\right)$ and constant stress $T_{ij}^\infty = \mathcal{C}_{ijkh}^{(1)}\epsilon_{kh}^\infty$. If we now embed the inhomogeneity in the matrix, we must cope with the problem of evaluating the perturbation induced in the elastic fields, both inside and outside the particle. In order to utilize the infinitesimal theory of elasticity we must consider $R_1 \approx R_2$ or, equivalently $|\epsilon_0| \ll 1$ if $\epsilon_0 = R_1/R_2 - 1$. All the quantity in our system are reported in Fig.7, together with the conceptual scheme utilized to solve the problem. We start with the description of the equivalence principle used to obtain the elastic fields in the system. The original problem with the prestrained (or prestressed) inhomogeneity is approached through the superimposition of two subproblems A and B. The subproblem A is described by an entirely homogeneous matrix subjected to the remote load $\hat{\epsilon}^\infty$ or $\hat{T}^\infty = \hat{\mathcal{C}}^{(1)}\hat{\epsilon}^\infty$. In this simple case the following elastic fields apply at any point of the body

$$\hat{\epsilon}^A = \hat{\epsilon}^\infty \text{ and } \hat{T}^A = \hat{T}^\infty = \hat{\mathcal{C}}^{(1)}\hat{\epsilon}^\infty \tag{2.26}$$

The subproblem B corresponds to a spherical or cylindrical inclusion (with radius R_1) described by the eigenstrain $\hat{\epsilon}^*$. The results summa-

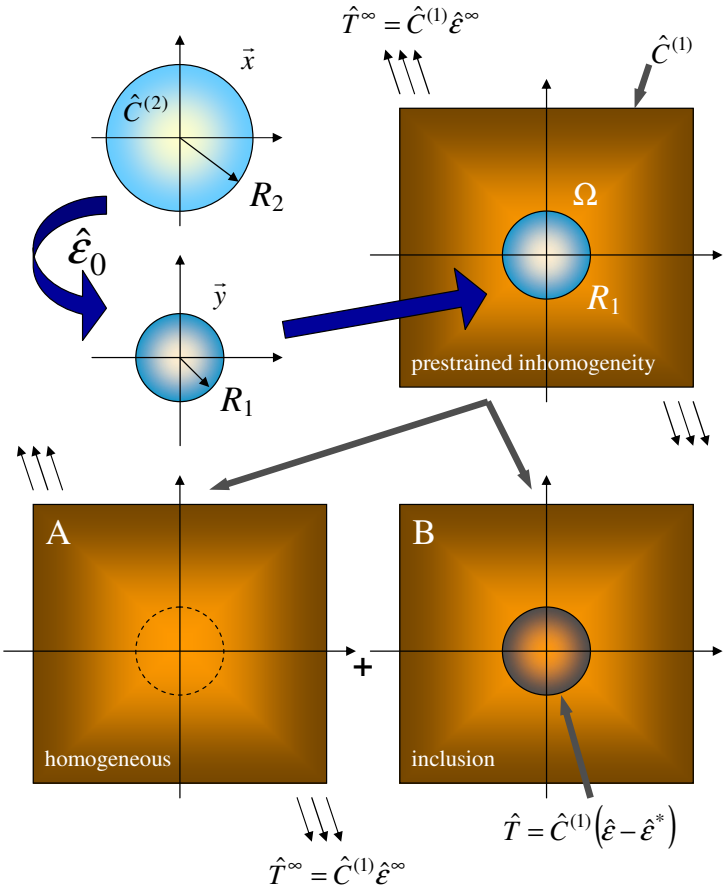

Figure 7: Scheme of a prestrained (cylindrical or spherical) inhomogeneity (stiffness $\hat{\mathcal{C}}^{(2)}$ and radius R_2) embedded into a homogeneous matrix (stiffness $\hat{\mathcal{C}}^{(1)}$ and cavity with radius R_1). One can see the initial deformation $\hat{\varepsilon}_0$ and the superimposition of the subproblems A and B corresponding to the homogeneous loaded matrix and to the inclusion with eigenstrain $\hat{\varepsilon}^*$.

rized in the previous Section allow us to obtain the following uniform elastic fields in the region of the inclusion

$$\hat{\varepsilon}^B = \hat{\mathbb{S}}\hat{\varepsilon}^* \text{ and } \hat{T}^B = \hat{\mathcal{C}}^{(1)}\left(\hat{\varepsilon}^B - \hat{\varepsilon}^*\right) \tag{2.27}$$

The superimposition of the stress and the strain for the situations A and B leads to the relations

$$\begin{aligned} \hat{\varepsilon} &= \hat{\varepsilon}^A + \hat{\varepsilon}^B = \hat{\varepsilon}^\infty + \hat{\mathbb{S}}\hat{\varepsilon}^* \\ \hat{T} &= \hat{T}^A + \hat{T}^B = \hat{\mathcal{C}}^{(1)}\hat{\varepsilon}^\infty + \hat{\mathcal{C}}^{(1)}\left(\hat{\varepsilon}^B - \hat{\varepsilon}^*\right) \\ &= \hat{\mathcal{C}}^{(1)}\hat{\varepsilon}^\infty + \hat{\mathcal{C}}^{(1)}\left(\hat{\mathbb{S}}\hat{\varepsilon}^* - \hat{\varepsilon}^*\right) \end{aligned} \tag{2.28}$$

which are correct for any point in the region of the inclusion. At this point, it is important to investigate the relation between $\hat{\varepsilon}$ and $\hat{T}$ inside the inhomogeneity, i.e. the constitutive relation of the embedded particle. This is a crucial point because this relation is described by the stiffness tensor $\hat{\mathcal{C}}^{(2)}$ in the reference frame $\{\vec{x}\}$, where the particle is not deformed (see Fig.7). However, this is not true in the reference

frame $\{\vec{y}\}$ where the particle is radially deformed in order to achieve the radius R_1 of the cavity. It must be underlined that the equivalence principle must be used with the constitutive equation of the particle written in the reference frame where the particle itself has the same shape and size of the cavity. The linear displacement field changing the radius of the particle from R_2 to R_1 is $\vec{u}_0(\vec{x}) = (R_1 - R_2)/R_2\vec{x}$ and, therefore, the corresponding strain tensor is $\hat{\epsilon}_0 = (R_1 - R_2)/R_2\hat{I}_2 = \epsilon_0\hat{I}_2$ for a cylinder and $\hat{\epsilon}_0 = (R_1 - R_2)/R_2\hat{I}_3 = \epsilon_0\hat{I}_3$ for a sphere, where $\epsilon_0 = (R_1 - R_2)/R_2$. In other words, each point of the particle is transformed accordingly to $\vec{y} = \vec{x} + \hat{\epsilon}_0\vec{x}$ in order to fit the cavity. In this configuration the surfaces of the prestrained circular inhomogeneity and of the cavity are firmly bonded. An arbitrary deformation $\vec{u}_T(\vec{x})$ of the particle can be described by two successive steps: a first deformation described by $\vec{u}_0(\vec{x})$ and a further deformation $\vec{u}(\vec{y})$ defined on the reference frame $\{\vec{y}\}$. Therefore, the arbitrary deformation $\vec{u}_T(\vec{x})$ can be written in the form $\vec{u}_T(\vec{x}) = \vec{u}_0(\vec{x}) + \vec{u}(\vec{y}) = \vec{u}_0(\vec{x}) + \vec{u}(\vec{x} + \hat{\epsilon}_0\vec{x})$. The subscript T means *true*, i.e. the displacement $\vec{u}_T(\vec{x})$ is the actual or total displacement measured in the reference configuration where the material is in own elastic equilibrium. On the other hands, the second step of the deformation, described by the vector $\vec{u}(\vec{y})$, defines a standard strain tensor $\epsilon_{ij}(\vec{y}) = \frac{1}{2}\left(\frac{\partial u_i}{\partial y_j} + \frac{\partial u_j}{\partial y_i}\right)$ working in the reference frame $\{\vec{y}\}$. The relation between $\hat{\epsilon}_T(\vec{x})$ and $\hat{\epsilon}(\vec{y})$ is

$$\begin{aligned}
\epsilon_{T,ij} &= \frac{1}{2}\left(\frac{\partial u_{T,i}}{\partial x_j} + \frac{\partial u_{T,j}}{\partial x_i}\right) \\
&= \frac{1}{2}\left(\frac{\partial u_{0,i}}{\partial x_j} + \frac{\partial u_{0,j}}{\partial x_i} + \frac{\partial u_i}{\partial y_j} + \frac{\partial u_j}{\partial y_i} + \frac{\partial u_i}{\partial y_s}\epsilon_{0,sj} + \frac{\partial u_j}{\partial y_s}\epsilon_{0,si}\right) \\
&= \epsilon_0\delta_{ij} + (1 + \epsilon_0)\,\epsilon_{ij}
\end{aligned} \tag{2.29}$$

In the reference frame $\{\vec{x}\}$ we have the standard constitutive equation $\hat{T}(\vec{x}) = \hat{\mathcal{C}}^{(2)}\hat{\epsilon}_T(\vec{x})$ while, in the reference frame $\{\vec{y}\}$ (where the particle has the same radius of the hosting cavity) we simply obtain $\hat{T}(\vec{y}) = \hat{\mathcal{C}}^{(2)}\left[\epsilon_0\hat{I} + (1 + \epsilon_0)\hat{\epsilon}(\vec{y})\right]$ where $\hat{I} = \hat{I}_2$ for a cylindrical particle and $\hat{I} = \hat{I}_3$ for a spherical one. By considering that $\epsilon_0 = (R_1 - R_2)/R_2$ we obtain

$$\hat{T}(\vec{y}) = \hat{\mathcal{C}}^{(2)}\left[\frac{R_1 - R_2}{R_2}\hat{I} + \frac{R_1}{R_2}\hat{\epsilon}(\vec{y})\right] = \frac{R_1}{R_2}\hat{\mathcal{C}}^{(2)}\left[\hat{\epsilon}(\vec{y}) - \frac{R_2 - R_1}{R_1}\hat{I}\right] \tag{2.30}$$

This is the constitutive equation of the prestrained (or prestressed) inhomogeneity in the reference frame $\{\vec{y}\}$. It must be utilized with the strain and stress fields defined in Eq.(2.28), by obtaining

$$\underbrace{\hat{\mathcal{C}}^{(1)}\hat{\epsilon}^{\infty} + \hat{\mathcal{C}}^{(1)}\left(\hat{\mathcal{S}}\hat{\epsilon}^* - \hat{\epsilon}^*\right)}_{\hat{T}(\vec{y})} = \frac{R_1}{R_2}\hat{\mathcal{C}}^{(2)}\left[\underbrace{\left(\hat{\epsilon}^{\infty} + \hat{\mathcal{S}}\hat{\epsilon}^*\right)}_{\hat{\epsilon}(\vec{y})} - \frac{R_2 - R_1}{R_1}\hat{I}\right] \tag{2.31}$$

Eq.(2.31) represents an equation for the eigenstrain $\hat{\epsilon}^*$ assuring the equivalence between the original (prestrained) inhomogeneity problem and the superimposition of the subproblems A and B. The eigenstrain $\hat{\epsilon}^*$ can be obtained through straightforward tensor calculations

$$\begin{aligned}
\hat{\epsilon}^* &= \left[\left(\hat{\jmath} - \frac{R_1}{R_2}\left(\hat{\mathcal{C}}^{(1)}\right)^{-1}\hat{\mathcal{C}}^{(2)}\right)^{-1} - \hat{\mathcal{S}}\right]^{-1} \\
&\quad \times \left[\hat{\epsilon}^{\infty} - \left(\hat{\jmath} - \frac{R_2}{R_1}\left(\hat{\mathcal{C}}^{(2)}\right)^{-1}\hat{\mathcal{C}}^{(1)}\right)^{-1}\frac{R_2 - R_1}{R_1}\hat{I}\right]
\end{aligned} \tag{2.32}$$

where $\hat{\mathcal{I}}$ stands for the fourth-rank identity operator. Moreover, Eq.(2.31) can be written in the alternative form

$$\hat{\mathcal{C}}^{(1)}\left[\underbrace{\left(\hat{\varepsilon}^{\infty}+\hat{\mathcal{S}}\hat{\varepsilon}^{*}\right)}_{\hat{\varepsilon}(\vec{y})}-\hat{\varepsilon}^{*}\right]=\frac{R_1}{R_2}\hat{\mathcal{C}}^{(2)}\left[\underbrace{\left(\hat{\varepsilon}^{\infty}+\hat{\mathcal{S}}\hat{\varepsilon}^{*}\right)}_{\hat{\varepsilon}(\vec{y})}-\frac{R_2-R_1}{R_1}\hat{\mathcal{I}}\right] \tag{2.33}$$

which is useful to evaluate the strain $\hat{\varepsilon}(\vec{y})$ in the inhomogeneity. A long manipulation leads to the following relation between the internal strain $\hat{\varepsilon}(\vec{y})$ and the eigenstrain $\hat{\varepsilon}^{*}$

$$\begin{aligned}\hat{\varepsilon}=&\left[\hat{\mathcal{I}}-\frac{R_1}{R_2}\left(\hat{\mathcal{C}}^{(1)}\right)^{-1}\hat{\mathcal{C}}^{(2)}\right]^{-1}\hat{\varepsilon}^{*}+\\&\left[\hat{\mathcal{I}}-\frac{R_2}{R_1}\left(\hat{\mathcal{C}}^{(2)}\right)^{-1}\hat{\mathcal{C}}^{(1)}\right]^{-1}\frac{R_2-R_1}{R_1}\hat{\mathcal{I}}\end{aligned} \tag{2.34}$$

Now, we can substitute Eq.(2.32) in Eq.(2.34), obtaining the internal strain measured in the reference frame $\{\vec{y}\}$

$$\hat{\varepsilon}=\hat{\mathcal{A}}\left[\hat{\varepsilon}^{\infty}+\hat{\mathcal{S}}\left(\hat{\mathcal{C}}^{(1)}\right)^{-1}\hat{\mathcal{C}}^{(2)}\frac{R_2-R_1}{R_2}\hat{\mathcal{I}}\right] \tag{2.35}$$

where we have defined the tensor $\hat{\mathcal{A}}$ as

$$\hat{\mathcal{A}}=\left\{\hat{\mathcal{I}}-\hat{\mathcal{S}}\left[\hat{\mathcal{I}}-\frac{R_1}{R_2}\left(\hat{\mathcal{C}}^{(1)}\right)^{-1}\hat{\mathcal{C}}^{(2)}\right]\right\}^{-1} \tag{2.36}$$

It is also important to obtain the *true* internal strain, measured in the reference frame $\{\vec{x}\}$. To this aim we obtain from Eq.(2.29) the relation giving the *true* strain $\hat{\varepsilon}_T$ as

$$\hat{\varepsilon}_T=\frac{R_1-R_2}{R_2}\hat{\mathcal{I}}+\frac{R_1}{R_2}\hat{\varepsilon}=\frac{R_1}{R_2}\hat{\mathcal{A}}\left[\hat{\varepsilon}^{\infty}-\left(\hat{\mathcal{I}}-\hat{\mathcal{S}}\right)\frac{R_2-R_1}{R_1}\hat{\mathcal{I}}\right] \tag{2.37}$$

Finally, by recalling the definition of $\hat{\mathcal{A}}$ in Eq.(2.36), we obtain the explicit expression

Internal strain of a prestressed cylindrical or spherical inclusion under remote loading

$$\begin{aligned}\hat{\varepsilon}_T\;=\;&\frac{R_1}{R_2}\left\{\hat{\mathcal{I}}-\hat{\mathcal{S}}\left[\hat{\mathcal{I}}-\frac{R_1}{R_2}\left(\hat{\mathcal{C}}^{(1)}\right)^{-1}\hat{\mathcal{C}}^{(2)}\right]\right\}^{-1}\\&\times\left[\hat{\varepsilon}^{\infty}-\left(\hat{\mathcal{I}}-\hat{\mathcal{S}}\right)\frac{R_2-R_1}{R_1}\hat{\mathcal{I}}\right]\end{aligned} \tag{2.38}$$

This is the most important result of the present Section. It is important to remark that, if we consider $R_1=R_2$, we obtain the standard Eshelby result for not prestrained inhomogeneities. In fact, if $R_1=R_2$ both Eqs.(2.35) and (2.38) reduce to Eq.(2.23) , as expected. Furthermore, we can calculate the state of strain in the sourrounding matrix; the counterpart of Eq.(2.28) for the external region reads

$$\begin{aligned}\hat{\varepsilon}\,(\vec{y})\;&=\;\hat{\varepsilon}^{\infty}+\hat{\mathcal{S}}^{\infty}_{ijkh}\,(\vec{y})\,\hat{\varepsilon}^{*}\\\hat{\mathrm{T}}\,(\vec{y})\;&=\;\hat{\mathcal{C}}^{(1)}\hat{\varepsilon}^{\infty}+\hat{\mathcal{C}}^{(1)}\hat{\mathcal{S}}^{\infty}_{ijkh}\,(\vec{y})\,\hat{\varepsilon}^{*}\end{aligned} \tag{2.39}$$

where the eigenstrain $\hat{\varepsilon}^{*}$ is given by Eq.(2.32). The final expression for the external strain assumes the form

External strain of a prestressed cylindrical or spherical inclusion under remote loading

$$\begin{aligned}\hat{\varepsilon}\,(\vec{y})\;=\;&\hat{\varepsilon}^{\infty}+\hat{\mathcal{S}}^{\infty}_{ijkh}\,(\vec{y})\left[\left(\hat{\mathcal{I}}-\frac{R_1}{R_2}\left(\hat{\mathcal{C}}^{(1)}\right)^{-1}\hat{\mathcal{C}}^{(2)}\right)^{-1}-\hat{\mathcal{S}}\right]^{-1}\\&\times\left[\hat{\varepsilon}^{\infty}-\left(\hat{\mathcal{I}}-\frac{R_2}{R_1}\left(\hat{\mathcal{C}}^{(2)}\right)^{-1}\hat{\mathcal{C}}^{(1)}\right)^{-1}\frac{R_2-R_1}{R_1}\hat{\mathcal{I}}\right]\end{aligned} \tag{2.40}$$

The spherical inhomogeneity

Here, we apply the result stated in Eq.(2.38) to the specific case of a spherical particle. The constitutive equations for the sphere ($j = 2$) and the matrix ($j = 1$) can be represented in the explicit form $\hat{T} = \hat{\mathcal{C}}^{(j)}\hat{\epsilon} = 2\mu_j\hat{\epsilon} + \lambda_j \mathrm{Tr}(\hat{\epsilon})\hat{I}_3$. We also introduce the notation $K_j = \lambda_j + \frac{2}{3}\mu_j$ for the three-dimensional bulk moduli (see 1) in the medium j. The explicit expression of the Eshelby tensor for a sphere embedded in a matrix with Poisson ratio ν_1 is reported in literature [68, 45]

$$\begin{aligned} \mathcal{S}_{ijkh} &= \frac{1}{15(1-\nu_1)}\left[\left(\delta_{ik}\delta_{jh} + \delta_{ih}\delta_{jk}\right)(4-5\nu_1)\right. \\ &+ \left.\delta_{kh}\delta_{ij}(5\nu_1 - 1)\right] \end{aligned} \tag{2.41}$$

To obtain a more useful form, we can evaluate the effect of $\mathcal{S}_{ijkh}$ over an arbitrary tensor w_{kh}, getting

$$\mathcal{S}_{ijkh}w_{kh} = \frac{2(4-5\nu_1)}{15(1-\nu_1)}w_{ij} + \frac{5\nu_1 - 1}{15(1-\nu_1)}w_{kk}\delta_{ij} \tag{2.42}$$

Now, the Poisson ratio ν_1 of the matrix can be written in terms of the moduli K_1 and μ_1 through the standard relation $\nu_1 = \frac{3K_1 - 2\mu_1}{2(3K_1+\mu_1)}$, obtaining

$$\hat{\mathcal{S}}\hat{\epsilon} = \frac{6}{5}\frac{K_1 + 2\mu_1}{3K_1 + 4\mu_1}\hat{w} + \frac{1}{5}\frac{3K_1 - 4\mu_1}{3K_1 + 4\mu_1}\mathrm{Tr}(\hat{w})\hat{I}_3 \tag{2.43}$$

At this point we have in hand all the ingredients to develop Eq.(2.38). We define the parameters

$$\begin{aligned} L_3 &= 1 + \frac{6}{5}\frac{K_1 + 2\mu_1}{3K_1 + 4\mu_1}\left(\frac{R_1}{R_2}\frac{\mu_2}{\mu_1} - 1\right) \\ M_3 &= \frac{1}{5(3K_1 + 4\mu_1)}\left[5\frac{R_1}{R_2}K_2 - K_1\left(3 + 2\frac{R_1}{R_2}\frac{\mu_2}{\mu_1}\right) - 4\left(\frac{R_1}{R_2}\mu_2 - \mu_1\right)\right] \end{aligned} \tag{2.44}$$

which are useful to write in explicit form the effect of $\hat{\mathcal{A}}$ defined in Eq.(2.36) over an arbitrary tensor $\hat{w}$

$$\hat{\mathcal{A}}\hat{w} = \frac{1}{L_3}\hat{w} - \frac{M_3}{L_3}\frac{1}{L_3 + 3M_3}\mathrm{Tr}(\hat{w})\hat{I}_3 \tag{2.45}$$

The following expression is useful in the following calculations

$$L_3 + 3M_3 = \frac{3\frac{R_1}{R_2}K_2 + 4\mu_1}{3K_1 + 4\mu_1} \tag{2.46}$$

By means of a long but straightforward calculation we obtain the final expression for the *true* strain in the following form

$$\begin{aligned} \hat{\epsilon}_T &= \frac{R_1}{R_2}\frac{1}{L_3}\hat{\epsilon}^\infty - \frac{R_1}{R_2}\frac{M_3}{L_3}\frac{1}{L_3 + 3M_3}\mathrm{Tr}\hat{\epsilon}^\infty\hat{I}_3 \\ &- \frac{R_2 - R_1}{R_2}\frac{4\mu_1}{3\frac{R_1}{R_2}K_2 + 4\mu_1}\hat{I}_3 \end{aligned} \tag{2.47}$$

The cylindrical inhomogeneity

We apply now Eq.(2.38) to the case of a cylindrical particle embedded in the homogeneous matrix. We suppose to deform both the particle and the matrix under the plane strain condition defined in Section 1.2.2 (on the plane perpendicular to the axis of the cylindrical particle). Therefore (see 1.2.3 and Table 3), we introduce the two-dimensional bulk moduli

$k_j = K_j + \frac{1}{3}\mu_j$ $(j = 1, 2)$. Accordingly, we adopt the constitutive relations in the form $\hat{T} = \hat{\mathcal{C}}^{(j)}\hat{e} = 2\mu_j\hat{e} + \left(k_j - \mu_j\right)\mathrm{Tr}\left(\hat{e}\right)\hat{I}_2$ where $j = 1$ for the matrix and $j = 2$ for the inhomogeneity. Moreover, we remember that the result of the application of the Eshelby tensor $\hat{S}$ (for a cylindrical geometry) over an arbitrary tensor $\hat{w}$ is given by [45]

$$\hat{S}\hat{w} = \frac{1}{2}\frac{k_1 + 2\mu_1}{k_1 + \mu_1}\hat{w} + \frac{1}{4}\frac{k_1 - 2\mu_1}{k_1 + \mu_1}\mathrm{Tr}\left(\hat{w}\right)\hat{I}_2 \tag{2.48}$$

The development of Eq.(2.38) can be made easier by the definition of the parameters

$$\begin{aligned} L_2 &= 1 + \frac{1}{2}\frac{k_1 + 2\mu_1}{k_1 + \mu_1}\left(\frac{R_1}{R_2}\frac{\mu_2}{\mu_1} - 1\right) \\ M_2 &= \frac{1}{4\left(k_1 + \mu_1\right)}\left[2\frac{R_1}{R_2}k_2 - k_1\left(1 + \frac{R_1}{R_2}\frac{\mu_2}{\mu_1}\right) - 2\left(\frac{R_1}{R_2}\mu_2 - \mu_1\right)\right] \end{aligned} \tag{2.49}$$

which are useful to write in explicit form the effect of $\hat{\mathcal{A}}$ defined in Eq.(2.36) over an arbitrary tensor $\hat{w}$

$$\hat{\mathcal{A}}\hat{w} = \frac{1}{L_2}\hat{w} - \frac{M_2}{L_2}\frac{1}{L_2 + 2M_2}\mathrm{Tr}\left(\hat{w}\right)\hat{I}_2 \tag{2.50}$$

The following expression is useful in the following calculations

$$L_2 + 2M_2 = \frac{\frac{R_1}{R_2}k_2 + \mu_1}{k_1 + \mu_1} \tag{2.51}$$

A straightforward algebraic manipulation leads to the following final result

$$\begin{aligned} \hat{e}_T &= \frac{R_1}{R_2}\frac{1}{L_2}\hat{e}^\infty - \frac{R_1}{R_2}\frac{M_2}{L_2}\frac{1}{L_2 + 2M_2}\mathrm{Tr}\hat{e}^\infty\hat{I}_2 \\ &- \frac{R_2 - R_1}{R_2}\frac{\mu_1}{\frac{R_1}{R_2}k_2 + \mu_1}\hat{I}_2 \end{aligned} \tag{2.52}$$

Since Eq.(2.52) is a result obtained for the two-dimensional elasticity (plane strain condition), it can be also verified by means of the complex potentials method [83, 84, 85] (see Section 5.2.4).

Features of the generalized Eshelby model

For nano-science applications the typical sizes of the particles range in the interval 5 nm $< R_1 \approx R_2 <$ 50 nm, while the possible difference between the radii lies in the range 0 Å$< |R_2 - R_1| <$ 5 Å. In order to describe the new features of the generalized inclusion model, in this Section we show an example of cylindrical particle (with moduli μ_2 = 85 GPa and k_2 = 115 GPa) embedded in a matrix (having moduli μ_1 = 50 GPa and k_1 = 110 GPa). By means of Eq.(2.52) we obtain the true internal strain field $\hat{e}_T$ for 2 nm$< R_1 <$20 nm and 0.1 Å$< R_2 - R_1 <$0.5 Å. In Fig. 8 (a) one can find the results for the case without external loads applied to the system. In this case the isotropy leads to the hydrostatic condition $\varepsilon_{xx} = \varepsilon_{yy}$. The effect generated by the condition $R_1 \neq R_2$ can be compared with the constant value of the strain predicted by the classical Eshelby theory when $R_1 = R_2$. Moreover, in Fig. 8 (b) the effects of a remotely applied uniaxial load are shown. We note that, for a given value of $|R_2 - R_1|$, the difference between the two predictions decreases with increasing radius of the inclusion. Therefore, the condition $R_1 \neq R_2$ induces a scale effect that become negligible only

scale effects...

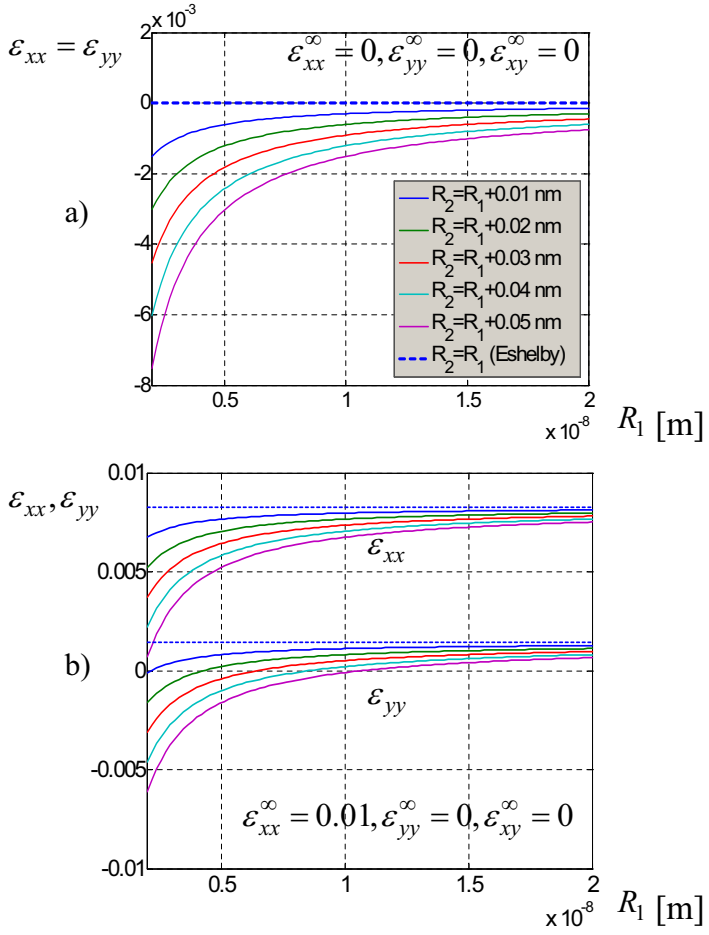

Figure 8: Internal components ε_{xx} and ε_{yy} of the strain tensor $\hat{e}_T$ for a pre-strained cylindrical inhomogeneity (stiffness $\hat{C}^{(2)}$ and radius R_2) embedded into a homogeneous matrix (stiffness $\hat{C}^{(1)}$ and cavity with radius R_1). One can find the results without external load (a) and the effects of a remotely applied deformation (b).

when the radius R_1 is larger than a given threshold.

We have also analyzed the external fields, described by Eq.(2.40). In particular, in Fig. 9 the true displacement field components $u_x(x,0) - u^{\infty}_x(x,0)$ (a) and $u_y(0,y) - u^{\infty}_y(0,y)$ (b) are shown for $\varepsilon^{\infty}_{xx} = 0.01$, $\varepsilon^{\infty}_{yy} = 0$ and $\varepsilon^{\infty}_{xy} = 0$. We have used the fixed radius R_1 =20 nm and the difference 0.1 Å$< |R_2 - R_1| <$ 1Å. The dashed lines correspond to the Eshelby theory ($R_1 = R_2$) and, therefore, they are continuous at the cylinder-matrix interface. When $R_1 \neq R_2$ the displacement field shows a discontinuity at the interface due to the gluing of the surfaces having different radius (it is the typical behavior of the elastic fields generated by a dislocation distributed over the interface). The jump of the discontinuity is an increasing function of $R_2 - R_1$ both for the longitudinal and the transversal components. By comparing the Eshelby solution with the results for $R_1 \neq R_2$ we note that the behavior can be largely different, depending on the quantity $R_2 - R_1$. As for the longitudinal component, we observe that a value of $R_2 - R_1$ exists (of about 0.7 Å for the example shown in Fig. 9 (a)) which leads to a very

...and localizations effects

fast decay to zero of $u_x(x,0) - u_x^\infty(x,0)$. In other words, in such a case, the prestrain causes a strong localization of the elastic fields around the interface. On the other hand, the transversal component shown in Fig. 9 (b) shows a decay to zero that is more and more slower for incrasing values of $R_2 - R_1$.

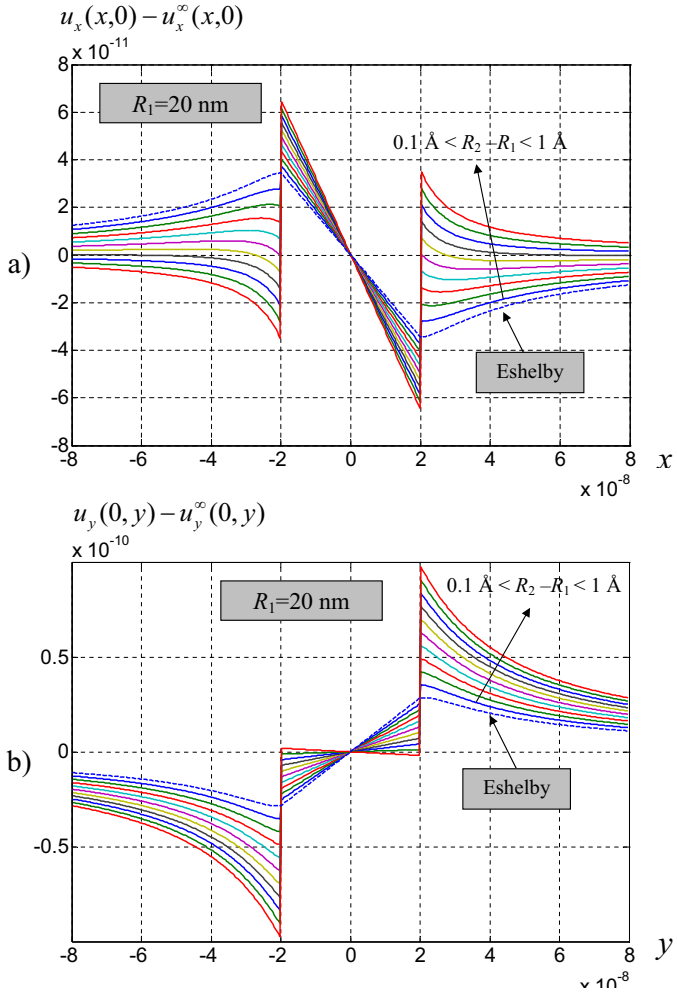

Figure 9: True displacement field components $u_x(x,0) - u_x^\infty(x,0)$ (a) and $u_y(0,y) - u_y^\infty(0,y)$ (b) for a prestrained cylindrical inhomogeneity (radius R_2) embedded into a homogeneous matrix (cavity with radius R_1).

All the features described in this Section have been confirmed by molecular dynamics experiments conducted in order to show the role of the interface elasticity in nanostructured silicon [86] (see Section 5.2). It is interesting to observe that such atomistic simulations perfectly take into account both the fast decay and the displacement discontinuity, being in good agreement with the present model.

2.2.2 *Ellipsoidal inclusions*

We consider an elastic particle (stiffness $\hat{\mathcal{C}}^{(2)}$) with an ellipsoidal shape given by $\vec{x} \cdot \hat{a}^{-2}\vec{x} = 1$ in the reference frame $\{\vec{x}\}$. This particle must be embedded in the matrix (stiffness $\hat{\mathcal{C}}^{(1)}$) showing an ellipsoidal cavity described by $\vec{y} \cdot \hat{b}^{-2}\vec{y} = 1$ in the reference frame $\{\vec{y}\}$ (see Fig.10

for details). These ellipsoids have the semiaxes aligned to reference frames and, therefore, the tensors $\hat{a}$ and $\hat{b}$ are diagonal and their entries represent the semiaxes length of the ellipsoids. To begin, we search for the geometrical transformation, which converts the first ellipsoid (representing the particle) in the second ellipsoid (representing the cavity). The general form of such a transformation is assumed in the form $\vec{y} = \hat{F}\vec{x}$ where $\hat{F}$ is an unknown non singular tensor (the inverse transformation is $\vec{x} = \hat{F}^{-1}\vec{y}$). The application of the tensor $\hat{F}$ to the ellipsoid $\vec{x}\cdot\hat{a}^{-2}\vec{x} = 1$ leads to the transformed ellipsoid $\vec{y}\cdot\hat{F}^{-T}\hat{a}^{-2}\hat{F}^{-1}\vec{y} = 1$. Therefore, the tensor $\hat{F}$ must fulfill the condition

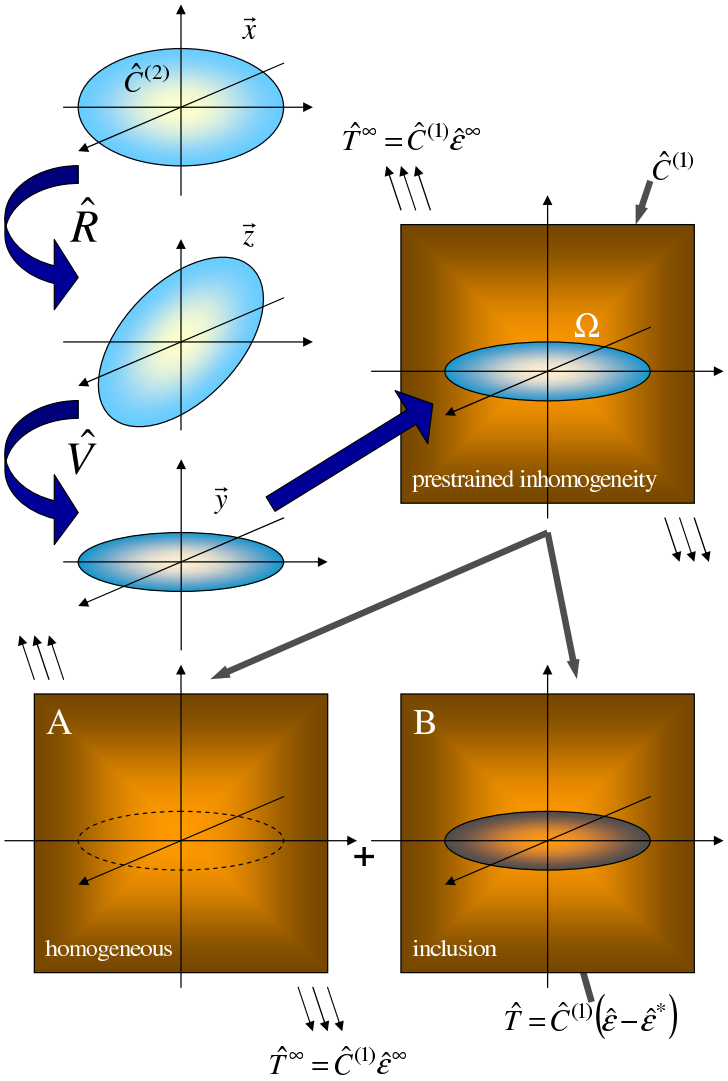

Figure 10: Scheme of a prestrained ellipsoidal inhomogeneity (stiffness $\hat{\mathcal{C}}^{(2)}$) embedded into a matrix (stiffness $\hat{\mathcal{C}}^{(1)}$). One can see the initial rotation $\hat{R}$, the further deformation $\hat{V}$ and the superimposition of the subproblems A and B corresponding to the homogeneous loaded matrix and to the inclusion with eigenstrain $\hat{e}^{*}$.

$$\hat{b}^{-2} = \hat{F}^{-T}\hat{a}^{-2}\hat{F}^{-1} \tag{2.53}$$

It is easy to recognize that it exists an infinite number of tensors $\hat{F}$ fulfilling the previous relation: in fact, reasoning in $\mathfrak{R}^n$, the tensor $\hat{F}$ corresponds to n^2 unknowns, while Eq.(2.53) corresponds to $n(n+1)/2$

equations (in fact, both sides are symmetric). In order to characterize all the possible tensors satisfying Eq.(2.53) we invoke the polar decomposition $\hat{F} = \hat{R}\hat{U} = \hat{V}\hat{R}$, which is correct for any non singular tensor $\hat{F}$. We adopt the left version $\hat{F} = \hat{V}\hat{R}$ where $\hat{R}$ is an orthogonal tensor and $\hat{V}$ is symmetric and positive definite. From the above statement we simply obtain $\hat{F}^{-1} = \hat{R}^T\hat{V}^{-1}$ and $\hat{F}^{-T} = \hat{V}^{-1}\hat{R}$. Therefore, Eq.(2.53) can be rewritten in the form

$$\hat{b}^{-2} = \hat{V}^{-1}\hat{R}\hat{a}^{-2}\hat{R}^T\hat{V}^{-1} \tag{2.54}$$

Now, we suppose to consider a given orthogonal tensor $\hat{R}$ and we prove that it exists a unique tensor $\hat{V}$ fulfilling Eq.(2.54). In other words, we have decomposed the transformation $\vec{y} = \hat{F}\vec{x}$ in two steps: $\vec{z} = \hat{R}\vec{x}$ and $\vec{y} = \hat{V}\vec{z}$ (see Fig.10 for details). In the reference frame $\{\vec{z}\}$ the ellipsoid assumes the form $\vec{z}\cdot\hat{c}^{-2}\vec{z} = 1$ where $\hat{c} = \hat{R}\hat{a}\hat{R}^T$ is a positive definite symmetric tensor. Since the tensor $\hat{R}$ is now considered fixed, Eq.(2.54) can be written as follows

$$\hat{b}^{-2} = \hat{V}^{-1}\hat{c}^{-2}\hat{V}^{-1} \tag{2.55}$$

We must now find the solution $\hat{V}$ of the previous Eq.(2.55). This equation can be represented in the form $\hat{c}^{-1}\hat{b}^{-2}\hat{c}^{-1} = (\hat{c}^{-1}\hat{V}^{-1}\hat{c}^{-1})(\hat{c}^{-1}\hat{V}^{-1}\hat{c}^{-1})$ or, equivalently, in the form $\hat{c}^{-1}\hat{b}^{-2}\hat{c}^{-1} = (\hat{c}^{-1}\hat{V}^{-1}\hat{c}^{-1})^2$. Therefore, we obtain $\hat{c}^{-1}\hat{V}^{-1}\hat{c}^{-1} = \sqrt{\hat{c}^{-1}\hat{b}^{-2}\hat{c}^{-1}}$ since the tensor $\hat{c}^{-1}\hat{b}^{-2}\hat{c}^{-1}$ is symmetric and positive definite (having a regular square root). At the end, the transformation tensor $\hat{F}^{-1}$ or $\hat{F}^{-T}$ is explicitely given

$$\begin{aligned}\hat{F}^{-1} &= \hat{R}^T\hat{V}^{-1} = \hat{R}^T\hat{c}\sqrt{\hat{c}^{-1}\hat{b}^{-2}\hat{c}^{-1}}\hat{c} \qquad (2.56)\\ &= \hat{a}\hat{R}^T\sqrt{(\hat{R}\hat{a}\hat{R}^T)^{-1}\hat{b}^{-2}(\hat{R}\hat{a}\hat{R}^T)^{-1}}\hat{R}\hat{a}\hat{R}^T\\ \hat{F}^{-T} &= \hat{V}^{-1}\hat{R} = \hat{c}\sqrt{\hat{c}^{-1}\hat{b}^{-2}\hat{c}^{-1}}\hat{c}\hat{R} \qquad (2.57)\\ &= \hat{R}\hat{a}\hat{R}^T\sqrt{(\hat{R}\hat{a}\hat{R}^T)^{-1}\hat{b}^{-2}(\hat{R}\hat{a}\hat{R}^T)^{-1}}\hat{R}\hat{a}\end{aligned}$$

It is simple to verify by substitution that our solution satisfies Eq.(2.53) as requested. Moreover, if $\hat{R} = \hat{I}_3$ we obtain the simple solution $\hat{F} = \hat{a}^{-1}\hat{b}$ as expected.

For the following purposes we suppose to fix the rotation tensor $\hat{R}$ and to obtain the transformation tensors $\hat{V}$ and $\hat{F}$ through the previous procedure based upon the knowledge of the shape of the ellipsoids (the tensors $\hat{a}$ and $\hat{b}$). Moreover, the shape of the ellipsoid assumed in the reference $\{\vec{z}\}$ must be very similar to that assumed in the reference $\{\vec{y}\}$ in order to satisfy the requirements of the infinitesimal theory of elasticity.

We suppose to measure the *true* strain of the embedded ellipsoid in the reference frame $\{\vec{z}\}$, i.e. after the first rotation. The ellipsoid in the reference frame $\{\vec{z}\}$ assumes the role of reference configuration. In order to describe the generalized version of the Eshelby equivalence principle, the complete transformation, from the reference configuration to the deformed one, can be accomplished in two steps: firstly, we apply the tensor $\hat{V}$, which gives to the elliposidal particle the exact shape of the cavity (in the reference frame $\{\vec{y}\}$) and, successively, we consider the final change leading to the actual current configuration.

The transformation $\vec{y} = \hat{V}\vec{z}$ between the reference frames $\{\vec{z}\}$ and $\{\vec{y}\}$ corresponds to a displacement field $\vec{u}_V(\vec{z}) = \vec{y} - \vec{z} = \left(\hat{V} - \hat{I}\right)\vec{z}$. In this configuration the surfaces of the prestrained ellipsoidal inhomogeneity and of the cavity are firmly bonded. The current configuration, after

relaxation, is then reached through a further displacement field $\vec{u}(\vec{y})$, which represents the main unknown in our system, depending upon the shape tensors $\hat{a}$ and $\hat{b}$ and on the externally applied loadings. It is now important to find a relation between the *true* strain measured in the reference frame $\{\vec{z}\}$ and the displacement fields $\vec{u}_V(\vec{z})$ and $\vec{u}(\vec{y})$; the total displacement is $\vec{u}_T(\vec{z}) = \vec{u}_V(\vec{z}) + \vec{u}(\vec{y}) = \vec{u}_V(\vec{z}) + \vec{u}[\vec{z} + \vec{u}_V(\vec{z})]$. The strain in the reference frame $\{\vec{y}\}$ is defined as $\epsilon_{ij}(\vec{y}) = \frac{1}{2}\left(J_{ij} + J_{ji}\right)$ where $J_{ij}(\vec{y}) = \frac{\partial u_i}{\partial y_j}$ and, therefore, the *true* strain is given by

$$\begin{aligned} \epsilon_{T,ij}(\vec{z}) &= \frac{1}{2}\left(\frac{\partial u_{T,i}}{\partial z_j} + \frac{\partial u_{T,j}}{\partial z_i}\right) \\ &= \frac{1}{2}\left(\frac{\partial u_{V,i}}{\partial z_j} + \frac{\partial u_{V,j}}{\partial z_i} + \frac{\partial u_i}{\partial y_s}\frac{\partial y_s}{\partial z_j} + \frac{\partial u_j}{\partial y_s}\frac{\partial y_s}{\partial z_i}\right) \\ &= \frac{1}{2}\left[V_{ij} - \delta_{ij} + V_{ji} - \delta_{ji} + J_{is}(\vec{y})V_{sj} + J_{js}(\vec{y})V_{si}\right]_{\vec{y}=\hat{V}\vec{z}} \end{aligned} \tag{2.58}$$

Since the tensor $\hat{V}$ is symmetric we simply obtain

$$\hat{\epsilon}_T(\vec{z}) = \hat{V} - \hat{I} + \frac{1}{2}\left[\hat{J}(\vec{y})\hat{V} + \hat{V}\hat{J}^\top(\vec{y})\right]_{\vec{y}=\hat{V}\vec{z}} \tag{2.59}$$

where $\hat{J}\hat{V}$ and $\hat{V}\hat{J}^\top$ represent two standard matrix multiplications and $\hat{J}^\top$ is the transpose of $\hat{J}$. The constitutive equation in the reference frame $\{\vec{z}\}$ is $\hat{T}(\vec{z}) = \hat{\mathcal{C}}^{(2)}\hat{\epsilon}_T(\vec{z})$ and, consequently, in the reference frame $\{\vec{y}\}$ we immediatly obtain

$$\hat{T}(\vec{y}) = \hat{\mathcal{C}}^{(2)}\left\{\hat{V} - \hat{I} + \frac{1}{2}\left[\hat{J}(\vec{y})\hat{V} + \hat{V}\hat{J}^\top(\vec{y})\right]\right\} \tag{2.60}$$

It is important to remark that, in order to adopt the equivalence principle approach, we must utilize in the region Ω the constitutive equation of the inhomogeneity written in the reference frame $\{\vec{y}\}$, i.e. in the deformed configuration close-fitting the cavity of the homogeneous matrix. In these conditions, the problem can be splitted in the superimposition of two different subproblems (see Fig.10): the problem A corresponds to a very simple situation of an entirely homogeneous material (stiffness $\hat{\mathcal{C}}^{(1)}$ without inclusions or inhomogeneities) loaded by the remotely applied stress $\hat{T}^\infty$. The corresponding elastic fields can be summed up as follows

$$\hat{\epsilon}^A = \hat{\epsilon}^\infty,\ \hat{J}^A = \hat{\epsilon}^\infty \text{ and } \hat{T}^A = \hat{T}^\infty = \hat{\mathcal{C}}^{(1)}\hat{\epsilon}^\infty \tag{2.61}$$

The second problem B corresponds to an inclusion confined in the region Ω and described by the eigenstrain $\hat{\epsilon}^*$. The related fields have been discussed in Section 2 and they are summarized below

$$\hat{\epsilon}^B = \hat{\mathcal{S}}\hat{\epsilon}^*,\ \hat{J}^B = \hat{\mathcal{D}}\hat{\epsilon}^* \text{ and } \hat{T}^B = \hat{\mathcal{C}}^{(1)}\left(\hat{\epsilon}^B - \hat{\epsilon}^*\right) \tag{2.62}$$

where the tensors $\hat{\mathcal{D}}$ and $\hat{\mathcal{S}}$ have been defined in Eqs.(2.14) and (2.15), respectively. The superimpositions of strain, gradient of displacement and stress in the schemes A and B define the elastic field in the region Ω as follows

$$\begin{aligned} \hat{\epsilon} &= \hat{\epsilon}^A + \hat{\epsilon}^B = \hat{\epsilon}^\infty + \hat{\mathcal{S}}\hat{\epsilon}^* \\ \hat{J} &= \hat{J}^A + \hat{J}^B = \hat{\epsilon}^\infty + \hat{\mathcal{D}}\hat{\epsilon}^* \\ \hat{T} &= \hat{T}^A + \hat{T}^B = \hat{\mathcal{C}}^{(1)}\hat{\epsilon}^\infty + \hat{\mathcal{C}}^{(1)}\left(\hat{\epsilon}^B - \hat{\epsilon}^*\right) = \hat{\mathcal{C}}^{(1)}\hat{\epsilon}^\infty + \hat{\mathcal{C}}^{(1)}\left(\hat{\mathcal{S}}\hat{\epsilon}^* - \hat{\epsilon}^*\right) \end{aligned} \tag{2.63}$$

The equivalence principle becomes operative by combining Eq.(2.63) for the fields in the region Ω with the constitutive relation given in Eq.(2.60)

$$\begin{aligned} \hat{\mathcal{C}}^{(1)}\hat{\epsilon}^{\infty} \;+\; & \hat{\mathcal{C}}^{(1)}\left(\hat{\mathcal{S}}-\hat{\mathcal{I}}\right)\hat{\epsilon}^{*} \\ & = \hat{\mathcal{C}}^{(2)}\left\{\hat{V}-\hat{I}+\frac{1}{2}\left[(\hat{\epsilon}^{\infty}+\hat{\mathcal{D}}\hat{\epsilon}^{*})\hat{V}+\hat{V}(\hat{\epsilon}^{\infty}+\hat{\mathcal{D}}\hat{\epsilon}^{*})^{\top}\right]\right\} \end{aligned} \tag{2.64}$$

This is an equation for the eigenstrain ensuring the equivalence between the superimposition of the problems A and B and the original prestrained inhomogeneity problem. This relation can be written in the following form

$$\begin{aligned} \hat{\mathcal{C}}^{(1)}\hat{\epsilon}^{\infty}-\hat{\mathcal{C}}^{(2)}\left(\hat{V}-\hat{I}\right) \;-\; & \frac{1}{2}\hat{\mathcal{C}}^{(2)}\left(\hat{\epsilon}^{\infty}\hat{V}+\hat{V}\hat{\epsilon}^{\infty}\right) \\ = -\hat{\mathcal{C}}^{(1)}\left(\hat{\mathcal{S}}-\hat{\mathcal{I}}\right)\hat{\epsilon}^{*} \;+\; & \frac{1}{2}\hat{\mathcal{C}}^{(2)}\left[(\hat{\mathcal{D}}\hat{\epsilon}^{*})\hat{V}+\hat{V}(\hat{\mathcal{D}}\hat{\epsilon}^{*})^{\top}\right] \end{aligned} \tag{2.65}$$

which represents a linear equation in the eigenstrain $\hat{\epsilon}^{*}$. It can be written in components through the standard form $M_{ij} = N_{ijkh}\epsilon^{*}_{kh}$, where

$$M_{ij} = \mathcal{C}^{(1)}_{ijst}\epsilon^{\infty}_{st} - \mathcal{C}^{(2)}_{ijst}\left(V_{st}-\delta_{st}\right) - \frac{1}{2}\mathcal{C}^{(2)}_{ijst}\left(\epsilon^{\infty}_{sk}V_{kt}+V_{sk}\epsilon^{\infty}_{kt}\right) \tag{2.66}$$

$$N_{ijkh} = \mathcal{C}^{(1)}_{ijkh} - \mathcal{C}^{(1)}_{ijst}\mathcal{S}_{stkh} + \frac{1}{2}\mathcal{C}^{(2)}_{ijst}\left[\mathcal{D}_{srkh}V_{rt}+\mathcal{D}_{trkh}V_{rs}\right] \tag{2.67}$$

Alternatively, Eq.(2.65) can be solved in tensor notation by means of the definition of the following operation

$$\left[\hat{\mathcal{D}}\odot\hat{V}\right]\hat{\epsilon}^{*} = \frac{1}{2}\left[(\hat{\mathcal{D}}\hat{\epsilon}^{*})\hat{V}+\hat{V}(\hat{\mathcal{D}}\hat{\epsilon}^{*})^{\top}\right] \tag{2.68}$$

where the tensor $\hat{\mathcal{D}}\odot\hat{V}$ corresponds to the components

$$\left[\hat{\mathcal{D}}\odot\hat{V}\right]_{stkh} = \frac{1}{2}\left[\mathcal{D}_{srkh}V_{rt}+\mathcal{D}_{trkh}V_{rs}\right] \tag{2.69}$$

By this definition, Eq.(2.65) can be easily solved and the equivalent eigenstrain is eventually obtained as

$$\begin{aligned} \hat{\epsilon}^{*} \;=\; & \left[\hat{\mathcal{C}}^{(2)}\left(\hat{\mathcal{D}}\odot\hat{V}\right)-\hat{\mathcal{C}}^{(1)}\left(\hat{\mathcal{S}}-\hat{\mathcal{I}}\right)\right]^{-1} \\ & \times\left[\hat{\mathcal{C}}^{(1)}\hat{\epsilon}^{\infty}-\hat{\mathcal{C}}^{(2)}\left(\hat{V}-\hat{I}\right)-\frac{1}{2}\hat{\mathcal{C}}^{(2)}\left(\hat{\epsilon}^{\infty}\hat{V}+\hat{V}\hat{\epsilon}^{\infty}\right)\right] \end{aligned} \tag{2.70}$$

Moreover, the *true* internal strain, defined in the reference frame $\{\vec{z}\}$ is given by Eq.(2.59). By utilizing Eqs.(2.63) and (2.64), it assumes, after some straightforward calculations, the following final form

Internal strain

$$\begin{aligned} \hat{\epsilon}_{T}(\vec{z}) \;=\; & \left(\hat{\mathcal{C}}^{(2)}\right)^{-1}\hat{\mathcal{C}}^{(1)}\left\{\hat{\epsilon}^{\infty}+\left(\hat{\mathcal{S}}-\hat{\mathcal{I}}\right)\left[\hat{\mathcal{C}}^{(2)}\left(\hat{\mathcal{D}}\odot\hat{V}\right)-\hat{\mathcal{C}}^{(1)}\left(\hat{\mathcal{S}}-\hat{\mathcal{I}}\right)\right]^{-1}\right. \\ & \left.\times\left[\hat{\mathcal{C}}^{(1)}\hat{\epsilon}^{\infty}-\hat{\mathcal{C}}^{(2)}\left(\hat{V}-\hat{I}\right)-\frac{1}{2}\hat{\mathcal{C}}^{(2)}\left(\hat{\epsilon}^{\infty}\hat{V}+\hat{V}\hat{\epsilon}^{\infty}\right)\right]\right\} \end{aligned} \tag{2.71}$$

This is the most important result of this Section, stating that the internal strain is uniform inside the inhomogeneiy having shape and size different from those of the hosting cavity. We remark that if one is interested in the *true* internal strain in the original reference frame $\{\vec{x}\}$ it is sufficient to use the rotation $\hat{\epsilon}_{T}(\vec{x}) = \hat{R}^{\top}\hat{\epsilon}_{T}(\vec{z})\hat{R}$. When $\hat{V} = \hat{I}$

the inhomogeneity is not strained (deformed) to fit the cavity and the results of the standard Eshelby theory must be obtained. In fact, if $\hat{V} = \hat{I}$ we have $\hat{\mathcal{D}} \odot \hat{V} = \hat{\mathcal{S}}$ and the true strain assumes the simpler form $\hat{\epsilon}_T = \left\{ \hat{\jmath} - \hat{\mathcal{S}} \left[\hat{\jmath} - \left(\hat{\mathcal{C}}^{(1)} \right)^{-1} \hat{\mathcal{C}}^{(2)} \right] \right\}^{-1} \hat{\epsilon}^{\infty}$, as expected.

Furthermore, we can calculate the state of strain in the sourrounding matrix; the equivalence principle for the external region reads

$$\begin{aligned} \hat{\epsilon}(\vec{y}) &= \hat{\epsilon}^{\infty} + \hat{\mathcal{S}}^{\infty}_{ijkh}(\vec{y})\, \hat{\epsilon}^{*} \\ \hat{T}(\vec{y}) &= \hat{\mathcal{C}}^{(1)} \hat{\epsilon}^{\infty} + \hat{\mathcal{C}}^{(1)} \hat{\mathcal{S}}^{\infty}_{ijkh}(\vec{y})\, \hat{\epsilon}^{*} \end{aligned} \tag{2.72}$$

where the eigenstrain $\hat{\epsilon}^{*}$ is given by Eq.(2.70). The final expression for the external strain assumes the form

External strain

$$\begin{aligned} \hat{\epsilon}(\vec{y}) &= \hat{\epsilon}^{\infty} + \hat{\mathcal{S}}^{\infty}_{ijkh}(\vec{y}) \left[\hat{\mathcal{C}}^{(2)} \left(\hat{\mathcal{D}} \odot \hat{V} \right) - \hat{\mathcal{C}}^{(1)} \left(\hat{\mathcal{S}} - \hat{\jmath} \right) \right]^{-1} \\ &\quad \times \left[\hat{\mathcal{C}}^{(1)} \hat{\epsilon}^{\infty} - \hat{\mathcal{C}}^{(2)} \left(\hat{V} - \hat{I} \right) - \frac{1}{2} \hat{\mathcal{C}}^{(2)} \left(\hat{\epsilon}^{\infty} \hat{V} + \hat{V} \hat{\epsilon}^{\infty} \right) \right] \end{aligned} \tag{2.73}$$

Example of application

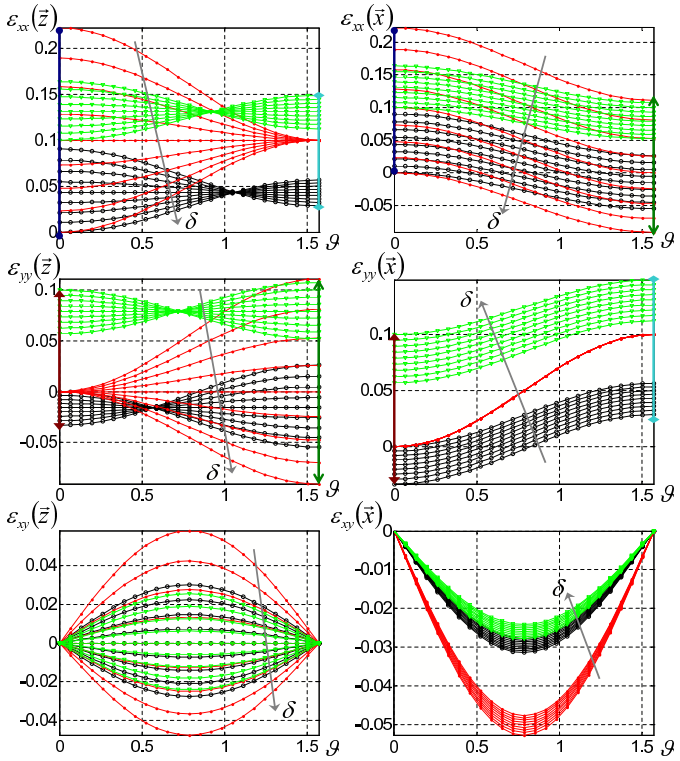

Figure 11: Planar components $\varepsilon_{xx}, \varepsilon_{yy}$ and ε_{xy} of the strain $\hat{\epsilon}_T$ versus the angle ϑ [rad], in both reference frames $\{\vec{z}\}$ and $\{\vec{x}\}$ with the following parameters: $K_1 = K_2 = 1$, $\mu_1 = \mu_2 = 0.1$, $\hat{a} = \mathrm{diag}(\delta, 1, 1)$ with $0.9 < \delta < 1.1$ and $\hat{b} = \mathrm{diag}(1.1, 1, 1)$. The load is given by $\hat{\epsilon}^{\infty} = \mathrm{diag}(0.1, 0.1, 0)$. Dotted red lines: prestrain before relaxation; black lines with circles: strain after relaxation without load; green lines with triangles: strain after relaxation with applied load.

We describe now a series of examples of application of the previous theory to prestrained ellipsoidal inhomogeneities inserted into different ellipsoidal cavities. For the sake of simplicity we have used the same material for the embedded particle and the hosting matrix

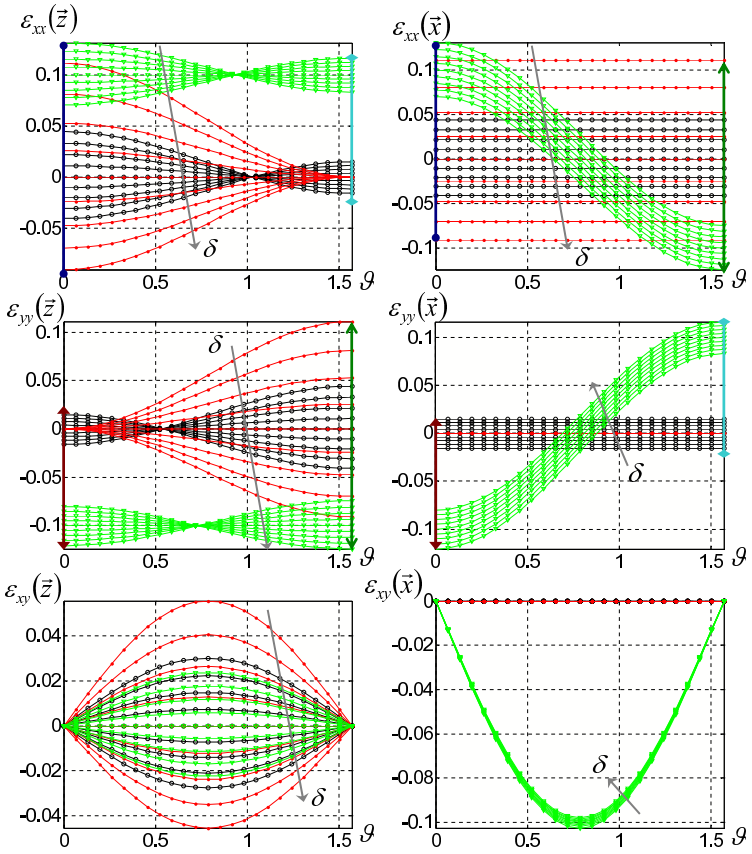

Figure 12: Planar components $\varepsilon_{xx}, \varepsilon_{yy}$ and ε_{xy} of the strain $\hat{\varepsilon}_T$ versus the angle ϑ [rad], in both reference frames $\{\vec{z}\}$ and $\{\vec{x}\}$ with the following parameters: $K_1 = K_2 = 1$, $\mu_1 = \mu_2 = 0.1$, $\hat{a} = \mathrm{diag}(\delta, 1, 1)$ with $0.9 < \delta < 1.1$ and $\hat{b} = \mathrm{diag}(1, 1, 1)$. The load is given by $\hat{\varepsilon}^{\infty} = \mathrm{diag}(0.1, -0.1, 0)$. Dotted red lines: prestrain before relaxation; black lines with circles: strain after relaxation without load; green lines with triangles: strain after relaxation with applied load.

($K_1 = K_2 = 1$ and $\mu_1 = \mu_2 = 0.1$ in arbitrary units). The geometry of the inhomogeneity is described by the tensor $\hat{a} = \mathrm{diag}(\delta, 1, 1)$ (a.u.) for $0.9 < \delta < 1.1$, in order to investigate the effects of the aspect ratio on the elastic response of the system. More precisely, we have utilized nine values of δ regularly distributed over its range of variation (moving from prolate to oblate ellipsoid of revolution). On the other hand, for the geometry of the cavity we have chosen three different possibilities, namely $\hat{b} = \mathrm{diag}(1.1, 1, 1)$ (a.u.) (prolate spheroid), $\hat{b} = \mathrm{diag}(1, 1, 1)$ (a.u.) (sphere) and $\hat{b} = \mathrm{diag}(0.9, 1, 1)$ (a.u.) (oblate spheroid). For any possible geometry of the ellipsoids, the inhomogeneity is embedded in the cavity after a rotation of an angle ϑ around the $x_3 \equiv z$ axis of the reference frame $\{\vec{x}\}$. It corresponds to a rotation matrix of the form

$$\hat{R} = \begin{bmatrix} \cos\vartheta & -\sin\vartheta & 0 \\ \sin\vartheta & \cos\vartheta & 0 \\ 0 & 0 & 1 \end{bmatrix} \tag{2.74}$$

We have explored the entire interval $0 < \vartheta < \pi/2$ [rad] by means of 25 regularly spaced values. The results have been organized as follows:

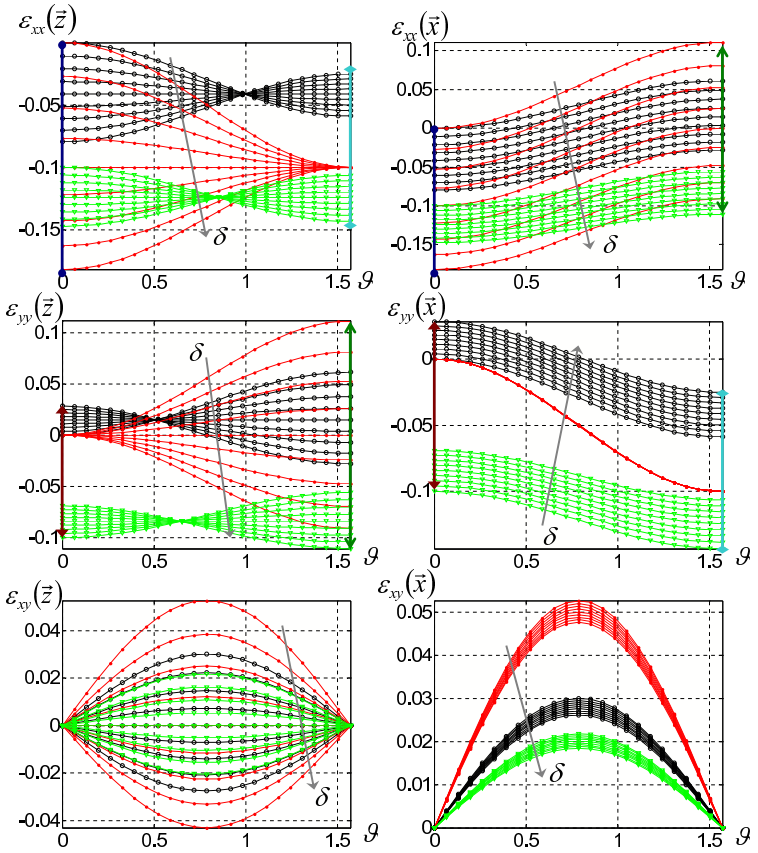

Figure 13: Planar components $\varepsilon_{xx}, \varepsilon_{yy}$ and ε_{xy} of the strain $\hat{\varepsilon}_T$ versus the angle ϑ [rad], in both reference frames $\{\vec{z}\}$ and $\{\vec{x}\}$ with the following parameters: $K_1 = K_2 = 1$, $\mu_1 = \mu_2 = 0.1$, $\hat{a} = \mathrm{diag}(\delta, 1, 1)$ with $0.9 < \delta < 1.1$ and $\hat{b} = \mathrm{diag}(0.9, 1, 1)$. The load is given by $\hat{\varepsilon}^\infty = \mathrm{diag}(-0.1, -0.1, 0)$. Dotted red lines: prestrain before relaxation; black lines with circles: strain after relaxation without load; green lines with triangles: strain after relaxation with applied load.

- in Fig. 11 the planar components $\varepsilon_{xx}, \varepsilon_{yy}$ and ε_{xy} of the true strain $\hat{\varepsilon}_T$ are shown versus the angle ϑ [rad], in both reference frames $\{\vec{z}\}$ and $\{\vec{x}\}$, for $\hat{b} = \mathrm{diag}(1.1, 1, 1)$. The load is given by $\hat{\varepsilon}^\infty = \mathrm{diag}(0.1, 0.1, 0)$.

- in Fig. 12 the planar components $\varepsilon_{xx}, \varepsilon_{yy}$ and ε_{xy} of the true strain $\hat{\varepsilon}_T$ are shown versus the angle ϑ [rad], in both reference frames $\{\vec{z}\}$ and $\{\vec{x}\}$, for $\hat{b} = \mathrm{diag}(1, 1, 1)$. The load is given by $\hat{\varepsilon}^\infty = \mathrm{diag}(0.1, -0.1, 0)$.

- in Fig. 13 the planar components $\varepsilon_{xx}, \varepsilon_{yy}$ and ε_{xy} of the true strain $\hat{\varepsilon}_T$ are shown versus the angle ϑ [rad], in both reference frames $\{\vec{z}\}$ and $\{\vec{x}\}$, for $\hat{b} = \mathrm{diag}(0.9, 1, 1)$. The load is given by $\hat{\varepsilon}^\infty = \mathrm{diag}(-0.1, -0.1, 0)$.

In each plot the dotted red lines correspond to the prestrain before relaxation, i.e. $\hat{\varepsilon}_T(\vec{z}) = \hat{V} - \hat{I}$ and $\hat{\varepsilon}_T(\vec{x}) = \hat{R}^\top \hat{\varepsilon}_T(\vec{z}) \hat{R} = \hat{R}^\top (\hat{V} - \hat{I}) \hat{R}$ (this is the deformation of the inhomogeneity applied for fitting closely the undeformed cavity); the black lines with circles correspond to the strain after relaxation without load, i.e. to Eq.(2.71) with $\hat{\varepsilon}^\infty = 0$ or its rotated version; finally, the green lines with triangles correspond to the

strain after relaxation with applied load, i.e. to Eq.(2.71) with $\hat{\epsilon}^{\infty} \neq 0$ or its rotated version.

It is interersting to observe the following properties of the plots: for $\vartheta = 0$ we have $\varepsilon_{xx}(\vec{z}) = \varepsilon_{xx}(\vec{x})$ (see dark-blu arrows in Figs.11-13) and $\varepsilon_{yy}(\vec{z}) = \varepsilon_{yy}(\vec{x})$ (see red arrows in Figs.11-13); similarly, for $\vartheta = \pi/2$ we have $\varepsilon_{xx}(\vec{z}) = \varepsilon_{yy}(\vec{x})$ (see sky-blu arrows in Figs.11-13) and $\varepsilon_{yy}(\vec{z}) = \varepsilon_{xx}(\vec{x})$ (see green arrows in Figs.11-13). These properties simply derive from the rotation of the strain tensor and, therefore, hold on for all the strain plots (unrelaxed, relaxed without load and relaxed with load).

Some more comments of the results follow. In Fig.11, related to the case with the prolate cavity $\hat{b} = \mathrm{diag}(1.1, 1, 1)$, the unrelaxed strain $\varepsilon_{xx}(\vec{z})$ (dotted red lines) in the reference frame fixed on the matrix must start at the value $(1.1 - \delta)/\delta$ for $\vartheta = 0$ and it must end at the value $(1.1 - 1)/1 = 0.1$ for $\vartheta = \pi/2$; on the other hand, the unrelaxed strain $\varepsilon_{xx}(\vec{x})$ (dotted red lines) in the reference frame fixed on the inhomogeneity must start at the value $(1.1 - \delta)/\delta$ for $\vartheta = 0$ as before while it must end at the value $(1 - \delta)/\delta$ for $\vartheta = \pi/2$. Moreover, for the same case, the unrelaxed strain $\varepsilon_{yy}(\vec{z})$ (dotted red lines) in the reference frame fixed on the matrix must start at the value 0 for $\vartheta = 0$ and it must end at the value $(1 - \delta)/\delta$ for $\vartheta = \pi/2$; on the other hand, the unrelaxed strain $\varepsilon_{yy}(\vec{x})$ (dotted red lines) in the reference frame fixed on the inhomogeneity must start at the value 0 for $\vartheta = 0$ as before while it must end at the value $(1.1 - 1)/1 = 0.1$ for $\vartheta = \pi/2$. These considerations, dealing with the unrelaxed strains, are related just to geometrical factors. On the contrary, the elastic response can be observed in the relaxed strain curves (black lines without load and green lines with load), obtained by means of the present theory, i.e. through Eq.(2.71). It is interesting to observe that the intersection points of the curves (of $\varepsilon_{xx}(\vec{z})$ for $\vartheta = \pi/2$ and of $\varepsilon_{yy}(\vec{z})$ for $\vartheta = 0$) of the unrelaxed strains (dotted red lines) are shifted by the elastic relaxation process to a different value of the angle ϑ (see black lines), preserving the property that all the curves pass through the same point. This property is manteined also with an externally applied load (see green lines). We also note that a shear strain appear inside the inhomogeneity when it is rotated of an angle ϑ different from 0 and $\pi/2$.

The second case, represented in Fig.12, is simpler because the cavity is a sphere (of radius 1) and, therefore, the embedding of the inhomogeneity does not depend on the angle ϑ. This can be seen by means of the (dotted red) curves of the unrelaxed strain $\varepsilon_{xx}(\vec{x})$, which are constant at the values $(1 - \delta)/\delta$ and the curves of the unrelaxed strain $\varepsilon_{yy}(\vec{x})$, which are constant at the values 0. Also the relaxed version of these strain curves (black lines without load) are constant for the same reasons. Only when the load is applied to the system we observe the dependence on the angle ϑ, due to the rotation of the reference frame $\{\vec{x}\}$, rigidly bonded to the inhomogeneity (see green lines). As for the reference frame $\{\vec{z}\}$, fixed in the matrix, we observe in Fig.12 that the red lines for $\varepsilon_{xx}(\vec{z})$ start at $(1 - \delta)/\delta$ and end in 0. Conversely, the red lines for $\varepsilon_{yy}(\vec{z})$ start at 0 and end in $(1 - \delta)/\delta$. The elastic relaxation with or without load allows us to conclude that the intersection points of the curves have the same behavior described for the previous case, represented in Fig.11.

The third case, shown in Fig.13 is similar to the first one. Here an oblate particle with $\hat{b} = \mathrm{diag}(0.9, 1, 1)$ is considered.

2.3 NONLINEAR ESHELBY THEORY

In this Section, we develop a further generalization of the original Eshelby theory. Such a new development [87] allows us to treat the inclusion configuration also under the hypothesis of nonlinear elastic behavior of the inclusion. In the following, we firstly describe several different approach to nonlinear elasticity.

2.3.1 *Nonlinear Elasticity*

geometrical nonlinearity and physical nonlinearity

It is known that the concept of nonlinearity can be introduced in the theory of elasticity in two different ways [31]. Firstly, nonlinearity can be taken into account by means of the exact relation for the strain not limited to small deformations (see Section 1.1.1). This approach is referred to as *geometrical nonlinearity* since it is related to the equations not depending on the material under consideration. Secondly, another nonlinear aspect can be considered through the arbitrarieness of the (generically not Hookean) stress-strain constitutive relation. This approach is referred to as *physical nonlinearity* since it is related to properties of the material under consideration. Therefore, by combining the two previous contributions, it follows that there are four different types of problems in the theory of elasticity [33]

- those having both physical and geometrical linearity;
- those which are physically nonlinear but geometrically linear;
- those linear physically but nonlinear geometrically;
- those nonlinear both physically and geometrically.

The problems of the first type are the subject of the classical theory of elasticity (small deformation in Hookean materials). In this work, we adopt the second conceptual framework. Therefore, the deformations are still represented by the strain tensor $\hat{\epsilon}$ defined in Eq.(1.7), but, the elongations can exceed the Hookean limit of proportionality between stress and strain: this requires a *nonlinear stress-strain relationship*. This conceptual framework is sometimes referred to as *hypoelasticity*: it is intended to model perfectly reversible nonlinear stress-strain behavior but restricted to infinitesimal strains. Such a description has been already adopted in the past in order to model nonlinear cubic polycrystals with perturbative and self consistent methods [88].

Nonlinear elastic constitutive equations

In geometrically linear but physically nonlinear elasticity, the balance of linear and angular momentum still holds for all materials, regardless of their constitution. Therefore, the balance of the linear momentum leads to the equation of motion in the usual form of Eq.1.26, while the balance of the angular momentum leads to the symmetry of the stress tensor ($T_{ij} = T_{ji}$). As stated above, in this case the nonlinearity of the mechanical response of the material is taken into account by means of a nonlinear constitutive equation

$$T_{ij} = f_{ij}(\hat{\epsilon}) \quad \text{or} \quad \hat{T} = f(\hat{\epsilon}) \tag{2.75}$$

where the functions f_{ij} are chosen so that $f_{ij} = f_{ji}$ in order to satisfy the required symmetry. In particular, this generic stress-strain relation

can be developped up to the second order term in the strain taking into account the deviation from the stress-strain proportionality [89, 90]

$$T_{ij} = \mathcal{C}_{ijkh}\epsilon_{kh} + \frac{1}{2}\mathcal{L}_{ijkhnm}\epsilon_{kh}\epsilon_{nm} + \mathcal{O}(\epsilon_{kh}^2) \tag{2.76}$$

where $\mathcal{C}_{ijkh}$ are the components of the, linear, stiffness tensor while the coefficients $\mathcal{L}_{ijkhnm}$ represent the nonlinear behavior of the system. Such a constitutive relation can also be written in the following form

$$T_{ij} = \mathcal{C}^{NL}_{ijkh}(\hat{\epsilon})\,\epsilon_{kh} \tag{2.77}$$

where

$$\hat{\mathcal{C}}^{NL}(\hat{\epsilon}) = \left(\mathcal{C}_{ijkh} + \frac{1}{2}\mathcal{L}_{ijkhnm}\epsilon_{nm}\right) \tag{2.78}$$

is the nonlinear (strain dependent) stiffness tensor. It can be noticed that while the tensor $\hat{\mathcal{C}}$ has 21 independent entries, the second order tensor $\hat{\mathcal{L}}$ has 56 independent components. Tables for the values of $\mathcal{C}_{ijkh}$ and $\mathcal{L}_{ijkhnm}$ can be found in literature [88]. These values can be obtained by experimental procedure [91, 92] and by computational techniques (e.g., molecular dynamics [93] or first-principles calculations [94]). For the following purpose we are interested in the isotropic nonlinear constitutive equations expanded up to the second order in the strain components. In order to introduce these forms of physical nonlinearities we can take into account two different approaches, as described below.

Isotropic nonlinear constitutive equations in Cauchy elasticity

The Cauchy approach to the constitutive equations is the less restrictive starting point for the elasticity theory since it does not consider the strain energy function. It is simply based on the Eq.(2.75). To develop this approach in an isotropic context an assumption must be made concerning the behavior of Eq.(2.75) under rigid-body rotations. The function $f(\hat{\epsilon})$ must satisfy the identity [31]

Invariance under rotation of the stress

$$\hat{R}^T f(\hat{\epsilon})\,\hat{R} = f\left(\hat{R}^T\hat{\epsilon}\hat{R}\right) \tag{2.79}$$

for all proper orthogonal tensor $\hat{R}$ representing the rotation. A function satisfying the previous identity is known as an isotropic tensor function, and it can be represented in the form [31]

$$\hat{T} = f(\hat{\epsilon}) = q_1\hat{I} + q_2\hat{\epsilon} + q_3\hat{\epsilon}^2 \tag{2.80}$$

where $\hat{I}$ is the identity operator and q_1, q_2 and q_3 are scalar functions of the invariants $Tr(\hat{\epsilon})$, $Tr(\hat{\epsilon}^2)$ e $Tr(\hat{\epsilon}^3)$ of the strain tensor $\hat{\epsilon}$

$$q_\alpha = q_\alpha\left(Tr(\hat{\epsilon}), Tr(\hat{\epsilon}^2), Tr(\hat{\epsilon}^3)\right) \tag{2.81}$$

The development of Eq.(2.80), up to the second order in the powers of $\hat{\epsilon}$, provides the following constitutive equation

Second order Cauchy elasticity

$$\begin{aligned}\hat{T} &= 2\mu\hat{\epsilon} + \lambda Tr(\hat{\epsilon})\,\hat{I} \\ &+ A\hat{\epsilon}^2 + BTr\left(\hat{\epsilon}^2\right)\hat{I} + C\left[Tr(\hat{\epsilon})\right]^2\hat{I} + D\hat{\epsilon}Tr(\hat{\epsilon})\end{aligned} \tag{2.82}$$

where μ and λ are the standard Lamè moduli concerning the linear contribution and A, B, C and D are the coefficients describing the nonlinear behavior of the material.

Isotropic nonlinear constitutive equations in Green elasticity

The Green elasticity is based on Eq.(2.75) with an additional hypothesis: we suppose that the stress power, in a given deformation, is absorbed into a strain energy function $U(\hat{\epsilon})$, representing the density of elastic potential energy (see Section 1.3). The existence of such a function and the consideration of energy balance in the continuum, lead to the evolution equation

$$\frac{dU(\hat{\epsilon})}{dt} = T_{ij}(\hat{\epsilon})\frac{d\epsilon_{ij}}{dt} \tag{2.83}$$

affirming that the function $U(\hat{\epsilon})$ is an exact differential form such that

$$T_{ij}(\hat{\epsilon}) = \frac{\partial U(\hat{\epsilon})}{\partial \epsilon_{ij}} \tag{2.84}$$

So, if a function $U(\hat{\epsilon})$ exists, the (arbitrarily nonlinear) constitutive equation for a given material can be determined by Eq.(2.84) [36, 39]. From the thermodynamics point of view, the strain energy function can be identified with the internal energy per unit volume in an isentropic process, or with the Helmholtz free energy per unit volume in an isothermal process. Such an approach can be further developed for isotropic media: in this case, the function $U(\hat{\epsilon})$ must satisfy the relation [31]

Invariance under rotation of the elastic energy

$$U(\hat{\epsilon}) = U\left(\hat{R}^T\hat{\epsilon}\hat{R}\right) \tag{2.85}$$

for any rotation tensor $\hat{R}$. Eq.(2.85) represents the scalar counterpart of the tensor relation Eq.(2.79). If Eq.(2.85) is true then it follows that the function $U(\hat{\epsilon})$ can depend only on the principal invariants of the strain tensor

$$U = U\left(Tr(\hat{\epsilon}), Tr(\hat{\epsilon}^2), Tr(\hat{\epsilon}^3)\right) \tag{2.86}$$

We may expand Eq.(2.86) up to the third order in the strain components, obtaining [39]

$$\begin{aligned} U(\hat{\epsilon}) &= \mu Tr\left(\hat{\epsilon}^2\right) + \frac{\lambda}{2}\left[Tr\left(\hat{\epsilon}\right)\right]^2 \\ &+ \frac{A}{3}Tr\left(\hat{\epsilon}^3\right) + BTr\left(\hat{\epsilon}\right)Tr\left(\hat{\epsilon}^2\right) + \frac{C}{3}\left[Tr\left(\hat{\epsilon}\right)\right]^3 \end{aligned} \tag{2.87}$$

Finally, performing the derivatives indicated in Eq. (2.84), we obtain the nonlinear isotropic constitutive equation (within the Green approach) expanded up to the second order in the strain tensor

Second order Green elasticity

$$\begin{aligned} \hat{T} &= 2\mu\hat{\epsilon} + \lambda Tr\left(\hat{\epsilon}\right)\hat{I} \\ &+ A\hat{\epsilon}^2 + B\left\{Tr\left(\hat{\epsilon}^2\right)\hat{I} + 2\hat{\epsilon}Tr\left(\hat{\epsilon}\right)\right\} + C\left[Tr\left(\hat{\epsilon}\right)\right]^2\hat{I} \end{aligned} \tag{2.88}$$

It is evident by comparison of Eq.(2.82) and Eq.(2.88) that the Green elasticity is more restrictive than the Cauchy elasticity: we obtain the Green formulation from the Cauchy formulation by imposing $D = 2B$. We use four independent parameters (A, B, C and D) in the Cauchy elasticity and three independent parameters (A, B and C) in the Green elasticity. These parameters are called Landau coefficients [39].

Landau coefficients

2.3.2 *Eshelby theory for nonlinear inhomogeneities*

A nonlinear isotropic and homogeneous ellipsoid can be generically described by the relation $\hat{\mathbf{T}} = \hat{\mathcal{C}}^{(2)}(\hat{\mathbf{e}})\,\hat{\mathbf{e}}$ (see Eq.(2.77)). Let's now place this inhomogeneity in a linear matrix characterized by a stiffness tensor $\hat{\mathcal{C}}^{(1)}$ (see Fig.4) and let's calculate the strain field inside the particle when a uniform field $\hat{\mathbf{T}}^{\infty} = \hat{\mathcal{C}}^{(1)}\hat{\mathbf{e}}^{\infty}$ is remotely applied to the system. If the particle were linear, with $\hat{\mathcal{C}}^{(2)}$ independent from the strain, we would have, inside the ellipsoid, a uniform strain field $\hat{\mathbf{e}}^{s}$ given by the Eq.(2.23) [8, 49] Conversely, if the ellipsoid were nonlinear, it is easy to prove that the internal uniform field must satisfy the equation

Internal strain field for nonlinear inclusions

$$\hat{\mathbf{e}}^{s} = \left[\hat{\mathbf{I}} - \hat{\mathbb{S}}\left(\hat{\mathbf{I}} - \left(\hat{\mathcal{C}}^{(1)}\right)^{-1}\hat{\mathcal{C}}^{(2)}(\hat{\mathbf{e}}^{s})\right)\right]^{-1}\hat{\mathbf{e}}^{\infty} \tag{2.89}$$

obtained form Eq.(2.23) through the substitution $\hat{\mathcal{C}}^{(2)} \to \hat{\mathcal{C}}^{(2)}(\hat{\mathbf{e}}^{s})$. If a solution $\hat{\mathbf{e}}^{s*}$ exists for a given $\hat{\mathbf{e}}^{\infty}$, it means that the nonlinear inhomogeneity could be replaced by a linear one with constant stiffness $\hat{\mathcal{C}}^{(2)} = \hat{\mathcal{C}}^{(2)}(\hat{\mathbf{e}}^{s*})$, without modifications of the elastic fields at any point. Therefore, if a solution exists, then Eq.(2.89) exactly describes, through self-consistency, the elastic behavior of the nonlinear anisotropic inclusion. This is not a trivial result: for instance, such a generalization of Eq.(2.23) is not valid if a nonlinear behavior is assumed for material 1 (matrix). The calculation of the internal strain field from Eq.(2.89) is very complicated and it strongly depends on the kind of nonlinearity $\hat{\mathbf{T}} = \hat{\mathcal{C}}^{(2)}(\hat{\mathbf{e}})\,\hat{\mathbf{e}}$. This task will be accomplished in the following, dealing with a sphere or a cylinder described by physical nonlinearities as those in Eq.(2.82) (Cauchy) or Eq.(2.88) (Green).

To conclude, we have verified the following general statement: if the linear elastic space with a single inhomogeneity of ellipsoidal shape is subjected to remote uniform loading, the stress field inside the inhomogeneity will be uniform independently of the constitutive law for the inhomogeneity, provided that both the matrix and the particle be homogeneous bodies. Some similar properties can be found in earlier literature [95, 96, 97].

When the Green approach is considered it is also possible to verify the existence and the uniqueness for the solution of Eq.(2.89). The proof is reported in the following Section.

Nonlinear Eshelby theory within Green elasticity

In order to prove the existence and the uniqueness of the solution of Eq.(2.89), we adopt the Green formulation of the elasticity theory. A strain energy function $U(\hat{\mathbf{e}})$ defines the constitutive equation $\hat{\mathbf{T}}(\hat{\mathbf{e}}) = \frac{\partial U(\hat{\mathbf{e}})}{\partial \hat{\mathbf{e}}}$ of the inhomogeneity, which is equivalent to $\hat{\mathbf{T}}(\hat{\mathbf{e}}) = \hat{\mathcal{C}}^{(2)}(\hat{\mathbf{e}})\,\hat{\mathbf{e}}$. In these conditions, the existence and uniqueness of a solution for Eq.(2.89) can be exactly proved under the sole hypothesis of convexity for the

strain energy function $U(\hat{\varepsilon})$. To prove this statement, we rearrange Eq.(2.89) as follows

$$\begin{aligned}
\left\{\hat{I}-\hat{S}\left[\hat{I}-\left(\hat{\mathcal{C}}^{(1)}\right)^{-1}\hat{\mathcal{C}}^{(2)}\left(\hat{\varepsilon}^{s}\right)\right]\right\}\hat{\varepsilon}^{s} &= \hat{\varepsilon}^{\infty}\\
\hat{\varepsilon}^{s}-\hat{S}\left[\hat{I}-\left(\hat{\mathcal{C}}^{(1)}\right)^{-1}\hat{\mathcal{C}}^{(2)}\left(\hat{\varepsilon}^{s}\right)\right]\hat{\varepsilon}^{s} &= \hat{\varepsilon}^{\infty}\\
\hat{\varepsilon}^{s}-\hat{S}\hat{\varepsilon}^{s}+\hat{S}\left(\hat{\mathcal{C}}^{(1)}\right)^{-1}\hat{\mathcal{C}}^{(2)}\left(\hat{\varepsilon}^{s}\right)\hat{\varepsilon}^{s} &= \hat{\varepsilon}^{\infty}\\
\left[\hat{I}-\hat{S}\right]\hat{\varepsilon}^{s}+\hat{S}\left(\hat{\mathcal{C}}^{(1)}\right)^{-1}\frac{\partial U(\hat{\varepsilon}^{s})}{\partial\hat{\varepsilon}^{s}} &= \hat{\varepsilon}^{\infty}\\
\hat{\mathcal{C}}^{(1)}\left[\hat{S}^{-1}-\hat{I}\right]\hat{\varepsilon}^{s}-\hat{\mathcal{C}}^{(1)}\hat{S}^{-1}\hat{\varepsilon}^{\infty}+\frac{\partial U(\hat{\varepsilon}^{s})}{\partial\hat{\varepsilon}^{s}} &= 0
\end{aligned} \tag{2.90}$$

Now, the first linear term can be converted to the gradient of a quadratic form and the second constant term can be converted to the gradient of a linear form. At the end we observe that the internal strain field must satify the following relation

$$\frac{\partial}{\partial\hat{\varepsilon}}\left\{\frac{1}{2}\hat{\varepsilon}\hat{\mathcal{C}}^{(1)}\left[\hat{S}^{-1}-\hat{I}\right]\hat{\varepsilon}-\hat{\varepsilon}\hat{\mathcal{C}}^{(1)}\hat{S}^{-1}\hat{\varepsilon}^{\infty}+U(\hat{\varepsilon})\right\}=0 \tag{2.91}$$

which is exactly equivalent to Eq.(2.89). The first term represents a symmetric and positive definite quadratic form in $\hat{\varepsilon}$. In fact, in Appendix A.2, we prove the symmetry and the definiteness of the tensor

$$\hat{q}=\hat{\mathcal{C}}^{(1)}\left[\hat{S}^{-1}-\hat{I}\right] \tag{2.92}$$

The second term in Eq.(2.91) is a linear function of $\hat{\varepsilon}$. Therefore, the sum of these two terms is a convex functional with relative minimum at $\left[\hat{I}-\hat{S}\right]\hat{\varepsilon}^{\infty}$. This value represents the strain field in a void ($\hat{\mathcal{C}}^{(2)}\left(\hat{\varepsilon}\right)=0$ in Eq.(2.89) or $U(\hat{\varepsilon})=0$ in Eq.(2.91)) embedded in the matrix with stiffness $\hat{\mathcal{C}}^{(1)}$. If $U(\hat{\varepsilon})$ is a convex functional (with $U(0)=0$) the brackets in Eq.(2.91) contain the sum of two convex terms: they result in an overall convex functional with a unique minimal extremum at $\hat{\varepsilon}^{s}$.

3

NONLINEAR ELASTICITY OF COMPOSITE MATERIALS

Contents

3.1 STATE OF THE ART AND PRESENT DEVELOPMENT

In recent years the characterization of linear and nonlinear heterogeneous materials has attracted an ever increasing interest. A problem of considerable technological importance is the evaluation of the effective physical properties governing the behavior of a given composite material on the macroscopic scale, taking into account the actual microscale material features [98]. At present, it is well known that it does not exist a universal mixing formula giving the effective properties of the heterogeneous materials as some sort of average of the properties of the constituents. In fact, the details of the morphology or micro-geometry play a central role in determining the overall properties, particularly when the crystalline grains have highly anisotropic or nonlinear behavior or when there is a large difference in the properties of the constituent materials. The primary aim in the study of materials is to understand and classify the relationship between the internal micro-structure and the physical properties. Such a relationship may be used for designing and improving materials or, conversely, for interpreting experimental data in terms of micro-structural features. A great number of theoretical investigations have been developed in order to describe the behavior of composite materials when a specific microstructure is considered. On the other hands, a different class of theories does not assume a given microstructure, searching for general results of broad applicability. The most important properties are the classical Hashin-Shtrikman variational bounds [99, 100], which provide an upper and lower bound for composite materials properties, and the expansions of Brown [101] and Torquato [102, 103] which take into account the spatial correlation function of the constituents.

Effective properties of heterogeneous materials

Hashin-Shtrikman bounds

Dispersions or suspensions of inhomogeneities in a matrix are examples of widely studied heterogeneous materials: these media have been extensively analyzed both from the electrical and the elastic point of view. One of the first attempts to characterize dielectric dispersions of spheres was developed by Maxwell [104], which found out a famous formula valid for very diluted suspensions. A better model has been

provided by the differential scheme [67, 105]. In this case the results maintain the validity also for less diluted suspensions.

Recent progresses in this field concern dielectrically linear and nonlinear spheroidal inhomogeneities with geometric factors probabilistically distributed [106]. The size-dependent Bruggeman theory, which considers the effective particle dimension for non dilute dispersions, has been introduced as well [107]. A wide survey of mixture theory applications to metamaterials can be found in literature [108]. Finally, the dielectric (focusing or defocusing) Kerr nonlinearity [109] has been utilized to explore the importance of the particle shape [110].

On the other hands, dealing with the elastic characterization of dispersions, a similar line of research has been developed [68, 111]. A famous result exists for a material composed by a very dilute concentration of linear spherical inhomogeneities dispersed in a linear solid matrix [69]. To adapt this theory to the case of any finite volume fraction, the differential method is also applied to the elastic theories for spherical [112], cylindrical [73] and ellipsoidal particles [74]. Recent works focus on microstructures that can be characterized as continuous matrices containing inhomogeneities of diverse shapes, properties and orientations [77, 70]. The evaluation of the effective elastic properties of a body containing a given distribution of cracks belongs to the field of homogenization techniques as well [113]. Recent investigations consider the effects of the orientational statistical distribution of cracks in a given material [80, 114].

Effective nonlinear elastic behavior of heterogeneous materials

In heterogeneous materials the nonlinear elastic regime has been investigated under specific conditions [115, 116, 117]. Nevertheless, the general nonlinear elastic features are relevant in many materials science problems. For example, in biomechanics, transient elastography has shown its efficiency to map the nonlinear properties of soft tissues and it can be used as diagnostic technique [118, 119]. In material science the linear theory is incapable of fully capturing all fracture phenomena and hyperelasticity plays a governing role in the dynamics of fracture [120, 121]. The quantum dots growth, ordering and orientation (occuring during processing) are largely affected by elastic phenomena, even beyond the linear regime [122, 123]. Finally, many problems of fracture mechanics in composite materials do contain nonlinear features like, e.g., the interaction between a moving crack and a fiber (or, more generally, an inclusion) [124].

In this Section we consider[125] the linear and nonlinear elastic behavior of a composite material. In particular we take into account a dispersion of isotropic nonlinear inhomogeneities (spheres or parallel cylinders) embedded into a linear isotropic host matrix. The nonlinearity of the inhomogeneities is described either by the Cauchy model (four parameters) or by the energy-based Green approach (three parameters) discussed in Section 2.3.1.

We have introduced two simplifying hypotheses: the small volume fraction of the embedded particles and the small deformations of the whole solid body. Nevertheless, we obtain useful results both for analyzing the mechanical properties of a given heterogeneous structure and for designing a composite material with a desired linear and nonlinear elastic behavior.

The homogenization method is based on the nonlinear generalization of the Eshelby theory

The main concept applied in order to homogenize the heterogeneous structures is the nonlinear generalization of the Eshelby theory developed in the previous Chapter. This approach has been analytically

applied to perform a linear and nonlinear micromechanical averaging in the composite structure and, therefore, to develop a complete homogenizing procedure yielding the mechanical behavior of the solid body at the macro-scale.

As for the linear properties, we have obtained a series of results in perfect agreement with earlier researches on this subject. This point can be considered as a check of the mathematical procedure. As for the nonlinear properties, firstly, we have obtained the expressions of the four effective elastic moduli of the composite medium with inhomogeneities described by the Cauchy constitutive equations, which represent the less restrictive way to model the nonlinear elasticity. Then, we have considered, as a particular case, the Green elasticity to describe the nonlinear behavior of the particles. In this case we have verified that if a strain energy function exists for the inhomogeneities, then an overall strain energy function exists for the whole composite structure. This point confirms the perfect coherence between our micromechanical averaging procedure and the thermodynamics of the composite material.

3.2 DISPERSION OF SPHERICAL INCLUSIONS

3.2.1 *Effective elastic moduli*

We consider an assembly of spherical inhomogeneities (see Fig.14) described by a Cauchy constitutive relation

$$\begin{aligned} \hat{T}^s &= 2\mu_2 \hat{e}^s + \lambda_2 \mathrm{Tr}\,(\hat{e}^s)\,\hat{I} + A\,(\hat{e}^s)^2 \\ &+ B\mathrm{Tr}\left[(\hat{e}^s)^2\right]\hat{I} + C\,[\mathrm{Tr}\,(\hat{e}^s)]^2\,\hat{I} + D\hat{e}^s\mathrm{Tr}\,(\hat{e}^s) \end{aligned} \tag{3.1}$$

randomly embedded in a linear matrix with stiffness tensor $\hat{\mathcal{C}}^{(1)}$ (moduli λ_1 and μ_1). We also introduce the bulk moduli $K_1 = \lambda_1 + \frac{2}{3}\mu_1$ and $K_2 = \lambda_2 + \frac{2}{3}\mu_2$. If needed, we can easily move to the Green elasticity by assuming $D = 2B$. We suppose that the volume fraction c of the embedded phase is small (dilute dispersion). Since the elastic interac-

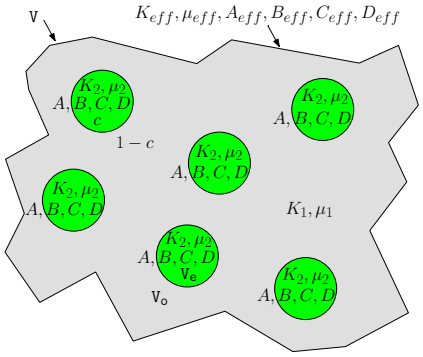

Figure 14: Scheme of a dispersion of nonlinear spheres embedded in a linear matrix

tions can be neglected, each sphere behaves as an isolated one under the effect of a remote load $\hat{T}^\infty = \hat{\mathcal{C}}^{(1)}\hat{e}^\infty$. The starting point for the

evaluation of the induced internal strain $\hat{\epsilon}^s$ is Eq.(2.89), which can be usefully rearranged as follows

$$\hat{\epsilon}^s - \hat{\mathcal{S}}\hat{\epsilon}^s + \hat{\mathcal{S}}\left(\hat{\mathcal{C}}^{(1)}\right)^{-1}\hat{T}^s = \hat{\epsilon}^\infty \tag{3.2}$$

Here, we have introduced the internal stress given by the relation $\hat{T}^s = \hat{\mathcal{C}}^{(2)}(\hat{\epsilon}^s)\,\hat{\epsilon}^s$. The result of the application of $\left(\hat{\mathcal{C}}^{(1)}\right)^{-1}$ over the stress tensor $\hat{T}^s$ can be easily written in explicit form

$$\left(\hat{\mathcal{C}}^{(1)}\right)^{-1}\hat{T}^s = \frac{1}{2\mu_1}\hat{T}^s - \frac{\lambda_1}{2\mu_1(2\mu_1+3\lambda_1)}\mathrm{Tr}\left(\hat{T}^s\right)\hat{I} \tag{3.3}$$

Moreover, the explicit expression of the Eshelby tensor for a sphere is reported in literature [68, 45]

$$\begin{aligned}\mathcal{S}_{ijkh} &= \frac{1}{15(1-\nu_1)}\left[\left(\delta_{ik}\delta_{jh}+\delta_{ih}\delta_{jk}\right)(4-5\nu_1)\right. \\ &+ \left.\delta_{kh}\delta_{ij}(5\nu_1-1)\right]\end{aligned} \tag{3.4}$$

We can evaluate the effect of $\mathcal{S}_{ijkh}$ over an arbitrary strain ϵ^s_{kh}, getting

$$\mathcal{S}_{ijkh}\epsilon^s_{kh} = \frac{2(4-5\nu_1)}{15(1-\nu_1)}\epsilon^s_{ij} + \frac{5\nu_1-1}{15(1-\nu_1)}\epsilon^s_{kk}\delta_{ij} \tag{3.5}$$

Now, the Poisson ratio ν_1 of the matrix can be written in terms of the bulk modulus K_1 and the shear modulus μ_1 according to Table 1, obtaining

$$\hat{\mathcal{S}}\hat{\epsilon}^s = \frac{6}{5}\frac{K_1+2\mu_1}{3K_1+4\mu_1}\hat{\epsilon}^s + \frac{1}{5}\frac{3K_1-4\mu_1}{3K_1+4\mu_1}\mathrm{Tr}\left(\hat{\epsilon}^s\right)\hat{I} \tag{3.6}$$

In order to find a single equation for the internal strain $\hat{\epsilon}^s$, we can substitute Eqs.(3.1), (3.3) and (3.6) in Eq.(3.2). A long algebraic calculation leads to the important equation

$$\begin{aligned}L\hat{\epsilon}^s &+ M\mathrm{Tr}\left(\hat{\epsilon}^s\right)\hat{I} + N\left(\hat{\epsilon}^s\right)^2 + O\hat{\epsilon}^s\mathrm{Tr}\left(\hat{\epsilon}^s\right) \\ &+ P\mathrm{Tr}\left[\left(\hat{\epsilon}^s\right)^2\right]\hat{I} + Q\left[\mathrm{Tr}\left(\hat{\epsilon}^s\right)\right]^2\hat{I} = \hat{\epsilon}^\infty\end{aligned} \tag{3.7}$$

which completely defines the internal strain induced in a nonlinear sphere by the uniform remote deformation $\hat{\epsilon}^\infty$. The parameters L, M, N, O, P and Q have been written in terms of the shear moduli, bulk moduli and nonlinear coefficients as follows

$$L = 1 + \frac{6}{5}\frac{K_1+2\mu_1}{3K_1+4\mu_1}\left(\frac{\mu_2}{\mu_1}-1\right) \tag{3.8}$$

$$\begin{aligned}M &= \frac{1}{5(3K_1+4\mu_1)} \\ &\times \left[5K_2 - K_1\left(3+2\frac{\mu_2}{\mu_1}\right) - 4(\mu_2-\mu_1)\right]\end{aligned} \tag{3.9}$$

$$N = \frac{3}{5}\frac{A}{\mu_1}\frac{K_1+2\mu_1}{3K_1+4\mu_1} \tag{3.10}$$

$$O = \frac{3}{5}\frac{D}{\mu_1}\frac{K_1+2\mu_1}{3K_1+4\mu_1} \tag{3.11}$$

$$P = \frac{1}{15(3K_1+4\mu_1)}\left[15B - A\left(1+3\frac{K_1}{\mu_1}\right)\right] \tag{3.12}$$

$$Q = \frac{1}{15(3K_1+4\mu_1)}\left[15C - D\left(1+3\frac{K_1}{\mu_1}\right)\right] \tag{3.13}$$

At this point we take into consideration the actual dispersion of spheres. We define V as the total volume of the composite material, V_e as the volume corresponding to the spheres and V_o as the volume of the matrix ($V = V_o \cup V_e$, see Fig.14). Since we are working under the hypothesis of small volume fraction c, we can consider the average value of the strain in the matrix equal to the externally applied strain $\hat{\varepsilon}^\infty$. Therefore, the average value of the strain in the overall system is given by

$$\langle \hat{\varepsilon} \rangle = c\hat{\varepsilon}^s + (1-c)\hat{\varepsilon}^\infty \tag{3.14}$$

On the other hand, the average value of the stress over the entire structure can be calculated as follows

$$\begin{aligned}
\langle \hat{T} \rangle &= \frac{1}{V}\int_V \hat{T}dv = \frac{1}{V}\hat{\mathcal{C}}^{(1)}\int_{V_o}\hat{\varepsilon}dv + \frac{1}{V}\int_{V_e}\hat{T}dv \\
&= \frac{1}{V}\hat{\mathcal{C}}^{(1)}\int_{V_o}\hat{\varepsilon}dv + \frac{1}{V}\int_{V_e}\hat{T}dv \\
&\quad + \frac{1}{V}\hat{\mathcal{C}}^{(1)}\int_{V_e}\hat{\varepsilon}dv - \frac{1}{V}\hat{\mathcal{C}}^{(1)}\int_{V_e}\hat{\varepsilon}dv \\
&= \frac{1}{V}\hat{\mathcal{C}}^{(1)}\int_V \hat{\varepsilon}dv + \frac{1}{V}\left[\int_{V_e}\hat{T}dv + \hat{\mathcal{C}}^{(1)}\int_{V_e}\hat{\varepsilon}dv\right] \\
&= \hat{\mathcal{C}}^{(1)}\langle\hat{\varepsilon}\rangle + c\left[\hat{T}^s - \hat{\mathcal{C}}^{(1)}\hat{\varepsilon}^s\right]
\end{aligned} \tag{3.15}$$

In order to obtain the macroscopic characterization of the material, we search for the relationship between $\langle\hat{T}\rangle$ and $\langle\hat{\varepsilon}\rangle$, given in Eqs.(3.14) and (3.15), respectively.

By substituting Eq.(3.7) in Eq.(3.14), we obtain the average strain $\langle\hat{\varepsilon}\rangle$ in terms of the internal strain $\hat{\varepsilon}^s$

$$\begin{aligned}
\langle\hat{\varepsilon}\rangle &= [c + (1-c)L]\,\hat{\varepsilon}^s \\
&+ (1-c)\left\{M\mathrm{Tr}(\hat{\varepsilon}^s)\hat{I} + N(\hat{\varepsilon}^s)^2\right. \\
&+ \left. O\hat{\varepsilon}^s\mathrm{Tr}(\hat{\varepsilon}^s) + P\mathrm{Tr}\left[(\hat{\varepsilon}^s)^2\right]\hat{I} + Q[\mathrm{Tr}(\hat{\varepsilon}^s)]^2\hat{I}\right\}
\end{aligned} \tag{3.16}$$

and by substituting the constitutive relations in Eq.(3.15), we obtain the average stress $\langle\hat{T}\rangle$ in terms of $\hat{\varepsilon}^s$

$$\begin{aligned}
\langle\hat{T}\rangle &= 2\mu_1\langle\hat{\varepsilon}\rangle + \left(K_1 - \frac{2}{3}\mu_1\right)\mathrm{Tr}\langle\hat{\varepsilon}\rangle\hat{I} \\
&+ c\{2(\mu_2-\mu_1)\hat{\varepsilon}^s \\
&+ \left[K_2 - K_1 - \frac{2}{3}(\mu_2-\mu_1)\right]\mathrm{Tr}(\hat{\varepsilon}^s)\hat{I} \\
&+ A(\hat{\varepsilon}^s)^2 + B\mathrm{Tr}\left[(\hat{\varepsilon}^s)^2\right]\hat{I} \\
&+ C[\mathrm{Tr}(\hat{\varepsilon}^s)]^2\hat{I} + D\hat{\varepsilon}^s\mathrm{Tr}(\hat{\varepsilon}^s)\Big\}
\end{aligned} \tag{3.17}$$

The last two expressions, although in implicit form, define the macroscopic contitutive equation relating $\langle\hat{T}\rangle$ and $\langle\hat{\varepsilon}\rangle$. In fact, we may obtain $\hat{\varepsilon}^s$ in terms of $\langle\hat{\varepsilon}\rangle$ from Eq.(3.16) and this result can be replaced in Eq.(3.17), leading to the final characterization. In order to follow this scheme, we rewrite Eq.(3.16) in a simpler form

$$\begin{aligned}
\langle\hat{\varepsilon}\rangle &= L'\hat{\varepsilon}^s + M'\mathrm{Tr}(\hat{\varepsilon}^s)\hat{I} + N'(\hat{\varepsilon}^s)^2 \\
&+ O'\hat{\varepsilon}^s\mathrm{Tr}(\hat{\varepsilon}^s) + P'\mathrm{Tr}\left[(\hat{\varepsilon}^s)^2\right]\hat{I} + Q'[\mathrm{Tr}(\hat{\varepsilon}^s)]^2\hat{I}
\end{aligned} \tag{3.18}$$

where we have used the definitions

$$L' = c + (1-c)\,L \tag{3.19}$$
$$M' = (1-c)M \tag{3.20}$$
$$N' = (1-c)N \tag{3.21}$$
$$O' = (1-c)O \tag{3.22}$$
$$P' = (1-c)P \tag{3.23}$$
$$Q' = (1-c)Q \tag{3.24}$$

Starting from Eq.(3.18), we can straightforwardly calculate the quantities $\mathrm{Tr}\,\langle\hat{e}\rangle$, $\langle\hat{e}\rangle^2$, $\langle\hat{e}\rangle\,\mathrm{Tr}\,\langle\hat{e}\rangle$, $\mathrm{Tr}\left(\langle\hat{e}\rangle^2\right)$ and $[\mathrm{Tr}\,\langle\hat{e}\rangle]^2$ in terms of the internal strain $\hat{e}^s$ (by using the relation $\mathrm{Tr}(\hat{I}) = 3$). These set of relations can be written neglecting the terms of order greater than two in $\hat{e}^s$, since we are interested in the characterization of the nonlinear elastic properties of the dispersion up to the second order. Therefore, this set of equations can be arranged in a matrix form, as follows

$$\tilde{U}\begin{bmatrix} \hat{e}^s \\ \mathrm{Tr}\,(\hat{e}^s)\,\hat{I} \\ (\hat{e}^s)^2 \\ \hat{e}^s\mathrm{Tr}\,(\hat{e}^s) \\ \mathrm{Tr}\left[(\hat{e}^s)^2\right]\hat{I} \\ [\mathrm{Tr}\,(\hat{e}^s)]^2\,\hat{I} \end{bmatrix} = \begin{bmatrix} \langle\hat{e}\rangle \\ \mathrm{Tr}\,\langle\hat{e}\rangle\,\hat{I} \\ \langle\hat{e}\rangle^2 \\ \langle\hat{e}\rangle\,\mathrm{Tr}\langle\hat{e}\rangle \\ \mathrm{Tr}\left[\langle\hat{e}\rangle^2\right]\hat{I} \\ [\mathrm{Tr}\,\langle\hat{e}\rangle]^2\,\hat{I} \end{bmatrix} \tag{3.25}$$

The elements of the matrix $\tilde{U}$ have been written in terms of the parameters defined in Eqs.(3.19)-(3.24)

$$\tilde{U} = \begin{bmatrix} L' & M' & N' & O' & P' & Q' \\ 0 & L'+3M' & 0 & 0 & N'+3P' & O'+3Q' \\ 0 & 0 & L'^2 & 2L'M' & 0 & M'^2 \\ 0 & 0 & 0 & L'(L'+3M') & 0 & M'(L'+3M') \\ 0 & 0 & 0 & 0 & L'^2 & M'(2L'+3M') \\ 0 & 0 & 0 & 0 & 0 & (L'+3M')^2 \end{bmatrix} \tag{3.26}$$

Finally, by using Eq.(3.17) and by inverting Eq.(3.25), we may obtain the matrix form of the complete constitutive relation

$$\langle \hat{T} \rangle = \left(c \begin{bmatrix} 2(\mu_2 - \mu_1) \\ K_2 - K_1 - \frac{2}{3}(\mu_2 - \mu_1) \\ A \\ D \\ B \\ C \end{bmatrix}^T \tilde{U}^{-1} \right. \tag{3.27}$$

$$\left. + \begin{bmatrix} 2\mu_1 \\ K_1 - \frac{2}{3}\mu_1 \\ 0 \\ 0 \\ 0 \\ 0 \end{bmatrix}^T \right) \begin{bmatrix} \langle \hat{e} \rangle \\ \mathrm{Tr}\langle \hat{e} \rangle \hat{I} \\ \langle \hat{e} \rangle^2 \\ \langle \hat{e} \rangle \mathrm{Tr}\langle \hat{e} \rangle \\ \mathrm{Tr}\left(\langle \hat{e} \rangle^2 \right) \hat{I} \\ [\mathrm{Tr}\langle \hat{e} \rangle]^2 \hat{I} \end{bmatrix} \tag{3.28}$$

The constitutive equation in the form of Eq.(3.28) can be written in terms of the effective linear and nonlinear elastic moduli as follows

$$\begin{aligned} \langle \hat{T} \rangle &= 2\mu_{eff} \langle \hat{e} \rangle + \left(K_{eff} - \frac{2}{3}\mu_{eff} \right) \mathrm{Tr}\langle \hat{e} \rangle \hat{I} \\ &+ A_{eff} \langle \hat{e} \rangle^2 + B_{eff} \mathrm{Tr}\left[\langle \hat{e} \rangle^2 \right] \hat{I} \\ &+ C_{eff} [\mathrm{Tr}\langle \hat{e} \rangle]^2 \hat{I} + D_{eff} \langle \hat{e} \rangle \mathrm{Tr}\langle \hat{e} \rangle \end{aligned} \tag{3.29}$$

As for the linear elastic moduli, we obtain

Effective linear elastic moduli for a dispersion of spheres

$$\mu_{eff} = \mu_1 + c\frac{\mu_2 - \mu_1}{L'} \tag{3.30}$$

$$K_{eff} = K_1 + c\frac{K_2 - K_1}{L' + 3M'} \tag{3.31}$$

and, as for the nonlinear elastic moduli, we have

Effective nonlinear elastic moduli for a dispersion of spheres

$$A_{eff} = c\frac{A}{L'^2} - 2c\frac{N'(\mu_2 - \mu_1)}{L'^3} \tag{3.32}$$

$$\begin{aligned} B_{eff} &= 2c\frac{(N'M' - L'P')(\mu_2 - \mu_1)}{L'^3 (L' + 3M')} + \\ &- c\frac{(N' + 3P')\left[K_2 - K_1 - \frac{2}{3}(\mu_2 - \mu_1)\right]}{L'^2 (L' + 3M')} + c\frac{B}{L'^2} \end{aligned} \tag{3.33}$$

$$\begin{aligned} C_{eff} &= \frac{1}{9}\frac{c\,(9C+3B+3D+A)}{(L'+3M')^2}+\frac{1}{9}\frac{c\,(A-3B)}{L'^2} \\ &- \frac{4}{9}\frac{N'\,(\mu_2-\mu_1)\,c}{L'^3}-\frac{1}{9}\frac{c\,(3D+2A)}{L'\,(L'+3M')} \\ &+ \frac{1}{9}\frac{c(4N'+6O')(\mu_2-\mu_1)}{L'^2\,(L'+3M')} \\ &+ \frac{1}{9}\frac{c(3N'+9P')(K_2-K_1)}{L'^2\,(L'+3M')} \\ &- \frac{1}{3}\frac{c(9Q'+3O'+3P'+N')(K_2-K_1)}{(L'+3M')^3} \end{aligned} \tag{3.34}$$

$$\begin{aligned} D_{eff} &= 2c\frac{(2N'M'-L'O')\,(\mu_2-\mu_1)}{L'^3\,(L'+3M')} \\ &- 2c\frac{M'A}{L'^2\,(L'+3M')}+c\frac{D}{L'\,(L'+3M')} \end{aligned} \tag{3.35}$$

If we use the definitions of the parameters L' and M', given in Eqs.(3.19) and (3.20), we obtain for the effective shear and bulk moduli the explicit expressions

$$\mu_{eff}=\mu_1+c\frac{\mu_2-\mu_1}{c+(1-c)\left[1+\frac{6}{5}\left(\frac{\mu_2}{\mu_1}-1\right)\frac{K_1+2\mu_1}{3K_1+4\mu_1}\right]} \tag{3.36}$$

$$K_{eff}=K_1+\frac{(3K_1+4\mu_1)\,(K_2-K_1)\,c}{3K_2+4\mu_1-3c(K_2-K_1)} \tag{3.37}$$

These two expressions are coincident with those obtained for a linear dispersion of elastic spheres [69]. However, they are completed by Eqs.(3.32)-(3.35) in order to characterize the nonlinear properties of the mixture. These expressions are a generalization[125] of those presented in recent literature, obtained within the framework of the Green elasticity [87].

3.2.2 *Properties of the dispersion of spheres*

The set of results obtained in the previous Section for the effective moduli of a dispersion of nonlinear spheres fulfills a series of important general properties:

1. Eqs.(3.32)-(3.37) are also true for $c = 1$; in this case (very high volume fraction of spheres) the procedure is not expected to be valid but nonetheless the results appears to be exact (if $c = 1$ then $\mu_{eff} = \mu_2$, $K_{eff} = K_2$, $A_{eff} = A$, $B_{eff} = B$, $C_{eff} = C$, $D_{eff} = D$).

Universal mixing scheme

2. The nonlinear elastic moduli A, B, C and D influence the effective nonlinear moduli of the composite material following the universal scheme showed in Fig.15. Therefore, there is a complicated mixing of the nonlinear elastic modes induced by the heterogeneity of the structure. The results for the nonlinear effective parameters, obtained with a single coefficient (A, B, C or D) different from zero, are reported in Appendix A.3 , in form of series expansions in the volume fraction up to the first order. They are coherent with the scheme shown in Fig.15.

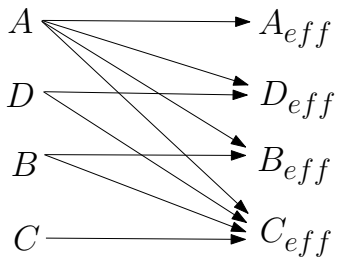

Figure 15: Mixing scheme for the nonlinear modes

3. If the linear elastic moduli of the matrix and of the spheres are the very same ($K_1 = K_2$ and $\mu_1 = \mu_2$), we simply obtain $K_{eff} = K_1$, $\mu_{eff} = \mu_1$ and the following special set of results for the nonlinear components

$$A_{eff} = cA \tag{3.38}$$
$$B_{eff} = cB \tag{3.39}$$
$$C_{eff} = cC \tag{3.40}$$
$$D_{eff} = cD \tag{3.41}$$

It means that the nonlinearity of the overall system is simply proportional to the nonlinearity of the spheres.

4. We have developed our procedure under the hypotesis of Cauchy nonlinear elasticity for the spheres embedded in the linear matrix. If we let $D = 2B$ we move from the Cauchy elasticity to the Green elasticity, assuming the existence of a strain energy function for the inhomogeneities. It is important to remark that the following property holds: if $D = 2B$ then the relation $D_{eff} = 2B_{eff}$ is true for the effective nonlinear moduli. It can be verified by direct calculation and it means that our approach is perfectly consistent with the energy balance of the composite material. In other words, we have verified that if a strain energy function exists for the embedded spheres, then an overall strain energy function exists for the whole composite structure.

From Cauchy elasticity to Green elasticity

5. If we consider the special value of the Poisson ratio $\nu_1 = \nu_2 = 1/5$ (both for the matrix and the spheres) and different values for the Young moduli $E_1 \neq E_2$, we obtain another interesting result: the effective Poisson ratio assume the same value $\nu_{eff} = 1/5$, the effective Young modulus E_{eff} assumes the value

Special value of the Poisson ratio $\nu = 1/5$

$$E_{eff} = \frac{E_1(1-c) + E_2(1+c)}{E_1(1+c) + E_2(1-c)} E_1 \tag{3.42}$$

and the effective nonlinear elastic moduli can be calculated as follows

$$X_{eff} = \frac{8E_1^3 c}{[E_1(1+c) + E_2(1-c)]^3} X \tag{3.43}$$

where the symbol X represents any modulus A, B, C or D (the four effective parameters exhibit the same behavior). Therefore, we can

say that the special value $\nu_1 = \nu_2 = 1/5$ uncouples the behavior of the nonlinear elastic modes (described at the point 2), generating a direct correspondence among the nonlinear moduli of the spheres and the effective nonlinear moduli. Furthermore, if we add the condition $E_1 = E_2$, we get back to the point 3. The special value 1/5 for the Poisson ratio comes out in several issues considering a dispersion of spheres. For example, for linear porous materials (with spherical pores) and for linear dispersions of rigid spheres the value 1/5 is a fixed points for the Poisson ratio: if $\nu_1 = 1/5$, then we have $\nu_{eff} = 1/5$ for all spheres concentrations [74, 126]. Moreover, there is another interesting behaviour of the effective Poisson ratio for high volume fraction of pores or rigid spheres: in both cases for $c \to 1$ the effective Poisson ratio converges to the fixed value $\nu_{eff} = 1/5$, irrespective of the matrix Poisson ratio [74, 126].

Incompressible inhomogeneities

6. Finally, we analyze the properties of the dispersion when incompressible material is utilized for the embedded spheres: the constitutive relation Eq.(3.1) describes an incompressible medium in the limit $\lambda_2 \to \infty$ (or, equivalently, $K_2 \to \infty$ since $K_2 = \lambda_2 + 2\mu_2/3$); by inverting Eq.(3.1), writing the strain tensor in terms of the stress tensor and performing such a limit, we obtain (up to the second order)

$$\begin{aligned} \hat{\epsilon}^s &= \frac{1}{2\mu_2}\hat{T}^s - \frac{1}{6\mu_2}\mathrm{Tr}\left(\hat{T}^s\right)\hat{I} - \frac{A}{8\mu_2^3}\left(\hat{T}^s\right)^2 \\ &+ \frac{A}{24\mu_2^3}\mathrm{Tr}\left[\left(\hat{T}^s\right)^2\right]\hat{I} - \frac{A}{36\mu_2^3}\left[\mathrm{Tr}\left(\hat{T}^s\right)\right]^2\hat{I} \\ &+ \frac{A}{12\mu_2^3}\hat{T}^s\mathrm{Tr}\left(\hat{T}^s\right) \end{aligned} \tag{3.44}$$

which describes a nonlinear isotropic and incompressible material. We remark that only the nonlinear modulus A intervenes in defining such a constitutive equation and that Eq.(3.44) imposes $\mathrm{Tr}\left(\hat{\epsilon}^s\right) = 0$, as requested by the incompressibility. In this limiting condition, as for the effective linear moduli, we observe that Eq.(3.36) for μ_{eff} remains unchanged and Eq.(3.37) leads to

$$K_{eff} = K_1 + \left(K_1 + \frac{4}{3}\mu_1\right)\frac{c}{1-c} \tag{3.45}$$

On the other hand, the nonlinear elastic moduli have been eventually found as

$$A_{eff} = 125A\theta \tag{3.46}$$

$$B_{eff} = -\frac{125}{3}A\theta \tag{3.47}$$

$$C_{eff} = \frac{250}{9}A\theta \tag{3.48}$$

$$D_{eff} = -\frac{250}{3}A\theta \tag{3.49}$$

where

$$\theta = \frac{c\left(3K_1 + 4\mu_1\right)^3\mu_1^3}{\psi^3} \tag{3.50}$$

$$\begin{aligned} \psi &= 6\left(K_1 + 2\mu_1\right)\left[c\mu_1 + (1-c)\mu_2\right] \\ &+ \mu_1\left(9K_1 + 8\mu_1\right) \end{aligned} \tag{3.51}$$

One can observe that, as expected, the effective nonlinear elastic moduli depend only on the modulus A describing the nonlinearity of the spheres, as shown in Eq.(3.44). Moreover, we remark that a single modulus A for the spheres can generate four different effective nonlinear moduli, as predicted by the scheme in Fig.15.

To conclude we present some numerical results obtained by the implementation of Eqs.(3.32)-(3.37). In Fig. 16 we have considered Green nonlinear elasticity and the mixture parameters: $\mu_1 = 1, \mu_2 = 4, K_1 = 7, K_2 = 1, A = 2, B = 3, C = 5, D = 2B$ in arbitrary units. In Fig. 17 we have considered Cauchy nonlinear elasticity and the mixture parameters: $\mu_1 = 1, \mu_2 = 4, K_1 = 10, K_2 = 1, A = 2, B = -3, C = -5, D = 4$ in arbitrary units. The results have been presented in terms

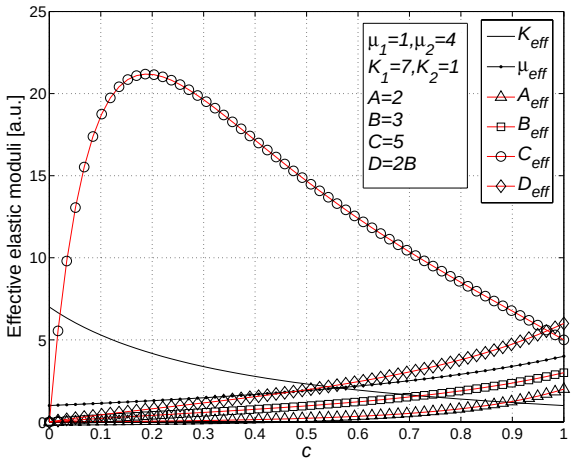

Figure 16: Linear and nonlinear effective elastic moduli of a dispersion of spheres in terms of the volume fraction c. We have used the values $\mu_1 = 1, \mu_2 = 4, K_1 = 7, K_2 = 1, A = 2, B = 3, C = 5, D = 2B$ in arbitrary units.

of the volume fraction c of the spheres. In both cases we may observe a consistent amplification of the nonlinear effective modulus C_{eff}. We have verified that such a phenomenon is always exhibited when $K_1 \gg K_2$ (i.e. when the matrix is much more incompressible than the spheres) and that the higher values of C_{eff} appear for small values of the volume fraction c, belonging to the range of applicability of the present theory.

As it is well known, simple limitations for the values of the linear effective moduli are well established

Voigt and Reuss bounds

$$\frac{1}{\frac{1-c}{K_1}+\frac{c}{K_2}} \leqslant K_{eff} \leqslant (1-c)K_1 + cK_2 \tag{3.52}$$

$$\frac{1}{\frac{1-c}{\mu_1}+\frac{c}{\mu_2}} \leqslant \mu_{eff} \leqslant (1-c)\mu_1 + c\mu_2 \tag{3.53}$$

The lower bounds in Eqs.(3.52) and (3.53) are referred to as the Voigt bounds, and the upper bounds are designated as the Reuss bounds [111]. Unfortunately, these bounds are of no practical value, but more refined bounds, with realistic applications, have been derived by Hashin and Shtrikman [100]. From our numerical results, shown in Figs.16 and

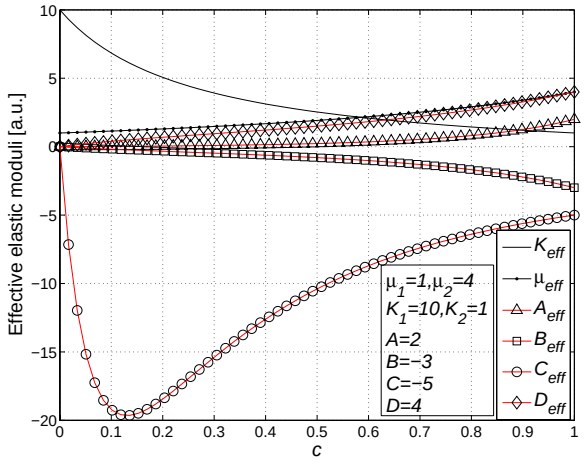

Figure 17: Linear and nonlinear effective elastic moduli of a dispersion of spheres in terms of the volume fraction c. We have used the values $\mu_1 = 1, \mu_2 = 4, K_1 = 10, K_2 = 1, A = 2, B = -3, C = -5, D = 4$ in arbitrary units

17, we may observe that the nonlinear properties, contrarily to the linear ones, are not bounded by some given values, exhibiting, in certain conditions, a strong amplification leading to nonlinear effective moduli much greater than those of the constituents. This point is important in the topic of designing materials with desired properties and functions.

3.3 DISPERSION OF PARALLEL CYLINDRICAL INCLUSIONS

3.3.1 *Effective elastic moduli*

We take now into consideration an assembly of parallel cylinders, as represented in Fig.18, described by an arbitrary Cauchy constitutive relation (see Eq.(3.1)). As before, when needed, we can easily move to the Green elasticity by assuming $D = 2B$. The cylindrical inhomogeneities are randomly embedded in a linear matrix with elastic moduli K_1 and μ_1. This is a simple but complete way for modeling a nonlinear fibrous material. In earlier works the linear analysis for a parallel distribution of fibres has been developed by means of the Eshelby methodology and of the differential effective medium theory [73, 127]. Moreover, the mechanical response of elastic and inelastic fibre-strengthened materials has been investigated, also with self-consistent models [128, 129, 130]. Here, in order to deal with the nonlinear properties, we suppose that the volume fraction c of the embedded phase is small (dilute dispersion). It means that each cylinder can be considered isolated in the space (non interacting with other inhomogeneities) and subjected to the same external loading. In order to simplify the modeling and considering that the system shows a transverse isotropic symmetry (otherwise said uniaxial symmetry), we assume the plane strain condition on an arbitrary plane π (see Fig.18) orthogonal to the cylinders. It means that we are dealing with a problem belonging to the two-dimensional elasticity. Moreover, in plain strain condition, it is a common choice to introduce the two dimensional elastic moduli (see Section 1.2.1)

Two-dimensional elasticity approach

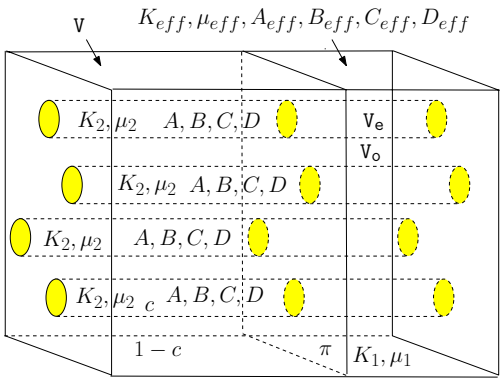

Figure 18: Scheme of a dispersion of nonlinear parallel cylinders embedded in a linear matrix

$\mu^{2D} = \mu$ and $K^{2D} = K + \mu/3$, where K and μ are the customarily used three-dimensional moduli [127]. Throughout this Section we indicate for brevity K and μ alluding to the two-dimensional version of the elastic moduli. It means that the linear matrix is described by

$$\hat{T} = 2\mu_1 \hat{e} + (K_1 - \mu_1)\,\mathrm{Tr}\,(\hat{e})\,\hat{I} \tag{3.54}$$

and the cylindrical inhomogeneities are described by the Cauchy constitutive relation

$$\begin{aligned} \hat{T}^s &= 2\mu_2 \hat{e}^s + (K_2 - \mu_2)\,\mathrm{Tr}\,(\hat{e}^s)\,\hat{I} + A\,(\hat{e}^s)^2 \\ &+ B\mathrm{Tr}\left[(\hat{e}^s)^2\right]\hat{I} + C\,[\mathrm{Tr}\,(\hat{e}^s)]^2\,\hat{I} + D\hat{e}^s\mathrm{Tr}\,(\hat{e}^s) \end{aligned} \tag{3.55}$$

where any strain or stress tensor is represented by a square matrix of order two, working in the framework of the two-dimensional elasticity. Now, we remark that Eq.(2.89) or, equivalently, Eq.(3.2) are correct for any geometry and, therefore, they can be directly used in the present analysis. Nevertheless, in order to use Eq.(3.2) we need to consider some ingredients: the result of the application of the compliance tensor of the matrix on the stress tensor $\hat{T}^s$ can be written as

$$\left(\hat{\mathcal{C}}^{(1)}\right)^{-1}\hat{T}^s = \frac{1}{2\mu_1}\hat{T}^s - \frac{K_1 - \mu_1}{4\mu_1 K_1}\mathrm{Tr}\left(\hat{T}^s\right)\hat{I} \tag{3.56}$$

Moreover, the effect of the Eshelby tensor $\hat{S}$ for a cylinder over an arbitrary strain tensor $\hat{e}^s$ is given by [45]

$$\hat{S}\hat{e}^s = \frac{1}{2}\frac{K_1 + 2\mu_1}{K_1 + \mu_1}\hat{e}^s + \frac{1}{4}\frac{K_1 - 2\mu_1}{K_1 + \mu_1}\mathrm{Tr}\,(\hat{e}^s)\,\hat{I} \tag{3.57}$$

Now, in order to obtain a single equation for the internal strain $\hat{e}^s$, we can substitute Eqs.(3.55), (3.56) and (3.57) in the starting Eq.(3.2). A tedious calculation leads to the equation

$$\begin{aligned} L\hat{e}^s &+ M\mathrm{Tr}\,(\hat{e}^s)\,\hat{I} + N\,(\hat{e}^s)^2 + O\hat{e}^s\mathrm{Tr}\,(\hat{e}^s) \\ &+ P\mathrm{Tr}\left[(\hat{e}^s)^2\right]\hat{I} + Q\,[\mathrm{Tr}\,(\hat{e}^s)]^2\,\hat{I} = \hat{e}^\infty \end{aligned} \tag{3.58}$$

which completely defines the internal strain induced in a nonlinear cylinder by the uniform externally applied deformation $\hat{e}^{\infty}$. The parameters L, M, N, O, P and Q have been defined as

$$L = 1+\frac{1}{2}\frac{K_1+2\mu_1}{K_1+\mu_1}\left(\frac{\mu_2}{\mu_1}-1\right) \tag{3.59}$$

$$M = \frac{1}{4(K_1+\mu_1)} \tag{3.60}$$
$$\times \left[2K_2-K_1\left(1+\frac{\mu_2}{\mu_1}\right)-2(\mu_2-\mu_1)\right]$$

$$N = \frac{A}{4\mu_1}\frac{K_1+2\mu_1}{K_1+\mu_1} \tag{3.61}$$

$$O = \frac{D}{4\mu_1}\frac{K_1+2\mu_1}{K_1+\mu_1} \tag{3.62}$$

$$P = \frac{1}{8(K_1+\mu_1)}\left(4B-A\frac{K_1}{\mu_1}\right) \tag{3.63}$$

$$Q = \frac{1}{8(K_1+\mu_1)}\left(4C-D\frac{K_1}{\mu_1}\right) \tag{3.64}$$

We follow a procedure similar to that described in Section 4. We use again Eqs.(3.15) and (3.18) for the average values of the stress and the strain over the whole composite material. At this point, starting from Eq.(3.18), we obtain the system given in Eq.(3.25) (by using the two-dimensional relation $\mathrm{Tr}(\hat{I})=2$). It is defined by the matrix $\tilde{U}$ where the elements depend on the parameters defined in Eqs.(3.19)-(3.24) and calculated by means of Eqs.(3.59)-(3.64)

$$\tilde{U} = \begin{bmatrix} L' & M' & N' & O' & P' & Q' \\ 0 & L'+2M' & 0 & 0 & N'+2P' & O'+2Q' \\ 0 & 0 & L'^2 & 2L'M' & 0 & M'^2 \\ 0 & 0 & 0 & L'(L'+2M') & 0 & M'(L'+2M') \\ 0 & 0 & 0 & 0 & L'^2 & 2M'(L'+M') \\ 0 & 0 & 0 & 0 & 0 & (L'+2M')^2 \end{bmatrix} \tag{3.65}$$

Finally, by inverting Eq.(3.25), we may obtain the matrix form of the complete constitutive relation

$$\langle\hat{T}\rangle = \left(c \begin{bmatrix} 2(\mu_2-\mu_1) \\ K_2-K_1-(\mu_2-\mu_1) \\ A \\ D \\ B \\ C \end{bmatrix}^T \tilde{U}^{-1} + \begin{bmatrix} 2\mu_1 \\ K_1-\mu_1 \\ 0 \\ 0 \\ 0 \\ 0 \end{bmatrix}^T \right) \begin{bmatrix} \langle\hat{e}\rangle \\ \mathrm{Tr}\langle\hat{e}\rangle\hat{I} \\ \langle\hat{e}\rangle^2 \\ \langle\hat{e}\rangle \mathrm{Tr}\langle\hat{e}\rangle \\ \mathrm{Tr}\left(\langle\hat{e}\rangle^2\right)\hat{I} \\ [\mathrm{Tr}\langle\hat{e}\rangle]^2\hat{I} \end{bmatrix} \tag{3.66}$$

The constitutive equation in the form of Eq.(3.66) can be written in terms of the effective linear and nonlinear elastic moduli as follows

$$\begin{aligned} \langle\hat{T}\rangle &= 2\mu_{eff}\langle\hat{e}\rangle + (K_{eff}-\mu_{eff})\,\mathrm{Tr}\langle\hat{e}\rangle\hat{I} \\ &+ A_{eff}\langle\hat{e}\rangle^2 + B_{eff}\mathrm{Tr}\left[\langle\hat{e}\rangle^2\right]\hat{I} \\ &+ C_{eff}\,[\mathrm{Tr}\langle\hat{e}\rangle]^2\,\hat{I} + D_{eff}\langle\hat{e}\rangle\mathrm{Tr}\langle\hat{e}\rangle \end{aligned} \tag{3.67}$$

As for the linear elastic moduli, we obtain

Effective linear moduli of a dispersion of a dispersion of cylinders

$$\begin{aligned} \mu_{eff} &= \mu_1 + c\frac{\mu_2-\mu_1}{L'} \\ &= \mu_1 + c\frac{\mu_2-\mu_1}{c+(1-c)\left[1+\frac{1}{2}\left(\frac{\mu_2}{\mu_1}-1\right)\frac{K_1+2\mu_1}{K_1+\mu_1}\right]} \end{aligned} \tag{3.68}$$

$$\begin{aligned} K_{eff} &= K_1 + c\frac{K_2-K_1}{L'+2M'} \\ &= K_1 + c\frac{K_2-K_1}{c+(1-c)\frac{\mu_1+K_2}{\mu_1+K_1}} \end{aligned} \tag{3.69}$$

It is important to remember that the bulk modulus K_{eff} represents the two-dimensional version, as above defined. Moreover, the two linear results given in Eqs.(3.68) and (3.69) are perfectly coincident with earlier literature [76]. As for the effective nonlinear elastic moduli, we have the following results

Effective nonlinear moduli of a dispersion of a dispersion of cylinders

$$A_{eff} = \frac{Ac}{L'^2} - 2c\frac{N'(\mu_2-\mu_1)}{L'^3} \tag{3.70}$$

$$\begin{aligned} B_{eff} &= \frac{c\,[N'(\mu_2-\mu_1)+BL']}{L'^3} \\ &- \frac{c\,(2P'+N')\,(K_2-K_1)}{L'^2\,(L'+2M')} \end{aligned} \tag{3.71}$$

$$
\begin{aligned}
C_{eff} &= c\frac{4C+2B+2D+A}{4\left(L'+2M'\right)^2}+c\frac{A-2B}{4L'^2} \\
&+ c\frac{2\left(O'+N'\right)\left(\mu_2-\mu_1\right)+\left(2P'+N'\right)\left(K_2-K_1\right)}{2L'^2\left(L'+2M'\right)} \\
&- \frac{c\left(2P'+N'+4Q'+2O'\right)\left(K_2-K_1\right)}{2\left(L'+2M'\right)^3} \\
&- \frac{cN'\left(\mu_2-\mu_1\right)}{L'^3}-c\frac{A+D}{2L'\left(L'+2M'\right)}
\end{aligned}
\tag{3.72}
$$

$$
\begin{aligned}
D_{eff} &= 2\frac{\left(2N'M'-L'O'\right)\left(\mu_2-\mu_1\right)c}{L'^3\left(L'+2M'\right)} \\
&- 2c\frac{M'A}{L'^2\left(L'+2M'\right)}+\frac{cD}{L'\left(L'+2M'\right)}
\end{aligned}
\tag{3.73}
$$

They represent the complete nonlinear characterization of the random dispersion of parallel cylinders.

3.3.2 *Properties of the dispersion of parallel cylinders*

It is interesting to observe that all the properties described in Section 3.2.2 for the dispersion of spheres (points 1-6) can be easily verified also for the present case. In particular, the scheme represented in Fig. 15 remains valid. In Appendix A.4 we have reported the explicit results giving the first order expansions of the nonlinear elastic moduli with respect of the volume fraction, corresponding to the simple cases where only one nonlinear parameter of the cylinders is different from zero. We analyze the case corresponding to the point 5 of Section 3.2.2: we consider the special value of the three-dimensional Poisson ratio $\nu_1=\nu_2=1/4$ (corresponding to the two-dimensional Poisson ratio $\nu_{2D}=\nu_{3D}/(1-\nu_{3D})=1/3$ [127]) and different values for the three-dimensional Young moduli $E_1\neq E_2$. In this case, the effective 3D Poisson ratio assume the value $\nu_{eff}=1/4$ and the effective 3D Young modulus E_{eff} assumes the value

$$
E_{eff}=\frac{E_1\left(1-c\right)+E_2\left(2+c\right)}{E_1\left(1+2c\right)+2E_2\left(1-c\right)}E_1 \tag{3.74}
$$

Moreover, the effective nonlinear elastic moduli can be calculated as follows

$$
X_{eff}=\frac{27E_1^3c}{\left[E_1\left(1+2c\right)+2E_2\left(1-c\right)\right]^3}X \tag{3.75}
$$

where the symbol X represents any modulus A, B, C or D (the four effective parameters exhibit the same behavior). Therefore, as before, we can say that the special value $\nu_1=\nu_2=1/4$ uncouples the behavior of the nonlinear elastic modes, generating a direct correspondence among the nonlinear moduli of the spheres and the effective nonlinear moduli.

Special value of the Poisson ratio $\nu=1/4$

Finally, we have numerically implemented Eqs.(3.68)-(3.73) in order to shown some explicit result. In Fig. 19 we have considered Green nonlinear elasticity and the mixture parameters: $\mu_1=1,\mu_2=5,K_1=10,K_2=1,A=-8,B=-2,C=-1,D=2B$ in arbitrary units. In Fig. 20 we have considered Cauchy nonlinear elasticity and the mixture parameters: $\mu_1=1,\mu_2=5,K_1=10,K_2=1,A=8,B=-2,C=-1,D=6$ in arbitrary units. As in the previous section, we may observe

a consistent amplification of the nonlinear effective modulus C_{eff}. We have also verified that such a phenomenon is exhibited when $K_1 \gg K_2$ (i.e. when the matrix is much more incompressible than the spheres) and that the higher values of C_{eff} appear for small values of the volume fraction c, belonging to the range of applicability of the present theory.

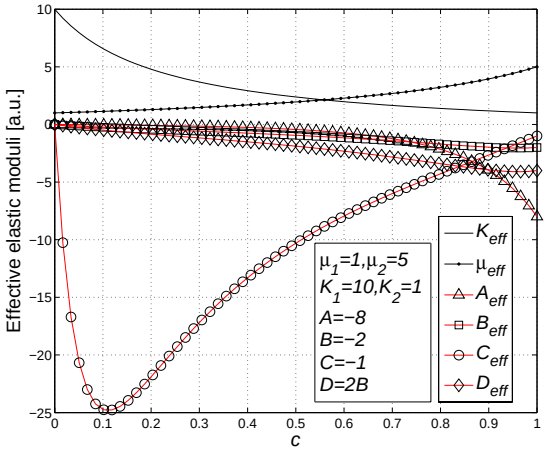

Figure 19: Linear and nonlinear effective elastic moduli for a dispersion of cylinders in terms of the volume fraction c. We have used the values $\mu_1 = 1, \mu_2 = 5, K_1 = 10, K_2 = 1, A = -8, B = -2, C = -1, D = 2B$ in arbitrary units

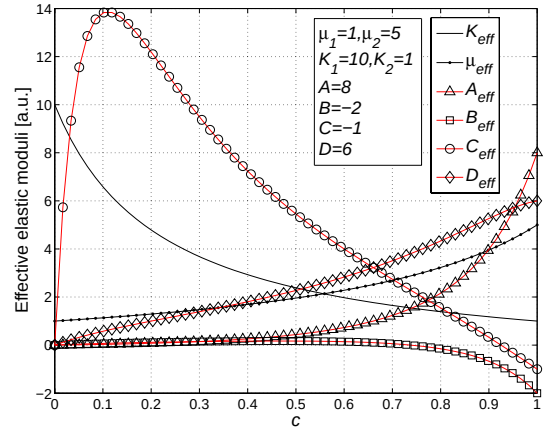

Figure 20: Linear and nonlinear effective elastic moduli for a dispersion of cylinders in terms of the volume fraction c. We have used the values $\mu_1 = 1, \mu_2 = 5, K_1 = 10, K_2 = 1, A = 8, B = -2, C = -1, D = 6$ in arbitrary units

Part II

ATOMISTIC SIMULATIONS

4 MICROSCOPIC THEORY OF ELASTICITY

Contents

In this Chapter we present an introduction to the atomistic theory of elasticity where the macroscopic elastic properties of a material are obtained by explicitly taking into account its atomic-scale structure and the fundamental interactions among its constituents. Although this subject has been widely investigated in the past [131], the connection between the continuum and the atomistic approach still remains a topic of crucial importance in modern materials science.

Firstly, we will show the connection between the macroscopic elastic moduli of a medium and the features of the interatomic potential describing the microscopic dynamics of the corresponding atom-resolved system. In particular, we will elaborate a general conceptual framework that can be used to generate improved force fields for applications in the realm of solid mechanics [132] (In Chapter 6 we will discuss a straightforward application of such a framework). In the second part of the Chapter we introduce some typical interaction potentials used in molecular dynamics simulations. Finally, we work out the complete theory for the calculation of the stress tensor at the atomic scale. We will discuss the calculation of the nonlinear elastic effects and we will address some important conceptual and technical issues which are tricky and often cause incorrect implementations of stress calculations.

4.1 MACROSCOPIC ELASTIC PROPERTIES OF ATOMISTIC MODELS

We develop an atomistic version of the elasticity theory for an isotropic and homogeneous material and we establish the minimum level of complexity that any microscopic model of atomic interactions must exploit in order to obtain results consistent with the continuum theory. In particular, we will examine two situations: a two-dimensional triangular lattice with two-body interactions and a two-dimensional triangular lattice with both two-body and three-body interactions. Such a case study is paradigmatic under two remarkably important standpoints. On one hand, the two-dimensional (perfect) triangular lattice is the only

The role of the microscopic interactions in predicting the macroscopic elastic behavior

(homogeneous) isotropic crystal structure; therefore, it represents the simplest crystalline counterpart of the continuum medium discussed in the previous Sections. On the other hand, by considering either a two-body or a more sophisticated force field we can understand the role of the microscopic interaction model in predicting elastic features. Anyway, we remark that our conclusions will be of general validity, although our arguments are developed for two-dimensional crystals only. We will prove that two-body force fields provide an elastic picture that is not consistent with continuum mechanics, because they describe the elastic behavior of the material with only one elastic modulus. On the contrary, force fields including both two-body and three-body interactions provide results in formal agreement with continuum elasticity theory, i.e., they predict the existence of two independent elastic constants.

4.1.1 *Atomistic interaction with central forces*

We begin by considering an arbitrary lattice of point masses that interact through simple central forces (two-body interaction), acting between nearest neighbors only. We focus on a pair of particles placed in positions $\vec{r}_1^{(0)}$ and $\vec{r}_2^{(0)}$ at equilibrium or, equivalently, in a configuration of minimum energy. If a small deformation is applied, the new positions will be given by

Atomistic displacement

$$\vec{r}_\alpha = \vec{r}_\alpha^{(0)} + \vec{u}\left(\vec{r}_\alpha^{(0)}\right) \tag{4.1}$$

where, according to Eq.(1.3), we have introduced the displacement vector field $\vec{u}\left(\vec{r}_\alpha^{(0)}\right)$ for any equilibrium lattice site. We further assume that the two-body interaction may be represented by an harmonic spring of constant k_s. If the particles in $\vec{r}_1$ and $\vec{r}_2$ are nearest neighbors, the force on the first particle due to the second one is

$$\vec{F}_1^{2B} = k_s \vec{n}\,(|\vec{r}_2 - \vec{r}_1| - l) \tag{4.2}$$

where $l = \left|\vec{r}_2^{(0)} - \vec{r}_1^{(0)}\right|$ is the equilibrium distance and $\vec{n}$ is the unit vector in the direction of the central force (see Fig.21 for details). This force corresponds to a two-body interaction potential energy $U^{2B} = (1/2)k_s\,(|\vec{r}_2 - \vec{r}_1| - l)^2$. By assuming slow variations of the displacement over the atomic scale (this is actually the case of deformations due to applied loads at the macroscale), we can expand this force up to the first order in the difference $\vec{u}\left(\vec{r}_2^{(0)}\right) - \vec{u}\left(\vec{r}_1^{(0)}\right)$. Then, writing

$$\vec{u}\left(\vec{r}_2^{(0)}\right) = \vec{u}\left(\vec{r}_1^{(0)}\right) + \left[\frac{\partial \vec{u}}{\partial \vec{r}}\right]\left(\vec{r}_2^{(0)} - \vec{r}_1^{(0)}\right) \tag{4.3}$$

we obtain

$$\vec{F}_1^{2B} = k_s\, l\, \vec{n}\left(\vec{n} \cdot \left[\frac{\partial \vec{u}}{\partial \vec{r}}\right] \vec{n}\right) \tag{4.4}$$

Finally, defining the strain tensor as in Eq.(1.7), we find

$$\vec{F}_1^{2B} = k_s\, l\, \vec{n}\,(\vec{n} \cdot \hat{\epsilon}\, \vec{n}) \tag{4.5}$$

This is the force acting on a given particle caused by a neighboring atom, placed at distance l and aligned in direction $\vec{n}$, when the local

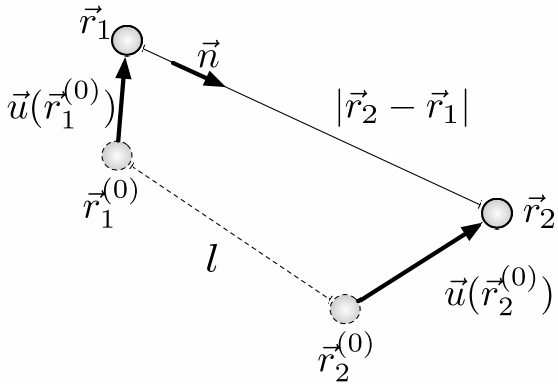

Figure 21: Displacement ($\vec{u}$) and distance ($\vec{r}$) vectors for a pair of atoms, before (this configuration is labelled by suffix $^{(0)}$) and after deformation. The unit vector $\vec{n}$ along the direction of the central force acting between atoms 1 and 2 is shown as well.

deformation is characterized by the strain tensor $\hat{e}$. In this derivation we have implicitly assumed the Cauchy-Born rule [133] stating that within a body under a small strain the positions of the atoms follow the overall deformation of the material. This approximation generally holds for face-centered cubic and body-centered cubic crystals (in general for Bravais lattices), while for lattices with a basis of two (or more) atoms in the unit cell the rule has to be modified to allow for internal degrees of freedom between the sublattices.

Cauchy-Born rule

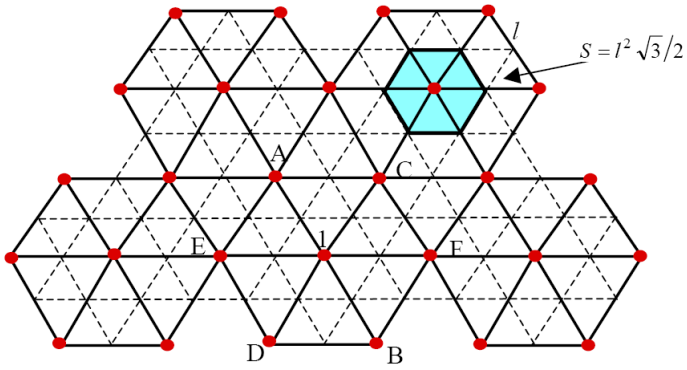

Figure 22: Planar (2-dimensional) triangular crystal with lattice constant l. One can easily find the area S of the unit cell and the six first-next-neighbors A, B, C, D, E, and F of atom 1.

We now apply the result given in Eq.(4.5) to the specific case of the two-dimensional triangular lattice shown in Fig.22 and representing the only case of isotropic crystal. Any particle has six nearest neighbors placed at distance l (corresponding to the edge of the triangular mesh). By computing the force due to the opposite neighbors A and B of atom 1, we find $\vec{F}^{2B}_{1,AB} = k_s\, l\, \vec{n} \cdot (\hat{e}_A - \hat{e}_B)\, \vec{n}$ where we indicated the unit vector connecting A to B with $\vec{n}$. The total force on atom 1 is given by the sum of three terms calculated along the three directions A-B, C-D and E-F (see Fig.22). In order to match the continuum formalism we

must divide the total force by $S = l^2\sqrt{3}/2$, namely by the area occupied by each atom. The resulting force density is

$$\vec{f}^{\,2B}_{1,AB} = \frac{2\sqrt{3}}{3} k_s \; \vec{n} \cdot \frac{(\hat{e}_A - \hat{e}_B)}{l} \vec{n} \tag{4.6}$$

The ratio $\frac{1}{l}(\hat{e}_A - \hat{e}_B)$ in Eq.(4.6) is identified with $(\vec{n} \cdot \partial/\partial \vec{r})\,\hat{e}$, i.e. with the projection of the gradient of the strain tensor. Therefore, the total force due to the couple *AB* is written as

$$\vec{f}^{\,2B}_{1,AB} = \frac{2\sqrt{3}}{3} k_s \; \vec{n} \cdot (\vec{n} \cdot \partial/\partial \vec{r}) \; \hat{e}\vec{n} \tag{4.7}$$

Finally, the Newtonian law describing the motion of atom 1 is obtained as $\vec{f}^{\,2B}_{1,AB} + \vec{f}^{\,2B}_{1,CD} + \vec{f}^{\,2B}_{1,EF} + \vec{b} = \rho\,\ddot{\vec{u}}$ where $\vec{b}$ is the density of external forces applied to the system, ρ is the mass density and $\ddot{\vec{u}}$ is the acceleration. Each force term can be developed through the Eq.(4.7), leading to the final elasticity equation

$$\frac{\sqrt{3}}{4} k_s \left[\nabla^2 \vec{u} + 2\nabla(\nabla \cdot \vec{u})\right] + \vec{b} = \rho\,\ddot{\vec{u}} \tag{4.8}$$

By comparing Eq.(4.8) to Eq.(1.61) we obtain the effective elastic moduli of the triangular lattice

Elastic properties of an atomistic model with two-body interactions

$$\lambda = \mu = \frac{\sqrt{3}}{4} k_s \tag{4.9}$$

or, equivalently, the Young modulus and the Poisson ratio

$$E = \frac{5\sqrt{3}}{8} k_s \quad \text{and} \quad \nu = \frac{1}{4} \tag{4.10}$$

Eqs.(4.9) and (4.10) prove that an atomistic model for the triangular lattice with first next-neighbors central forces only is not able to take into account all the elastic features predicted by the continuum elastic theory (and confirmed experimentally). In particular, Eq.(4.9) indicates that, according to this model, the material should have only one characteristic elastic constant, while Eq.(4.10) implies that a universal value of the Poisson ratio should exist, independent of the actual physical properties of the material.

4.1.2 *Atomistic model with two-body and three-body interactions*

We now consider a more refined force field, including three-body interactions among nearest neighbors. In this case we begin by defining a potential function involving three atomic positions $\vec{r}_1$, $\vec{r}_2$ and $\vec{r}_3$. We assume that the three angles ϑ_1, ϑ_2 and ϑ_3 (see Fig.23) are respectively equal to α_1, α_2 and α_3 at equilibrium.

Therefore, we can choose a potential energy of the form

$$\begin{aligned} U^{3B} \;=\; & \frac{1}{2}\Big\{H_1 [\cos\vartheta_1 - \cos\alpha_1]^2 + H_2 [\cos\vartheta_2 - \cos\alpha_2]^2 \\ & + H_3 [\cos\vartheta_3 - \cos\alpha_3]^2\Big\} \end{aligned} \tag{4.11}$$

where H_1, H_2, H_3 are suitable constants. For a triangular lattice, we have $\alpha_1 = \alpha_2 = \alpha_3 = \pi/3$ and therefore

$$U^{3B} = \frac{1}{2} h l^2 \left\{ \left[\cos\vartheta_1 - \frac{1}{2}\right]^2 + \left[\cos\vartheta_2 - \frac{1}{2}\right]^2 + \left[\cos\vartheta_3 - \frac{1}{2}\right]^2 \right\} \tag{4.12}$$

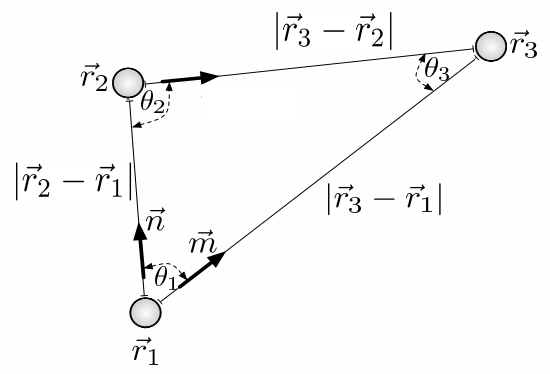

Figure 23: Distances and angles for a three-atom cluster. The unit vector $\vec{n}$ ($\vec{m}$) in the direction of the central force acting between atoms 1 and 2 (1 and 3) is shown as well.

where for simplicity we set $H_1 = H_2 = H_3 = hl^2$, with l being the interatomic distance in the unstrained lattice. In such a way, the constant k_s (describing the two-body interactions) and the constant h (describing the three-body interactions) usefully assume the same physical units.

By applying the same approximations used to derive Eq.(4.5), we find the following net force on atom 1

$$\begin{aligned}\vec{F}_1^{3B} &= \frac{3}{2} h l \left\{ \left(\vec{m} \cdot \hat{e}\, \vec{n} + \frac{1}{2} \vec{m} \cdot \hat{e}\, \vec{m} - \vec{n} \cdot \hat{e}\, \vec{n} \right) \vec{m} \right. \\ &\left. + \left(\vec{m} \cdot \hat{e}\, \vec{n} + \frac{1}{2} \vec{n} \cdot \hat{e}\, \vec{n} - \vec{m} \cdot \hat{e}\, \vec{m} \right) \vec{n} \right\} \end{aligned} \tag{4.13}$$

where $\vec{m}$ and $\vec{n}$ are the unit vectors defined in Fig.23. We remark that the bilinear form $\vec{m} \cdot \hat{e}\, \vec{n}$ is directly connected to the variation of the angle between $\vec{m}$ and $\vec{n}$, induced by the deformation described by $\hat{e}$. As expected, the force term given in Eq.(4.13) depends on the angular distortion of the triangle represented in Fig.23. Moreover, if ϑ_2 and ϑ_3 are equal, then the force is oriented along the bisector of the angle ϑ_1 in such a way to increase ϑ_1 if $\vartheta_1 < \pi/3$ and to decrease ϑ_1 if $\vartheta_1 > \pi/3$.

By adopting the angular dependent force defined in Eq.(4.13), we can itemize the full set of forces at work as follows: (i) two-body interaction forces, as given in Eq.(4.7); (ii) three-body interaction forces: six angular terms are working on atom 1 of Fig.22, as calculated in Eq.(4.13) (they correspond to the angles A1C, C1F, F1B, B1D, D1E and E1A); (iii) the external forces applied to the lattice. Following the same procedure outlined in the previous Section, we get

$$\frac{3}{4} \left(\frac{\sqrt{3}}{3} k_s + \frac{3}{2} h \right) \nabla^2 \vec{u} + \frac{\sqrt{3}}{2} k_s \nabla (\nabla \cdot \vec{u}) + \vec{b} = \rho\, \ddot{\vec{u}} \tag{4.14}$$

By comparing Eq.(4.14) to Eq.(1.61) we easily find the effective elastic moduli of the lattice

Elastic properties of an atomistic model with two-body and three-body interactions

$$\lambda = \frac{3}{4} \left(\frac{\sqrt{3}}{3} k_s - \frac{3}{2} h \right) \quad \text{and} \quad \mu = \frac{3}{4} \left(\frac{\sqrt{3}}{3} k_s + \frac{3}{2} h \right) \tag{4.15}$$

or, equivalently, the Young modulus and the Poisson ratio

$$E = \frac{3\sqrt{3}}{8} k_s \left(\frac{\sqrt{3}}{3} + \frac{3}{2} \frac{h}{k_s} \right) \left(\frac{5\sqrt{3}}{3} - \frac{3}{2} \frac{h}{k_s} \right) \quad \text{and} \quad \nu = \frac{1}{4} - \frac{3\sqrt{3}}{8} \frac{h}{k_s}$$

(4.16)

In conclusion, only this improved lattice model can correctly describe the elastic behavior of any isotropic media, since it provides the atomistic expression for *both independent* elastic constants. In other words, we can state that at least three-body interactions are mandatory to reproduce the complex mechanical behavior of real isotropic materials accurately.

Finally, we introduce some energetic considerations. The Lamé constants must obey the inequalities $\mu > 0$ and $2\mu + 3\lambda > 0$. Consequently, the interaction parameters k_s and h must be as follows: $k_s > 0$ and $-\frac{2\sqrt{3}}{9}k_s < h < \frac{10\sqrt{3}}{9}k_s$. When h approaches the value $-\frac{2\sqrt{3}}{9}k_s$, the Poisson ratio becomes equal to $1/2$ (a situation found in rubbery materials): the system is *volume* (*area*) *preserving* since the three-body interactions are working contrarily ($h < 0$) to what is expected. On the other hand, when h approaches the value $\frac{10\sqrt{3}}{9}k_s$, the Poisson ratio has the negative value of -1 (a situation common in some *re-entrant polymer foams* [46]): in this case the structure is *shape preserving*, allowing only deformations described by isotropic rescaling of the body.

In our approach we considered some hypotheses in order to simplify the mathematical complexity of the interaction models. The main assumptions are summarized here: (i) we described only two-dimensional systems; (ii) the interaction potentials are linear (springs); (iii) their action is limited to between nearest neighbors only; (iv) we have analyzed simple Bravais lattices where internal strains do not occur. Nevertheless, the final conclusions, about the primary importance of the three-body interactions for obtaining the correct number of independent elastic constants, can be applied to arbitrary crystals (in three dimensions) with arbitrarily nonlinear and long-range interaction potentials.

Method of the homogeneous deformation

In many earlier publications the method of homogeneous deformations was used to analytically derive expressions for the elastic constants of a crystalline solid in which the energy density can be separated into contributions from many-body interactions of different order [134, 135]. For example the exact explicit expressions for the body-centered cubic lattice [136, 137] and for hexagonal closed packing lattice [138, 139] have been derived for an arbitrary many-body interatomic potential. In these complicated expressions, if we reset the three-body interaction (and higher order multi-body terms) to zero, we then obtain a reduction in the number of the independent elastic constants, confirming our predictions. We remark however that this result is valid only if we determine the elastic constants of the crystalline structure in the reference equilibrium configuration, i.e., when the external pressure applied to the body is exactly reset to zero. In a recent publication [140], the two-dimensional triangular lattice with two-body (arbitrarily nonlinear and long-range) interactions was studied under an external pressure P and it was proved that the lattice can show a negative Poisson ratio behavior, as long as certain conditions involving the two-body interaction potential are satisfied. The result is given by the relation [140]

Effect of the external pressure on the Poisson ratio

$$\nu(P) = \frac{1 + 2PK_T}{4} \tag{4.17}$$

where $P = -\frac{dU}{dV}$ is the applied pressure and $K_T = -\frac{1}{V}\frac{dV}{dP}$ is the compressibility (U is the total energy and V is the volume of the body).

If we let $P = 0$ in Eq.(4.17) we obtain the value of the Poisson ratio given in Eq.(4.10). Therefore, Eq.(4.10) is exact also with nonlinear and long-range interaction potentials. Moreover, Eq.(4.17) shows that with $P < 0$ we can obtain a negative Poisson ratio.

4.2 INTERATOMIC POTENTIALS FOR SOLID MECHANICS

In computational atomic-scale solid mechanics it is important to use interatomic interaction potentials that can correctly describe the mechanical properties of the atomistic systems under consideration subjected to arbitrary deformations. The development of accurate and predictive representations of the interaction forces is an open and active research field.

An accurate description of interatomic forces can be achieved by ab initio quantum mechanical methods. They are more fundamental and often superior with respect to empirical force fields. Nevertheless, such methods are computationally very demanding, so, their use is limited to a relatively small number of atoms (typically < 1000) which is not large enough to investigate many important problems in the mechanics of solids. In fact, dealing with heterogeneous materials, the typical sizes of the systems needed to properly reproduce their structural complexity ($> 10^4$) is much larger than those achievable through quantum mechanical methods. Moreover, the main theoretical tool devoted to the analysis of the elastic behavior of materials, the continuum theory of elasticity, has been developed in order to consider actual macroscopic systems (where the number of atoms approaches the Avogadro number). So, in order to apply (and verify) such a theory to atom-resolved systems we need to increase the sizes of the simulated systems as much as possible. Therefore, while ab initio methods have been successfully applied to study specific aspects of homogeneous materials, the development of more general pictures usually exploits empirical methods. In the following a brief review of the main adopted potentials, with increasing complexity, is reported.

The simplest interatomic potential is obtained by taking into account only two-body interactions

The two-body interaction

$$U = \sum_{\alpha<\beta} U^{2B}(x_{\alpha\beta}) \tag{4.18}$$

As explained earlier, such a two-body interaction is not sound enough for simulations in the realm of solid mechanics. However, it can be used in this field when simple, qualitative and paradigmatic computations must be performed on very large systems. This is the case of the renowned Lennard-Jones potential, originally developed for describing the properties of gases. In this model two distinct forces are considered in the interaction between two atoms: in the limit of large separation an attractive force (van der Waals force, or dispersion force) and a repulsive force at short ranges (the result of overlapping electron orbitals). The Lennard-Jones potential (also referred to as the L-J potential or 6-12 potential) was proposed in 1924 by John Lennard-Jones [141]. It assumes the form

The Lennard-Jones potential

$$U^{2B}(r) = 4\epsilon\left[\left(\frac{\sigma}{r}\right)^{12} - \left(\frac{\sigma}{r}\right)^{6}\right] \tag{4.19}$$

where ϵ is the depth of the potential well and σ is the distance at which the interparticle potential is zero and r is the distance between the

particles. The $(1/r)^{12}$ term describes repulsion and the $(1/r)^6$ term describes attraction.

The L-J potential is particularly accurate for describing noble gas. Concerning condensed matter, the L-J is able to describe, at a qualitative level, the physics of metals with a close-packed crystalline structure. As a matter of fact the lowest energy arrangement of an infinite number of atoms is the hexagonal close-packing. Upon raising temperature, the lowest free energy arrangement becomes cubic close packing and then liquid. Under pressure the lowest energy structure switches between cubic and hexagonal close packing [142]. Accordingly the applicability of the L-J model for solids is limited.

To achieve more realistic interatomic force models, it is necessary to go beyond the two body approximation. An important example is the Stillinger-Weber (SW) potential, which was developed to describe covalently bonded silicon [26]. The SW potential takes into account both two-body and three-body terms

The Stillinger and Weber potential

$$\mathcal{U} = \sum_{\alpha<\beta} \mathcal{U}^{2B}(x_{\alpha\beta}) + \sum_{\alpha<\beta<\gamma} \mathcal{U}^{3B}(\vec{x}_\alpha, \vec{x}_\beta, \vec{x}_\gamma) \tag{4.20}$$

where $\vec{x}_\alpha$ is the position of the α-th atom and $x_{\alpha\beta} = |\vec{x}_\alpha - \vec{x}_\beta|$. The potential terms for two-body interactions can be written as $\mathcal{U}^{2B}(x_{\alpha\beta}) = \epsilon f_2(x_{\alpha\beta}/\sigma)$ and $\mathcal{U}^{3B}(\vec{x}_\alpha, \vec{x}_\beta, \vec{x}_\gamma) = \epsilon f_3(\vec{x}_\alpha/\sigma, \vec{x}_\beta/\sigma, \vec{x}_\gamma/\sigma)$. The function f_2 is given by

$$f_2(r) = A\left(Br^{-p} - r^{-q}\right)\exp\left[(r-a)^{-1}\right] \tag{4.21}$$

if $r < a$ and $f_2 = 0$ if $r > a$, where A, B, p, q and a are positive constants. The three-body term is given by

$$\begin{aligned} f_3(\vec{x}_\alpha, \vec{x}_\beta, \vec{x}_\gamma) &= h(x_{\beta\alpha}, x_{\beta\gamma}, \theta_{\alpha\beta\gamma}) + h(x_{\alpha\beta}, x_{\alpha\gamma}, \theta_{\beta\alpha\gamma}) \\ &\quad + h(x_{\gamma\alpha}, x_{\gamma\beta}, \theta_{\alpha\gamma\beta}) \end{aligned} \tag{4.22}$$

where $\theta_{\alpha\beta\gamma}$ is the angle between $\vec{x}_\alpha$ and $\vec{x}_\gamma$ subtended at vertex β and

$$\begin{aligned} h(x_{\beta\alpha}, x_{\beta\gamma}, \theta_{\alpha\beta\gamma}) &= \lambda \exp\left[\xi\left(x_{\beta\alpha} - a\right)^{-1} + \xi\left(x_{\beta\gamma} - a\right)^{-1}\right] \\ &\quad \times \left(\cos\theta_{\alpha\beta\gamma} + \frac{1}{3}\right)^2 \end{aligned} \tag{4.23}$$

where λ and ξ are constants. The object of the three-body component of the potential is to enforce the tetrahedral bond angle (109.47°) among triplets of bonded atoms. This model has been developed for describing interactions in solid and liquid forms of Si but it appears only moderately accurate to describe the amorphous phase [143]. Deficiencies of the SW force model are furthermore found when studying the brittle cleavage of silicon [144].

To improve the reliability of the models and to extend their applicability to configurations far from equilibrium, it is possible to use higher-order (up to five-body) expansion terms [145]. Despite the increased complexity, similar models improve only selectively the description of the solid system and often at a considerable increase of the computational cost.

A computationally more convenient approach is to use an Environment Dependent Interatomic Potential (EDIP) [146, 147]. The interaction model includes only two-body and three-body terms as is the case of

The EDIP potential

the SW model but, in addition, it has an explicit dependence on the local atomic environment through an effective coordination number

$$Z_\alpha = \sum_{\gamma \neq \alpha} f(x_{\alpha\gamma}) \tag{4.24}$$

where $f(x_{\alpha\gamma})$ is a cutoff function that measures the contribution of neighbor γ to the coordination of atom α in terms of the separation $x_{\alpha\gamma}$. In the case of silicon [146, 147], the environment-dependent formulation is able to capture successfully (i) the energetics and elastic properties of the ground-state diamond lattice, (ii) the covalent rehybridization of undercoordinated atoms, and (iii) a smooth transition to metallic bonding for overcoordinated atoms.

The primary importance of the local coordination Z_α to describe bonding in solids properly was first pointed out by Abell [148]. In fact, it can be shown by quantum-mechanical arguments that the more neighbors an atom has, the weaker the bond to each neighbor will be. Abell proposed an interatomic potential formed by a sum over nearest-neighbors two body terms in the form

$$\mathcal{U} = \frac{1}{2} \sum_{\alpha \neq \beta} \left[f_r(x_{\alpha\beta}) + b_{\alpha\beta} f_a(x_{\alpha\beta}) \right] \tag{4.25}$$

where $f_r(r_{\alpha\beta})$ and $f_a(r_{\alpha\beta})$ are pair-additive repulsive and attractive interactions, respectively. The bond strength $b_{\alpha\beta}(Z_\alpha)$ (also named bond order) is a monotonically decreasing function of the coordination number $b_{\alpha\beta} \sim Z_\alpha^{-\frac{1}{2}}$. With Morse-type repulsive and attractive pair interactions

$$f_r(r) = A \exp(-\lambda_1 r) \tag{4.26}$$

$$f_a(r) = -B \exp(-\lambda_2 r) \tag{4.27}$$

the above Eq.(2.25) yields an energy versus volume relationship similar to the universal binding energy curve for solids [149]. Furthermore, at variance with a simple two-body potential, by using the bond order b_{ij} environment dependence it is possible to reproduce both the open (e.g., diamond) or close-packed crystalline structures depending on the actual choice of the parameters. This point is crucial for determining the equilibrium state of a crystal structure.

Recognizing the utility of the Abell's approach, Tersoff proposed a model for Si, Ge, C and SiC by taking into account the environment-dependent bond strength [27]. In Tersoff formulation the total energy is

The Tersoff potential

$$\mathcal{U} = \frac{1}{2} \sum_{\alpha \neq \beta} f_c(x_{\alpha\beta}) \left[f_r(x_{\alpha\beta}) + b_{\alpha\beta} f_a(x_{\alpha\beta}) \right] \tag{4.28}$$

where a cutoff function is introduced to limit the sum over nearest neighbors

$$f_c(r) = \begin{cases} 1 & r < R - D \\ \frac{1}{2} - \frac{1}{2} \sin\left[\pi(r-R)/D\right] & R - D < r < R + D \\ 0 & r > R + D \end{cases} \tag{4.29}$$

The bond-order parameter $b_{\alpha\beta}$ is given by

$$b_{\alpha\beta} = \left(1 + \beta \zeta_{\alpha\beta}^n\right)^{-1/(2n)} \tag{4.30}$$

with

$$\zeta_{\alpha\beta} = \sum_{\gamma\neq\alpha,\beta} f_c(x_{\alpha\gamma})g(\theta_{\alpha\beta\gamma})\exp\left[\lambda_3^3(x_{\alpha\beta}-x_{\alpha\gamma})^3\right] \tag{4.31}$$

$$g(\theta) = 1+\frac{c^2}{d^2}-\frac{c^2}{d^2+(h-\cos\theta)^2} \tag{4.32}$$

The function $b_{\alpha\beta}$ is a measure of the bond-order, and it is assumed to be a monotonically decreasing function of the coordination of atoms α and β. In addition, terms that act to limit the range of interaction to the first neighbor shell are included in $b_{\alpha\beta}$. This model can be modified in order to describe multicomponent mixtures, and more specifically SiC and SiGe mixtures.

The Brenner potential

In 1990 [150] Brenner extended the analytic form of the Tersoff potential by introducing two additional ad hoc terms into the bond order to counter the overbinding of radicals. A second-generation Brenner potential [151] leads to a significantly better description of bond energies, lengths, and force constants for hydrocarbon molecules, as well as elastic properties of diamond. This prominent model has been applied successfully in several atomic scale studies of complex processes involving hydrocarbon molecules, graphite, graphene and diamond lattice.

4.3 ATOMIC-SCALE STRESS

In order to properly compare the results obtained through molecular dynamics simulations with those achieved within the continuum elasticity theory, the identification of the macroscopic stress tensor with a suitable atomistic quantity is a crucial point. In the following a straightforward derivation of the standard atomistic expression of the stress, the so-called viral stress, is presented. Moreover, we show how this expression is modified in order to allow for the calculation of the nonlinear elastic behavior within the Green elasticity.

4.3.1 *The virial stress*

To obtain the atomic-scale counterpart of the Cauchy stress tensor (see Eqs.(1.22) and (1.23)), we consider a small portion of a given elastic body with volume V and surface S. We suppose that in this region there are N atoms, described by positions $\vec{x}_\alpha$ for $\alpha = 1,...,N$. The number of the atoms is large enough to allow the definition of the macroscopic elastic fields (stress and strain) in that region, but it is also small enough to identify the local stress with its average on the volume. To get the continuum-to-molecular equivalence it is useful to introduce the so-called virial form $\sum_{\alpha=1}^{N}\vec{x}_\alpha\otimes\vec{F}_\alpha$ where the symbol $\otimes$ represents the tensor product of vectors. The quantity $\vec{F}_\alpha$ is the total force acting on the α-th atom and, therefore, the equation of motion $\vec{F}_\alpha = m_\alpha\vec{a}_\alpha$ (m_α is the mass of the α-th atom) leads to the balance

Definition of virial

$$\sum_{\alpha=1}^{N}\vec{x}_\alpha\otimes\vec{F}_\alpha = \sum_{\alpha=1}^{N} m_\alpha\vec{x}_\alpha\otimes\vec{a}_\alpha \tag{4.33}$$

Now, the total force $\vec{F}_\alpha$ can be written as the sum of two contributions: $\vec{F}_\alpha^{int}$, which is the internal force on the α-th atom due to the atoms contained in the volume V; and $\vec{F}_\alpha^{ext}$, which is the external force on the

α-th atom due to the atoms falling outside the volume V and by any external action. By exploiting this contributions we get

$$\sum_{\alpha=1}^{N} \vec{x}_\alpha \otimes \vec{F}_\alpha^{int} + \sum_{\alpha=1}^{N} \vec{x}_\alpha \otimes \vec{F}_\alpha^{ext} = \sum_{\alpha=1}^{N} m_\alpha \vec{x}_\alpha \otimes \vec{a}_\alpha \tag{4.34}$$

The external force $\vec{F}_\alpha^{ext}$ is, in turn, given by the surface force $\vec{F}_\alpha^{ext}(S)$ (due to atoms nearby the surface S) and by the body force $\vec{F}_\alpha^{ext}(V)$ (due to external fields). Therefore, Eq.(4.34) can be cast in the form

$$\begin{aligned} \sum_{\alpha=1}^{N} \vec{x}_\alpha \otimes \vec{F}_\alpha^{int} \quad + \quad & \sum_{\alpha=1}^{N} \vec{x}_\alpha \otimes \left[\vec{F}_\alpha^{ext}(V) + \vec{F}_\alpha^{ext}(S)\right] \\ = \quad & \sum_{\alpha=1}^{N} m_\alpha \vec{x}_\alpha \otimes \frac{d\vec{v}_\alpha}{dt} \end{aligned} \tag{4.35}$$

where $\vec{v}_\alpha$ is the velocity of the α-th atom. We observe that the velocity $\vec{v}_\alpha$ of each atom is the sum $\vec{v}_\alpha = \vec{v}_\alpha^{d} + \vec{v}_\alpha^{th}$ of a macroscopic drift $\vec{v}_\alpha^{d}$ and a thermal fluctuation $\vec{v}_\alpha^{th}$. The macroscopic drift velocities $\vec{v}_\alpha^{d}$ of the α-th atom is defined as the mean value of the velocities $\vec{v}_\beta$ of the atoms belonging to a given neighborhood of the α-th site. Evidently, this mean value removes the statistical fluctuations, resulting in a macroscopic quantity. Therefore, we get

$$\begin{aligned} \sum_{\alpha=1}^{N} \vec{x}_\alpha \otimes \vec{F}_\alpha^{int} + \sum_{\alpha=1}^{N} \vec{x}_\alpha \otimes \vec{F}_\alpha^{ext}(V) + \sum_{\alpha=1}^{N} \vec{x}_\alpha \otimes \vec{F}_\alpha^{ext}(S) \\ = \sum_{\alpha=1}^{N} m_\alpha \vec{x}_\alpha \otimes \frac{d\vec{v}_\alpha^{d}}{dt} + \sum_{\alpha=1}^{N} m_\alpha \vec{x}_\alpha \otimes \frac{d\vec{v}_\alpha^{th}}{dt} \end{aligned} \tag{4.36}$$

Any quantity appearing in Eq.(4.36) must be understood as instantaneous. To obtain the corresponding average values, we introduce the time average $\langle\cdot\rangle = \lim_{\tau\to\infty} \frac{1}{\tau}\int_0^\tau (\cdot)\, dt$. As for the last term of the right hand side of Eq.(4.36) we get

$$\begin{aligned} & \left\langle \sum_{\alpha=1}^{N} m_\alpha \vec{x}_\alpha \otimes \frac{d\vec{v}_\alpha^{th}}{dt} \right\rangle \\ = & \left\langle \sum_{\alpha=1}^{N} m_\alpha \left[\frac{d}{dt}\left(\vec{x}_\alpha \otimes \vec{v}_\alpha^{th}\right) - \vec{v}_\alpha \otimes \vec{v}_\alpha^{th}\right] \right\rangle \\ = & \lim_{\tau\to\infty} \frac{1}{\tau}\int_0^\tau \sum_{\alpha=1}^{N} m_\alpha \frac{d}{dt}\left(\vec{x}_\alpha \otimes \vec{v}_\alpha^{th}\right) dt - \left\langle \sum_{\alpha=1}^{N} m_\alpha \vec{v}_\alpha \otimes \vec{v}_\alpha^{th} \right\rangle \\ = & \lim_{\tau\to\infty} \frac{1}{\tau} \sum_{\alpha=1}^{N} m_\alpha \vec{x}_\alpha \otimes \vec{v}_\alpha^{th}\Big|_{t=0}^{t=\tau} - \left\langle \sum_{\alpha=1}^{N} m_\alpha \vec{v}_\alpha \otimes \vec{v}_\alpha^{th} \right\rangle \end{aligned} \tag{4.37}$$

We are dealing with an elastic solid body which is a stable bound system, i.e., a system that hangs together forever. In other words, coordinates and velocities for all particles are expressed by finite quantities forever. In this case, the function $G(t) = \sum_{\alpha=1}^{N} m_\alpha \vec{x}_\alpha \otimes \vec{v}_\alpha^{th}$ is bounded between two extremes, G_{min} and G_{max}, and the first term in Eq.(4.37) is therefore zero in the limit of very long times τ

$$\begin{aligned} \lim_{\tau\to\infty} \frac{1}{\tau} \sum_{\alpha=1}^{N} m_\alpha \vec{x}_\alpha \otimes \vec{v}_\alpha^{th}\Big|_{t=0}^{t=\tau} \quad &= \quad \lim_{\tau\to\infty} \frac{G(\tau) - G(0)}{\tau} \\ &\leqslant \quad \lim_{\tau\to\infty} \frac{G_{max} - G_{min}}{\tau} = 0 \end{aligned} \tag{4.38}$$

On the other hand, the last term in Eq.(4.37) can be easily computed

$$\left\langle \sum_{\alpha=1}^{N} m_\alpha \vec{v}_\alpha \otimes \vec{v}_\alpha^{\,th} \right\rangle = \left\langle \sum_{\alpha=1}^{N} m_\alpha \vec{v}_\alpha^{\,d} \otimes \vec{v}_\alpha^{\,th} \right\rangle + \left\langle \sum_{\alpha=1}^{N} m_\alpha \vec{v}_\alpha^{\,th} \otimes \vec{v}_\alpha^{\,th} \right\rangle \tag{4.39}$$

The first term is zero since $\langle \vec{v}_\alpha^{\,th} \rangle = 0$ (we have also used the statistical indipendence of $\vec{v}_\alpha^{\,d}$ and $\vec{v}_\alpha^{\,th}$). Conversely, the second term is quadratic in the fluctuation $\vec{v}_\alpha^{\,th}$ and it is not negligible. So far, we have proved the following important result

$$\left\langle \sum_{\alpha=1}^{N} m_\alpha \vec{x}_\alpha \otimes \frac{d\vec{v}_\alpha^{\,th}}{dt} \right\rangle = -\left\langle \sum_{\alpha=1}^{N} m_\alpha \vec{v}_\alpha^{\,th} \otimes \vec{v}_\alpha^{\,th} \right\rangle \tag{4.40}$$

and, therefore, the virial balance given in Eq.(4.36) can be written as

$$\left\langle \sum_{\alpha=1}^{N} \vec{x}_\alpha \otimes \vec{F}_\alpha^{int} \right\rangle + \left\langle \sum_{\alpha=1}^{N} \vec{x}_\alpha \otimes \vec{F}_\alpha^{ext}(V) \right\rangle + \left\langle \sum_{\alpha=1}^{N} \vec{x}_\alpha \otimes \vec{F}_\alpha^{ext}(S) \right\rangle = \left\langle \sum_{\alpha=1}^{N} m_\alpha \vec{x}_\alpha \otimes \frac{d\vec{v}_\alpha^{\,d}}{dt} \right\rangle - \left\langle \sum_{\alpha=1}^{N} m_\alpha \vec{v}_\alpha^{\,th} \otimes \vec{v}_\alpha^{\,th} \right\rangle \tag{4.41}$$

To proceed further we must link some atomic terms with their continuum counterparts. In fact, we have that: the term depending on body forces corresponds to a volume integral; the term depending on surface forces corresponds to a surface integral; the first term in the right hand side can be converted to a volume integral by observing that $d\vec{v}_\alpha^{\,d}/dt$ is the macroscopic acceleration field $\vec{a}$. Accordingly,

$$\left\langle \sum_{\alpha=1}^{N} \vec{x}_\alpha \otimes \vec{F}_\alpha^{int} \right\rangle + \left\langle \int_V \vec{x} \otimes \vec{F}^{ext}(V) d\vec{x} \right\rangle + \left\langle \int_S \vec{x} \otimes \vec{F}^{ext}(S) dS \right\rangle = \left\langle \int_V \rho \vec{x} \otimes \vec{a} d\vec{x} \right\rangle - \left\langle \sum_{i=1}^{N} m_\alpha \vec{v}_\alpha^{\,th} \otimes \vec{v}_\alpha^{\,th} \right\rangle \tag{4.42}$$

As described in Sec.1.1.3, in continuum elasticity we have external bulk forces $\vec{F}^{ext}(V) = \vec{b}$ and surface external forces $\vec{F}^{ext}(S) = \hat{T}\vec{n}$. Therefore, the balance equation given in Eq.(4.41) becomes

$$\left\langle \sum_{\alpha=1}^{N} \vec{x}_\alpha \otimes \vec{F}_\alpha^{int} \right\rangle + \left\langle \int_V \vec{x} \otimes \vec{b} d\vec{x} \right\rangle + \left\langle \int_S \vec{x} \otimes (\hat{T}\vec{n})\, dS \right\rangle = \left\langle \int_V \rho \vec{x} \otimes \vec{a} d\vec{x} \right\rangle - \left\langle \sum_{\alpha=1}^{N} m_\alpha \vec{v}_\alpha^{\,th} \otimes \vec{v}_\alpha^{\,th} \right\rangle \tag{4.43}$$

or, equivalently

$$\left\langle \sum_{\alpha=1}^{N} x_{\alpha,k} F_{\alpha,h}^{int} \right\rangle + \left\langle \int_V x_k b_h d\vec{x} \right\rangle + \left\langle \int_S x_k T_{hp} n_p dS \right\rangle = \left\langle \int_V \rho x_k a_h d\vec{x} \right\rangle - \left\langle \sum_{\alpha=1}^{N} m_\alpha v_{\alpha,k}^{th} v_{\alpha,h}^{th} \right\rangle \tag{4.44}$$

By applying the divergence theorem to the surface integral, we get

$$\left\langle \sum_{\alpha=1}^{N} x_{\alpha,k} F_{\alpha,h}^{int} \right\rangle + \left\langle \int_V x_k b_h d\vec{x} \right\rangle + \left\langle \int_V \frac{\partial}{\partial x_p} \left(x_k T_{hp} \right) d\vec{x} \right\rangle = \left\langle \int_V \rho x_k a_h d\vec{x} \right\rangle - \left\langle \sum_{\alpha=1}^{N} m_\alpha v_{\alpha,k}^{th} v_{\alpha,h}^{th} \right\rangle \tag{4.45}$$

We can now develop the derivative

$$\left\langle \sum_{\alpha=1}^{N} x_{\alpha,k} F_{\alpha,h}^{int} \right\rangle + \left\langle \int_V x_k b_h d\vec{x} \right\rangle + \left\langle \int_V \left(\delta_{kp} T_{hp} + x_k \frac{\partial T_{hp}}{\partial x_p} \right) d\vec{x} \right\rangle = \left\langle \int_V \rho x_k a_h d\vec{x} \right\rangle - \left\langle \sum_{\alpha=1}^{N} m_\alpha v_{\alpha,k}^{th} v_{\alpha,h}^{th} \right\rangle \tag{4.46}$$

so that

$$\left\langle \sum_{\alpha=1}^{N} x_{\alpha,k} F_{\alpha,h}^{int} \right\rangle + \left\langle \int_V T_{hk} d\vec{x} \right\rangle + \left\langle \int_V x_k \left(\frac{\partial T_{hp}}{\partial x_p} + b_h - \rho a_h \right) d\vec{x} \right\rangle + \left\langle \sum_{\alpha=1}^{N} m_\alpha v_{\alpha,k}^{th} v_{\alpha,h}^{th} \right\rangle = 0 \tag{4.47}$$

The third term is zero because of Eq.(1.26). Moreover, we can define the local average value

$$\mathcal{T}_{hk} = \frac{1}{V} \int_V T_{hk} d\vec{x} \tag{4.48}$$

of the stress tensor over the volume V. In conclusion, the balance equation for the virial sum leads to the following definition of stress

$$\langle \mathcal{T}_{hk} \rangle = -\frac{1}{V} \left\langle \sum_{\alpha=1}^{N} m_\alpha v_{\alpha,k}^{th} v_{\alpha,h}^{th} \right\rangle - \frac{1}{V} \left\langle \sum_{\alpha=1}^{N} x_{\alpha,k} F_{\alpha,h}^{int} \right\rangle \tag{4.49}$$

where only atomic-scale quantities are used, namely: particle positions and velocities, and interatomic forces. This very important relation links atomistic to continuum elasticity; it can be written in tensor form

The microscopic form of the Cauchy stress

$$\left\langle \hat{\mathcal{T}} \right\rangle = -\frac{1}{V} \left\langle \sum_{\alpha=1}^{N} m_\alpha \vec{v}_\alpha^{th} \otimes \vec{v}_\alpha^{th} \right\rangle - \frac{1}{V} \left\langle \sum_{\alpha=1}^{N} \vec{x}_\alpha \otimes \vec{F}_\alpha^{int} \right\rangle \tag{4.50}$$

This result has innumerable applications in molecular dynamics simulations of mechanical properties. In fact, it enables us to evaluate the macroscopic Cauchy stress in an elastic solid system defined at the atomic or molecular level. We remark that we have identified a macroscopic field (the stress tensor introduced in Sec.1.1.3) with a combination of microscopic quantities by means of two average procedures: the first one performed over the volume V (denoted by $\hat{\mathcal{T}}$) and the second one over the time (denoted by the angle brackets). It is also important to observe that the first kinetic term depends on the velocity contribution due to thermal fluctuations only, while it does not depend on drift velocities. This contribution plays a key role in finite-temperature thermoelasticity [152]. We point out that Eq.(4.50) is exactly correct for systems undergoing arbitrary time-dependent deformations.

It is possible to reformulate the result given in Eq.(4.50) by writing

$$\left\langle \hat{\mathcal{T}} \right\rangle = -\frac{1}{N\omega}\left\langle \sum_{\alpha=1}^{N} m_\alpha \vec{v}_\alpha^{\,th} \otimes \vec{v}_\alpha^{\,th} \right\rangle - \frac{1}{N\omega}\left\langle \sum_{\alpha=1}^{N} \vec{x}_\alpha \otimes \vec{F}_\alpha^{int} \right\rangle \tag{4.51}$$

where we have attributed to any atom the same average volume $\omega = V/N$. Although this assumption is widely used in atomistic simulations on materials mechanical behavior, it should be nevertheless noted that it is in principle correct for atomic-scale homogeneous systems only. Actually, many interesting problems in modern nano-mechanics (including fracture) refer to systems that do not fulfill such an assumption. We need therefore to better refine the volume concept, by introducing a suitable criterion for dividing the space into locally proper sub-domains that we will refer to as atomic volumes ω_α

$$\left\langle \hat{\mathcal{T}} \right\rangle = -\frac{1}{N}\left\langle \sum_{\alpha=1}^{N} \frac{m_\alpha}{\omega_\alpha} \vec{v}_\alpha^{\,th} \otimes \vec{v}_\alpha^{\,th} \right\rangle - \frac{1}{N}\left\langle \sum_{\alpha=1}^{N} \frac{1}{\omega_\alpha} \vec{x}_\alpha \otimes \vec{F}_\alpha^{int} \right\rangle \tag{4.52}$$

A possible solution is offered by the following discretization procedure. We can work out a partitioning of the total available space into elementary volumes (much smaller than ω_α). Then, each elementary volume is uniquely assigned to its next-neighbor atom site [153]. The atomic volume of any given lattice site is finally defined as the sum of the elementary volumes attributed to that atom site. It can be proved that such a discretization procedure is basically equivalent to the Voronoi tessellation, it is unique, and unambiguously attributes to each atom a proper value of the volume.

Finally, we observe that, at thermodynamic equilibrium, the first tensor term in Eq.(4.50) is directly proportional to the temperature since it contains the average values of the kinetic quantities $m_\alpha \vec{v}_\alpha^{\,th} \otimes \vec{v}_\alpha^{\,th}$. Therefore, in the thermal linear approximation, we can write

$$-\frac{1}{V}\left\langle \sum_{\alpha=1}^{N} m_\alpha \vec{v}_\alpha^{\,th} \otimes \vec{v}_\alpha^{\,th} \right\rangle = -\hat{\mathcal{C}}\hat{\alpha}T \tag{4.53}$$

where $\hat{\mathcal{C}}$ is the (fourth-order) stiffness tensor, $\hat{\alpha}$ is the (second-order) thermal expansion coefficient tensor (satisfying the symmetry relation $\alpha_{ij} = \alpha_{ji}$) and T is the temperature. So, Eq.(4.50) assumes the form

$$\left\langle \hat{\mathcal{T}} \right\rangle = -\hat{\mathcal{C}}\hat{\alpha}T - \left\langle \frac{1}{V}\sum_{\alpha=1}^{N} \vec{x}_\alpha \otimes \vec{F}_\alpha \right\rangle \tag{4.54}$$

Now, in the following Section we prove that, in linear elasticity

$$\frac{\partial U}{\partial \hat{\varepsilon}} = -\left\langle \frac{1}{V}\sum_{\alpha=1}^{N} \vec{x}_\alpha \otimes \vec{F}_\alpha \right\rangle \tag{4.55}$$

and, therefore

$$\left\langle \hat{\mathcal{T}} \right\rangle = -\hat{\mathcal{C}}\hat{\alpha}T + \frac{\partial U}{\partial \hat{\varepsilon}} \tag{4.56}$$

Moreover, for a linear elastic material we have $\frac{\partial U}{\partial \hat{\varepsilon}} = \hat{\mathcal{C}}\hat{\varepsilon}$ and, therefore, Eq.(4.56) is simplified as

$$\left\langle \hat{\mathcal{T}} \right\rangle = -\hat{\mathcal{C}}\hat{\alpha}T + \hat{\mathcal{C}}\hat{\varepsilon} = \hat{\mathcal{C}}\left(\hat{\varepsilon} - \hat{\alpha}T\right) \tag{4.57}$$

The thermal expansion coefficient tensor

When the stress tensor is zero we must have $\hat{\varepsilon} = \hat{\alpha}T$, obtaining the physical meaning of the thermal expansion coefficient tensor $\hat{\alpha}$: it represents the thermal-induced strain for any degree of temperature.

4.3.2 *The atomistic nonlinear Cauchy stress*

It is possible to find a direct relation between the atomic stress and the Cauchy stress tensor derived by the strain energy function, as in Eq.(2.84). By means of such a derivation, we find that the viral stress in Eq.(4.50) corresponds to the Cauchy stress only under the linear approximation. While, if we are interested in the nonlinear elastic behavior of the system, a different form of the atomistic stress have to be considered.

Thermodynamical identification of the strain energy

In a given dynamic system, the strain energy function $U(\hat{\epsilon})$ can be identified with the thermodynamic potential of the corresponding statistical ensemble (i.e. the internal energy for an isolated system, the Helmholtz free energy for a system in equilibrium with a thermal bath, etc...). By considering the basic case of an isolated system at $T = 0$ K, the internal energy corresponds to the interatomic potential energy $\mathcal{U}$ that is a function of the atomic positions $\vec{x}_\alpha \quad \alpha = 1, ..., N$, namely: $\mathcal{U} = \mathcal{U}(\{\vec{x}_\alpha\})$. In absence of any external load, the system lies in the minimum energy configuration $\{\vec{x}^0_\alpha\}$. On the contrary, if a uniform strain field $\hat{\epsilon}$ is applied, the new atomic positions can be expressed as $\vec{x}_\alpha = (\hat{I} + \hat{\epsilon})\vec{x}^0_\alpha$ and the corresponding internal energy is given by $\mathcal{U}\left(\{(\hat{I} + \hat{\epsilon})\vec{x}^0_\alpha\}\right)$. Therefore, the strain energy density is

$$U(\hat{\epsilon}) = \frac{1}{V}\mathcal{U}\left(\left\{(\hat{I} + \hat{\epsilon})\vec{x}^0_\alpha\right\}\right) \tag{4.58}$$

The nonlinear form of the Cauchy stress

where V is the volume of the system. According to Eq.(2.84), the stress tensor is given by

$$\begin{aligned}
\hat{T} = \frac{\partial U(\hat{\epsilon})}{\partial \hat{\epsilon}} &= \frac{1}{V}\sum_\alpha^N \frac{\partial \mathcal{U}}{\partial \vec{x}_\alpha}\frac{\partial \vec{x}_\alpha}{\partial \hat{\epsilon}} \\
&= \frac{1}{V}\sum_\alpha^N \frac{\partial \mathcal{U}}{\partial \vec{x}_\alpha}\frac{\partial}{\partial \hat{\epsilon}}(\hat{I} + \hat{\epsilon})\vec{x}^0_\alpha \\
&= \frac{1}{V}\sum_\alpha^N \frac{\partial \mathcal{U}}{\partial \vec{x}_\alpha} \otimes \vec{x}^0_\alpha \\
&= -\frac{1}{V}\sum_\alpha^N \vec{x}^0_\alpha \otimes \vec{F}^{int}_\alpha
\end{aligned} \tag{4.59}$$

This expression corresponds to that in Eq.(4.50) if the positions $\vec{x}_\alpha$ in the deformed configuration are replaced by the positions $\vec{x}^0_\alpha$ of the system in the minimum energy state. It easy to prove that Eq.(4.50) is coincident with the first order expansion in ϵ of Eq.(4.59). In fact

$$\vec{x}^0_\alpha = \vec{x}_\alpha + o(\epsilon) \tag{4.60}$$

and $\frac{\partial V}{\partial \vec{x}_\alpha} = o(\epsilon)$, therefore

$$\frac{1}{V}\sum_\alpha^N \frac{\partial \mathcal{U}}{\partial \vec{x}_\alpha} \otimes \vec{x}^0_\alpha = \frac{1}{V}\sum_\alpha^N \frac{\partial \mathcal{U}}{\partial \vec{x}_\alpha} \otimes \vec{x}_\alpha + o(\epsilon^2) \tag{4.61}$$

This means that if we are interested in the evaluation of the stress up to the second order in the strain (nonlinear Green elasticity described in Section 2.3.1) we have to apply the expression in Eq.(4.59) in spite of that in Eq.(4.50).

4.3.3 *A different definition of the virial stress*

We add some comments so the reader can avoid possible misunderstandings, which are often encountered in literature when discussing the stress concept. As a matter of fact, the virial stress is one of the most commonly used stress-like quantities in discrete particle systems (it is also called the *pressure tensor*) and it is sometimes defined as [154, 155]

$$\left\langle \hat{\mathcal{T}} \right\rangle = -\frac{1}{V}\left\langle \sum_{\alpha=1}^{N} m_\alpha \frac{d\vec{x}_\alpha}{dt} \otimes \frac{d\vec{x}_\alpha}{dt} \right\rangle - \frac{1}{V}\left\langle \sum_{\alpha=1}^{N} \vec{x}_\alpha \otimes \vec{F}_\alpha^{int} \right\rangle \quad (4.62)$$

Such a virial stress concept is typically obtained by generalizing the Clausius and Maxwell theories for pressure [156, 157]. The first term depends on the mass and on the absolute velocity of atomic particles, reflecting that mass transfer generates a pressure on stationary spatial surfaces external to an atomic-particle system. The second term depends on interatomic forces and atomic positions, providing a continuum measure for the internal mechanical interactions between particles. However, the *virial stress* defined in Eq.(4.62) is not a measure of the Cauchy mechanical stress within an elastic body undergoing an arbitrary deformation [158]. As shown in the previous Section, it can be proved that the absolute velocities $\vec{v}_\alpha = d\vec{x}_\alpha/dt$ in Eq.(4.62) must be replaced with thermal velocities $\vec{v}_\alpha^{th}$ in order to properly obtain the Cauchy stress [159].

Virial Stress and external pressure

We also remark that the virial approach or virial theorem (Clausius 1870), as applied to gas systems for the evaluation of external pressure, captures this effect correctly. The key concept is that the pressure represents external forces between an atomic system and a container (where the pressure is generated by the collisions of the atoms on the inner surface of the container). In contrast, stress represents internal forces between particles inside a body (and it is not generated by collisions against a wall). Indeed, Eq.(4.62) describes the macroscopic pressure of a gas system correctly under the three following conditions: (i) the system is in statistical equilibrium, (ii) the pressure is to be interpreted in a time and volume averaged sense, i.e., fluctuations at the molecular level are assumed to average out over time and space and, (iii) the pressure must be recognized as the average force per unit area on the wall of a physical container holding the gas system. The *virial stress* given in Eq.(4.62) must be applied in molecular dynamics simulations when one is analyzing the pressure (or pressure tensor) of a gas or a fluid at thermodynamic equilibrium onto the inner surface of its container.

We recall that, in continuum mechanics, the Lagrangian reference frame is a way of looking at the motion where the observer follows individual body particles as they move through space and time. Therefore, in this picture, the key quantity is the trajectory of a given volume element identified by its initial conditions. On the other hand, the Eulerian reference frame is a way of looking at the motion that focuses on specific locations in the space through which the body particles pass. In this case the physical observables are described by scalar or vector fields, defined in a given point of the space. Eq.(4.50) represents the atomic counterpart of the Cauchy stress when it is considered in an Eulerian (spatial) reference frame. Andia, Costanzo, and Gray [160, 161] have taken a Lagrangian (material) frame of reference to show that the

stress in the atomic system does not contain a velocity term at all, by obtaining the further relation

Microscopic stress in Lagrangian reference frame

$$\left\langle \hat{\mathfrak{T}}_{\mathcal{L}} \right\rangle = -\frac{1}{V}\left\langle \sum_{\alpha=1}^{N} \vec{x}_\alpha \otimes \vec{F}_\alpha^{int} \right\rangle \tag{4.63}$$

Gao and Weiner [162] clearly show that the dynamic term is included only in an Eulerian (spatial) reference frame and not in a Lagrangian frame of reference. They also show the equivalence between the Eulerian (spatial) and the Lagrangian (material) definitions of virial stress [162]. Anyway, in molecular dynamics simulations the Eulerian point of view must be always considered in order to draw meaningful comparisons among numerical and continuum results [152].

4.3.4 *Implementation of the atomic stress*

In the previous Sections we have derived the atomistic counterpart of the Cauchy stress. It has been obtained from the calculation of the virial defined in terms of the atomic positions, Eq.(4.50). On the other hand, in Molecular Dynamics, typically the so-called Periodic Boundary Conditions (PBC) are applied. In such a case, in spite of the absolute positions of the particles, the interatomic distances carry on all the informations on the dynamics of the system. Therefore, as discussed in Section 4.3.5, it is crucial to express all the system properties in terms of the atomic distances.

Two-body interactions

Here, we specialize the general result given in Eq.(4.50) to the case of two-body interactions between the atoms within a solid elastic body. The quantity $\vec{F}_\alpha^{int}$ can be written as the sum $\sum_{\beta\neq\alpha}^{N} \vec{f}_{\alpha\beta}$, where $\vec{f}_{\alpha\beta}$ is the force applied on atom α by atom β. Eq.(4.50) can be converted to

$$\left\langle \hat{\mathfrak{T}} \right\rangle = -\frac{1}{V}\left\langle \sum_{\alpha=1}^{N} m_\alpha \vec{v}_\alpha^{th} \otimes \vec{v}_\alpha^{th} \right\rangle - \frac{1}{V}\left\langle \sum_{\alpha=1}^{N} \vec{x}_\alpha \otimes \sum_{\beta\neq\alpha}^{N} \vec{f}_{\alpha\beta} \right\rangle \tag{4.64}$$

The last term can be split into two identical terms as follows

$$\begin{aligned} \left\langle \hat{\mathfrak{T}} \right\rangle &= -\frac{1}{V}\left\langle \sum_{\alpha=1}^{N} m_\alpha \vec{v}_\alpha^{th} \otimes \vec{v}_\alpha^{th} \right\rangle \\ &- \frac{1}{2V}\left\langle \sum_{\alpha=1}^{N} \vec{x}_\alpha \otimes \sum_{\beta\neq\alpha}^{N} \vec{f}_{\alpha\beta} \right\rangle + \frac{1}{2V}\left\langle \sum_{\alpha=1}^{N} \vec{x}_\alpha \otimes \sum_{\beta\neq\alpha}^{N} \vec{f}_{\beta\alpha} \right\rangle \end{aligned} \tag{4.65}$$

since $\vec{f}_{\beta\alpha} = -\vec{f}_{\alpha\beta}$. After some algebra we get

$$\left\langle \hat{\mathfrak{T}} \right\rangle = -\frac{1}{V}\left\langle \sum_{\alpha=1}^{N} m_\alpha \vec{v}_\alpha^{th} \otimes \vec{v}_\alpha^{th} \right\rangle + \frac{1}{2V}\left\langle \sum_{\alpha=1}^{N} \sum_{\beta\neq\alpha}^{N} \vec{x}_{\alpha\beta} \otimes \vec{f}_{\alpha\beta} \right\rangle \tag{4.66}$$

where $\vec{x}_{\alpha\beta} = \vec{x}_\beta - \vec{x}_\alpha$. This form is particularly useful for molecular dynamics simulations because the force term $\vec{f}_{\alpha\beta}$ is linked directly with the interaction potential energy $\mathcal{U}^{2B}(r)$

$$\vec{f}_{\alpha\beta} = \left.\frac{d\mathcal{U}^{2B}(r)}{dr}\right|_{r=|\vec{x}_{\alpha\beta}|} \frac{\vec{x}_{\alpha\beta}}{|\vec{x}_{\alpha\beta}|} \tag{4.67}$$

By substituting Eq.(4.67) into Eq.(4.66) we obtain

$$\begin{aligned}\left\langle \hat{\mathcal{T}} \right\rangle &= -\frac{1}{V}\left\langle \sum_{\alpha=1}^{N} m_\alpha \vec{v}_\alpha^{\,th} \otimes \vec{v}_\alpha^{\,th} \right\rangle \\ &+ \frac{1}{2V}\left\langle \sum_{\alpha=1}^{N}\sum_{\beta\neq\alpha}^{N} \vec{x}_{\alpha\beta} \otimes \vec{x}_{\alpha\beta} \left(\frac{1}{r}\frac{d\mathcal{U}^{2B}(r)}{dr}\right)\Big|_{r=|\vec{x}_{\alpha\beta}|} \right\rangle\end{aligned} \tag{4.68}$$

This form is useful because it depends only on quantities available during any simulations and it is well suited for being used under the typical assumption of periodic boundary conditions.

Many-body interactions

We derive now a formulation of Eq.(4.50) in terms of the atomic distances that can be used for any many-body force field. We observe that many-body interactions such as Stillinger-Weber, Tersoff, Brenner and EDIP, as well as tight-binding ones, have a total potential energy $\mathcal{U}$ which can be written in terms of all the possible (scalar) distances between each couple of atoms. If we define $x_{\alpha\beta} = |\vec{x}_{\alpha\beta}| = |\vec{x}_\beta - \vec{x}_\alpha|$, we then get $\mathcal{U} = \mathcal{U}(\{x_{\alpha\beta}\})$.

For a system of N atoms we have $N(N-1)/2$ independent distances $x_{\alpha\beta}$ which define the positions of the particles up to a nonessential roto-translation (the potential energy $\mathcal{U}$ must be invariant under roto-translation of the particle system). From Eq.(4.49) we obtain

$$\langle \mathcal{T}_{hk} \rangle = -\frac{1}{V}\left\langle \sum_{\alpha=1}^{N} m_\alpha v_{\alpha,k}^{th} v_{\alpha,h}^{th} \right\rangle - \frac{1}{V}\langle \Gamma_{hk} \rangle \tag{4.69}$$

where

$$\begin{aligned}\Gamma_{hk} &= \sum_{\alpha=1}^{N} x_{\alpha,k} F_{\alpha,h}^{int} = -\sum_{\alpha=1}^{N} x_{\alpha,k}\frac{\partial \mathcal{U}}{\partial x_{\alpha,h}} \\ &= -\sum_{\alpha=1}^{N} x_{\alpha,k}\frac{1}{2}\sum_{\delta=1}^{N}\sum_{\rho=1}^{N}\frac{\partial \mathcal{U}}{\partial x_{\delta\rho}}\frac{\partial x_{\delta\rho}}{\partial x_{\alpha,h}}\end{aligned} \tag{4.70}$$

where $\partial\mathcal{U}/\partial x_{\gamma\gamma}$ is zero by definition ($\mathcal{U}$ does not depend on $x_{\gamma\gamma}$ since $x_{\gamma\gamma} = 0$ for any atom γ). We simply obtain

$$\frac{\partial x_{\delta\rho}}{\partial x_{\alpha,h}} = \frac{\partial|\vec{x}_\rho - \vec{x}_\delta|}{\partial x_{\alpha,h}} = \frac{(\delta_{\delta\alpha} - \delta_{\rho\alpha})(x_{\delta,h} - x_{\rho,h})}{x_{\delta\rho}} \tag{4.71}$$

We also define $x_{\alpha\beta,s} = \vec{x}_{\alpha\beta}\cdot\vec{e}_s$ and therefore

$$\begin{aligned}\Gamma_{hk} &= \sum_{\alpha=1}^{N} x_{\alpha,k}\frac{1}{2}\sum_{\delta=1}^{N}\sum_{\rho=1}^{N}\frac{\partial \mathcal{U}}{\partial x_{\delta\rho}}\frac{(\delta_{\delta\alpha} - \delta_{\rho\alpha})x_{\delta\rho,h}}{x_{\delta\rho}} \\ &= \sum_{\alpha=1}^{N}\sum_{\rho=1}^{N}\frac{x_{\alpha,k}}{2}\frac{\partial \mathcal{U}}{\partial x_{\alpha\rho}}\frac{x_{\alpha\rho,h}}{x_{\alpha\rho}} - \sum_{\beta=1}^{N}\sum_{\delta=1}^{N}\frac{x_{\beta,k}}{2}\frac{\partial \mathcal{U}}{\partial x_{\delta\beta}}\frac{x_{\delta\beta,h}}{x_{\delta\beta}} \\ &= \sum_{\alpha=1}^{N}\sum_{\rho=1}^{N}\frac{x_{\alpha,k}}{2}\frac{\partial \mathcal{U}}{\partial x_{\alpha\rho}}\frac{x_{\alpha\rho,h}}{x_{\alpha\rho}} - \sum_{\rho=1}^{N}\sum_{\alpha=1}^{N}\frac{x_{\rho,k}}{2}\frac{\partial \mathcal{U}}{\partial x_{\alpha\rho}}\frac{x_{\alpha\rho,h}}{x_{\alpha\rho}} \\ &= -\sum_{\alpha=1}^{N}\sum_{\rho=1}^{N}\frac{x_{\alpha\rho,h}x_{\alpha\rho,k}}{2}\frac{1}{x_{\alpha\rho}}\frac{\partial \mathcal{U}}{\partial x_{\alpha\rho}}\end{aligned} \tag{4.72}$$

By substituting Eq.(4.72) in Eq.(4.69) we get

$$\begin{aligned}\langle \mathcal{T}_{hk} \rangle &= -\frac{1}{V}\left\langle \sum_{\alpha=1}^{N} m_\alpha v_{\alpha,k}^{th} v_{\alpha,h}^{th} \right\rangle \\ &\quad + \frac{1}{V}\left\langle \sum_{\alpha=1}^{N}\sum_{\beta=1}^{N} \frac{x_{\alpha\beta,h} x_{\alpha\beta,k}}{2} \frac{1}{x_{\alpha\beta}} \frac{\partial \mathcal{U}}{\partial x_{\alpha\beta}} \right\rangle \end{aligned} \tag{4.73}$$

or, equivalently, in tensor form

$$\begin{aligned}\left\langle \hat{\mathcal{T}} \right\rangle &= -\frac{1}{V}\left\langle \sum_{\alpha=1}^{N} m_\alpha \vec{v}_\alpha^{th} \otimes \vec{v}_\alpha^{th} \right\rangle \\ &\quad + \frac{1}{2V}\left\langle \sum_{\alpha=1}^{N}\sum_{\beta\neq\alpha}^{N} \vec{x}_{\alpha\beta} \otimes \vec{x}_{\alpha\beta} \frac{1}{x_{\alpha\beta}} \frac{\partial \mathcal{U}}{\partial x_{\alpha\beta}} \right\rangle \end{aligned} \tag{4.74}$$

Note that when the interaction energy represents a system of two-body interactions, Eq.(4.74) reduces to Eq.(4.68), as expected. Once again and as discussed in the next Section, Eq.(4.74) can be used under the typical assumption of Periodic Boundary Conditions.

4.3.5 *Virial stress and Periodic Boundary Conditions*

As a final consideration on the stress definition in Molecular Dynamics, we present a discussion on the calculation of the virial stress in a system under Periodic Boundary Conditions. More precisely, we will clarify that the expressions obtained in Section 4.3.4 (where the virial is expressed in terms of the interatomic distances, Eqs.(4.66) and (4.74), in spite of the atomic positions as in Eq.(4.50)) are suitable for the implementation under PBC. To this aim, we can consider the simple case of a one-dimensional chain of atoms at zero temperature. We assume that the system is subjected to nearest neighbors interactions of magnitude f^{int}.

The volume is fixed by external forces

Firstly, in Fig.24 we show a configuration of such a system where the volume (the length L of the chain) is kept fixed by the external forces f^{ext}. In such a case, the virial stress can be obtained by means of its

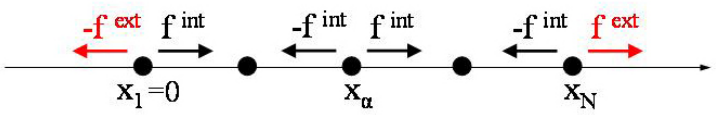

Figure 24: One-dimensional chain of atoms subjected to a nearest neighbors internal interaction, f^{int}, and to external forces f^{ext}.

expression in terms of the atomic positions x_α:

$$T = \frac{1}{L}\sum_{\alpha} x_\alpha F_\alpha^{int} = -\frac{1}{L} x_N f^{int} \tag{4.75}$$

where F_α^{int} is the total internal force acting on the atom α. We note that, at the equilibrium, the total force on each atoms is zero. Therefore, the

internal force acting on the atom in x_N, i.e. $-f^{int}$, is equal in absolute value to the external one f^{ext}. As a consequence, the virial stress is

$$T = f^{ext} \tag{4.76}$$

that is zero, as expected, only in absence of external forces.

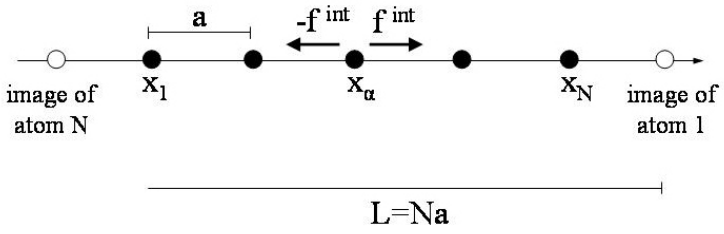

Figure 25: One-dimensional chain of atoms subjected to internal forces and to Periodic Boundary Conditions.

The volume is fixed by the P.B.C.

On the other hand, in Molecular Dynamics simulations (typically) the system is not subjected to surface forces but the volume is fixed by means of the Periodic Boundary Conditions, i.e. by the interactions with the periodic images of the atoms (see Fig.25). In order to apply such conditions the interatomic distance $x_{\alpha\beta}$ are calculated by

Interatomic distances under Periodic Boundary Conditions

$$x_{\alpha\beta}|_{PBC} = x_\alpha - x_\beta - L \text{ int}\left[\frac{(x_\alpha - x_\beta)}{l} - \frac{1}{2}\right] \tag{4.77}$$

In particular, this means that $x_{1N}|_{PBC} = a$, being a the lattice parameter.

Now, if we calculate the stress in terms of the atomic positions, i.e. by a straightforward application of Eq.(4.50), we get

$$T = \frac{1}{L}\sum_\alpha x_\alpha F_\alpha^{int} = -\frac{1}{L}\sum_\alpha x_\alpha (f^{int} - f^{int}) = 0 \tag{4.78}$$

In this calculation we have not take into account the effect of the PBC. obtaining $T = 0$ independently of the possible deformation of the system. In order to get the correct result, we must properly consider the boundary conditions. This can be done by calculating the virial stress in terms of the interatomic distances $x_{\alpha\beta}|_{PBC}$

$$T = \frac{1}{L}\sum_{\alpha\beta} x_{\alpha\beta}|_{PBC} f^{int} = \frac{1}{L}\sum_{\alpha\beta} a\, f^{int} = \frac{1}{L} N\, a\, f^{int} = f^{int} \tag{4.79}$$

which was to be demonstrated.

5

INTERFACE LINEAR ELASTICITY AT THE NANOSCALE

Contents

Interface between different media is the most common structure in composites and complex materials. It represents the main feature of atomistic models of materials generally not taken into account by continuum theories. In fact, in the continuum based theory the interface between media is considered devoid of any inner structure or specific elastic response. On the other hand, the effective elastic behavior of heterogeneous materials where the inhomogeneity shows up at the nano-scale (i.e. nanocomposite, multi-layered or nanostructured materials) is deeply affected by interface features, occurring between phases characterized by different elastic moduli and different atomic structure [98, 163, 164]. In particular, a key issue consists in evaluating the stress and the strain fields nearly or just across the interface between such phases. While this problem has been extensively investigated by continuum mechanics [165, 166, 167, 168], comparatively little work has been based on atomistic simulations. This is in spite of the maturity they reached in dealing with solid mechanics [169] and even though they allow for a detailed atomic-scale modeling of the structural complexity of heterogeneous materials [170, 171, 172, 173]. In the first Section of this Chapter, we show the analysis of the elastic features of a planar interface. We describe its macroscopic behavior by means of a set of continuity conditions. Moreover, through atomistic simulations, we apply such a general scheme to a specific atom-resolved interface model. In the second part of the Chapter, we consider a rather different physical system where the interface between different media plays a crucial role. We describe the elastic behavior of an inclusion embedded in matrix with different elastic properties. This is the subject of the Eshelby theory described in the previous Chapters. In particular, we show that the interface formation at the boundary between matrix and inclusion leads to prestrain (or prestress) effects not considered by the standard Eshelby approach. This effects shows up only at the nanoscale, i.e. when an inclusion size of a few nanometers is considered. Furthermore, we apply the generalization of the Eshelby theory discussed in Section 2.2 to the qualitative and quantitative description of these size-effects.

5.1 FLAT INTERFACE ELASTIC PROPERTIES: THE A-SI/C-SI CASE

In this Section we compare [174] continuum and atomistic solid mechanics to establish a general picture about the continuity of the elastic fields (i.e. strain and stress) across a planar interface between two different media. In particular, we firstly derive, in the framework of continuum elasticity, a set of conditions for strain and stress at the interface. Then, we apply such relations of general validity to an atom-resolved interface system. To this aim, we atomistically model an amorphous/crystalline silicon interface (a-Si/c-Si) which involves both elastically different phases and structures quite differing at the atomic scale. In other words, the a-Si/c-Si interface is an interesting model system containing the two most relevant features of heterogeneous materials. It also represents a system of paramount importance for applications in microelectronics, photovoltaics, or opto-electronics.

5.1.1 *Continuity conditions at the interface*

In continuum mechanics the dynamics of a deformable body under infinitesimal strain is described by the equation of motion in Eq.(1.26). Let us consider a plane interface between two different linear elastic

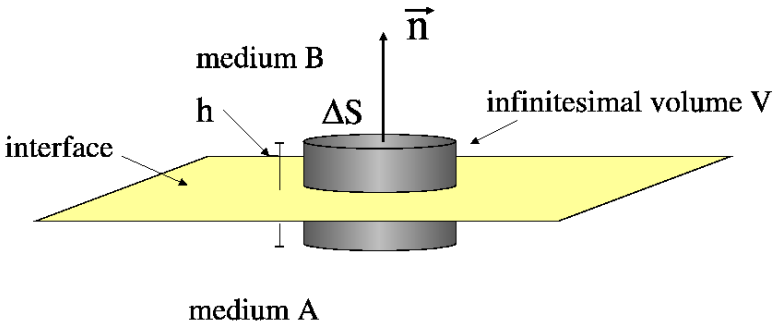

Figure 26: Infinitesimal volume across an interface between two elastically different media.

media, having stiffness $\hat{\mathcal{C}}^{(a)}$ and $\hat{\mathcal{C}}^{(b)}$. Close to the interface, the stress and the strain fields within material a (b) are, respectively, $\hat{T}^{(a)}$ and $\hat{\epsilon}^{(a)}$ ($\hat{T}^{(b)}$ and $\hat{\epsilon}^{(b)}$).

The first continuity condition is obtained by integrating the equation of motion Eq.(1.26) on the infinitesimal volume V across the interface (see Fig.26)

$$\int_V \vec{\nabla}\hat{T}dV + \int_V \vec{b}dV = \int_V \rho\vec{a}dV \tag{5.1}$$

By applying the divergence theorem to the first term of the last equation

$$\int_S \hat{T}\vec{n}dS + \int_V \vec{b}dV = \int_V \rho\vec{a}dV \tag{5.2}$$

where $\vec{n}$ is the unitary vector orthogonal to the interface plane defined in Fig.26. We now consider the integration volume as $V = \Delta S\, h$ where h is the infinitesimal quantity. Therefore

$$\hat{T}^{(b)} \Delta S\, \vec{n} - \hat{T}^{(a)} \Delta S\, \vec{n} + o(h) + \vec{b}\, \Delta S\, h = \rho\, \vec{a}\, \Delta S\, h \tag{5.3}$$

In the limit of vanishing h we finally find a first set of continuity conditions

Continuity of the orthogonal projection of stress field

$$\hat{T}^{(a)} \vec{n} = \hat{T}^{(b)} \vec{n} \tag{5.4}$$

for the stress field projected along the direction orthogonal to the interface plane.

In order to derive the continuity condition for the strain field, we preliminary consider the general expressions for the variation of length Δl and the variation of angle $\Delta\theta$ in a bulk material under deformation $\hat{e}$. According to Eqs. (1.10) and (1.11), if $\vec{t}$ is the unit vector aligned with a segment of length l, then its length variation is

$$\Delta l = \left(\vec{t} \cdot \hat{e}\, \vec{t}\right) l \tag{5.5}$$

Similarly, if $\vec{t}$ and $\vec{s}$ are unit vectors defining an angle θ, its variation under the same deformation is

$$\Delta\theta = \frac{1}{\sin(\theta)} \left[\cos(\theta) \left(\vec{t} \cdot \hat{e}\, \vec{t} + \vec{s} \cdot \hat{e}\, \vec{s}\right) - 2 \left(\vec{s} \cdot \hat{e}\, \vec{t}\right)\right] \tag{5.6}$$

We suppose now that $\vec{t}$ and $\vec{s}$ are arbitrary unit vectors lying on the interface plane. If we assume that interface debonding or sliding do not occur, then Δl and $\Delta\theta$ must to be continuous, i.e.

Continuity of the strain field projections

$$\begin{aligned} \vec{t} \cdot \hat{e}^{(a)}\, \vec{t} &= \vec{t} \cdot \hat{e}^{(b)}\, \vec{t} \\ \vec{s} \cdot \hat{e}^{(a)}\, \vec{t} &= \vec{s} \cdot \hat{e}^{(b)}\, \vec{t} \end{aligned} \tag{5.7}$$

These relations state the continuity of the strain field.

For linear elastic media, the interface relations provided by Eqs.(5.4) and (5.7) supply the further boundary conditions

Further continuity conditions under the linear hypothesis

$$\begin{aligned} \hat{C}^{(a)} \hat{e}^{(a)} \vec{n} &= \hat{C}^{(b)} \hat{e}^{(b)} \vec{n} \\ \vec{t} \cdot \left[\hat{C}^{(a)}\right]^{-1} \hat{T}^{(a)}\, \vec{t} &= \vec{t} \cdot \left[\hat{C}^{(b)}\right]^{-1} \hat{T}^{(b)}\, \vec{t} \\ \vec{s} \cdot \left[\hat{C}^{(a)}\right]^{-1} \hat{T}^{(a)}\, \vec{t} &= \vec{s} \cdot \left[\hat{C}^{(b)}\right]^{-1} \hat{T}^{(b)}\, \vec{t} \end{aligned} \tag{5.8}$$

They predict a discontinuity in some of the components of the strain and stress fields and allow for their evaluation.

In order to further proceed, we need to define the interface orientation, as well as the state of deformation. We therefore define a cartesian frame of reference (x, y, z), where (x, y) is the interface plane, and we assume that the unit vectors $\vec{s}, \vec{t}$ and $\vec{n}$ are aligned along the x-, y- and z-axis, respectively (see Fig.27). Moreover, in order to reduce the complexity of the stiffness tensors involved in the model, we fix a given symmetry for the elastic behavior of the media under consideration. For the following application, we can assume a cubic symmetry so that the

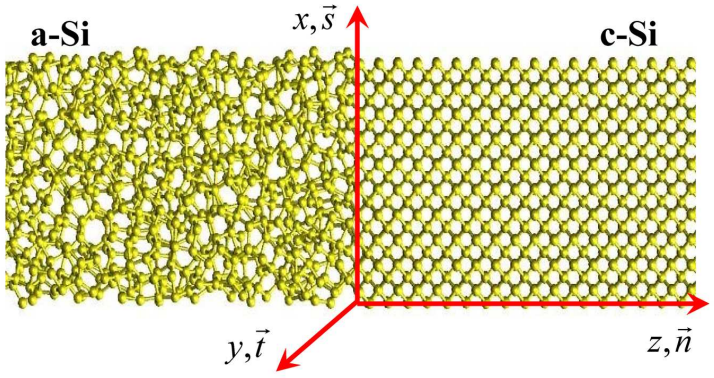

Figure 27: Atomistic structure of the a-Si/c-Si interface. The reference frame (x, y, z) and the basis $(\vec{s}, \vec{t}, \vec{n})$ have been represented.

behavior is described by three independent elastic moduli (see Section 1.1.5) and the resulting stiffness tensor is, in Voigt notation

$$\hat{\mathcal{C}} = \begin{pmatrix} \mathcal{C}_{11} & \mathcal{C}_{12} & \mathcal{C}_{12} & 0 & 0 & 0 \\ \mathcal{C}_{12} & \mathcal{C}_{11} & \mathcal{C}_{12} & 0 & 0 & 0 \\ \mathcal{C}_{12} & \mathcal{C}_{12} & \mathcal{C}_{11} & 0 & 0 & 0 \\ 0 & 0 & 0 & \mathcal{C}_{44} & 0 & 0 \\ 0 & 0 & 0 & 0 & \mathcal{C}_{44} & 0 \\ 0 & 0 & 0 & 0 & 0 & \mathcal{C}_{44} \end{pmatrix} \tag{5.9}$$

The full set of continuity conditions at the interface between two linear media under uniaxial elongation

Therefore, by imposing a uniaxial strain ϵ_{zz} (and $\epsilon_{ij} = 0 \; \forall \; i, j \neq z$) we get

$$T_{zz}^{(a)} = T_{zz}^{(b)} \tag{5.10}$$

$$\frac{\epsilon_{zz}^{(a)}}{\epsilon_{zz}^{(b)}} = \frac{\mathcal{C}_{11}^{(b)}}{\mathcal{C}_{11}^{(a)}} \tag{5.11}$$

$$\mathcal{D}_{12}^{(a)} \left(T_{yy}^{(a)} + T_{zz}^{(a)} \right) + \mathcal{D}_{11}^{(a)} T_{xx}^{(a)} = \mathcal{D}_{12}^{(b)} \left(T_{yy}^{(b)} + T_{zz}^{(b)} \right) + \mathcal{D}_{11}^{(b)} T_{xx}^{(b)} \tag{5.12}$$

$$\mathcal{D}_{12}^{(a)} \left(T_{xx}^{(a)} + T_{zz}^{(a)} \right) + \mathcal{D}_{11}^{(a)} T_{yy}^{(a)} = \mathcal{D}_{12}^{(b)} \left(T_{xx}^{(b)} + T_{zz}^{(b)} \right) + \mathcal{D}_{11}^{(b)} T_{yy}^{(b)} \tag{5.13}$$

Equation (5.10) states the continuity of the longitudinal component of the stress, while Eq.(5.11) predicts a discontinuity in the longitudinal strain; similarly, Eqs.(5.12) and (5.13) prove the discontinuity of the transverse components of the stress. Moreover, we note that the last two equations correspond to $\epsilon_{xx}^{(a)} = \epsilon_{xx}^{(b)}$ and $\epsilon_{yy}^{(a)} = \epsilon_{yy}^{(b)}$ (i.e. they correspond to Eq.(5.7) with $\vec{t} = (1, 0, 0)$ or $\vec{t} = (0, 1, 0)$). If an uniaxial deformation is considered, these transverse components of the strain vanish everywere and, therefore, both the left and right members of Eqs.(5.12) and (5.13) will be zero.

5.1.2 *The a-Si/c-Si interface model*

In our atomistic model, material (a) corresponds to a-Si and material (b) corresponds to c-Si. Therefore, we need at first to generate a bulk

Table 4: Elastic stiffness and compliance constants (at $T = 0$ K) for c-Si and a-Si obtained by present atomistic simulations (Stillinger-Weber potential). Ab initio calculations and experimental estimates for c-Si are reported as well. Results based on molecular dynamics simulations are also reported for the a-Si.

Elastic Moduli	a-Si	c-Si	c-Si[94] (ab initio)	a-Si[a][175] (MD)	c-Si[b][176] (Expt.)
$\mathcal{C}_{11}$[GPa]	135	151.26	162.07	150	166
$\mathcal{C}_{12}$[GPa]	94	76.14	63.51	86	64
$\mathcal{C}_{44}$[GPa]	20	56.4	77.26	33	79
$\mathcal{D}_{11}$[GPa^{-1}]	0.017	0.009988	0.00792	0.0114	0.0077
$\mathcal{D}_{12}$[GPa^{-1}]	-0.0071	-0.003347	-0.00222	-0.00417	-0.0021
$\mathcal{D}_{44}$[GPa^{-1}]	0.049	0.0177	0.0129	0.0303	0.013

[a] $T = 294$ K, [b] $T = 300$ K

a-Si sample. By using the Stillinger-Weber interatomic force field (described in the previous Chapter) an a-Si sample containing as many as 24000 atoms was obtained by quenching from the melt at the same density of c-Si. A simple cubic lattice of Si atoms was melted at $T = 2500$K. Then, a first quenching led to the liquid phase at $T = 1800$K. Finally, it was quenched again to the solid phase at $T = 0$K with a rate as slow as $3 \cdot 10^{12}$ K/s obtaining the amorphous configuration.Then, through small variations of the metric tensor (defining the volume and the shape of the periodically repeated simulation box) followed by relaxation of the internal degrees of freedom (through damped dynamics), all the components of the stress tensor have been reset to zero (actually to a value smaller than 10^{-2} GPa). In the amorphous structure so obtained 8% of the atoms are 3-fold coordinated, 75% are 4-fold coordinated and 17% are 5-fold coordinated corresponding to an average coordination close to 4.1 in agreement with experimental data. A c-Si sample containing the same number of atoms in the a-Si one has been arranged as well.

The a-Si bulk is obtained by quenching from the melt

In order to verify the continuity conditions in our atomistic system, we need to calculate the bulk elastic properties, i.e. the stiffness tensor components, of the two materials involved in the interface model. As for the c-Si, its lattice structure exhibits a cubic symmetry, therefore its macroscopic elastic behavior is described by the stiffness tensor in Eq.(5.9). On the other hand, the amorphous Si is a disordered atomic structure and, therefore, it exhibits an isotropic elastic behavior. In this case the stiffness tensor assumes the same form of the c-Si case but with the further (Cauchy) condition $2\mathcal{C}_{44} = \mathcal{C}_{11} - \mathcal{C}_{12}$. By appling a suitable set of uniaxial deformations in the range $0 \leqslant \epsilon_{zz} \leqslant 0.1$, we have obtained the longitudinal and transverse stress-strain curves reported in Fig.28 for both the media.

We remember that the local stress field deserves a careful definition and calculation: we have adopted the expression derived from the virial of the forces, as described in details in Section 4.3. Elastic and compliance constants have been obtained as the numerical derivative of the stress-strain curves at vanishing strain. In fact, if the uniaxial elongation in the z direction $\hat{e} = (0, 0, \epsilon_{zz}, 0, 0, 0)$ is applied to the system, the

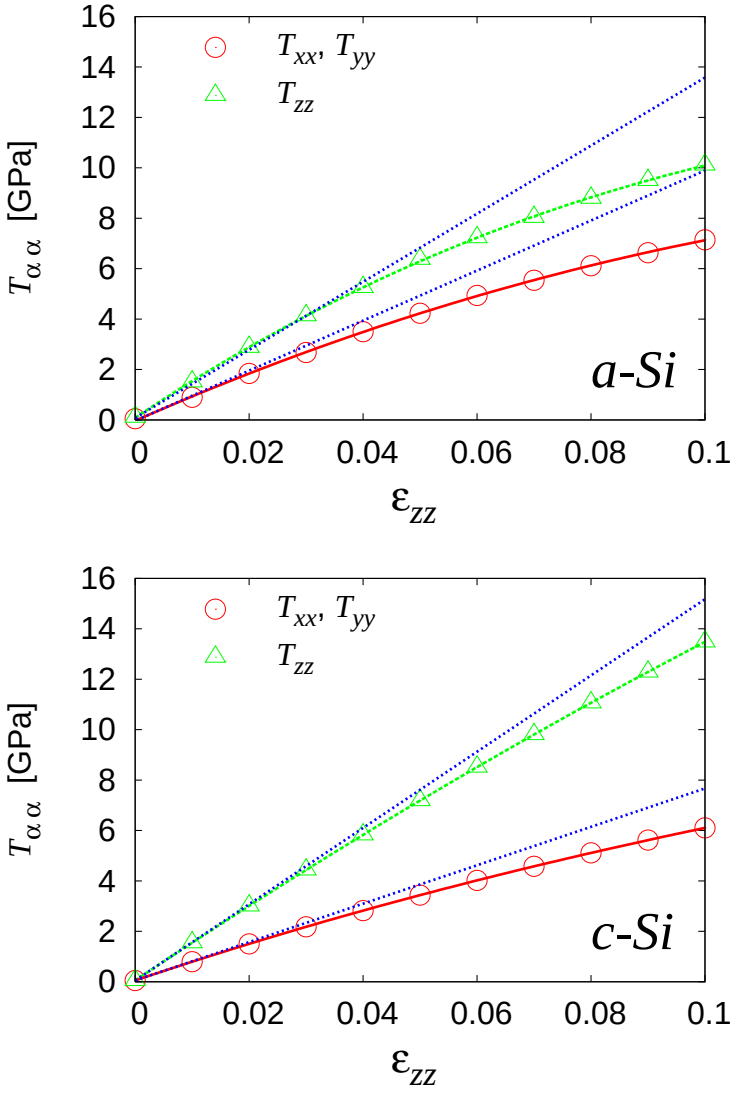

Figure 28: Longitudinal (T_{zz}) and tranverse (T_{xx}) stress-strain relations for the a-Si (top panel) and c-Si (bottom panel), obtained with molecular dynamics simulations.

resulting stress can be obtained from the constitutive equation $\hat{T} = \hat{\mathcal{C}}\hat{\epsilon}$ and from Eq.(5.9)

$$T_{xx} = T_{yy} = \mathcal{C}_{12}\epsilon_{zz} \tag{5.14}$$

$$T_{zz} = \mathcal{C}_{11}\epsilon_{zz} \tag{5.15}$$

Moreover, in order to calculate the third elastic constants $\mathcal{C}_{44}$, we have applied a shear deformation $\hat{\epsilon} = (0, 0, 0, \epsilon_{xy}, 0, 0)$ as well:

$$T_{xy} = \mathcal{C}_{44}\epsilon_{xy} \tag{5.16}$$

Present atomistic data are summarized in Table 4.

While for c-Si we have found three independent elastic moduli (cubic symmetry), in the case of the amorphous system the Cauchy relation is well reproduced. This proves that our computational procedure indeed generated an isotropic amorphous material: the a-Si slab, therefore,

represents the atomistic counterpart of an isotropic continuum. In Table 4 we also report experimental and ab initio elastic moduli for c-Si [94, 176] and molecular dynamics data for the amorphous phase [175]. The c-Si data show that our present simulations based on the Stillinger-Weber potential provide reasonably good elastic moduli. As for the a-Si, we observe that our results show a sizeable elastic softening with respect to the perfect crystal. The observed softening of the elastic properties of a-Si is consistent with previous investigations [175], as reported in Table 4. Overall these results stand for the reliability of the present estimation of bulk elastic properties.

The a-Si/c-Si interface was obtained by glueing the slabs and by relaxing the system by a damped molecular dynamics, thus allowing for the formation of chemical bonds across amorphous/crystalline boundary. A set of uniaxial homogeneous deformations in the range $0 \leqslant \epsilon_{zz} \leqslant 0.1$ was eventually applied to our composite system. After a suitable equilibration time, the linear applied displacement $u_z = \epsilon_{zz} z$ relaxed to $u_z = \epsilon_{zz} z + \Delta u_z(z)$, where Δu_z is the difference between the final and the applied displacement. In Fig.29 we show the results for a deformation as large as $\epsilon_{zz} = 0.04$. In Fig.29 (a) we report the perturbation Δu_z versus z: it is interesting to observe the fluctuations of the displacement in the a-Si slab induced by the structural disorder. Moreover, in Figs.29 (b) and (c), we show the longitudinal and the transverse components of the stress tensor, respectively. We plot the average value of the stress taken over slabs (normal to z) as thin as an interplanar distance. These planar averages will be hereafter referred to as $\overline{T}_{ij}(z)$. As a matter of fact, while in the crystalline system the atomic stress is practically uniform inside the sample, in the amorphous slab we find very large fluctuations due to the structural disorder. In order to point out the line-up of the stress tensor at the interface, we further average $\overline{T}_{ij}(z)$ over a distance d along the z-direction (Simple Moving Average) by defining

Planar average of the stress

Simple Moving Average of the noise in the amorphous bulk

$$\overline{\overline{T}}_{ij}(z) = \frac{1}{2d} \int_{z-d}^{z+d} \overline{T}_{ij}(z')dz' . \tag{5.17}$$

This is in fact the stress represented in Fig.29 (b) and (c) . Typically, we use $d \simeq 20$ Å, corresponding to 6 interplanar distances. This procedure allows for the estimation of $\overline{\overline{T}}_{zz}(z)$ in both the a-Si and c-Si, providing a typical value within each slab as large as 5.42 GPa and 5.48 GPa, respectively. So, as axpected from Eq.(5.10), the average zz-component of the stress is continuous. Similarly, the ratio between the average strain field in a-Si and the corresponding strain field in c-Si is found to be 1.108. On the other hand, from Table 4 we get $\mathcal{C}_{11}^{(c-Si)}/\mathcal{C}_{11}^{(a-Si)} = 1.12$. Once again, this result is in excellent agreement with the continuum condition given in Eq.(5.11). By inserting in Eqs.(5.12) and (5.13) the average stress values for any component, we obtain an almost perfect identity. We conclude that continuum and atomistic interface elasticity are perfectly consistent, provided that atomic-scale elastic fields are properly averaged.

Finally, we observe that the relaxed strain within the a-Si (c-Si) slab is always larger (smaller) than the applied strain ϵ_{zz}. This can be understood in terms of the quantity $\Delta u_z(z)$, previously defined and reported in Fig.30 for different values of the applied ϵ_{zz}. We can write: $\epsilon_{zz}^{(a-Si)} = \epsilon_{zz} + d\Delta u_z^{(a-Si)}/dz$ and $\epsilon_{zz}^{(c-Si)} = \epsilon_{zz} + d\Delta u_z^{(c-Si)}/dz$, where $d\Delta u_z^{(a-Si)}/dz$ and $d\Delta u_z^{(c-Si)}/dz$ are easly obtained from Fig.30.

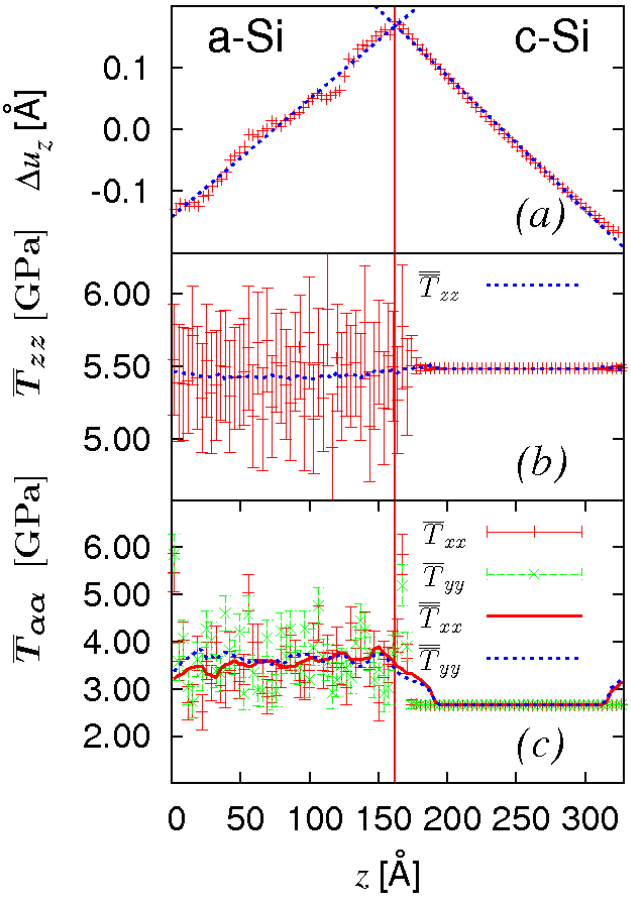

Figure 29: Perturbation to the imposed displacement after relaxation (a), transverse (b) and longitudinal (c) stress versus the z coordinate. For stress data the Simple Moving Average (SMA) has been considered to reduce the intensity of the fluctuations (dashed lines for $\overline{\overline{T}}_{zz}$ and $\overline{\overline{T}}_{yy}$, solid line for $\overline{\overline{T}}_{xx}$).

It is evident that $d\Delta u_z^{(a-Si)}/dz > 0$ and $d\Delta u_z^{(c-Si)}/dz < 0$ for any applied strain. Since this behavior is independent of the intensity of the applied strain, we conclude that the longitudinal stress-strain relations for a-Si and c-Si (see Fig.28) can not have intersection points: in other words, the amorphous phase is always softer than the crystalline one, for any state of deformation.

Nonlinear elastic behaviors of a-Si and c-Si

To conclude, we have verified that atomistic simulations for the interface behavior are consistent with continuum results, provided that appropriate averages are applied to the atomistic elastic fields. Moreover, we have obtained the stress-strain curves (transverse and longitudinal) of the Si amorphous and crystalline phases, proving that the a-Si is always softer than c-Si. Finally, we point out that the nonlinear character of amorphous silicon is larger than in crystalline silicon. This is qualitatively due to the complex disordered structure and to the rearrangements occurring during deformation. As a matter of fact, within a-Si atoms lie at distances that typically differ from the equilibrium crystalline ones. This means that they feel deviations from a purely harmonic potential.

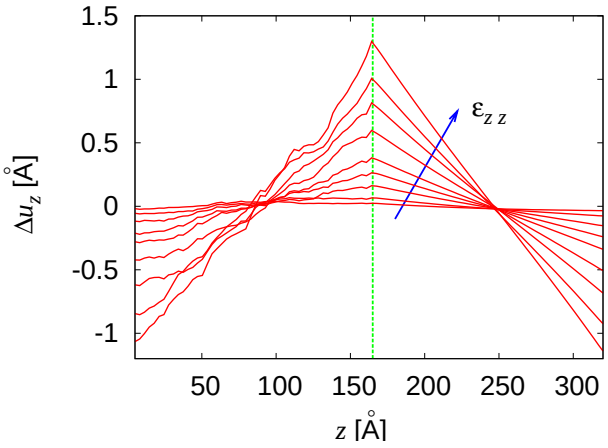

Figure 30: Perturbation to the imposed displacement obtained through relaxation for nine different values of the imposed strain (ranging from $\epsilon_{zz} = 0.02$ to $\epsilon_{zz} = 0.1$).

5.2 PRESTRAIN EFFECT INTO A SI NANOINCLUSION

The mechanical behavior of nanostructured materials is strongly affected by interface features, occurring at the boundary between phases characterized by different elastic constitutive equations or crystalline structures [167, 168]. In particular, the embedding of a given nanoinclusion in a hosting homogeneous matrix is deeply influenced by the lattice mismatch, which ultimately governs the effective elastic properties of the heterogeneous system. In fact, both the inclusion and the matrix accomplish an elastic relaxation to accommodate this mismatch and, therefore, they admit a state of deformation even if no external load is applied. We will refer to such a complex system as a prestressed (or, equivalently, prestrained) composite.

Prestress effect on the electronic behavior of actual nanostructures

A typical example of prestressed system is represented by semiconductor quantum dots or quantum wires, embedded in a matrix with different lattice parameter [122, 123]. Several works have been addressed to the calculation of the strain state in buried quantum dots [177, 178, 179]. Both quantitative and qualitative knowledge of stress and strain distributions are essential for characterizing and tailoring their optoelectronic properties [180, 181], as well as for understanding their self-organization [182]. Typically, the state of deformation is estimated using continuum elasticity and, then, used as input for an electronic structure calculation [183]. However, while continuum elasticity is inherently scale-independent, the elastic relaxation of a nanostructure depends on the actual length scale at which the heterogeneity shows up. In other words, surface effects become important, at the nanoscale, due to the increasing surface-to-volume ratio and induce a size dependency in the overall elastic behavior [184, 185].

In this Section we use [86] a combination of atomistic and continuum methods to describe the elastic behavior of a silicon nano-wire embedded in a silicon homogeneous matrix with different crystal orientation. This structure represents a good model for real systems of large technological interest [186, 187, 188]. Moreover, it also represents a conceptually relevant case where the atomic structure leads to de-

viations from the standard continuum picture. We describe how the presence of a disordered interface affects the elastic fields and generates a size-dependent prestrain in both the nano-wire and the surrounding matrix. In addition, by looking at the mechanical response of this model system to a remote load, we show how the prestrain induces a strong localization of the elastic fields nearby the inclusion. The atomistic simulations are developed to obtain a fully-resolved picture of the structural complexity of the disordered interface. On the other hand, the generalization of the Eshelby theory of Section 2.2 is here applied, fully reproducing the observed atomistic phenomena. This proves that such a generalization represents an atomically informed continuum model that includes the size-dependent effects described above.

Atomically informed continuum model

5.2.1 *The atomistic model*

We consider a crystalline silicon (c-Si) homogeneous matrix and we fix the x-axis along the (100) crystallographic direction of the diamond lattice (see Fig.31). The lattice parameter is set to the equilibrium value so as to obtain a stress-free configuration. A cylindrical portion of the matrix of radius R is then rotated by an angle ϑ around the z-axis (see Fig.31). Because of the cubic symmetry of the diamond lattice, the rotated cylinder behaves, upon loading along the y-axis, as an inclusion with a different elastic response than the hosting matrix. In addition, the elastic mismatch between the inclusion and the matrix depends on the angle of rotation and vanishes for $\vartheta = k\pi/2$ (k=integer). In most of our simulations we fixed $\vartheta = \pi/4$ since this angle supplies the largest difference in the elastic response between the inclusion and the matrix (see Sec. 5.2.3 for details).

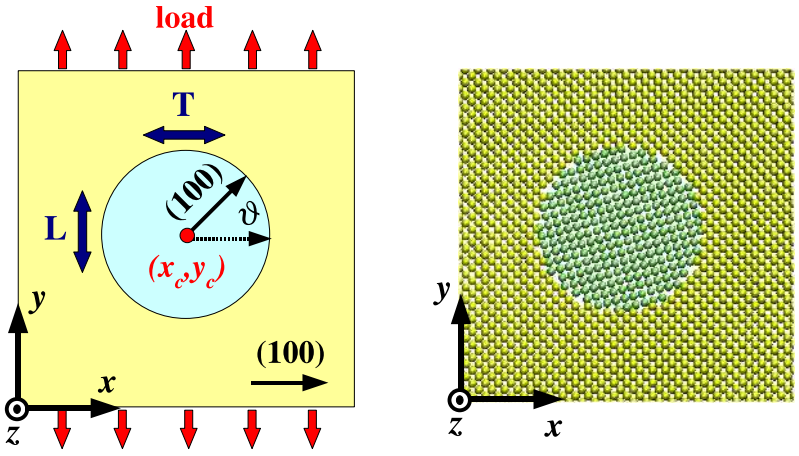

Figure 31: A c-Si inclusion of radius R embedded in a Si matrix. General scheme of the system geometry (left panel) and snapshot of an atomistic sample (right panel). The elastic mismatch between the inclusion and the matrix is obtained through a rotation by an angle ϑ of the inclusion. We also show the direction of the applied deformation (y-axis) and those of the longitudinal (L) and of the transverse (T) displacements.

The interaction among silicon atoms is described by the Tersoff potential (Section 4.2 and [189]). The simulation cell is a thin slab orthogonal to the z-axis; the PBC are applied so as to obtain an infinite cylindrical

inclusion. To minimizing the interaction between the periodic images, the width of the slab is ten times larger than the diameter of the inclusion, both in the x and in the y directions. As for the mechanical behavior, this structure is described by two dimensional elastic fields (plain strain conditions). It means that all the relevant quantities are functions only of the x and y coordinates.

Large scale atomistic simulations: 10^7 *atoms in a* 0.4 μm *Si slab*

By generating the input structure as above, we have arranged several samples with 2 nm $< R <$ 20 nm. The largest simulated system contains as many as 1.3×10^7 atoms and the corresponding length of the simulation cell along x and y is as large as 400 nm.

The initial configurations have been relaxed through damped dynamics in order to allow for chemical bonding at the interface between the inclusion and the matrix. The convergence criterion is set so to have interatomic forces in the final configuration not larger than 10^{-5} eV/Å. After this relaxation, we have computed the atomic displacement field $\vec{u}^0(x, y)$ and we have found that the disordered interface generates a uniform hydrostatic compression within the inclusion. Therefore, the present atomistic model correctly predicts that even in absence of any external load, the inclusions exhibit a state of uniform internal prestrain. In Fig.32 we show the variation of such a prestrain $\varepsilon^0 = \partial u_x^0/\partial x = \partial u_y^0/\partial y$ as function of the radius R. In order to obtain ε^0 for each sample, we have fit the $u_x^0(x, y)$ and $u_y^0(x, y)$ surfaces inside the inclusion guessing a linear dependence on x and y. In order to test the linear hypothesis, i.e. the uniformity of the internal strain field, we have used several fitting domains obtaining a constant trend.

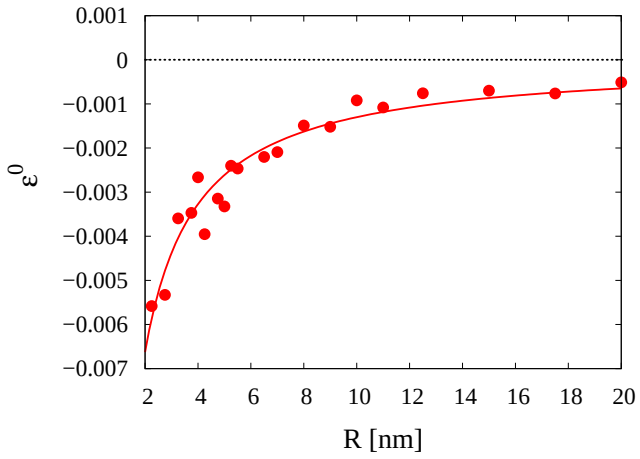

Figure 32: Internal prestrain ε^0 within the nano-wire as a function of the inclusion radius R. We report the atomistic result (full symbols) and the continuum theory prediction (solid line).

In Fig.32 we note that the prestrain ε^0 (in absolute value) reduces with increasing R. This effect can be explained as follows. In Fig.33 we report the atom number density and the energy per atom as a function of the distance r from the center of the inclusion; data are obtained from the sample with $R = 10$ nm. We note that the atom number density at a distance $r = R$, corresponding to the position of the interface, is lower than its value in the surrounding crystalline bulk. The interface region behaves as a coating of constant thickness d inserted between the matrix and the inclusion. Therefore, the volume available for the

inclusion is reduced with respect to the initial configuration by a factor $\left(\frac{R-d}{R}\right)^2$. When R increases this volume variation and the resulting prestrain tend to zero. We remark that, in principle, the thickness of the disordered interface could depend on the value of the angle ϑ defined in Fig.31. Nevertheless, in our calculations such a thickness was found to be pretty constant, as discussed below (see Sec.5.2.2). Further investigations about the disordered structure at an interface can be found elsewhere [190, 191].

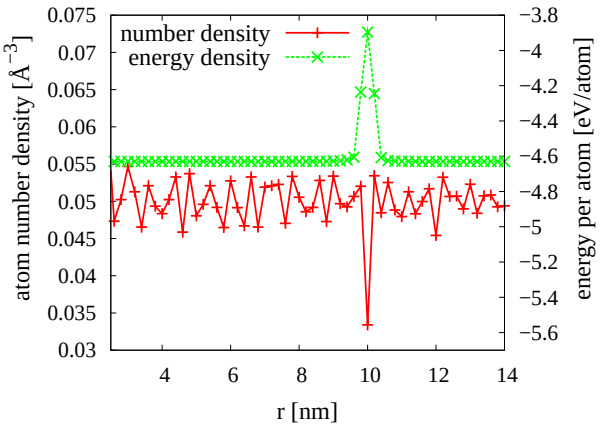

Figure 33: Energy per atom and atom number density as a function of the distance r from the center of the inclusion of radius R. The data correspond to a sample with $R = 10.0$ nm. For $r \simeq R$ the local number density is much smaller than elsewhere while the energy, as expected, is higher.

5.2.2 *The continuum model*

Here, we discuss the capability of the generalized Eshelby theory (see Section 2.2) to reproduce the size-dependent interface effects reported in the previous Section. As reported above, in the atomistic model, the prestress inside the inclusion is induced by the reduction of the available volume due to the interface formation. In order to mimic this volume variation in the context of continuum elasticity theory, we consider the configuration represented in Fig.34, where a cylinder of radius R_2 is forced to fit a similarly shaped void with radius $R_1 \neq R_2$. If $R_2 > R_1$ a uniform compression inside the cylinder is generated, as well as a radially decreasing compression in the external region. Actually such a configuration is the subject of Section 2.2.1 where we have calculated the complete solutions for the elastic fields assuming that both the hosting matrix and the cylinder are made of isotropic materials described by the elastic moduli (μ_1, ν_1) and (μ_2, ν_2), respectively. In order to apply these solutions to the problem described in Sec.5.2.1, we have to set its elastic parameters (i.e. μ_1, ν_1, μ_2 and ν_2) consistently. This implies that we must introduce two different isotropic media, respectively describing the elastic behavior of the nano-wire and of the matrix. If the linear elasticity of the matrix is described by the stiffness tensor $\hat{\mathcal{C}}^{(100)}$, then the inclusion is represented (in the same system of reference) by the tensor $\hat{\mathcal{C}}^{(100)}$ rotated upon the z-axis, namely $\hat{\mathcal{C}}(\vartheta)$ (remember that in our case both the matrix and the inclusion are made

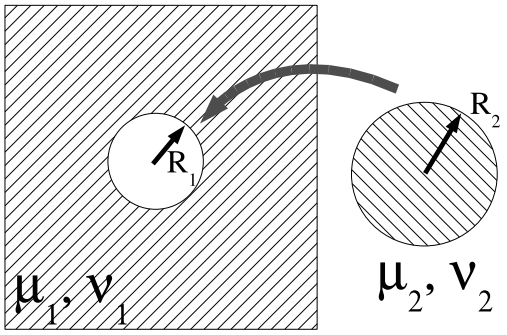

Figure 34: Scheme of the continuum theory model of a prestrained inclusion. Its radius R_2 is bigger then the radius R_1 of the hole in the host matrix (both defined in the reference undisturbed configuration). The elastic properties of the two media are represented by the shear modulus μ_α and by the Poisson ratio ν_α, where $\alpha = 1, 2$.

of c-Si). On the other hand, the isotropic elastic moduli μ and ν for the two phases depend upon the stiffness tensor components through the following relations:

$$\begin{aligned} \mu &= (\mathcal{C}_{11} - \mathcal{C}_{12})/2 \\ \nu &= \mathcal{C}_{12}/(\mathcal{C}_{11} + \mathcal{C}_{12}) \end{aligned} \tag{5.18}$$

Therefore, we set

$$\begin{aligned} \mu_1 &= (\mathcal{C}_{11}^{(100)} - \mathcal{C}_{12}^{(100)})/2 \\ \nu_1 &= \mathcal{C}_{12}^{(100)}/(\mathcal{C}_{11}^{(100)} + \mathcal{C}_{12}^{(100)}) \end{aligned} \tag{5.19}$$

in the matrix and

$$\begin{aligned} \mu_2 &= (\mathcal{C}_{11}(\vartheta) - \mathcal{C}_{12}(\vartheta))/2 \\ \nu_2 &= \mathcal{C}_{12}(\vartheta)/(\mathcal{C}_{11}(\vartheta) + \mathcal{C}_{12}(\vartheta)) \end{aligned} \tag{5.20}$$

in the inclusion. This approach is fully justified because we have calculated the exact internal strain field for some paradigmatic configurations with the anisotropic Eshelby model [45, 192] and we have verified that our isotropic approximation does not affect the results under uniaxial elongations or hydrostatic external loadings. On the other hand, the formalism for the isotropic case is much lighter than for the anisotropic one [32], thus providing a more clean picture.

In the last Section of this Chapter, we calculate the solution of the present prestressed configuration by means of a method rather different from that applied in Section 2.2. This calculation, suitable for the two-dimensional case only, has been applied in order to check the consistency of our Eshelby-like approach to prestressed system. The results obtained by means of the two methodologies are in perfect reciprocal agreement.

The atomistic data (full symbols in Fig.32) have been fitted by means of the following analytic expression (see Eq.(5.42)) for the prestrain

The continuum expression for the prestress effect at the nanoscale

$$\varepsilon^0 = \frac{\mu_1 (\chi_2 - 1)(R_1 - R_2)}{2\mu_2 R_1 - \mu_1 R_2 + R_2 \mu_1 \chi_2} \tag{5.21}$$

where $\chi_2 = 3 - 4\nu_2$. The radius difference $\Delta R = R_2 - R_1$ has been considered as the fitting parameter. Moreover, in order to draw the comparison with the atomistic simulations we have imposed $(R_1 + R_2)/2 = R$. Therefore, Eq.(5.21) is recast in the form

$$\varepsilon^0 = -\frac{\mu_1 (1 - 2\nu_2) \Delta R}{\mu_2 \left(R - \frac{\Delta R}{2}\right) + \mu_1 (1 - 2\nu_2) \left(R + \frac{\Delta R}{2}\right)} \tag{5.22}$$

The fitting procedure provided a value $\Delta R = R_2 - R_1 = 0.6$Å and proved that the present continuum model is consistent with atomistic data, as shown in Fig.32. This important result stands for the fact that the width of the disordered interface region can be considered independent from the curvature of the interface (at least in the present context); rather, it depends only on the crystalline structure of the two materials.

5.2.3 *The effect of external loading*

An uniaxial homogeneous elongation of 1% along the y direction (corresponding to a displacement field $u_x = 0$ and $u_y = \varepsilon^\infty_{yy} y$, where $\varepsilon^\infty_{yy} = 0.01$) was applied to the samples described in Sec.5.2.1. After the relaxation of the atomistic structure (performed through damped dynamics with the same convergence criterion reported in Sec.5.2.1), we have computed both the longitudinal $u_y(x, y)$ and the transverse $u_x(x, y)$ displacement fields inside and outside the embedded inclusion.

As a first step, we checked whether the internal strain could be considered as a uniform field, as predicted by the continuum elasticity. We have found that this prediction is indeed well verified by atomistic simulations, provided that we neglect a narrow disordered coating (about 0.5 nm thick) close to the interface. In order to obtain these estimations we have applied a fitting procedure similar to that used for the prestrain calculation (see Sec.5.2.1).

A further analysis has been performed to investigate the dependence of the internal strain upon the elastic mismatch between the inclusion and the matrix described by the rotation angle ϑ as shown in Eqs.(5.19) and (5.20). In Fig.35, we show the differences $\varepsilon_{xx} - \varepsilon^0$ and $\varepsilon_{yy} - \varepsilon^0$ between the resulting internal strain (after the application of the load) and the prestrain as function of ϑ for an inclusion with $R = 2$ nm. As expected for a cubic crystal like c-Si, both the longitudinal (empty symbols in Fig.35) and transverse (full symbols in Fig.35) strain components are $\pi/2$-periodic. Moreover, the angle $\vartheta = \pi/4$ leads to the largest difference between the internal strain and the applied one. In Fig.35 we also report the results obtained through the atomically informed continuum model described in Sec.5.2.2 (full and dashed lines). We note a good agreement between atomistics and continuum and we remark that for $\vartheta = \pi/2$ the inclusion has the same crystallographic orientation of the matrix. Nevertheless, a disordered interface and the corresponding prestrain are present. This is due to the fact that a pure $\pi/2$-rotation does not arrange the atoms consistently with the surrounding crystal (in order to obtain such a correspondence we have to apply a suitable translation along the (111) direction as well). Interesting enough, we found $\varepsilon_{xx} - \varepsilon^0 = \varepsilon^\infty_{xx}$ and $\varepsilon_{yy} - \varepsilon^0 = \varepsilon^\infty_{yy}$ for $\vartheta = \pi/2$, where ε^∞_{xx} and ε^∞_{yy} are the components of the remotely applied strain field. In other words, in spite of the complexity of the continuum equations described

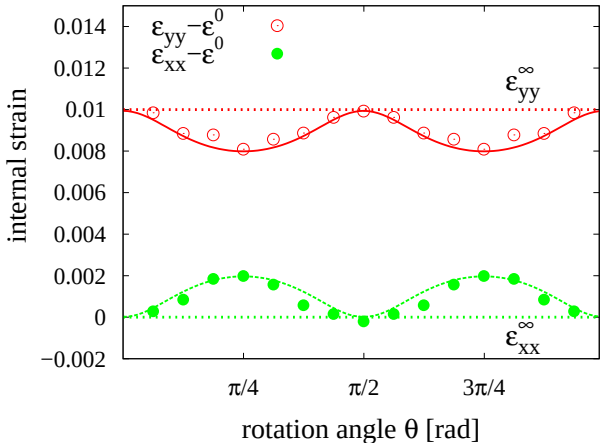

Figure 35: Longitudinal ε_{yy} (empty symbols) and transverse ε_{xx} (full symbols) strain inside the inclusion after the application of the load to the sample with $R = 2$ nm. We show the difference between these strain components and the corresponding prestrain (ε^0) as a function of the rotation angle ϑ. We also report the values ($\varepsilon^\infty_{yy} = 0.01$ and $\varepsilon^\infty_{xx} = 0$) of the strain applied to the overall system (horizontal dotted lines). The solid and the dashed curve represents the continuum theory predictions for the longitudinal and for the transverse field, respectively.

in Appendix 5.2.4, the prestrain roughly acts as an additive constant to the applied strain.

In Fig.36 we report the longitudinal (ε_{yy}) and transverse (ε_{xx}) strain fields inside the inclusion under load versus the inclusion radius R (for $\vartheta = \pi/4$). The results of the continuum theory are obtained by setting the prestrain to the value stated by the fitting procedure of the atomistic data (see Sec.5.2.2). For large values of the radius, the effect of the interface-induced prestrain is negligible (see also Fig.32) and the elastic fields become size-independent. Moreover, in the limit of vanishing prestrain (or equivalently for $R \to \infty$, as shown in Fig.32), the constant values approached by the atomistic data correspond to those predicted by the Eshelby continuum model [8].

Finally, we have investigated the effect of the inclusion on the surrounding matrix. Also in this case, we have found that the prestrain plays an important role in the determination of the elastic state of deformation of the system. In Fig.37 we show the longitudinal displacement field across the inclusion ($R = 10$ nm). In order to magnify the effects, we report the perturbation $u_y(x_c, y) - \varepsilon^\infty_{yy} y$ to the uniform applied displacement (where x_c is the abscissa of the center of the inclusion). We have reported two different predictions obtained through the continuum model described in Sec.5.2.2 and in Appendix 5.2.4. Corresponding atomistic data (red dots) are reported as well. The dashed green line represents the effect of the remotely applied load to the prestrained system and it is in good agreement with the atomistic scenario. The dotted blue curve shows the behavior of the system under load when the prestrain is absent. By comparing the two continuum models, we note that the internal fields are quite similar and the difference roughly corresponds to ε^0. On the contrary, the external fields are completely different. In the model including prestrain, the curve in Fig.37

Localization of the strain effect of the inclusion in the surrounding matrix

exhibits a very fast decay to zero. In other words, the prestrain causes a strong localization of the elastic fields around the interface. This effect is associated with a loss of continuity of the displacement field due to the narrow interface region which separates the two bulk zones. It is interesting to observe that our atomically informed continuum model perfectly takes into account both the fast decay and the displacement discontinuity, being in good agreement with the atomistic simulations.

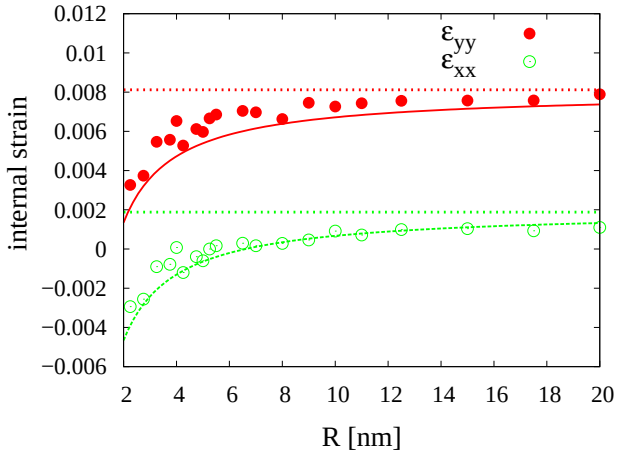

Figure 36: Longitudinal (ε_{yy}) and transverse (ε_{xx}) internal strain components as a function of the radius R of the cylindrical inclusion. Full and dashed lines represent the continuum theory. We also show by dotted lines the corresponding asymptotic values approached when the interface-induced prestrain becomes negligible.

5.2.4 *Solution of the continuum model through the complex variable method*

In order to solve the model presented in Sec.5.2.2, we use the complex variable method for the two-dimensional elasticity [31]. In each homogeneous region of the xy-plane the displacement vector field and the stress tensor field can be represented by means of a couple of Kolossov-Muskhelishvili elastic potentials [83, 84, 193]. We assume that the elastic state of a given homogeneous region α is exactly described by two holomorphic functions $\phi_\alpha(z)$ and $\psi_\alpha(z)$, where the complex number $z = x + iy$ represents the position on the plane. The Kolossov-Muskhelishvili equations allow for the determination of the elastic fields in each region [193]

$$u_x^\alpha + i\, u_y^\alpha = \frac{1}{2\mu_\alpha}[\chi_\alpha \phi_\alpha(z) - z\,\overline{\phi'_\alpha(z)} - \overline{\psi_\alpha(z)}] \tag{5.23}$$

$$\sigma_{xx}^\alpha + \sigma_{yy}^\alpha = 2[\phi'_\alpha(z) + \overline{\phi'_\alpha(z)}] \tag{5.24}$$

$$\sigma_{yy}^\alpha - \sigma_{xx}^\alpha + 2\, i\, \sigma_{xy}^{(\alpha)} = 2[\bar{z}\phi''_\alpha(z) + \psi''_\alpha(z)] \tag{5.25}$$

where $\bar{f}$ is the conjugate of f while f' and f'' indicate the first and the second derivative of the analytic function f, respectively. In our model the phase with $\alpha = 1$ corresponds to the matrix and the phase with $\alpha = 2$ corresponds to the inclusion. It means that $\phi_1(z)$ and $\psi_1(z)$ are defined for $|z| > R_1$ and $\phi_2(z)$ and $\psi_2(z)$ are defined for $|z| < R_2$. Moreover, the parameter χ_α introduced in Eq.(5.23) is given

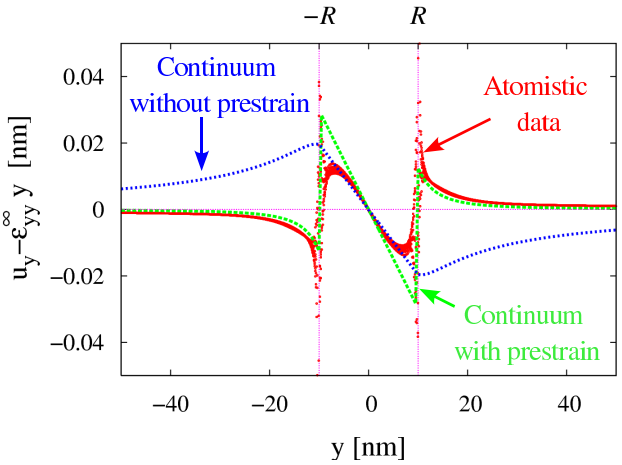

Figure 37: Longitudinal displacement $u_y(x,y)$ showing the behavior of the elastic field across the inclusion ($R = 10$ nm). The continuum predictions (blue and green curves) have been obtained by imposing $x = x_c$, where x_c corresponds to the center of the inclusion. The atomistic data (red dots) represent the displacement in the set of atoms having $x \in (x_c - \Delta x, x_c + \Delta x)$ where $\Delta x = 1$ nm. In order to better detect the effect of the inclusion, we report the difference, $u_y(x_c,y) - 0.01y$, between the longitudinal field and the uniform applied displacement of 1% in the y direction.

by $\chi_\alpha = 3 - 4\nu_\alpha$ under the assumed plane strain conditions [193]. The solution of the elastic problem can be obtained by imposing the perfect bonding at the interface described by the following continuity relations

$$\begin{aligned}\left(z + u_x^1 + i\, u_y^1\right)|_{z=R_1 e^{i\theta}} &= \left(z + u_x^2 + i\, u_y^2\right)|_{z=R_2 e^{i\theta}} \\ \left(\hat{\sigma}^1 \cdot \vec{n}\right)|_{z=R_1 e^{i\theta}} &= \left(\hat{\sigma}^2 \cdot \vec{n}\right)|_{z=R_2 e^{i\theta}}\end{aligned}$$

These boundary conditions can be expressed in terms of the elastic potentials:

$$\begin{aligned}\Big(z + \frac{1}{2\mu_1}[\chi_1\phi_1 &- z\,\overline{\phi_1'} - \overline{\psi_1}]\Big)|_{z=R_1 e^{i\theta}} = \\ \Big(z + \frac{1}{2\mu_2}[\chi_2\phi_2 &- z\,\overline{\phi_2'} - \overline{\psi_2}]\Big)|_{z=R_2 e^{i\theta}}\end{aligned} \tag{5.26}$$

$$\begin{aligned}\Big(\phi_1 &+ z\,\overline{\phi_1'} + \overline{\psi_1}\Big)|_{z=R_1 e^{i\theta}} = \\ \Big(\phi_2 &+ z\,\overline{\phi_2'} + \overline{\psi_2}\Big)|_{z=R_2 e^{i\theta}}\end{aligned} \tag{5.27}$$

The potentials $\phi_2(z)$ and $\psi_2(z)$ can be represented by Taylor series and $\phi_1(z)$ and $\psi_1(z)$ by Laurent series [31, 32]. A detailed analysis of the problem proves that the following simplified representations are sufficient to solve the problem

$$\psi_1(z) = \mu_1(\varepsilon_{yy}^\infty - \varepsilon_{xx}^\infty + 2i\varepsilon_{xy}^\infty)z + \frac{H_1}{z} + \frac{H_3}{z^3} \tag{5.28}$$

$$\phi_1(z) = \frac{\mu_1(\varepsilon_{xx}^\infty + \varepsilon_{yy}^\infty)z}{\chi_1 - 1} + \frac{F}{z} \tag{5.29}$$

$$\psi_2(z) = Az \tag{5.30}$$

$$\phi_2(z) = Bz \tag{5.31}$$

The linear terms in $\phi_1(z)$ and $\psi_1(z)$ represent the remotely applied load described by an arbitrary strain with components $\varepsilon^{\infty}_{xx}$, $\varepsilon^{\infty}_{yy}$ and $\varepsilon^{\infty}_{xy}$. The continuity relations given in Eq.(5.26) and Eq.(5.27) lead to a linear system for the complex parameters H_1, H_3, F, A and B. The parameters H_1, H_3 and F describe the elastic fields in the matrix around the inclusion and can be eventually obtained as

$$\begin{aligned}\mathfrak{Re}\{H_1\} = 4\frac{\mu_1\mu_2\,(R_1-R_2)\,R_1^2}{2\mu_2R_1-\mu_1R_2+R_2\mu_1\chi_2} \\ +2\frac{\left(\varepsilon^{\infty}_{xx}+\varepsilon^{\infty}_{yy}\right)\left[R_1\mu_2\,(\chi_1-1)-R_2\mu_1\,(\chi_2-1)\right]\mu_1R_1^2}{(2\mu_2R_1-\mu_1R_2+R_2\mu_1\chi_2)\,(\chi_1-1)}\end{aligned} \tag{5.32}$$

$$\mathfrak{Im}\{H_1\} = 0 \tag{5.33}$$

$$\mathfrak{Re}\{H_3\} = \frac{R_1^4\mu_1\left(\varepsilon^{\infty}_{yy}-\varepsilon^{\infty}_{xx}\right)(\mu_2R_1-\mu_1R_2)}{R_1\mu_2\chi_1+\mu_1R_2} \tag{5.34}$$

$$\mathfrak{Im}\{H_3\} = 2\frac{\mu_1R_1^4\varepsilon^{\infty}_{xy}\,(\mu_1R_2-\mu_2R_1)}{R_1\mu_2\chi_1+\mu_1R_2} \tag{5.35}$$

$$\mathfrak{Re}\{F\} = \frac{R_1^2\mu_1\left(\varepsilon^{\infty}_{yy}-\varepsilon^{\infty}_{xx}\right)(\mu_2R_1-\mu_1R_2)}{R_1\mu_2\chi_1+\mu_1R_2} \tag{5.36}$$

$$\mathfrak{Im}\{F\} = 2\frac{\mu_1R_1^2\varepsilon^{\infty}_{xy}\,(\mu_1R_2-\mu_2R_1)}{R_1\mu_2\chi_1+\mu_1R_2} \tag{5.37}$$

The parameters A and B represent the uniform field in the cylindrical inclusion

$$\mathfrak{Re}\{A\} = \frac{R_1\mu_1\mu_2\left(\varepsilon^{\infty}_{yy}-\varepsilon^{\infty}_{xx}\right)(\chi_1+1)}{R_1\mu_2\chi_1+\mu_1R_2} \tag{5.38}$$

$$\mathfrak{Im}\{A\} = 2\frac{\mu_1\mu_2R_1\varepsilon^{\infty}_{xy}\,(\chi_1+1)}{R_1\mu_2\chi_1+\mu_1R_2} \tag{5.39}$$

$$\begin{aligned}\mathfrak{Re}\{B\} &= 2\frac{\mu_1\mu_2\,(R_1-R_2)}{2\mu_2R_1-\mu_1R_2+R_2\mu_1\chi_2} \\ &+ \frac{\left(\varepsilon^{\infty}_{xx}+\varepsilon^{\infty}_{yy}\right)(\chi_1+1)\,R_1\mu_2\mu_1}{(2\mu_2R_1-\mu_1R_2+R_2\mu_1\chi_2)\,(\chi_1-1)}\end{aligned} \tag{5.40}$$

$$\mathfrak{Im}\{B\} = 0 \tag{5.41}$$

The knowledge of all the parameters allows us to obtain any component of any elastic field by means of the Kolossov-Muskhelishvili Eqs.(5.23), (5.24) and (5.25). It is possible to verify that, if we consider $R_1 = R_2$, we exactly obtain the results of the Eshelby theory for a cylindrical inclusion [45]. Our general solution takes into account both the effects of the remotely applied loads and those induced by the different size between the cylinder and the hosting hole (prestrain). If we suppose to consider the case where no loads are applied to the system, we obtain only two not vanishing parameters, namely $\mathfrak{Re}\{H_1\}$ and $\mathfrak{Re}\{B\}$. Indeed, in both Eq.(5.32) and Eq.(5.40) only the first term is independent on the applied loads. Therefore, the parameter $\mathfrak{Re}\{B\}$ describes the uniform isotropic compression inside the cylinder (internal prestrain) while

$\mathfrak{Re}\{H_1\}$ describes the asymptotically vanishing (as $1/z$) compression in the matrix (external prestrain). By substituting the expression of $\mathfrak{Re}\{B\}$ (with no loads) in Eq.(5.23) we eventually obtain the internal isotropic prestrain ε^0 as

$$\varepsilon^0 = \frac{\mu_1 (\chi_2 - 1)(R_1 - R_2)}{2\mu_2 R_1 - \mu_1 R_2 + R_2 \mu_1 \chi_2} \tag{5.42}$$

This equation has been used in the previous Section to obtain the fitting of the atomistic prestrain fields through suitable values of the difference $\Delta R = R_2 - R_1$.

Part III

THE CONSTITUTIVE FORCE FIELD

6

A VIRTUAL LABORATORY FOR NANOMECHANICS APPLICATIONS

Contents

In this Chapter we report the key idea and a paradigmatic implementation of a new constitutive force field. Such a model is addressed to the investigation of the mechanical behavior of complex materials and systems at the nano-scale by exploiting the atomistic features of condensed matter, but still conceiving the relevant elastic fields and phenomena according to continuum mechanics.

The force fields in molecular dynamics

In the context of atomistic simulations of complex systems, the force field approach is one of the most utilized methodology. It refers to a functional form (with a given set of parameters) adopted to describe the total potential energy of a system of atoms. Typically, the mathematical form of the potential function and the relative parameters are chosen in order to fit both experimental data and ab-initio quantum mechanical results, corresponding to the physical system under investigation. The standard implementations of the force field models have been devoted to perform atomistic simulations of large complex systems such as proteins (e.g. DNA and RNA) [194, 195] and other biological macromolecules. Therefore, the functional forms consider both covalent bonds and long-range electrostatics and van der Waals interactions. The main idea is that of introducing in the total potential energy several terms describing independently different physical phenomena. The advantage is that of controlling and modulating each physical contribution without affecting the other ones. Moreover, a nontrivial characteristic of these empirical models is the capability to reproduce the main physical features of complex atomic interactions without considering a, computationally very demanding, quanto-mechanical description.

Here, we adopt this conceptual scheme in order to introduce a force field model for applications in the physics and mechanics of solids. The key idea is that of developing a coarse graining procedure of the physical information, thus reducing the otherwise over-rich interatomic potentials nowadays available (see Section 4.2) into constitutive force fields optimized to describing mechanical behaviors. More specifically, we introduce a series of potential energy terms which model all the features of the classical linear and nonlinear elasticity theory. This approach allows us to lay the foundation of a virtual laboratory primarily focussed to the applications in micro- and nano-mechanics. In fact, in several fields ranging from the physics of the quantum dots [177, 178, 179] to the mechanics of composite materials [111], it is very

important to determine the actual strain and stress fields distributed within micro- and nano-structures.

The tunable nonlinear behavior of the constitutive force field

The development of this force field model in this context is essential for two main reasons: firstly, the continuum elasticity theory is inherently scale-independent while the elastic behavior of a nano-structure does depend on the actual length scale. Therefore, it is important to consider the real discretization of mass distribution in condensed matter systems i.e., the actual disposition of the atoms within a material body. Secondly, it allows us to straightforwardly control the nonlinear elastic effects which have shown a great importance in several topics such as fracture mechanics [120, 121], interfacial phenomena [196, 197], nanocomposite [87, 125] and graded structures [198]. Such nonlinear effects are usually very difficult to be considered through the continuum elasticity theory. Nevertheless, they can be simply introduced and controlled in a force field model. In other words, we will be able to construct a potential energy function for a discrete set of atoms corresponding to an arbitrarily nonlinear constitutive equation, relating the stress and the strain fields within a given medium. Moreover, we may consider models of complex materials with several different phases (each with a given constitutive relation) bonded at interfaces with arbitrary shape (modeling inclusions, precipitates, grain boundaries and other heterogeneities) as in a sort of *Atomistic Virtual Laboratory for Nanomechanics applications*.

6.1 THE CONSTITUTIVE FORCE FIELD

The development of our force field is addressed to the atomic-scale representation of the elastic behavior of a given material summarized in its constitutive equation. In continuum elasticity theory the constitutive equation can be obtained (within the Green formulation) from the strain energy function giving the elastic energy accumulated per unit volume of material (see Section 1.3 and, e.g., Ref. [31]). Such a function can be expressed in terms of the second-order linear elastic moduli and of the third-order nonlinear elastic moduli (Section 2.3.1). In the corresponding atomistic model we introduce a sufficient number of interactions so as to exactly reproduce the elastic behavior controlled by all the linear and nonlinear elastic moduli. More specifically, we introduce two-body interaction (described by axial springs with both harmonic and anharmonic behavior) as well as three-body interaction (angular springs having, as before, harmonic and anharmonic terms) and, possibly, many-body interactions. In fact, we have proved in Section 4.1 that a pure two-body force field describes the linear elastic behavior of a material with a single elastic modulus. On the contrary, a force field including both two-body and three-body interactions supplies the minimal complexity required to provide results in formal agreement with continuum elasticity theory, i.e., predicting the existence of two independent linear elastic constants.

Following this conceptual scheme, we need to understand the effects of any possible interaction between couples or groups of atoms on the linear and nonlinear elastic properties of the overall system.

If we take into consideration a system of N interacting particles the potential energy $\mathcal{U}$ must be a function of the vector distances $\{\vec{r}_{\alpha\beta}\}_{\alpha,\beta=1,\dots,N}$ between each couple of atoms, i.e. $\mathcal{U} = \mathcal{U}(\{\vec{r}_{\alpha\beta}\}_{\alpha,\beta=1,\dots,N})$.

For our purpose, it is convenient to develop this energy as a power series

$$\begin{aligned} \mathcal{U} = \mathcal{U}_0 \quad &+ \quad \sum K^{ij}_{\alpha\beta\gamma\delta} \; r^i_{\alpha\beta} \, r^j_{\gamma\delta} \\ &+ \quad \sum K^{ijk}_{\alpha\beta\gamma\delta\zeta\xi} \; r^i_{\alpha\beta} \, r^j_{\gamma\delta} \, r^k_{\zeta\xi} + \ldots \end{aligned} \tag{6.1}$$

where $r^i_{\alpha\beta}$ ($i = x, y, z$) is the $i-$th coordinate of the vector distance between the atom α and the atom β ($\mathcal{U}_0$, $K^{ij}_{\alpha\beta\gamma\delta}$, $K^{ijk}_{\alpha\beta\gamma\delta\zeta\xi}$,... are constants). This functional must show a minimum in a given configuration of the N particles: in the following, we will indicate such a reference configuration as $\{\vec{r}^{\,0}_{\alpha\beta}\}_{\alpha,\beta=1,N}$. Of course, this reference configuration is defined but for an arbitrary roto-traslation of the particles system.

The elastic behavior of a material is described by the linear elastic moduli $\mathcal{C}_{ij}$ and by the nonlinear moduli $\mathcal{C}_{ijk}$. These are the coefficients of the expansion in power series of the strain energy function $U(\hat{\varepsilon})$

The nonlinear strain energy function

$$U(\vec{\varepsilon}) \simeq \frac{1}{2}\mathcal{C}_{ij}\varepsilon_i\varepsilon_j + \frac{1}{6}\mathcal{C}_{ijk}\varepsilon_i\varepsilon_j\varepsilon_k \tag{6.2}$$

As discussed in Section 4.3.2, for an atomic system, this strain energy function can be easily obtained from the potential energy. In fact, if the system is subjected to a uniform strain field $\hat{\varepsilon}$, the vector distance between the atom α and the atom β is given by $\vec{r}_{\alpha\beta} = \vec{r}^{\,0}_{\alpha\beta} + \hat{\varepsilon}\ \vec{r}^{\,0}_{\alpha\beta}$. The strain energy function of this deformed system can be obtained through the following substitution

$$U(\hat{\varepsilon}) = \frac{1}{V}\mathcal{U}(\{\vec{r}^{\,0}_{\alpha\beta} + \hat{\varepsilon}\ \vec{r}^{\,0}_{\alpha\beta}\}_{\alpha,\beta=1,N}) \tag{6.3}$$

being V the volume of the system in reference configuration. By applying this rule to the interaction energy defined in Eq.(6.1) and by expanding the obtained energy function in powers of $\hat{\varepsilon}$ is easy to see that each elastic modulus ($\mathcal{C}_{ij}$ and $\mathcal{C}_{ijk}$) must be a linear functions of the potential parameters $K^{ij}_{\alpha\beta\gamma\delta}$, $K^{ijk}_{\alpha\beta\gamma\delta\zeta\xi}$... Therefore, generally speaking, it is possible to obtain any elastic behavior by properly setting the parameters of the potential. In conclusion, it is important to remark that a linear relation exists between the set of parameters defining the force field and the (linear and nonlinear) elastic constants describing the mechanical behavior of the particles system.

In order to provide an effective picture of the above analysis, we firstly take under consideration a simple harmonic spring with an equilibrium length r_0 between two interacting atoms placed in $\vec{r}_\alpha$ and $\vec{r}_\beta$ (see figure 38)

The harmonic two-body interaction

$$\mathcal{U}^{2b}_h(r_{\alpha\beta}; \kappa_h) = \frac{1}{2}\kappa_h(r_{\alpha\beta} - r_0)^2 \tag{6.4}$$

where h means harmonic, $r_{\alpha\beta} = \mid \vec{r}_{\alpha\beta} \mid = \mid \vec{r}_\alpha - \vec{r}_\beta \mid$ and κ_h is the spring constant. If we expand this interaction energy in the form of Eq.(6.1) all the coefficients $K^{ij}_{\alpha\beta\gamma\delta}$, $K^{ijk}_{\alpha\beta\gamma\delta\zeta\xi}$... will be simply proportional to the spring constant κ_h.

If the system is subjected to a displacement field $\vec{u}$, so that $\vec{r}_{\alpha\beta} = \vec{r}^{\,0}_{\alpha\beta} + \Delta\vec{u}_{\alpha\beta}$ being $\Delta\vec{u}_{\alpha\beta} = \vec{u}(\vec{r}^{\,0}_\alpha) - \vec{u}(\vec{r}^{\,0}_\beta)$, the corresponding potential energy is

$$\mathcal{U}^{2b}_h(\mid \vec{r}^{\,0}_{\alpha\beta} + \Delta\vec{u}_{\alpha\beta} \mid) = \frac{1}{2}\kappa_h(\mid \vec{r}^{\,0}_{\alpha\beta} + \Delta\vec{u}_{\alpha\beta} \mid - r_0)^2 \tag{6.5}$$

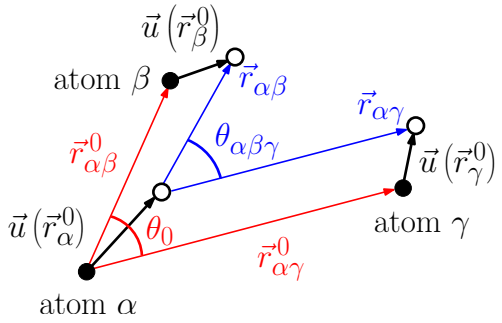

Figure 38: Definitions of the main quantities introduced to describe the deformation of an atomic system. Given three atoms α,β and γ, one can find the equilibrium positions $\vec{r}^{\,0}_\alpha$, $\vec{r}^{\,0}_\beta$ and $\vec{r}^{\,0}_\gamma$, the corresponding displacements $\vec{u}$, the vector distances $\vec{r}^{\,0}_{\alpha\beta}$, $\vec{r}^{\,0}_{\alpha\gamma}$ and $\vec{r}_{\alpha\beta}$, $\vec{r}_{\alpha\gamma}$, before and after the deformation, respectively and, finally, the angles θ_0 and $\theta_{\alpha\beta\gamma}$.

We can expand this function in powers of $\vec{u}$, eventually obtaining

$$U_h^{2b} = \frac{1}{2}\kappa_h \left(\vec{n}_{\alpha\beta}\cdot\Delta\vec{u}_{\alpha\beta}\right)^2 + \mathcal{O}(u^3) \tag{6.6}$$

being $\vec{n}_{\alpha\beta} = \frac{\vec{r}^{\,0}_{\alpha\beta}}{r_0}$. If the displacement field corresponds to a uniform strain $\hat{\varepsilon}$, it can be expressed as $\Delta\vec{u}_{\alpha\beta} = \hat{\varepsilon}\ \vec{r}^{\,0}_{\alpha\beta}$ and the strain energy function can be obtained through the rule in Eq.(6.3)

$$V\,U(\hat{\varepsilon}) = \frac{1}{2}\kappa_h \left(\vec{n}_{\alpha\beta}\cdot\hat{\varepsilon}\ \vec{r}^{\,0}_{\alpha\beta}\right)^2 + \mathcal{O}(\varepsilon^3) \tag{6.7}$$

By comparing this result with Eq.(6.2), we can verify that the linear elastic moduli $\mathcal{C}_{ij}$ are proportional to the potential parameter κ_h. Moreover, we can see that, through the $\mathcal{O}(\varepsilon^3)$ term in Eq.(6.7), not explicited for sake of brevity, the harmonic interaction affects also the nonlinear behavior, i.e. the $\mathcal{C}_{ijk}$ moduli will be proportional to κ_h as well. Therefore, if we are interested in a pure linear elastic system we can apply just the second order term in Eq.(6.6), by obtaining a particularly simple linear interaction potential. This consideration suggests to consider another different contribution to the potential energy: we name this interaction potential *linearized spring* and it assumes the form

The linearized two-body interaction

$$U_l^{2b} = \mathcal{L}\left[\frac{1}{2}\kappa_l\left(r_{\alpha\beta}-r_0\right)^2\right] = \frac{1}{2}\kappa_l\left(\vec{n}_{\alpha\beta}\cdot\Delta\vec{u}_{\alpha\beta}\right)^2 \tag{6.8}$$

where we have introduced a new spring constant k_l (l means linear) and the linearization operator $\mathcal{L}$.

A similar analysis can be performed on the following 3-body harmonic interaction

The harmonic three-body interaction

$$U_h^{3b}(\theta_{\alpha\beta\gamma};\gamma_h) = \frac{1}{2}\frac{\gamma_h}{{r_0}^2}(\cos\theta_{\alpha\beta\gamma}-\cos\theta_0)^2 \tag{6.9}$$

where $\cos\theta_{\alpha\beta\gamma} = \frac{\vec{r}_{\alpha\beta}\cdot\vec{r}_{\alpha\gamma}}{|\vec{r}_{\alpha\beta}||\vec{r}_{\alpha\gamma}|}$ is the cosine of the angle between the two bonds of the atom α with the atoms β and γ (see figure 38) and θ_0 is the equilibrium angle of the 3-body interaction. In this case we get

$$\begin{aligned} U_h^{3b} = \frac{1}{2}\frac{\gamma_h}{{r_0}^4}\big[&\vec{n}_{\alpha\beta}\cdot\Delta\vec{u}_{\alpha\gamma}+\vec{n}_{\alpha\gamma}\cdot\Delta\vec{u}_{\alpha\beta} \\ &-\cos\theta_0\left(\vec{n}_{\alpha\beta}\cdot\Delta\vec{u}_{\alpha\beta}+\vec{n}_{\alpha\gamma}\cdot\Delta\vec{u}_{\alpha\gamma}\right)\big]^2+\mathcal{O}(u^3)\end{aligned} \tag{6.10}$$

As for the two body term in Eq. (6.6), the harmonic interaction introduces both a linear and a nonlinear contribution to the strain energy function. Therefore, a pure linear elastic interaction can be obtained by applying to the dynamics the following linearized term

The linearized three-body interaction

$$\begin{aligned} \mathcal{U}_l^{3b} &= \mathcal{L}\left[\frac{1}{2}\frac{\gamma_l}{r_0^2}\left(\cos\theta_{\alpha\beta\gamma}-\cos\theta_0\right)^2\right] \\ &= \frac{1}{2}\frac{\gamma_l}{{r_0}^4}\left[\vec{n}_{\alpha\beta}\cdot\Delta\vec{u}_{\alpha\gamma}+\vec{n}_{\alpha\gamma}\cdot\Delta\vec{u}_{\alpha\beta}\right. \\ &\quad \left.-\cos\theta_0\left(\vec{n}_{\alpha\beta}\cdot\Delta\vec{u}_{\alpha\beta}+\vec{n}_{\alpha\gamma}\cdot\Delta\vec{u}_{\alpha\gamma}\right)\right]^2 \end{aligned} \tag{6.11}$$

Moreover, we may add other anharmonic terms:

The anharmonic interactions

$$\mathcal{U}_a^{2b}(r_{\alpha\beta};\kappa_a) = \frac{1}{2}\kappa_a(r_{\alpha\beta}-r_0)^3 \tag{6.12}$$

$$\mathcal{U}_a^{3b}(\theta_{\alpha\beta\gamma};\gamma_a) = \frac{1}{2}\frac{\gamma_a}{{r_0}^3}(\cos\theta_{\alpha\beta\gamma}-\cos\theta_0)^3 \tag{6.13}$$

which affects only the non linear behavior of the system.

As discussed in the next Section, the potential energy terms given in Eqs.(6.8) and (6.11) (corresponding to the linearized springs), in Eqs.(6.4) and (6.9) (corresponding to the harmonic springs) and in Eqs.(6.12) and (6.13) (corresponding to the anharmonic springs) can be superimposed for describing a complex behavior of the system of particles. This procedure is followed in order to increase the number of independent parameters and to produce the desired linear and nonlinear elastic behavior of the resulting material. This idea is the core of the present atomistic virtual laboratory based on the force field methodology. The elastic moduli of such a system will be linear combinations of the potential parameters κ_l, γ_l, κ_h, γ_h, κ_a and γ_a. If necessary, in order to further increase the complexity of the potential energy and the corresponding number of independent parameters, four-body (e.g. dihedral angular springs) or, in general, many-body interactions can be taken into account. In such a case, an analysis can be performed similarly to the two-body and three-body interactions discussed above. Finally, all the contributions to the force field can be extended beyond the first nearest neighbor interaction including, e.g., second and third nearest neighbors.

6.2 THE FORCE FIELD ON A TWO-DIMENSIONAL TRIANGULAR LATTICE

In this Section we show how the above formal setup is implemented in order to build a force for a two-dimensional triangular lattice with any possible linear and nonlinear elastic behavior.

6.2.1 *Nonlinear elasticity of the triangular lattice*

We consider now a triangular lattice of atoms (shown in Fig.39) belonging to the hexagonal crystal system. We search for the continuum elastic properties of such a structure. To this aim, we apply the fundamental principle of crystal physics, known as Neumann's principle, namely: the symmetry elements of any macroscopic physical property of a crystal must include the symmetry elements of the point group of the crystal [199]. Since the strain energy function is invariant under a

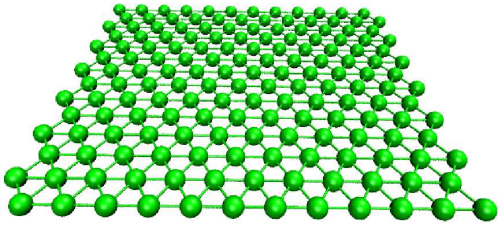

Figure 39: Scheme of a planar triangular lattice of atoms.

rotation of $\pi/3$ about the principal axis (normal to the lattice plane), the above general statement leads to the following conclusion: there are two linear moduli and three nonlinear independent elastic coefficients [200]. In particular, we easily proved that

Nonlinear strain energy function for the two-dimensional triangular lattice

$$\begin{aligned} U(\hat{\varepsilon}) &= \frac{\lambda}{2}[\mathrm{Tr}(\hat{\varepsilon})]^2 + \mu\,\mathrm{Tr}(\hat{\varepsilon}^2) \\ &+ \Lambda_1(\varepsilon_{xx}-\varepsilon_{yy})[(\varepsilon_{xx}-\varepsilon_{yy})^2 - 12\varepsilon_{xy}^2] \\ &+ \frac{1}{2}\Lambda_2\mathrm{Tr}(\hat{\varepsilon})[2\,\mathrm{Tr}(\hat{\varepsilon}^2) - \mathrm{Tr}(\hat{\varepsilon})^2] \\ &+ \frac{1}{2}\Lambda_3\mathrm{Tr}(\hat{\varepsilon})^3 \end{aligned} \tag{6.14}$$

where the nonlinear elastic moduli Λ_i, $i = 1,2,3$ can be expressed in terms of the stiffness parameters C_{ijk} in Eq.(6.2)

$$\Lambda_1 = \frac{1}{12}(C_{111} - C_{222}), \qquad \Lambda_2 = \frac{1}{4}(C_{222} - C_{112}),$$
$$\Lambda_3 = \frac{1}{12}(2C_{111} - C_{222} + 3C_{112}). \tag{6.15}$$

These results means that the triangular lattice shows a linear isotropic elastic behavior (described by the Lamé coefficients λ and μ) and an anisotropic nonlinear elasticity characterized by three independent elastic moduli Λ_1, Λ_2 and Λ_3. In the special case with $C_{111} = C_{222}$ we obtain a fully isotropic system. In fact, this nonlinear isotropic condition leads to $\Lambda_1 = 0$: in this case (as discussed in Section 7.1.1) the strain energy function depends only on the strain invariants and, as a consequence, it is fully invariant under arbitrary rotations. It is also interesting to remark that the hexagonal symmetry and the corresponding strain energy function given in Eq.(6.14) are exhibited by monolayer graphene, as recently discussed [201].

6.2.2 *Analysis and Synthesis of the elastic medium*

In order to apply the constitutive force field approach to the triangular lattice elasticity discussed in the previous Section, we consider a potential energy composed by two-body (U^{2b}) and three-body (U^{3b}) terms. In each case we can introduced three different interactions, namely:

- *linear*: U_l^{2b} and U_l^{3b} reported in Eqs. 6.8 and 6.11 respectively
- *harmonic*: U_h^{2b} and U_h^{3b} reported in Eqs. 6.4 and 6.9 respectively
- *anharmonic*: U_a^{2b} and U_a^{3b} reported in Eqs. 6.12 and 6.13 respectively

governed by different spring parameters. The overall interaction potential is the following

Potential energy of the constitutive force field

$$\begin{aligned} \mathcal{U} &= \mathcal{U}_0 + \frac{1}{2}\sum_{\alpha\beta}\left[\mathcal{U}_l^{2b}(r_{\alpha\beta}) + \mathcal{U}_h^{2b}(r_{\alpha\beta}) + \mathcal{U}_a^{2b}(r_{\alpha\beta})\right] \\ &+ \sum_{\alpha\beta\gamma}\left[\mathcal{U}_l^{3b}(\theta_{\alpha\beta\gamma}) + \mathcal{U}_h^{3b}(\theta_{\alpha\beta\gamma}) + \mathcal{U}_a^{3b}(\theta_{\alpha\beta\gamma})\right] \end{aligned} \tag{6.16}$$

where

$$\begin{aligned} \mathcal{U}_l^{2b}(r;\kappa_l) &= \mathcal{L}\left[\frac{1}{2}\kappa_l\,(r-r_0)^2\right] \\ \mathcal{U}_h^{2b}(r;\kappa_h) &= \frac{1}{2}\kappa_h\,(r-r_0)^2 \\ \mathcal{U}_a^{2b}(r;\kappa_a) &= \frac{1}{3}\frac{\kappa_a}{r_0}\,(r-r_0)^3 \\ \mathcal{U}_l^{3b}(\theta;\gamma_l) &= \mathcal{L}\left[\frac{1}{2}\frac{\gamma_l}{r_0^2}\,(\cos\theta-\cos\theta_0)^2\right] \\ \mathcal{U}_h^{3b}(\theta;\gamma_h) &= \frac{1}{2}\frac{\gamma_h}{r_0^2}\,(\cos\theta-\cos\theta_0)^2 \\ \mathcal{U}_a^{3b}(\theta;\gamma_a) &= \frac{1}{3}\frac{\gamma_a}{r_0^2}\,(\cos\theta-\cos\theta_0)^3 \end{aligned} \tag{6.17}$$

The analytical expressions giving the effects of each term in Eq.(6.16) on each elastic moduli of the resulting system can be obtained by means of a procedure similar to that reported in Section 4.1. In particular, we have shown the calculation of the effects of two-body and three-body harmonic interactions on the linear elastic parameters (Eq.(4.15) or Eq.(4.16)). For the present mono-component triangular lattice interacting with the force field in Eq.(6.16) the results of such a calculation for the linear and the nonlinear elastic moduli are reported in Table 5. These moduli have been calculated with the (rather cumbersome) algebra as in Section 4.1 and fully confirmed by a series of atomistic simulations based on our force field.

We can also calculate the dependence of the Poisson ratio and of the Young modulus from the force field parameters

$$\nu_{2D} = \frac{1}{3} - \frac{4(\gamma_l+\gamma_h)}{2(\kappa_l+\kappa_h)+3(\gamma_l+\gamma_h)} \tag{6.18}$$

and

$$E_{2D} = \frac{2\sqrt{3}}{3}(\kappa_l+\kappa_h)\left[\frac{(\kappa_l+\kappa_h)+\frac{9}{2}(\gamma_l+\gamma_h)}{(\kappa_l+\kappa_h)+\frac{3}{2}(\gamma_l+\gamma_h)}\right] \tag{6.19}$$

The relation in Eq.(6.18) confirms the general result that the Poisson ratio of a system subjected to only two-body interactions is constant (with value $1/3$) while it can change if angular interactions are present. Moreover, it is interesting to observe that the linear moduli ν_{2D} and E_{2D} depend only on the sums $\kappa_l+\kappa_h$ and $\gamma_l+\gamma_h$, which, therefore, govern the linear elastic behavior of our system.

Table 5: Linear and nonlinear stiffness tensor components $\mathcal{C}_{11}$, $\mathcal{C}_{12}$, $\mathcal{C}_{111}$, $\mathcal{C}_{222}$, $\mathcal{C}_{112}$ and elastic moduli λ, μ, Λ_1, Λ_2, Λ_3 of the planar triangular lattice in terms of the force field parameters.

	$\mathcal{U}_l^{2b}(r;\kappa_l)$	$\mathcal{U}_l^{3b}(\theta;\gamma_l)$	$\mathcal{U}_h^{2b}(r;\kappa_h)$	$\mathcal{U}_h^{3b}(\theta;\gamma_h)$	$\mathcal{U}_a^{2b}(r;\kappa_a)$	$\mathcal{U}_a^{3b}(\theta;\gamma_a)$
$\mathcal{C}_{11}$	$+\frac{3\sqrt{3}}{4}\kappa_l$	$+\frac{9\sqrt{3}}{8}\gamma_l$	$+\frac{3\sqrt{3}}{4}\kappa_h$	$+\frac{9\sqrt{3}}{8}\gamma_h$	0	0
$\mathcal{C}_{12}$	$+\frac{\sqrt{3}}{4}\kappa_l$	$-\frac{9\sqrt{3}}{8}\gamma_l$	$+\frac{\sqrt{3}}{4}\kappa_h$	$-\frac{9\sqrt{3}}{8}\gamma_h$	0	0
$\mathcal{C}_{111}$	0	0	$+\frac{9\sqrt{3}}{16}\kappa_h$	$-\frac{189\sqrt{3}}{32}\gamma_h$	$+\frac{9\sqrt{3}}{8}\kappa_a$	$+\frac{27\sqrt{3}}{32}\gamma_a$
$\mathcal{C}_{222}$	0	0	$+\frac{3\sqrt{3}}{16}\kappa_h$	$-\frac{27\sqrt{3}}{32}\gamma_h$	$+\frac{11\sqrt{3}}{8}\kappa_a$	$-\frac{27\sqrt{3}}{32}\gamma_a$
$\mathcal{C}_{112}$	0	0	$-\frac{5\sqrt{3}}{16}\kappa_h$	$+\frac{117\sqrt{3}}{32}\gamma_h$	$+\frac{3\sqrt{3}}{8}\kappa_a$	$-\frac{27\sqrt{3}}{32}\gamma_a$
λ	$+\frac{\sqrt{3}}{4}\kappa_l$	$-\frac{9\sqrt{3}}{8}\gamma_l$	$+\frac{\sqrt{3}}{4}\kappa_h$	$-\frac{9\sqrt{3}}{8}\gamma_h$	0	0
μ	$+\frac{\sqrt{3}}{4}\kappa_l$	$+\frac{9\sqrt{3}}{8}\gamma_l$	$+\frac{\sqrt{3}}{4}\kappa_h$	$+\frac{9\sqrt{3}}{8}\gamma_h$	0	0
Λ_1	0	0	$+\frac{\sqrt{3}}{32}\kappa_h$	$-\frac{27\sqrt{3}}{64}\gamma_h$	$-\frac{\sqrt{3}}{48}\kappa_a$	$+\frac{9\sqrt{3}}{64}\gamma_a$
Λ_2	0	0	$+\frac{\sqrt{3}}{8}\kappa_h$	$-\frac{36\sqrt{3}}{32}\gamma_h$	$+\frac{\sqrt{3}}{4}\kappa_a$	0
Λ_3	0	0	0	0	$+\frac{\sqrt{3}}{6}\kappa_a$	0

The results in Table 5 are summarized in the following equations reporting all the linear and nonlinear elastic constants in terms of all the contributions of the force field

$$\begin{aligned}
\mathcal{C}_{11} &= \frac{3\sqrt{3}}{4}(\kappa_l+\kappa_h)+\frac{9\sqrt{3}}{8}(\gamma_l+\gamma_h)\\
\mathcal{C}_{12} &= \frac{\sqrt{3}}{4}(\kappa_l+\kappa_h)-\frac{9\sqrt{3}}{8}(\gamma_l+\gamma_h)\\
\mathcal{C}_{44} &= \frac{\mathcal{C}_{11}-\mathcal{C}_{12}}{2}\\
\mathcal{C}_{111} &= \frac{9\sqrt{3}}{16}\kappa_h-\frac{189\sqrt{3}}{32}\gamma_h+\frac{9\sqrt{3}}{8}\kappa_a+\frac{27\sqrt{3}}{32}\gamma_a\\
\mathcal{C}_{222} &= \frac{3\sqrt{3}}{16}\kappa_h-\frac{27\sqrt{3}}{32}\gamma_h+\frac{11\sqrt{3}}{8}\kappa_a-\frac{27\sqrt{3}}{32}\gamma_a\\
\mathcal{C}_{112} &= -\frac{5\sqrt{3}}{16}\kappa_h+\frac{117\sqrt{3}}{32}\gamma_h+\frac{3\sqrt{3}}{8}\kappa_a-\frac{27\sqrt{3}}{32}\gamma_a
\end{aligned} \tag{6.20}$$

Macroscopic stiffness as a function of the potential parameters: analysis of the model

This set of five relations (the third one corresponds to the Cauchy relation for the isotropic linear behavior) solves the problem of the *analysis* of the linear and nonlinear behavior of a lattice with given set of parameters. The five elastic constants of an hexagonal bi-dimensional lattice ($\mathcal{C}_{11}$, $\mathcal{C}_{12}$, $\mathcal{C}_{111}$, $\mathcal{C}_{222}$ and $\mathcal{C}_{112}$) are linear functions of the six potential parameters introduced in the force field.

On the other hand, by inverting the system of equations (6.20) we can obtain the potential parameters for any required elastic behavior. In fact, a nonsingular system of five linear equations involving five variables can be obtained by fixing, e.g., $\gamma_a = 0$. In such a case we get

$$\begin{aligned}
\kappa_l &= \frac{\sqrt{3}}{3}\mathcal{C}_{11}+\frac{\sqrt{3}}{3}\mathcal{C}_{12}\\
&+ \frac{38\sqrt{3}}{9}\mathcal{C}_{111}-5\sqrt{3}\mathcal{C}_{222}+\frac{17\sqrt{3}}{3}\mathcal{C}_{112}\\
\gamma_l &= \frac{2\sqrt{3}}{27}\mathcal{C}_{11}-\frac{2\sqrt{3}}{9}\mathcal{C}_{12}\\
&+ \frac{32\sqrt{3}}{81}\mathcal{C}_{111}-\frac{4\sqrt{3}}{9}\mathcal{C}_{222}+\frac{4\sqrt{3}}{9}\mathcal{C}_{112}\\
\kappa_h &= -\frac{38\sqrt{3}}{9}\mathcal{C}_{111}+5\sqrt{3}\mathcal{C}_{222}-\frac{17\sqrt{3}}{3}\mathcal{C}_{112}\\
\gamma_h &= -\frac{32\sqrt{3}}{81}\mathcal{C}_{111}+\frac{4\sqrt{3}}{9}\mathcal{C}_{222}-\frac{4\sqrt{3}}{9}\mathcal{C}_{112}\\
\kappa_a &= \frac{\sqrt{3}}{3}\mathcal{C}_{111}-\frac{\sqrt{3}}{6}\mathcal{C}_{222}+\frac{\sqrt{3}}{2}\mathcal{C}_{112}
\end{aligned} \tag{6.21}$$

Potential parameters as a function of the required macroscopic stiffness: synthesis of the model

These relations solve the problem of the *synthesis* of the lattice with an arbitrary desired elastic behavior.

In Figs.40 one can find some examples of elastic behaviors synthetized through the above procedure. In particular, two linear materials have been generated: the first one (a) shows a standard positive Poisson ratio and the second one (b) exhibits a negative Poisson ratio (see Section 1.3). Moreover, isotropic nonlinear behaviors are reported: the first case (c) presents a longitudinal softening nonlinearity ($\mathcal{C}_{111} = \mathcal{C}_{222} < 0$) while the second one (d) shows a longitudinal stiffening nonlinearity ($\mathcal{C}_{111} = \mathcal{C}_{222} > 0$). For semplicity, the transversal behavior is stiffening in both cases ($\mathcal{C}_{112} > 0$). The possibility of controlling such softening and stiffening properties is crucial, i.e., in the dynamics of fracture, as discussed elsewhere [120, 121].

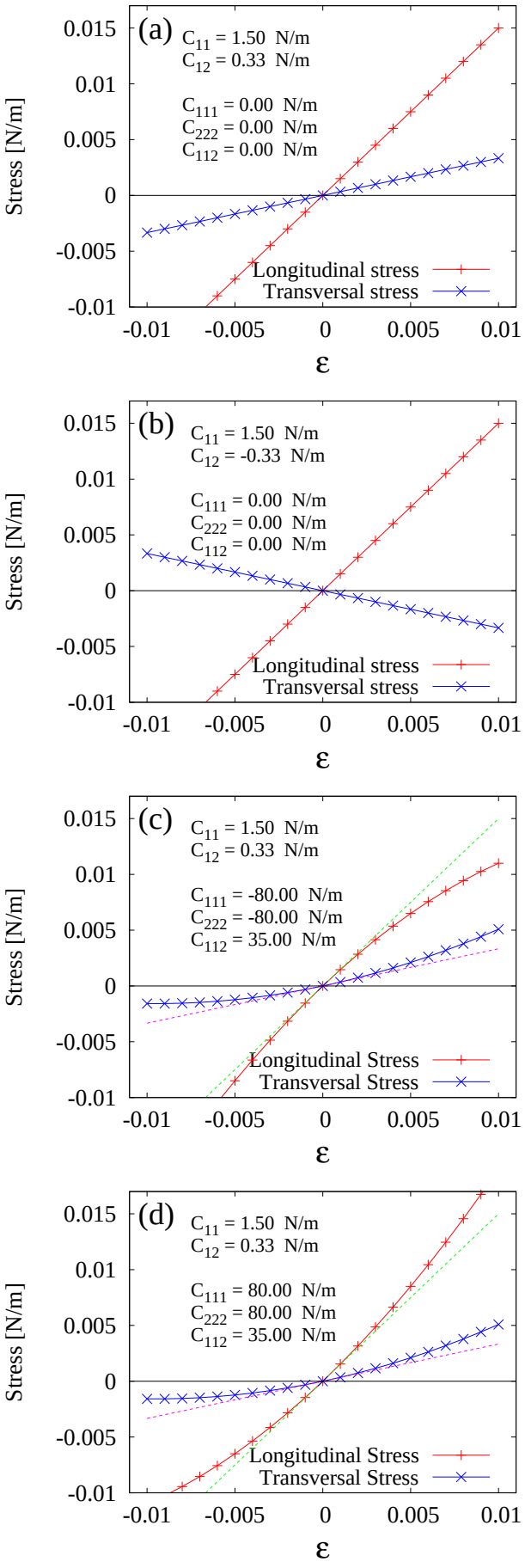

Figure 40: Examples of elastic behaviors achievable through our force field: (a) Isotropic linear, (b) Isotropic linear with negative Poisson ratio. (c) Isotropic nonlinear softening, (d) Isotropic nonlinear stiffening.

7

THE CONSTITUTIVE FORCE FIELD APPROACH TO NANOMECHANICS

Contents

In this Chapter we show several applications of the constitutive force field to the analysis of the elasticity of inhomogeneous materials. The goal of such analysis is the characterization of the possible onset of atomistic effects in the elastic behavior of complex systems where the inhomogeneity shows up at the nano-scale. In other words, we want to quantify the expected discrepancy between the mechanical behaviors of macroscopic complex materials and those of similar nano-structures.

To this aim, we use the continuum theory as a framework for the macroscale phenomena while force field-based simulations are considered in order to model at the atomic level the elastic behavior of nano-materials.

7.1 NONLINEAR ESHELBY PROBLEM

As a first application of the constitutive force field approach described in the previous Chapter, we show an atomistic investigation on the elastic behavior of a single nano-inclusion embedded in a given matrix under remote loading. The continuum mechanics supplies us the complete solution for this paradigmatic configuration in two cases: the first one considers a pure linear elastic behavior for both the inclusion and the matrix (standard Eshelby theory developed in Section 2.1). In the second case the hypotesis of linearity for the inclusion can be removed by introducing an arbitrary nonlinear behavior (nonlinear Eshelby theory in Section 2.3). These two situations have been studied through our atomistic force field in order to investigate the effects at the nano-scale of the discrete distribution of atoms on continuum-based results. By varing the radius of the inclusions and by drawing a comparison between the continuum and the atomistic results, we have quantified the scale effects on both the linear and the nonlinear behavior of the overall system. Moreover, we have used the atomistic model to study the other two configurations that can not be analyzed through the

continuum theory, namely: linear inclusion in nonlinear matrix and nonlinear inclusion in nonlinear matrix.

In Sections 2.1 and 2.3 we have derived the Eshelby solutions of the present problem for several shapes of the inclusion. Here, we consider the case of a two-dimensional circular inclusion embedded in a planar matrix. Accordingly to Section 1.2.3, from the continuum theory point of view, this configuration corresponds to the case of a three-dimensional cylindrical inclusion under plane strain conditions as well. Moreover, the Eshelby solutions can be exactly evaluated under the hypothesis of isotropic behavior of the involved materials. Consistently, such a condition has been introduced also in the atomistic models exploiting the capability of the constitutive force filed.

7.1.1 *Isotropic elastic behavior*

In this Section, we derive the nonlinear constitutive equation for a two-dimensional isotropic material. In particular we show that, in such a case, the nonlinear behavior is described by two independent elastic moduli.

When the strain energy function is known, the constitutive equation is derived as $\hat{T} = \frac{\partial U}{\partial \hat{\varepsilon}}$. Following the same procedure reported in Section 2.3.2, if the system under consideration is isotropic the strain energy function must depends only on the invariants of the tensor $\hat{\varepsilon}$. As a consequence, in the two-dimensional case, the following relation holds

$$U(\hat{\varepsilon}) = \left(\mathrm{Tr}(\hat{\varepsilon}), \mathrm{Tr}(\hat{\varepsilon}^2)\right) \tag{7.1}$$

The isotropic nonlinear strain energy function

In this case the expansion, up to the third order, becomes

$$calU(\hat{\varepsilon}) = \frac{\lambda}{2}\mathrm{Tr}(\hat{\varepsilon})^2 + \mu\ \mathrm{Tr}(\hat{\varepsilon}^2) + \mathbf{b}\ \mathrm{Tr}(\hat{\varepsilon})\mathrm{Tr}(\hat{\varepsilon}^2) + \frac{\mathbf{c}}{3}\ \mathrm{Tr}(\hat{\varepsilon})^3 \tag{7.2}$$

where λ and μ are the Lamé constants describing the linear elasticity of the medium, while the nonlinear behavior is modelled by the two coefficients $\mathbf{b}$ and $\mathbf{c}$, two-dimensional counterpart of the Landau coefficients in Eq.(2.87). The Lamé constants can be expressed in terms of the stiffness tensor components C_{ij}

$$\lambda = C_{12} \tag{7.3}$$

$$\mu = \frac{C_{11} - C_{12}}{2} = C_{44} \tag{7.4}$$

We remark that, since the system is isotropic, the Cauchy relation $2C_{44} = C_{11} - C_{12}$ is always fulfilled. Moreover, the coefficients $\mathbf{b}$ and $\mathbf{c}$ can be expressed in terms of the standard third order elastic moduli C_{ijk} through the following relations

$$\mathbf{b} = \frac{1}{4}(C_{111} - C_{112}) \qquad \mathbf{c} = \frac{3}{4}(C_{112} - \frac{1}{3}C_{111}) \tag{7.5}$$

or, in terms of the three nonlinear coefficients λ_1, λ_2, and λ_3 in Eqs. (6.14) and (6.15) adopted to describe the nonlinear elasticity of the hexagonal symmetry

$$\mathbf{b} = \Lambda_2 \qquad \mathbf{c} = \frac{3}{2}(\Lambda_3 - \Lambda_2) \tag{7.6}$$

As discussed in the previous Chapter, the isotropic condition implies that $\Lambda_3 = 0$. Finally, we note that the above system does not represent any symmetry group of the crystal classification since all of them are characterized by an anisotropic nonlinear elastic behavior [199].

7.1.2 *Eshelby theory for nonlinear inclusion in two-dimensional isotropic systems*

Here, we apply the nonlinear Eshelby theory described in Chapter 2.3 to the present case of a circular two-dimensional inclusion. The elastic properties of the linear matrix are described by two Lamé coefficients $\mu^{(1)}$ and $\lambda^{(1)}$ or, equivalently, by the stiffness tensor $\hat{\mathcal{C}}^{(1)}$. Moreover, the nonlinear elastic behavior of the inclusion is described by a constitutive relation similar to Eq.(7.2) and by the following elastic constants: $\mu^{(2)}$, $\lambda^{(2)}$ (for the linear elasticity), $\mathbf{b}$ and $\mathbf{c}$ (for the nonlinear one). It means that we adopt a nonlinear but isotropic circular inclusion. As above discussed the Eshelby theory states that the Cauchy stress $\hat{T}^{(2)}$ and the strain field $\hat{\varepsilon}^{(2)}$ within the inclusion are related to the remotely applied strain $\hat{\varepsilon}^{\infty}$ through the relation

$$\hat{\varepsilon}^{(2)} - \hat{S}\hat{\varepsilon}^{(2)} + \hat{S}\left(\hat{\mathcal{C}}^{(1)}\right)^{-1}\hat{T}^{(2)}(\hat{\varepsilon}^{(2)}) = \hat{\varepsilon}^{\infty} \tag{7.7}$$

where $\hat{S}$ is the Eshelby tensor for a circular inclusion depending only on the Poisson ratio of the host matrix. On the other hand, the constitutive relation in Eq.(7.2) supplies us the following stress strain relation

$$\begin{aligned}\hat{T}^{(2)}(\hat{\varepsilon}^{(2)}) &= 2\mu^{(2)}\hat{\varepsilon}^{(2)} + \lambda^{(2)}\mathrm{Tr}(\hat{\varepsilon}^{(2)})\hat{I} \\ &\quad + 2\mathbf{b}\mathrm{Tr}\left(\hat{\varepsilon}^{(2)}\right)\hat{\varepsilon}^{(2)} + \mathbf{b}\mathrm{Tr}\left[(\hat{\varepsilon}^{(2)})^2\right]\hat{I} \\ &\quad + \mathbf{c}\mathrm{Tr}^2\left(\hat{\varepsilon}^{(2)}\right)\hat{I}\end{aligned} \tag{7.8}$$

By replacing Eq.(7.8) into Eq.(7.7) we obtain the implicit equation for the internal field $\hat{\varepsilon}^{(2)}$

$$\begin{aligned}\hat{\varepsilon}^{\infty} &= A\hat{\varepsilon}^{(2)} + B\mathrm{Tr}(\hat{\varepsilon}^{(2)})\hat{I} + C\mathrm{Tr}(\hat{\varepsilon}^{(2)})\hat{\varepsilon}^{(2)} \\ &\quad + D\mathrm{Tr}\left[(\hat{\varepsilon}^{(2)})^2\right]\hat{I} + E\mathrm{Tr}^2\left(\hat{\varepsilon}^{(2)}\right)\hat{I}\end{aligned} \tag{7.9}$$

where

$$\begin{aligned}A &= 1 - \frac{\lambda^{(1)} + 3\mu^{(1)}}{2(\lambda^{(1)} + 2\mu^{(1)})}\left(1 - \frac{\mu^{(2)})}{\mu^{(1)})}\right) \\ B &= \frac{2(\lambda^{(2)} - \lambda^{(1)}) + \left(1 - \frac{\mu^{(2)}}{\mu^{(1)}}\right)\left(\lambda^{(1)} + \mu^{(1)}\right)}{4(\lambda^{(1)} + 2\mu^{(1)})} \\ C &= \frac{1}{2\mu^{(1)}}\frac{\lambda^{(1)} + 3\mu^{(1)}}{\lambda^{(1)} + 2\mu^{(1)}}\mathbf{b} \\ D &= \frac{1}{2}\frac{\mathbf{b}}{\lambda^{(1)} + 2\mu^{(1)}} \\ E &= \frac{1}{2}\frac{\mathbf{c}}{\lambda^{(1)} + 2\mu^{(1)}} - \frac{\lambda^{(1)} + \mu^{(1)}}{4\mu^{(1)}}\frac{\mathbf{b}}{\lambda^{(1)} + 2\mu^{(1)}}\end{aligned} \tag{7.10}$$

are constant parameters. In order to solve Eq.(7.9) for $\hat{\varepsilon}^{(2)}$ (up to the second order in $\hat{\varepsilon}^{\infty}$), it is useful to calculate the quantities $\hat{\varepsilon}^{\infty}$, $\mathrm{Tr}(\hat{\varepsilon}^{\infty})\hat{I}$, $\mathrm{Tr}(\hat{\varepsilon}^{\infty})\hat{\varepsilon}^{\infty}$, $\mathrm{Tr}\left[(\hat{\varepsilon}^{\infty})^2\right]\hat{I}$ and $\mathrm{Tr}^2\left(\hat{\varepsilon}^{\infty}\right)\hat{I}$ in terms of $\hat{\varepsilon}^{(2)}$. They can be arranged in matrix form as follows

$$\begin{pmatrix} \hat{\varepsilon}^{\infty} \\ \mathrm{Tr}(\hat{\varepsilon}^{\infty})\hat{I} \\ \mathrm{Tr}(\hat{\varepsilon}^{\infty})\hat{\varepsilon}^{\infty} \\ \mathrm{Tr}\left[(\hat{\varepsilon}^{\infty})^2\right]\hat{I} \\ \mathrm{Tr}^2\left(\hat{\varepsilon}^{\infty}\right)\hat{I} \end{pmatrix} = M \begin{pmatrix} \varepsilon^{(2)} \\ \mathrm{Tr}(\hat{\varepsilon}^{(2)})\hat{I} \\ \mathrm{Tr}(\hat{\varepsilon}^{(2)})\hat{\varepsilon}^{(2)} \\ \mathrm{Tr}\left[(\hat{\varepsilon}^{(2)})^2\right]\hat{I} \\ \mathrm{Tr}^2\left(\hat{\varepsilon}^{(2)}\right)\hat{I} \end{pmatrix} \tag{7.11}$$

where

$$M = \begin{pmatrix} A & B & C & D & E \\ 0 & A+2B & 0 & 2D & C+2E \\ 0 & 0 & A(A+2B) & 0 & B(A+2B) \\ 0 & 0 & 0 & A^2 & 2B(A+B) \\ 0 & 0 & 0 & 0 & (A+2B)^2 \end{pmatrix} \tag{7.12}$$

By inverting the above system of equations and by focusing on the first unknown we finally get the expression of the internal strain field $\hat{\varepsilon}^{(2)}$ as a function of the applied strain $\hat{\varepsilon}^{\infty}$

Internal strain in terms of the remotely applied strain

$$\begin{aligned} \hat{\varepsilon}^{(2)} &= \frac{\hat{\varepsilon}^{\infty}}{A} - \frac{B}{A(A+2B)} \mathrm{Tr}(\hat{\varepsilon}^{\infty})\hat{I} \\ &\quad - \frac{1}{A^2(A+2B)} \left(C\mathrm{Tr}(\hat{\varepsilon}^{\infty})\hat{\varepsilon}^{\infty} + D\mathrm{Tr}\left[(\hat{\varepsilon}^{\infty})^2\right] \hat{I} \right) \\ &\quad + \frac{2B(A+B)(C+D) - EA^2}{A^2(A+2B)^3} \mathrm{Tr}^2\left(\hat{\varepsilon}^{\infty}\right) \hat{I} \end{aligned} \tag{7.13}$$

This is the main result of the theory giving the uniform internal strain in terms of the remotely applied strain. For the following analysis is convenient to apply Eq.(7.13) for an applied homogeneous uniaxial elongation corresponding to

$$\hat{\varepsilon}^{\infty} = \begin{pmatrix} \varepsilon^{\infty}_{11} & \varepsilon^{\infty}_{12} \\ \varepsilon^{\infty}_{21} & \varepsilon^{\infty}_{22} \end{pmatrix} = \begin{pmatrix} \epsilon & 0 \\ 0 & 0 \end{pmatrix} \tag{7.14}$$

being ϵ a constant representing the magnitude of the axial deformation. In this case Eq.(7.13) assumes the form

The elastic coefficients providing the internal strain as a nonlinear function of the uniaxial applied load

$$\hat{\epsilon}^{(2)} = \begin{pmatrix} \varepsilon_l & 0 \\ 0 & \varepsilon_t \end{pmatrix} = \begin{pmatrix} L^I\epsilon + L^{II}\epsilon^2 & 0 \\ 0 & T^I\epsilon + T^{II}\epsilon^2 \end{pmatrix} \tag{7.15}$$

where we have introduced the simplified notations ε_l and ε_t to indicate the longitudinal strain $\varepsilon^{(2)}_{11}$ and the transverse strain $\varepsilon^{(2)}_{22}$, respectively (see Fig.41). According to Eqs.(7.13) and (7.15), these two components of the internal strain field are quadratic functions of the remotely applied strain ϵ and the four corresponding coefficients, L^I and T^I for the linear response and L^{II} and T^{II} for the nonlinear one, can be obtained as follows

$$L^I = \frac{A+B}{A(A+2B)} \tag{7.16}$$

$$T^I = \frac{-B}{A(A+2B)} \tag{7.17}$$

$$L^{II} = \frac{-(C+D)(A^2+2AB+2B^2) - EA^2}{A^2(A+2B)^3} \tag{7.18}$$

$$T^{II} = -\frac{A^2(D+E) + 2B(A+B)(D-C)}{A^2(A+2B)^3} \tag{7.19}$$

If the inclusion behavior is linear (i.e. $\mathbf{b} = 0$ and $\mathbf{c} = 0$) we get $L^{II} = 0$ and $T^{II} = 0$ and the original linear Eshelby result is recovered.

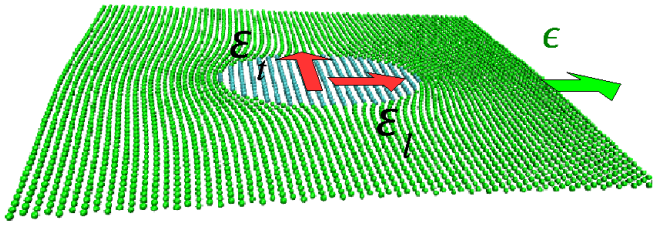

Figure 41: Scheme of the matrix-inclusion system. After the remote application of an uniaxial load ϵ we have computed both the longitudinal (ε_l) and the transverse (ε_t) strain fields inside the inclusion.

7.1.3 *Atomistic analysis of the Eshelby configuration*

In order to analyze the Eshelby configuration from the atomistic point of view, we have selected two different sets of parameters for the constitutive force field described in Sec.6.2.2 so as to obtain two different elastic media: a fully isotropic linear system, i.e. with $\mathcal{C}_{111} = \mathcal{C}_{222} = \mathcal{C}_{112} = 0$, and an isotropic nonlinear one, i.e. with $\mathcal{C}_{111} = \mathcal{C}_{222}$. According to the general scheme of Table 5, these requirements can be satisfied by several sets of the potential parameters. In order to simplify the simulation framework we have choosen to consider only 2-body terms in Eq.(6.16) (we note that, generally speaking, the introduction of 3-body interactions demands more computational resources than 2-body interactions). As a consequence of this choice, both the systems show a fixed Poisson ratio $\nu_{2d} = \frac{1}{3}$ (see Eq.(6.18) and following comments). In particular, we have set for the linear medium $\kappa_l = K$, $\kappa_h = 0$ and $\kappa_a = 0$ where K is a constant governing the stiffness of this first system. This setting corresponds to the application of the only *linear* 2-body interaction. As can be easily seen in Eq.(6.20), the resulting elastic behavior of the medium is

The isotropic linear atomistic model

$$\begin{aligned}
\mathcal{C}^{lin}_{11} &= \frac{3\sqrt{3}}{4}K \\
\mathcal{C}^{lin}_{12} &= \frac{\sqrt{3}}{4}K \\
\mathcal{C}^{lin}_{111} &= 0 \\
\mathcal{C}^{lin}_{222} &= 0 \\
\mathcal{C}^{lin}_{112} &= 0
\end{aligned} \tag{7.20}$$

In the interaction potential of the second system (the nonlinear medium) we have set $\kappa_l = 0$, $\kappa_h = K$ and $\kappa_a = \frac{3}{2}K$ where K is the constant governing the stiffness of the system. This means that the interaction is here composed by an *harmonic* term (affecting both the linear as the nonlinear elasticity) and an *anharmoinc* term (affecting

The isotropic nonlinear atomistic model

the only nonlinear elasticity) tuned to obtain an isotropic nonlinear behavior. In fact, in this case, the resulting elastic moduli are

$$\begin{aligned} \mathcal{C}^{nlin}_{11} &= \frac{3\sqrt{3}}{4}K \\ \mathcal{C}^{nlin}_{12} &= \frac{\sqrt{3}}{4}K \\ \mathcal{C}^{nlin}_{111} &= \frac{9}{4}\sqrt{3}K \\ \mathcal{C}^{nlin}_{222} &= \frac{9}{4}\sqrt{3}K \\ \mathcal{C}^{nlin}_{112} &= \frac{\sqrt{3}}{4}K \end{aligned} \tag{7.21}$$

The isotropy is confirmed by the validity of the relation $\mathcal{C}^{nlin}_{111} = \mathcal{C}^{nlin}_{222}$. Subsequently, different inclusion/matrix models have been obtained by arranging the two above systems according to the geometry shown in Fig.41. As a first case we have selected two linear media described by the elastic properties in Eq.(7.20) with different values of K (K_{mat} in the matrix and K_{inc} in the inclusion). This system has been utilized to validate the linear version of the Eshelby theory. A second analysis has been performed to investigate the case of a nonlinear inclusion in a linear matrix. Therefore, we have selected for the inclusion a nonlinear medium with elastic response given in Eq.(7.21) with $K = K_{inc}$ as stiffness parameter and for the matrix the linear medium described in Eq.(7.20) with stiffness given by K_{mat}. Finally, we have also studied the cases, not considered by the Eshelby theory, in which the matrix is nonlinear.

The interatomic distance parameter in the atomistic model

In order to avoid the formation of a disordered interface at the boundary between the two phases and the resulting effects on the mechanical behavior of the system [86], we have set the same equilibrium distance $r_0 = 3.405$ Å and the same crystallographic orientation for both the inclusion and matrix materials. In these conditions we have no lattice mismatches at the interface.

We have applied to the inclusion/matrix system described above a set of uniaxial elongations in the longitudinal direction (see Eq.(7.14)) with ϵ in the range $(-0.01, 0.01)$. For each value of the deformation we have calculated the internal longitudinal and transverse strain, as defined in Eq.(7.15). In particular, for each deformed sample, we have computed the displacement field inside the inclusion in the direction parallel to the load (the longitudinal displacement $u_1(x_1, x_2)$) and the displacement field in the direction perpendicular to the load (the transverse displacement $u_2(x_1, x_2)$). Subsequently, by fitting these surfaces, we have computed the longitudinal strain through the relation $\epsilon_l = \frac{\partial u_1}{\partial x_1}$ and the transverse strain through $\epsilon_t = \frac{\partial u_2}{\partial x_2}$.

This analysis has been performed for different values of the *elastic contrast* between matrix and inclusion defined as $\log_2(K_{mat}/K_{inc})$. This definition implies that a positive contrast means that the matrix is stiffer than the inclusion while a negative contrast means that the matrix is softer than the inclusion. Moreover, all the simulations are been repeated for several values of the radius R of the inclusion in order to study the scale effects.

The theoretical model discussed in Sec.7.1.2 concerns a single inclusion embedded into an infinite matrix. Therefore, the conventional Periodical Boundary Conditions (PBC), usually applied in the atomistic

simulations to avoid the finite size effects induced by the free surfaces, are in our case intrinsically inappropriate. So, in the present simulations we have applied the Asymptotic Boundary Conditions (ABC). To this aim, we have calculated for each sample, the theoretical displacement field due to the applied remote deformation (ε^{∞}) within an infinite two-dimensional elastic matrix with a single inclusion, as predicted by the Eshelby theory. Then, we have arranged all the atoms of a finite square simulation box (of side length equal to twenty times the radius R of the inclusion) according to this predicted displacement field. In this configuration, the atoms near the boundaries are subjected to a system of forces due to the free edges. We have therefore calculated such a system of forces generated by the atomistic interaction model. Finally, these values of forces have been applied, with opposite sign, to the atoms near the boundaries (ABC) so as to obtain the equilibrium state. After the application of the ABC, the system has been relaxed through dumped dynamics in order to allow for the relaxation of the internal degrees of freedom. The convergence criterion has been set so as to have the final interatomic forces not larger than 10^{-10} eV/Å.

The Asymptotic Boundary Conditions

Atomistic validation of the linear Eshelby theory

In this first analysis we have investigated the basic case of a single linear inclusion embedded into a linear matrix. The elastic behaviors of the media in the two phases are represented by the Eq.(7.20) with $K = K_{inc}$ in the inclusion and $K = K_{mat}$ in the matrix. At first, we have calculated the internal strain components as function of the contrast $\log_2(K_{mat}/K_{inc})$ for a radius of the inclusion $R = 10$ Å (corresponding to 30 atoms). The results are reported in Fig.42. The uniformity of the internal strain field is confirmed by the atomistic simulations with high degree of accuracy.

The zero contrast data corresponds to a system with the same medium inside and outside the inclusion (homogeneous material). Therefore, as aspected in this case, the external strain field is equal to the internal one ($L^I = 1, T^I = 0$). Interesting enough, when the contrast is positive (i.e. when the inclusion is softer than the hosting matrix) atomistic data show a behavior different from the continuum prediction while, elsewhere, a perfect agreement between the two approaches is present. As shown in Fig.43, such an atomistic effect increases with the contrast.

The observed discrepancy between Eshelby prediction and atomistic results has been analyzed by varying the radius of the inclusion. We have found that such an atomistic effect disappears with the increasing radius (see Fig.44). Therefore, we attribute this effect to the discrete (or atomistic) structure of the matter. The Eshelby theory can not take into account this phenomenon since it is based on the elasticity theory which is scale invariant by definition. From Figs.43 and 44 we deduce that such scale effects are much more pronounced for the longitudinal coefficient L^I than for the transversal one T^I.

The onset of atomistic effects

Atomistic validation of the nonlinear Eshelby theory

By following the generalization of the Eshelby theory discussed in Section 7.1.2, we take under consideration a nonlinear inclusion embedded in a linear matrix from the atomistic point of view. To this aim, we have considered for the inclusion medium the nonlinear isotropic

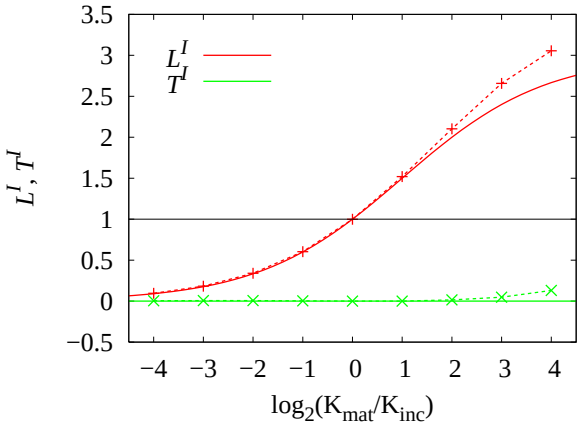

Figure 42: Mechanical behavior of a linear inclusion embedded in a linear matrix under remote load. The solid lines represent the Eshelby prediction (Eqs.(7.16) and (7.17)) while the symbols correspond to the atomistic results obtained for a radius of the inclusion $R = 10$ Å (30 particles).

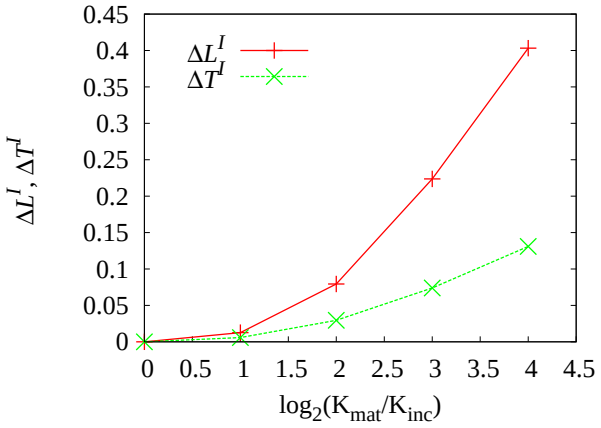

Figure 43: Atomistic effects on the linear elastic behavior of the inclusion. Differences ΔL^I and ΔT^I between the atomistic and continuum result as a function of the elastic contrast.

force field represented by the Eq.(7.21) with $K = K_{inc}$. The matrix is described by a linear material with $K = K_{mat}$ as before (see Eq.(7.20)). In Fig.45 we report the coefficients of the curves $\varepsilon_l = L^I\epsilon + L^{II}\epsilon^2$ and $\varepsilon_t = T^I\epsilon + T^{II}\epsilon^2$ for several values of the elastic contrast at fixed inclusion radius ($R = 10$ Å). Also in this case we have observed a quite perfect uniformity of the internal strain field.

By confronting these results with the corresponding fully linear case reported in Fig.42, we can note that the coefficients L^I and T^I assume exactly the same values. Also the linear atomistic scale effects are identical in the two models. This means that any feature of the linear part of the elastic behavior of the inclusion/matrix system is not affected by the presence of a nonlinearity in the behavior of inclusion. With respect to the nonlinear coefficients L^{II} and T^{II} we found, similarly to the linear ones, a perfect agreement between atomistic and Eshelby results if the inclusion is stiffer than the matrix (negative values of the

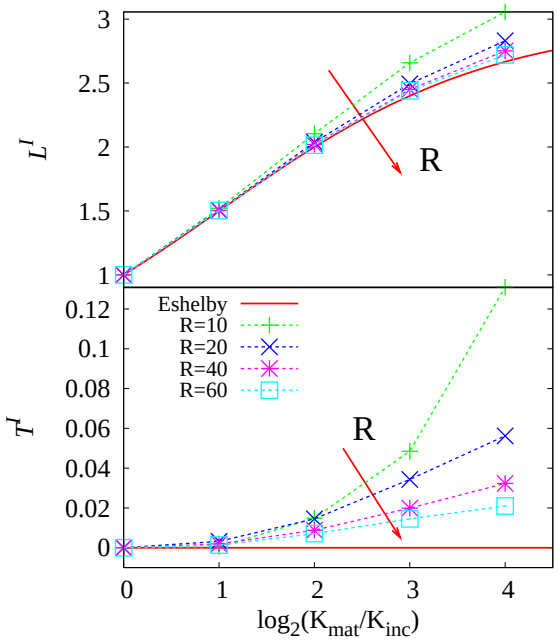

Figure 44: Atomistic effects on the linear elastic behavior of the inclusion. Linear coefficients L^I (top panel) and T^I (bottom panel) as a function of the elastic contrast for several values of the inclusion radius. For increasing radius the Eshelby results are recovered for each value of the contrast.

contrast). On the other hand, atomistic effects are present in the case of positive contrast, as shown in Fig.46 where the differences between atomistic and continuum results are quantified. We observe that the atomistic transversal nonlinear coefficient is practically coincident with the theoretical results for any value of the contrast. On the countrary, sizeable discrepancies have been found for the longitudinal coefficient. As represented in Fig.47, these effects depend on the contrast and cancel out when the radius of the inclusion increases. Both for the linear and nonlinear coefficients, we observe that the scale effects disappear for a radius greater than 10 nm when the lattice constant is about 3.4 Å.

The atomistic effects depend on the elastic contrast

Scaling laws for the atomistic effects

We have shown through the previous simulations that for positive contrast the Eshelby theory (both for linear and nonlinear behaviors) is recovered only in the limit of very large radius R of the inclusion. In the present Section, we show the results of the analysis of the scaling laws that drive this phenomenon. In Fig.48 we report the atomistic results for the longitudinal linear L^I and nonlinear L^{II} coefficients as a function of R. We do not take into consideration the transversal coefficients T^I and T^{II} since they show quite negligible scale effects creating some difficulties in performing the statistical analysis. In order to give an interpretation of the results, we have tested the following scaling power law

The hypothesis of scaling power low

$$\frac{L^I(R)}{L^I(\infty)} = 1 + \frac{a}{R^\alpha} \tag{7.22}$$

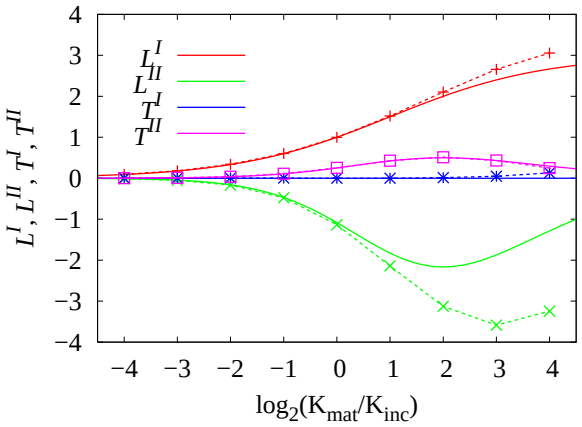

Figure 45: Linear and nonlinear coefficients of the curves $\varepsilon_l = L^I\epsilon + L^{II}\epsilon^2$ and $\varepsilon_t = T^I\epsilon + T^{II}\epsilon^2$ giving the internal longitudinal (ε_l) and transverse (ε_t) strain as a function of the magnitude ϵ of the remote load. The solid lines represent the Eshelby prediction while the symbols indicate the atomistic simulation results obtained for an inclusion of radius $R = 10$ Å.

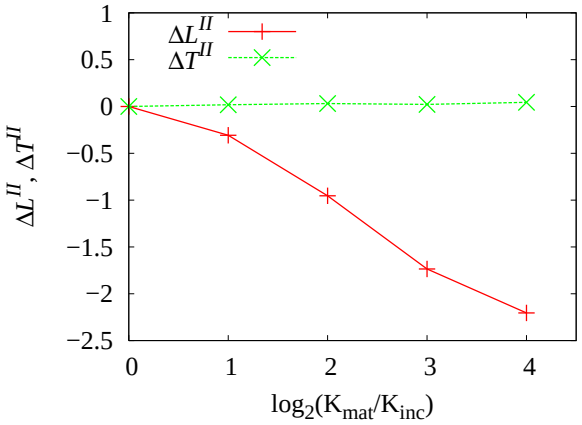

Figure 46: Atomistic effects on the nonlinear elastic behavior of the inclusion. Differences ΔL^{II} and ΔT^{II} between the atomistic and continuum results as a function of the elastic contrast.

for the longitudinal linear scale effects, where a and α are the fitting parameters. This choice implies the relation $\log_{10}[L^I(R)/L^I(\infty) - 1] = \log_{10} a - \alpha \log_{10} R$ which gives the meaning of angular coefficient to $-\alpha$ when the bi-logarithmic scale is adopted. Similarly, we use the representation

$$\frac{L^{II}(R)}{L^{II}(\infty)} = 1 + \frac{b}{R^\beta} \tag{7.23}$$

for the longitudinal nonlinear scale effects, where b and β are the fitting parameters. As before, the relation $\log_{10}[L^{II}(R)/L^{II}(\infty) - 1] = \log_{10} b - \beta \log_{10} R$ allows us to define $-\beta$ as the angular coefficient in bi-logarithmic scale. Accordingly, in Fig.49, the quantities $L^I(R)/L^I(\infty) - 1$ and $L^{II}(R)/L^{II}(\infty) - 1$ are represented in bi-logarithmic scale versus

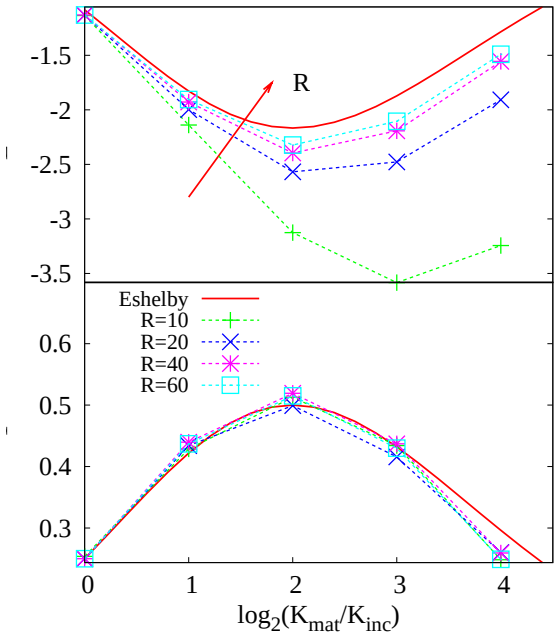

Figure 47: Atomistic effect on the nonlinear elastic behavior of the inclusion. Linear coefficients L^{II} (top panel) and T^{II} (bottom panel) as a function of the elastic contrast for several values of the inclusion radius. For increasing radius the Eshelby result is recovered for each value of the contrast.

the radius R of the inclusion. Then, a linear regression procedure has been utilized to fit all the sets of data. As one can observe, the scaling exponents α and β assume the quite constant value 1.1 both for linear and nonlinear data. This result can be interpretated by assuming that the linear and nonlinear behaviors of our elastic system belong to the same universality class. The emergence of the power laws and of the universality in our system can be attribuited to the fact that both linear and nonlinear properties depend upon the same force field and the same fundamental physical laws.

The same scaling exponent $\alpha = \beta = 1.1$ for both linear and nonlinear behavior

7.1.4 *The inclusion problem beyond the Eshelby theory*

Linear inclusion into nonlinear matrix

In this Section we consider the case of a linear inclusion embedded into a nonlinear matrix. As a first step we take under consideration the following setting of the potential parameters: the elastic behavior of the inclusion is described by the Eq.(7.20) with $K = K_{inc}$ while in the matrix we apply the force field so as to obtain the elastic behavior in Eq.(7.21) with $K = K_{mat}$. In Fig.50 we report the coefficients of the curves $\varepsilon_l = L^I\epsilon + L^{II}\epsilon^2$ and $\varepsilon_t = T^I\epsilon + T^{II}\epsilon^2$ giving the internal strain for several values of the elastic contrast at fixed inclusion radius ($R = 10$ Å). In this case the uniformity of the internal strain field is not demonstrated by the continuum theory but it has been, however, found by atomistic simulations. By drawing a comparison between Fig.50 and Fig.45, we discuss the following variations in the elastic behavior. When

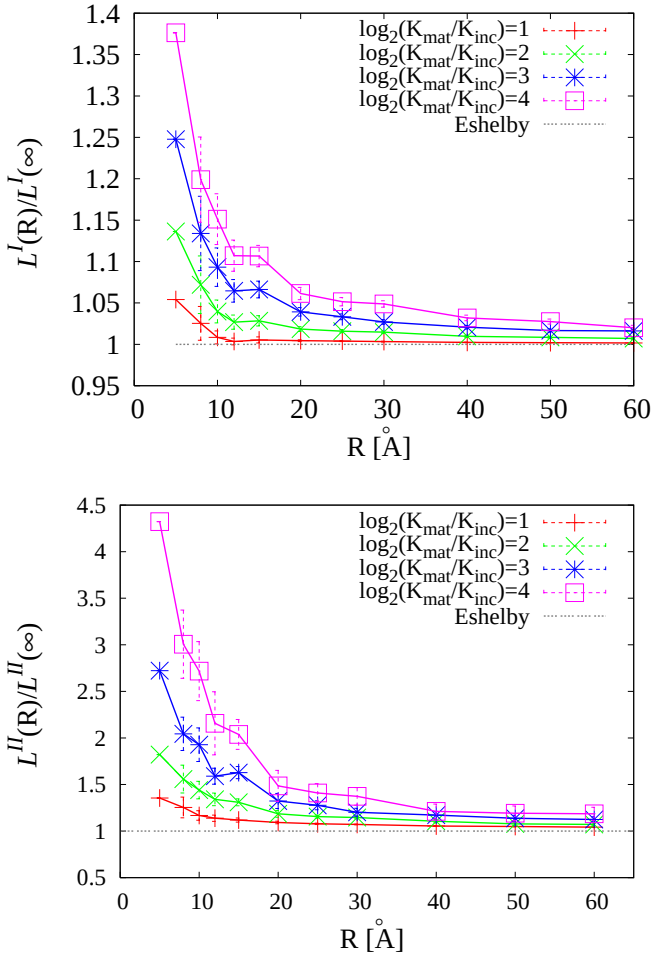

Figure 48: Atomistic effects on the elastic (longitudinal) behavior of the inclusion. Ratios $L^I(R)/L^I(\infty)$ (top) and $L^{II}(R)/L^{II}(\infty)$ (bottom) between atomistic data ($L^I(R)$, $L^{II}(R)$) and continuum results ($L^I(\infty)$, $L^{II}(\infty)$) as functions of the radius R of the inclusion.

For some value of the contrast, the nonlinearity of the matrix does not affect the internal stain

the inclusion is nonlinear the coefficients L^{II} and T^{II} have constant sign independently from the contrast and they exhibit a minimum and a maximum, respectively (see Fig.45). On the countrary, when the matrix is nonlinear it is remarkable to observe that two values of contrast exist which cancel out the second order nonlinear effects in the longitudinal and transversal direction, respectively (Fig.50).

As mentioned above, in this case a solution of problem within the continuum theory does not exist. Therefore, we also analyze the elastic behavior of the inclusion/matrix system by varying the nonlinearity of the matrix. To this aim, we have considered again a linear inclusion with elastic behavior represented by Eq.(7.20) with the stiffness constant $K = K_{inc}$ governing the linear elastic behavior of the inclusion.

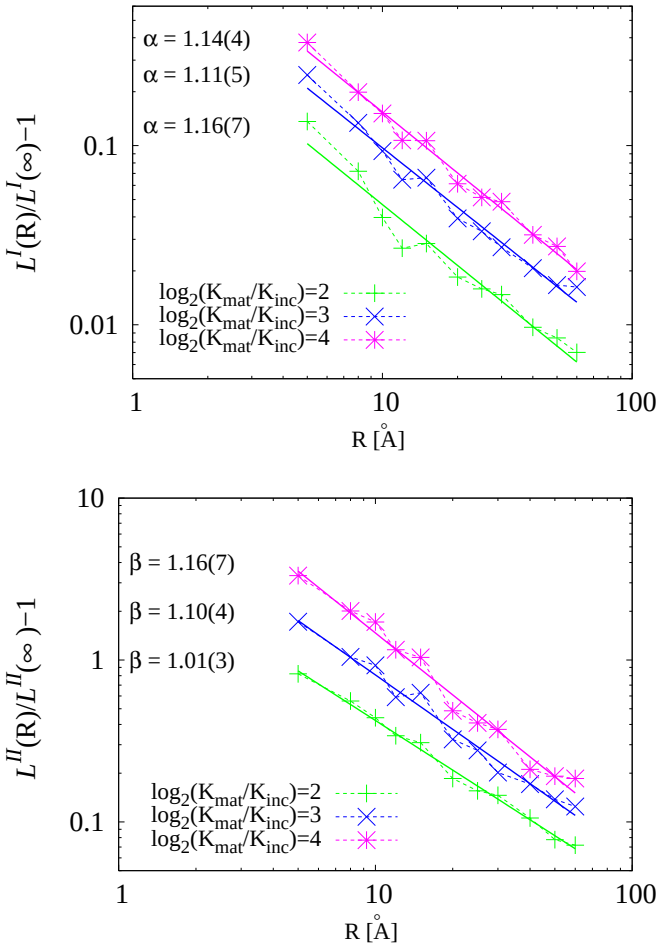

Figure 49: Atomistic effects on the elastic (longitudinal) behavior of the inclusion. The quantities $L^I(R)/L^I(\infty)-1$ (top) and $L^{II}(R)/L^{II}(\infty)-1$ (bottom) relating atomistic data ($L^I(R)$, $L^{II}(R)$) to continuum results ($L^I(\infty)$, $L^{II}(\infty)$) are represented in bi-logarithmic scale, as functions of the radius R.

On the other hand, within the nonlinear inclusion we have set $\kappa_l = K$, $\kappa_h = K'$ and $\kappa_a = \frac{3}{2}K'$ where K and K' are constants. The resulting elastic behavior of the matrix is the following

$$\begin{aligned}
\mathcal{C}^{nlin}_{11} &= \frac{3\sqrt{3}}{4}K^l_{mat} \\
\mathcal{C}^{nlin}_{12} &= \frac{\sqrt{3}}{4}K^l_{mat} \\
\mathcal{C}^{nlin}_{111} &= \frac{9}{4}\sqrt{3}K^{nl}_{mat} \\
\mathcal{C}^{nlin}_{222} &= \frac{9}{4}\sqrt{3}K^{nl}_{mat} \\
\mathcal{C}^{nlin}_{112} &= \frac{\sqrt{3}}{4}K^{nl}_{mat}
\end{aligned} \tag{7.24}$$

where $K^l_{mat} = K + K'$ is the stiffness constant governing the linear elasticity of the matrix and $K^{nl}_{mat} = K'$ is the constant governing its nonlinear elastic behavior. Therefore, by varing the value of K^{nl}_{mat} with

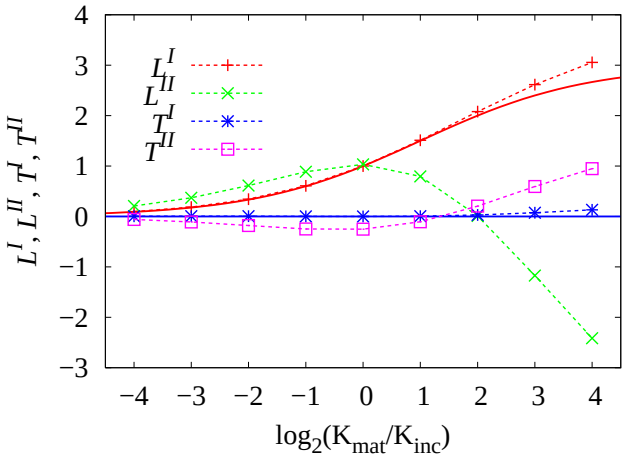

Figure 50: Linear and nonlinear coefficients of the curves $\varepsilon_l = L^I\epsilon + L^{II}\epsilon^2$ and $\varepsilon_t = T^I\epsilon + T^{II}\epsilon^2$ giving the internal longitudinal (ε_l) and transverse (ε_t) strain as a function of the magnitude ϵ of the remote load. The solid lines represent the linear Eshelby prediction while the symbols indicate the atomistic simulation results obtained for an inclusion of radius $R = 10$ Å.

respect to K^l_{mat}, we can achieve different levels of nonlinearity. In Fig.51 we report the atomistic results for the nonlinear coefficients L^{II} (top) and T^{II} (bottom) versus the (linear) elastic contrast $\log_2(K^l_{mat}/K_{inc})$ for different values of nonlinearity ratio K^{nl}_{mat}/K^l_{mat} in the matrix. We have not reported the results for the linear coefficients L^I and T^I since they are not affected by the nonlinear features of both inclusion and matrix; indeed, they assume the very same values reported in Fig.50. It is interesting to underline that the longitudinal coefficient L^{II} assumes the value zero for a given linear contrast $\log_2(K^l_{mat}/K_{inc})$ for any possible value of the nonlinear parameter K^{nl}_{mat} of the matrix. The same phenomenon has been observed for the transversal coefficient T^{II}.

Nonlinear inclusion into nonlinear matrix

In this Section we consider the case of a nonlinear inclusion embedded into a nonlinear matrix. In a first numerical analysis, the elastic behavior of both media is described by Eq.(7.21) with $K = K_{inc}$ in the inclusion and $K = K_{mat}$ in the matrix. In Fig.52 we report the coefficients of the curves $\varepsilon_l = L^I\epsilon + L^{II}\epsilon^2$ and $\varepsilon_t = T^I\epsilon + T^{II}\epsilon^2$ for several values of the elastic contrast at fixed inclusion radius ($R = 10$ Å). In this case the zero contrast value corresponds to a non linear but homogeneous material (without inclusion). Therefore, we obtained $L^{II} = T^{II} = 0$ and $L^I = 1$ for $K_{mat} = K_{inc}$ as expected and shown in Fig.52.

As before, since this configuration is not easily handled by continuum mechanics, we perform a more detailed analysis of the system with different nonlinearities for the hosting matrix. We have fixed the nonlinear elastic behavior of the inclusion accordingly to Eq.(7.21) with $K = K_{inc}$. Moreover, the matrix has been modelled by means of Eq.(7.24) where the linear and nonlinear stiffness constants K^l_{mat} and K^{nl}_{mat} modulate the response of the system. In Fig.53 we show the atomistic results for

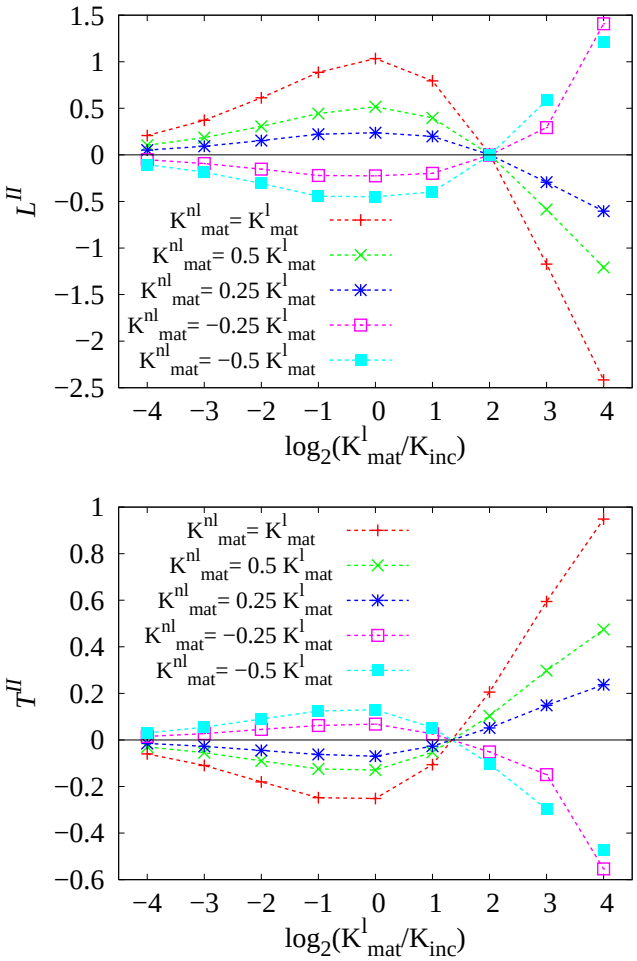

Figure 51: Atomistic results for the nonlinear coefficients L^{II} (top) and T^{II} (bottom) versus the (linear) elastic contrast $\log_2(K^{l}_{mat}/K_{inc})$ for different values of nonlinearity ratio K^{nl}_{mat}/K^{l}_{mat} in the matrix.

the nonlinear coefficients L^{II} (top) and T^{II} (bottom) versus the (linear) elastic contrast $\log_2(K^{l}_{mat}/K_{inc})$ for different values of nonlinearity ratio K^{nl}_{mat}/K^{l}_{mat} in the matrix for a fixed radius $R = 10$Å. We have not reported the results for the linear coefficients L^{I} and T^{I} since they are not affected by the nonlinear features of both inclusion and matrix; indeed, they assume the very same values reported in Fig.52. Interesting enough, we observe that there is a value of the linear contrast $\log_2(K^{l}_{mat}/K_{inc})$ which generates a constant value of L^{II} (see Fig.53, top) for any nonlinearity of the matrix. It means that, in such a specific condition, the nonlinear effects of the matrix are nullified. The same behavior is also observed for the transversal coefficient T^{II} (see Fig.53, bottom).

The nonlinear behavior of the inclusion can be independent from the nonlinearityof the matrix

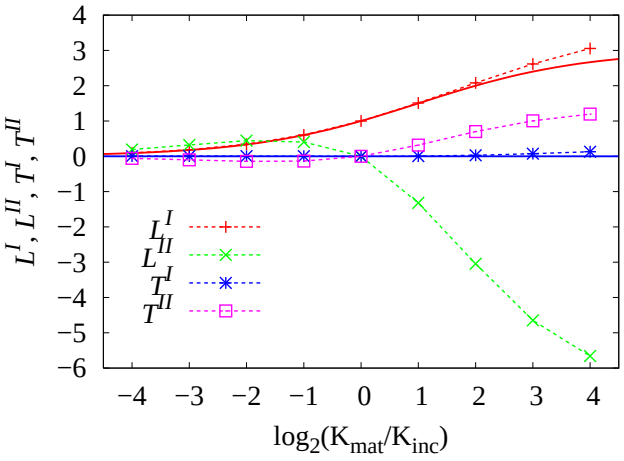

Figure 52: Linear and nonlinear coefficients of the curves $\varepsilon_l = L^I\epsilon + L^{II}\epsilon^2$ and $\varepsilon_t = T^I\epsilon + T^{II}\epsilon^2$ giving the internal longitudinal (ε_l) and transverse (ε_t) strain as a function of the magnitude ϵ of the remote load. The solid lines represent the linear Eshelby prediction while the symbols indicate the atomistic simulation results obtained for an inclusion radius $R = 10$ Å.

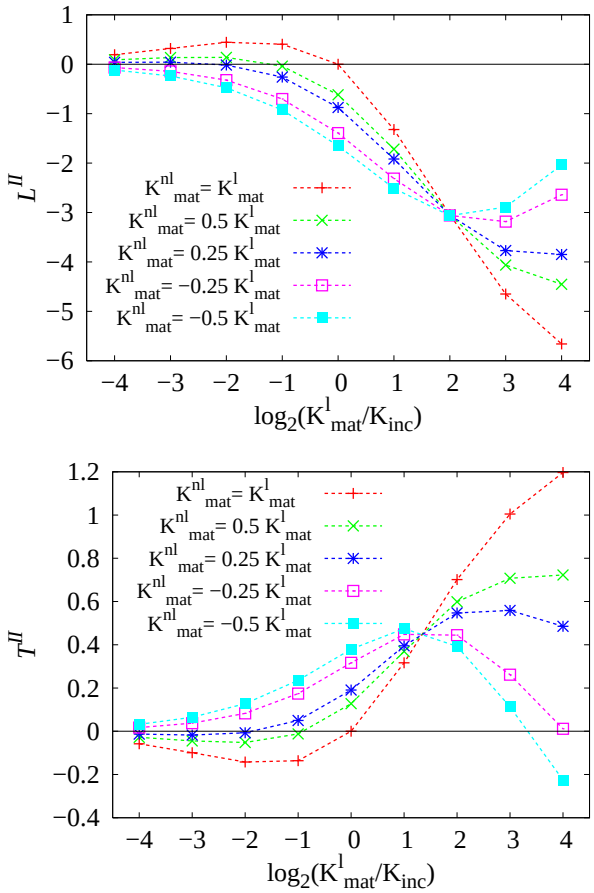

Figure 53: Atomistic results for the nonlinear coefficients L^{II} (top) and T^{II} (bottom) versus the (linear) elastic contrast $\log_2(K^l_{mat}/K_{inc})$ for different values of nonlinearity ratio K^{nl}_{mat}/K^l_{mat} in the matrix.

7.2 NONLINEAR NANO-COMPOSITES

In Chapter 3, we have considered the linear and nonlinear elastic behavior of heterogeneous materials composed by a dispersion of inclusions with elastic properties different from the hosting matrix. In particular, we have derived the expressions of the effective elastic properties of such a composite in terms of the elastic moduli of its components, i.e. of the homogeneous materials involved in the system. The applied procedure is based on the homogeneization method and exploits the nonlinear Eshelby solution for the elasticity of a single inhomogeneity. On the other hand, in the previous Sections we have investigated through atomistic simulations the applicability of the Eshelby theory at the nano-scale, finding and characterizing the onset of sizable atomistic scale-effects. We are now interested in the evaluation of these effects on the effective elastic behavior of nano-composites, i.e. on the elasticity of a dispersion of nano-inclusions.

We note that the continuum theory prediction supply us the following qualitative result: the effective behavior of the composite only dependents on the *volume fraction* $v = \frac{V_e}{V}$ of the particles (see Fig.54). Nevertheless, in order to investigate the effects of the size of the inhomogeneities, we have considered dispersions where the radius of the inclusions is constant.

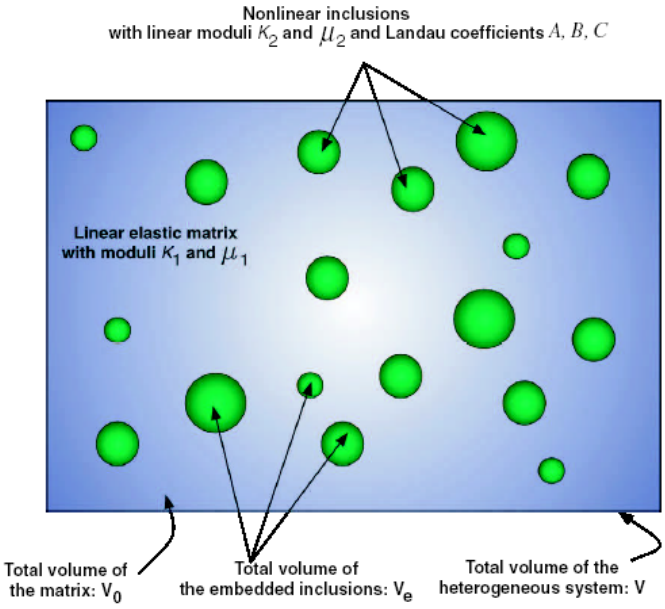

Figure 54: Scheme of a composite material. The inclusions exhibit a nonlinear behavior while the matrix is considered as a linear medium. The effective elastic behavior depends on the volume fraction $v = \frac{V_e}{V}$ and on the elastic features of the components.

Following the same procedures adopted in Section 7.1.3, we have set the constitutive force field so to define, on a triangular lattice, two elastically different media: an isotropic linear material for the matrix and an isotropic nonlinear one for the inclusions. In particular, two paradigmatic cases are considered: (i) the inclusion is twice stiffer than the matrix (negative elastic contrast) and (ii) the inclusion is twice softer than the matrix (positive elastic contrast). In fact, as observed

in the previous Sections, the onset of the size-effects for the single inhomogeneity depends on the sign of the elastic contrast.

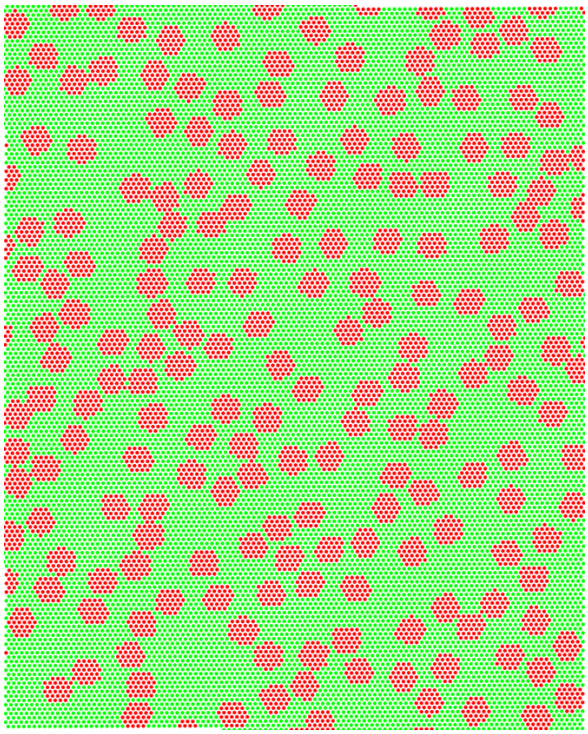

Figure 55: Atomistic configuration of a dispersion of circular inclusions (red atoms) arranged on a triangular lattice. In this sample, the volume fraction is equal to $v = 0.3$.

7.2.1 *Atomistic model of a dispersion of inclusions*

Generation algorithm for the dispersion atomistic model

We have arranged several samples of random dispersions of circular inclusions with constant radius $R \simeq 10$ Å and 20 Å (see Figs. 55 and 56) by applying the following algorithm. We note that any possible interface effects, similar to those observed in Section 5.2, are avoided by choosing the same equilibrium distance (potential parameter r_0) in both media. The center of the inclusions are generated by means of a uniform distribution. Each extraction is accepted only if it does not induce overlapping of the new inclusion with the previously defined ones. The procedure is stopped when the required volume fraction is obtained. We have verified that such a technique, allow us to generate samples with at most $v \simeq 0.5$ while the maximum value of the volume fraction in the two-dimensional random dispersion (random close-packing fraction) is $v = 0.82$ [202]. In order to approach this threshold a different algorithm should be adopted. Nevertheless, the continuum theory solutions are obtained in the limit of dilute dispersions and, therefore, we have considered the range $0 < v < 0.5$ appropriate for our purposes.

Elastic behavior of the dispersion model

By means of a set of suitable deformations we have computed the effective elastic moduli C^{eff}_{11}, C^{eff}_{22}, C^{eff}_{12}, C^{eff}_{44}, C^{eff}_{111}, C^{eff}_{222}, and C^{eff}_{112} of the atomistic systems through interpolations of the corresponding

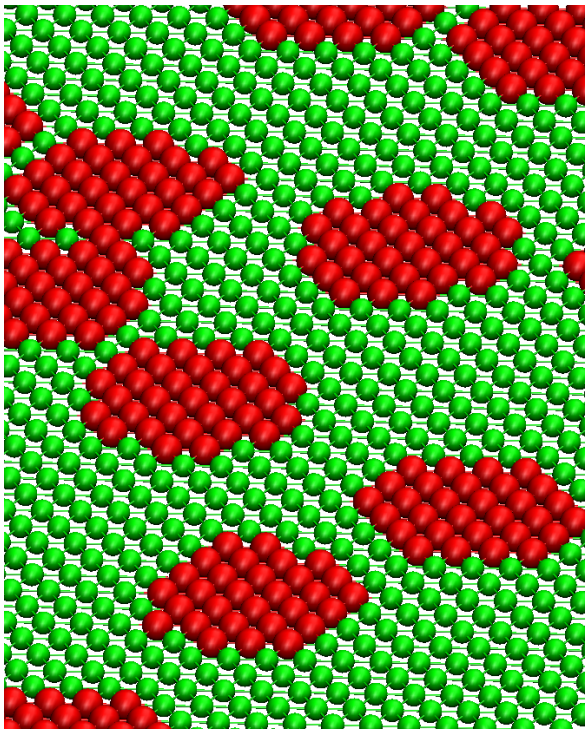

Figure 56: Configuration of the circular inclusions (red atoms) in the random dispersion arranged on a triangular lattice structure. In this sample, we fix the radius R of each inclusion as large as 10 Å corresponding to about 30 atoms.

stress/strain curves. In particular, we have applied (being (x,y) the reference frame of the two-dimensional lattice):

- Uniaxial elongations in the x direction:

$$\hat{\epsilon} = \begin{pmatrix} \varepsilon_{xx} & 0 \\ 0 & 0 \end{pmatrix} \tag{7.25}$$

The corresponding stress/strain curves have been fitted through

$$\begin{aligned} T_{xx} &= C_{11}^{eff}\epsilon_{xx} + C_{111}^{eff}\epsilon_{xx}^2 && (7.26)\\ T_{yy} &= C_{12}^{eff}\epsilon_{xx} + C_{112}^{eff}\epsilon_{xx}^2 && (7.27) \end{aligned}$$

- Uniaxial elongations in the y direction:

$$\hat{\epsilon} = \begin{pmatrix} 0 & 0 \\ 0 & \varepsilon_{yy} \end{pmatrix} \tag{7.28}$$

The corresponding stress/strain curves have been fitted through

$$\begin{aligned} T_{xx} &= C_{12}^{eff}\epsilon_{yy} + C_{112}^{eff}\epsilon_{yy}^2 && (7.29)\\ T_{yy} &= C_{22}^{eff}\epsilon_{yy} + C_{222}^{eff}\epsilon_{yy}^2 \end{aligned}$$

Table 6: Linear and nonlinear stiffness tensor components describing the effective elastic behavior of an atom-resolved dispersion of inclusions. The data are obtained by fitting the stress/strain curves in Eqs.(7.26), (7.29) and (7.31) for a sample composed by 100 inclusions corresponding to a volume fraction $v = 0.05$

$\mathcal{C}^{eff}_{11}$	$\mathcal{C}^{eff}_{22}$	$\mathcal{C}^{eff}_{12}$	$\mathcal{C}^{eff}_{44}$	$\mathcal{C}^{eff}_{111}$	$\mathcal{C}^{eff}_{222}$	$\mathcal{C}^{eff}_{112}$
0.2147	0.2148	0.07162	0.07156	0.0118	0.0123	0.00128

- Shear deformations:

$$\hat{\epsilon} = \begin{pmatrix} 0 & \epsilon_{xy} \\ \epsilon_{xy} & 0 \end{pmatrix} \tag{7.30}$$

The corresponding stress/strain curve has been fitted through

$$T_{xy} = \mathcal{C}^{eff}_{44}\epsilon_{xy} \tag{7.31}$$

Testing of the isotropy of the dispersion model

We note that we have considered a possible linear anisotropy by introducing the components $\mathcal{C}^{eff}_{22} \neq \mathcal{C}^{eff}_{11}$ in Eq.(7.29). In fact, by means of the set of deformations in Eqs.(7.26), (7.29) and (7.31), we have also verified if the size of the sample is statistically meaningful. This correspond to check if the population of inclusions is large enough to consider the overall system as a random structure. In such a case, the effective elastic response must exhibit an isotropy behavior and, therefore, the conditions

$$\mathcal{C}^{eff}_{11} = \mathcal{C}^{eff}_{22} \tag{7.32}$$
$$2\mathcal{C}^{eff}_{44} = \mathcal{C}^{eff}_{11} - \mathcal{C}^{eff}_{12} \tag{7.33}$$
$$\mathcal{C}^{eff}_{111} = \mathcal{C}^{eff}_{222} \tag{7.34}$$

must hold. In Table 6, we report the results of the above fitting procedure for a sample with 100 inclusion of radius $R = 10\text{Å}$ corresponding to a volume fraction $v = 0.05$. We can verify that this number of inclusions is large enough to obtain the isotropy with an error within 1%. In fact, we obtain

$$\left(\mathcal{C}^{eff}_{22} - \mathcal{C}^{eff}_{11}\right) / \frac{\mathcal{C}^{eff}_{22} + \mathcal{C}^{eff}_{11}}{2} = 0.0004$$

Moreover, we get from the shear deformation $2\mathcal{C}^{eff}_{44} = 0.14313$ while the Cauchy relation in Eq.(7.33) supplies us $2\mathcal{C}^{eff}_{44} = \mathcal{C}^{eff}_{11} - \mathcal{C}^{eff}_{12} = 0.14314$. As for the nonlinear isotropy we find

$$\left(\mathcal{C}^{eff}_{222} - \mathcal{C}^{eff}_{111}\right) / \frac{\mathcal{C}^{eff}_{222} + \mathcal{C}^{eff}_{111}}{2} = 0.01$$

In Fig.57 we report the stress/strain curves corresponding to the uniaxial elongations along the x and y directions. We easily verify the isotropic behavior by observing that the differences between the longitudinal responses $T_{xx}(\epsilon_{xx})$ and $T_{yy}(\epsilon_{yy})$ and between the transversal responses $T_{xx}(\epsilon_{yy})$ and $T_{yy}(\epsilon_{xx})$ are not detectable. The obtained isotropic behavior of the samples allows us to describe their effective

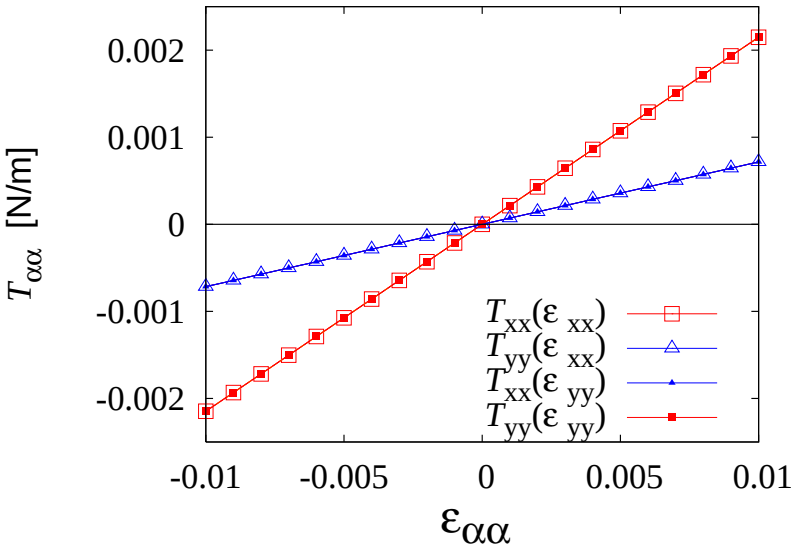

Figure 57: Stress/strain curves for a disperison containing 100 inclusions of radius $R = 10$ Å with a volume fraction $v = 0.05$. The empty symbols correspond to a uniaxial elongation in the x direction ($T_{xx}(\epsilon_{xx})$ and $T_{yy}(\epsilon_{xx})$) while the full symbols correspond to a uniaxial elongation in the y direction ($T_{xx}(\epsilon_{yy})$ and $T_{yy}(\epsilon_{yy})$). The system exhibits an isotropic behavior: both longitudinal (square symbols) and transversal (triangular symbols) responses in the two directions are not distinguishable.

elasticity by means of a strain energy relation similar to that in Eq.(7.2), namely

$$U(\hat{e}) = \frac{K^{eff} - \mu^{eff}}{2} Tr(\hat{e})^2 + \mu\, Tr(\hat{e}^2) + \mathbf{b^{eff}}\, Tr(\hat{e}) Tr(\hat{e}^2) + \frac{\mathbf{c^{eff}}}{3} Tr(\hat{e})^3 \tag{7.35}$$

Effective elastic moduli

where only two linear (K^{eff} and μ^{eff}) and two nonlinear ($\mathbf{b^{eff}}$ and $\mathbf{c^{eff}}$) independent elastic moduli are involved. These can be obtained from the stiffness components $\mathcal{C}^{eff}_{11}$, $\mathcal{C}^{eff}_{12}$, $\mathcal{C}^{eff}_{111}$, and $\mathcal{C}^{eff}_{112}$ by means of Eqs. (7.3), (7.4) and (7.5) (considering also that $\lambda^{eff} = K^{eff} - \mu^{eff}$).

7.2.2 *Atomistic versus continuum results*

In Section 3.3 we have derived the continuum theory prediction for the elastic behavior of a dispersion of parallel cylinders under plane strain conditions (Eqs. (3.68)-(3.73)). In particular, we have reported the effective nonlinear Landau moduli A^{eff}, B^{eff}, C^{eff}, and D^{eff} describing the Cauchy elasticity (see Section 2.3.1) in three-dimensions. From such a solution we can easily obtain the predictions for the present situation, where the nonlinear behavior is represented by $\mathbf{b^{eff}}$ and $\mathbf{c^{eff}}$. In fact, we can consider that if a strain energy function is present (Green elasticity developed in Section 2.3.1) the relation $D^{eff} = 2B^{eff}$

is satisfied. Moreover, the definitions of the two-dimensional coefficients $\mathbf{b^{eff}}$ and $\mathbf{c^{eff}}$ imply the following relations

$$\mathbf{b^{eff}} = B^{eff} + \frac{A^{eff}}{2} \qquad \mathbf{c^{eff}} = C^{eff} - \frac{A^{eff}}{2} \tag{7.36}$$

which furthermore reduce the number of the independent moduli. In this Section we compare the continuum predictions with the corresponding data obtained by means of the above discussed atomistic model. As for the linear moduli K^{eff} and μ^{eff} we also report the Hashin-Shtrikman variational bounds [99, 100]

The Hashin-Shtrikman variational bounds

$$F(K_1, K_2, 1-v, v, \mu_{min}) < K^{eff} < F(K_1, K_2, 1-v, v, \mu_{max}) \tag{7.37}$$

$$F(\mu_1, \mu_2, 1-v, v, \mu_{min}) < \mu^{eff} < F(\mu_1, \mu_2, 1-v, v, \mu_{max}) \tag{7.38}$$

where (K_1, μ_1) and (K_2, μ_2) are the elastic moduli of the matrix and of the inclusions, respectively, and μ_{max} (μ_{min}) is the largest (smallest) shear modulus between μ_1 and μ_2. Moreover

$$F(a_1, a_2, v_1, v_2, a) = v_1 a_1 + v_2 a_2 - \frac{v_1 v_2 (a_1 - a_2)^2}{v_2 a_1 + v_1 a_2 + a}$$

We also note that if v is the volume fraction of the inclusions then $1 - v$ is the volume fraction of the matrix.

Case 1: The inclusions are stiffer than the matrix (negative contrast)

The first considered case deals with a dispersion of circular inclusions twice stiffer than the surrounding matrix. In Fig. 58, we report the atomistic data and the continuum predictions for the effective shear and bulk moduli. We also plot the Hashin-Shtrikman bounds computed by means of Eqs. (7.37) and (7.38). The atomistic data are obtained from a sample where the radius of the inclusions is $R = 10$ Å. By comparing the results in Fig. 48, we can note that such a value is in a range where possible scale-effects are pronounced. In any case, we can observe that both the effective elastic properties (bulk and shear moduli) of the atomistic model are in good agreement with the continuum predictions. If a vary small discrepancy is present, it does not induce any violation of the Hashin-Shtrikman bounds. This is consistent with the conclusions obtained in Section 7.1: we didn't found any scale-effect if the inclusions are stiffer than the matrix. The same considerations hold for the effective nonlinear elastic properties reported in Fig. 59.

The continuum predictions are well verified also for large values of the volume fraction

On the other hand, by comparing the reported data, we note another (unexpected) result. As discussed in Chapter 3, the homogenization method supplies us the solution under the hypothesis of dilute dispersion. Therefore, we expect to see a validity breakdown of the continuum formulas for large values of the volume fraction, i.e. out of the range of their derivation. Interesting enough, the atomistic data prove that also for the very high value $v = 0.5$ the continuum predictions are well verified.

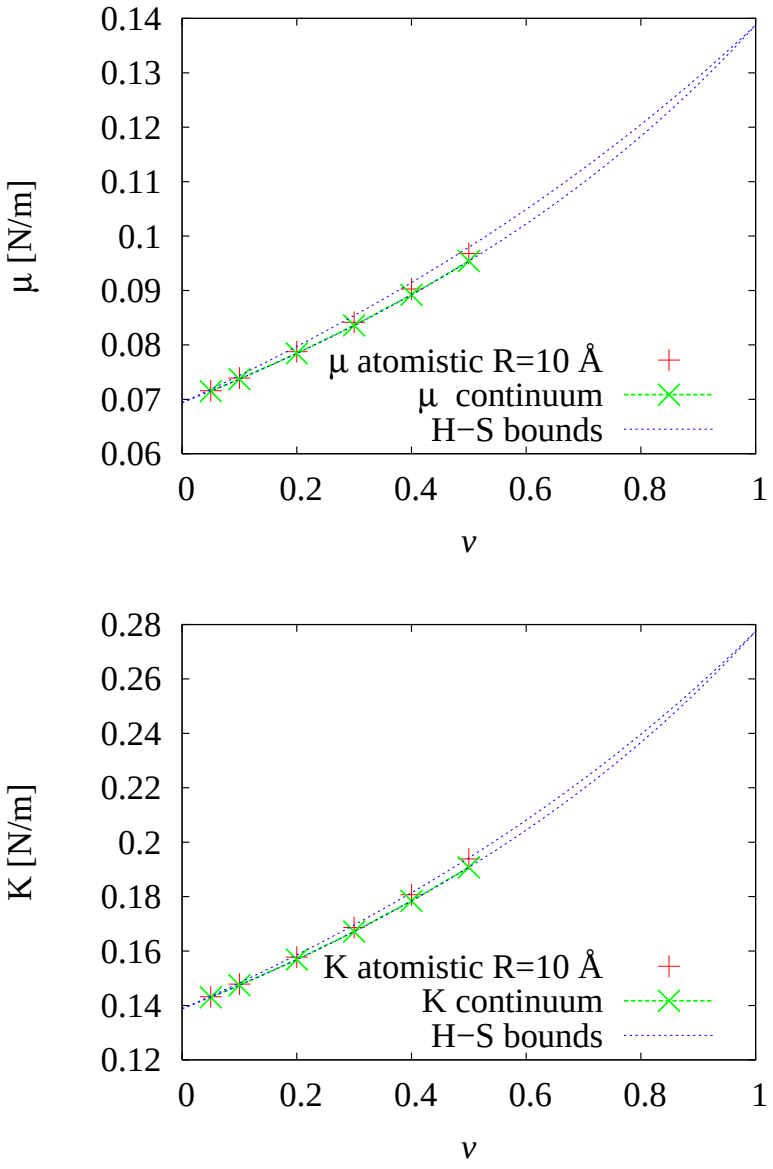

Figure 58: Effective shear (top) and bulk (bottom) moduli of a dispersion of circular inclusions of radius R = 10Å. The results correspond to the case of negative elastic contrast, i.e. the inclusions are stiffer than the matrix (Case 1). We report the atomistic data (pluses) and the corresponding continuum results (crosses) as functions of the volume fraction. The dashed lines represent the Hashin-Shtrikman bounds.

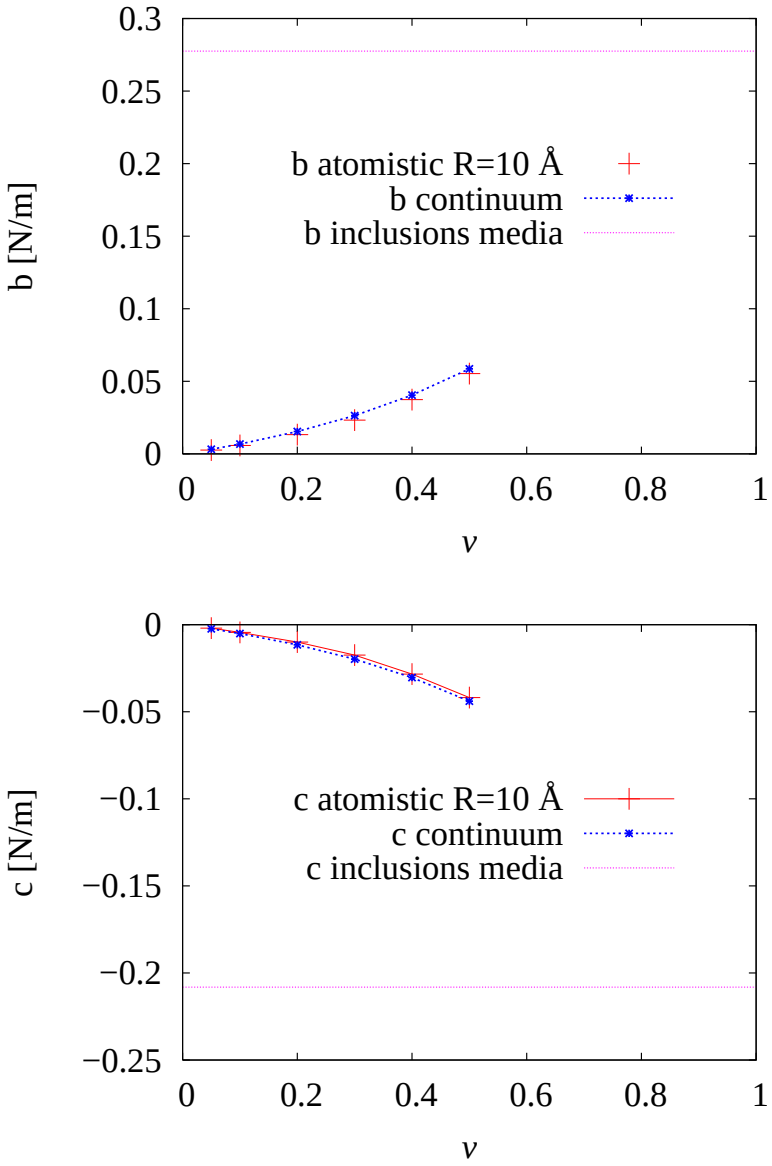

Figure 59: Effective nonlinear elastic properties ($\mathbf{b}^{\mathbf{eff}}$ in the top panel and $\mathbf{c}^{\mathbf{eff}}$ in the bottom panel) of a dispersion of circular inclusions of radius R = 10Å. The results correspond to the case of negative elastic contrast, i.e. the inclusions are stiffer than the matrix (Case 1). We report the atomistic data (pluses) and the corresponding continuum results (crosses) as functions of the volume fraction v. The dashed lines represent the elastic moduli of the medium in the inclusions. In the limit $v \to 1$ the effective moduli of the dispersion approach those of the inclusions.

Case 2: The inclusions are softer than the matrix (positive contrast)

In this second case, we consider a dispersion of inclusions twice softer than the surrounding matrix. In Fig. 60, the effective linear elastic properties are reported for $R = 20$ Å. In this case, we have verified that the samples with $R = 10$ Å exhibit an effective elastic behavior out of the range predicted by the Hashin-Shtrikman bounds. In order to find atomistic data consistent with such limitations we have to consider a larger radius of the inclusions. A similar effect is evident in the data reported in Fig.61 as well. The discrepancy between atomistic data and the corresponding continuum prediction is remarkable and decreases when R increases. Again, this is consistent with the conclusions of Section 7.1: positive values of the elastic contrast induce a size-dependence of the elastic behavior.

Scale-effects in the dispersion elasticity if the inclusions are softer than the matrix

In conclusion, we have proved that the size-effect observed in the atomistic simulation of a single inhomogeneity embedded in a stiffer matrix (Section 7.1) induce the onset of similar effects also in the elastic behavior of the dispersion. This result represents an meaningful example of a nano-scale phenomenon that carries out a macroscopic behavior unpredictable through the continuum theory approach. These effects turn out to be rather sizable and, as a consequence, their evaluation could play a crucial role in engineering and properly characterizing the elastic behavior of nanocomposite meterials.

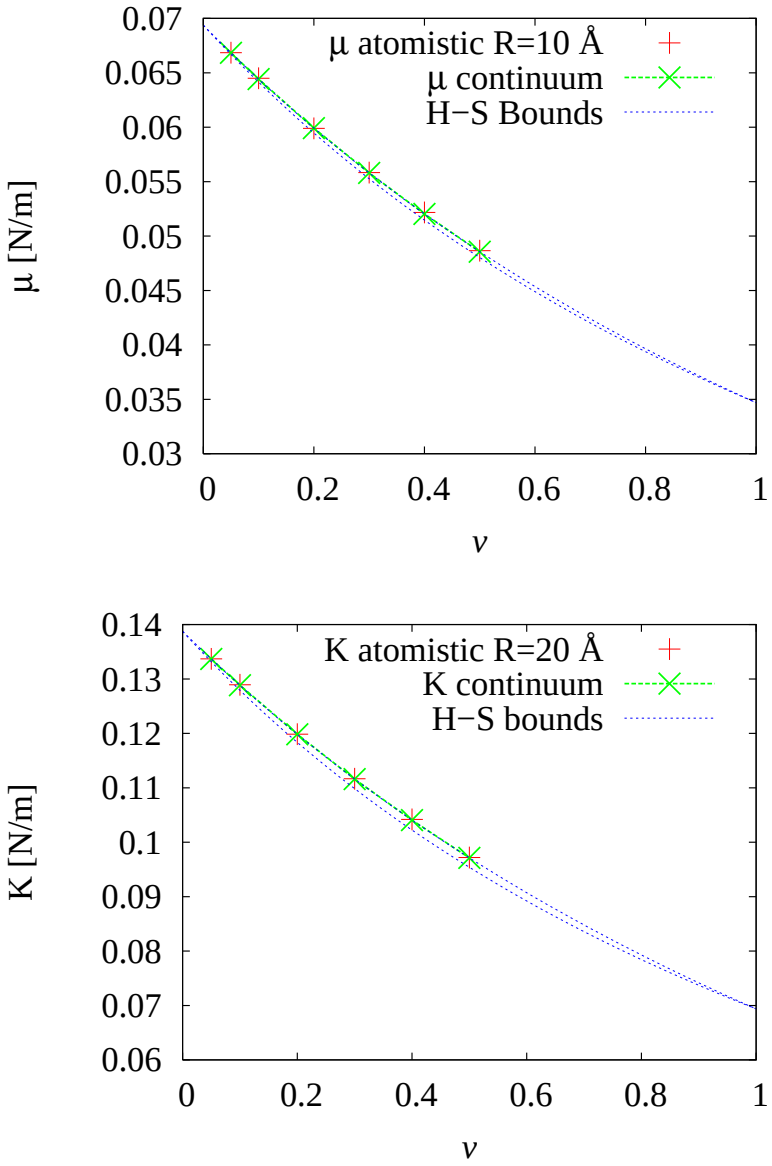

Figure 60: Effective shear (top) and bulk (bottom) moduli of a dispersion of circular inclusions of radius $R = 10$Å. The results correspond to the case of positive elastic contrast, i.e. the inclusions are softer than the matrix (Case 2). We report the atomistic data (pluses) and the corresponding continuum results (crosses) as functions of the volume fraction. The dashed lines represent the Hashin-Shtrikman bounds.

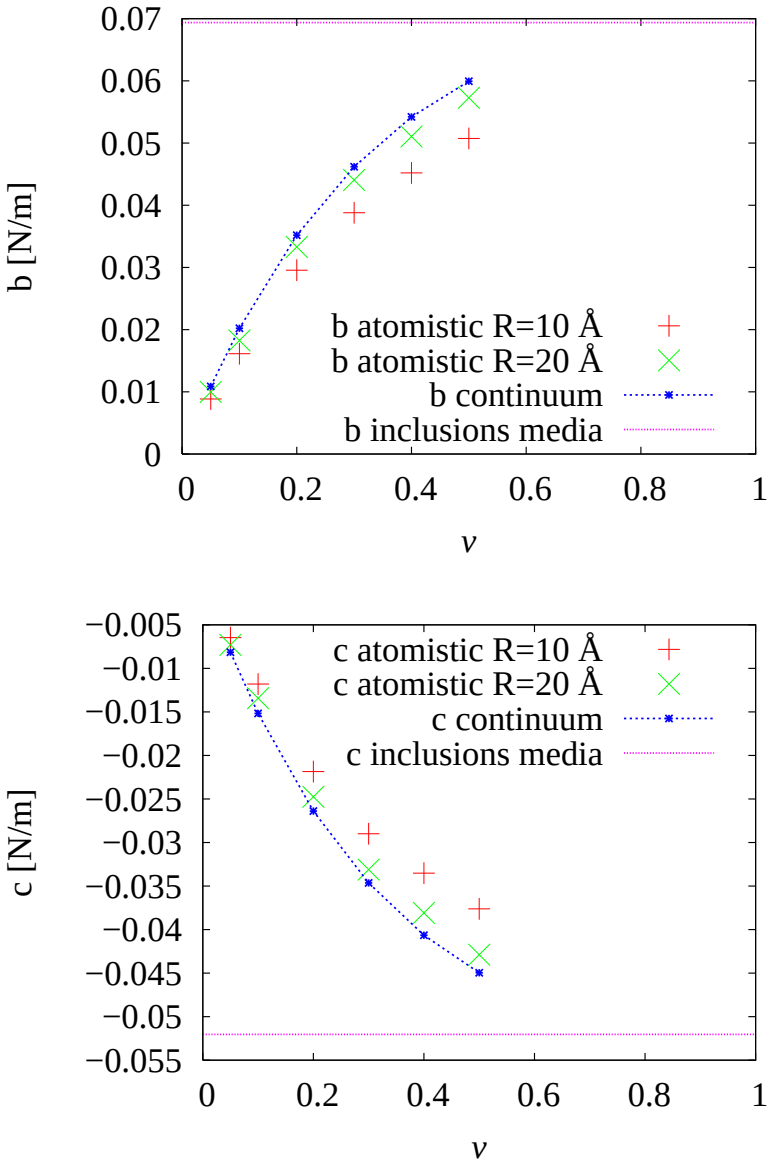

Figure 61: Effective nonlinear elastic properties of a dispersion of circular inclusions of radius R = 10Å: parameter $\mathbf{b}^{\mathbf{eff}}$ in the top panel and paramter $\mathbf{c}^{\mathbf{eff}}$ in the bottom panel . The results correspond to the case of positive elastic contrast, i.e. the inclusions are softer than the matrix (Case 2). We report the atomistic data (pluses) and the corresponding continuum results (crosses) as functions of the volume fraction v. The dashed lines represent the elastic moduli of the medium in the inclusions. In the limit $v \to 1$ the effective moduli of the dispersion approach those of the inclusions.

CONCLUSIONS

In this PhD thesis we have investigated the linear and nonlinear elastic behavior of nanocomposite materials both from the continuum and the atomistic point of view. As for the main advances on the elasticity theory, we have solved (Section 2.2) the problem of the elastic behavior of a prestressed single inclusion. This solution has been obtained as a meaningful generalization of the elegant Eshelby theory. A further generalization of such a theory has taken into account the elastic behavior of a nonlinear inclusion (Section 2.3). In particular, we have proved that the elastic fields inside the inclusion are uniform also if a non Hookean constitutive equation (i.e. nonlinear) is considered [87] (the standard Eshelby theory provides this result only under the linear hypothesis). Successively, we have considered a typical nanocomposite structure, i.e. a dispersion of nonlinear inhomogeneities (spheres or parallel cylinders) embedded into a host matrix with different elastic properties (Chapter 3). The previous result for a single nonlinear inclusion has been analytically applied to perform a linear and nonlinear micromechanical averaging of the elastic fields into the composite structure. Thus, a complete homogenizing procedure is provide, yielding the mechanical behavior of the solid body at the macro-scale in terms of the properties of its constituents [125]. In such a way, we have proved that the nonlinear effective elastic moduli, contrarily to the linear ones, are not subjected to specific bounds which limit their values when the behaviors of the constituents are chosen. We have indeed found some strong amplifications of the nonlinear behavior in certain given conditions. More specifically, we have observed that the nonlinear effective moduli of the heterogeneous structure can assume values much greater than those of the constituents if the matrix is much more incompressible than the inhomogeneities. This is a crucial point that can be applied in analyzing and designing composite materials with a given microstructure. Finally, some special values of the Poisson ratio of the materials have been found in order to obtain a direct correspondence among the nonlinear moduli of the inhomogeneities and the effective moduli of the composite structure. It means that, under the above conditions, we can realize a perfect scaling of the nonlinear properties (see Eq.(3.43) or (3.75)) modulated by the ratio E_1/E_2 between the Young moduli of the constituents.

The elastic fields into a single nonlinear inclusion are uniform

Amplifications of the nonlinear behavior in composite materials

We have also considered a series of atomistic investigations on Si-based nanostructures devoted to the analysis of the interface elasticity at the nanoscale (Chapter 5). We provided a full picture regarding the elastic fields across a planar interface. These results have been applied to a qualitative, as much as quantitative, description of the elastic behavior of the atomistic model of a flat interface between c-Si and a-Si [174]. Moreover, we have described several atomistic simulations performed to investigate the elastic behavior of a c-Si inclusion embedded in a differently oriented c-Si matrix [86]. In particular, we have described the effects of the presence of a prestrain, which is experimentally observed in many real cases [180]. In addition, we have analyzed the elastic strain field in the system both with and without a remotely applied external loading. We have proved that the above generalization of the

Elasticity of a planar a-Si/c-Si interface

standard Eshelby theory (with a simple hydrostatic prestrain inside the inclusion) is sufficient to correctly describe the overall elastic behavior of the embedded structure. In this work we have focused on a circular shape of the inclusion: of course, both the analytical model and the computational procedure can be generalized in order to take into account an elliptic shape with arbitrary aspect ratio. Moreover, it is important to remark that our results have been obtained for the crystalline silicon, but they can be transferred to other covalently bonded materials as well and, more generally, to brittle and ceramic systems. As for the applications, we underline that this investigation can be directly used to analyze the generation of prestrain during the embedding or the self-assembling of nanoparticles, such as quantum dots and quantum wires, in a matrix with different structure and physical properties. In particular, we have introduced and discussed the phenomenon of the localization of the elastic fields in the neighborhood of the inclusion, modulated by the actual prestrain.

Prestress-induced localization of the effect of inhomogeneities on the elastic fields

In the third Part of the thesis, we have developed a procedure for the analysis and the synthesis of an atomistic model of materials with a given linear and nonlinear macroscopic elastic properties (Chapter 6). The procedure is based on a constitutive force field with a given set of parameters directly related (linearly) to the second order and the third order elastic constants of the overall structure. The synthesis of a model with a desired linear and nonlinear elastic response is very simple and it allows to create both softening and stiffening behaviors, very useful for many practical applications. In particular, we have described the implementation of the force field on a two-dimensional lattice: the generalization to some three-dimensional ones (e.g. cubic or thetraedral) can be made straightforwardly. The development of the force field has been based on the understanding of the role of the atomistic interaction model in predicting the macroscopic elastic features [132]. From the linear point of view we have verified that two-body force fields provide an elastic picture that is not consistent with continuum mechanics, because they describe the linear elastic behavior of the material with only one elastic modulus (i.e. fixed Poisson ratio). On the contrary, force fields including both two-body and three-body interactions provide results in formal agreement with continuum elasticity theory, i.e., they predict the existence of two independent linear elastic constants. Moreover, from the nonlinear point of view, we proved that an *ad hoc* combination of anharmonic terms and angular springs allows the setting of all the third order elastic constants.

A novel constitutive force field for nonlinear elasticity of complex materials

We have utilized the constitutive force field to investigate the elastic behavior of the Eshelby configuration with different properties of the matrix and the inclusion (Section 7.1). The case of a fully linear matrix with a nonlinear inclusion can be handled through continuum mechanics, with a specific mathematical procedure discussed in the text. In fact, we have utilized this first case to check the validity of our atomistic model and to analyze the scale effects induced by the discretization of the matter (i.e. by the actual disposition of the atoms within the bodies). In particular, we have found a deviation from the continuum theory results for inclusions with radius smaller than about 10 nm; we have also verified the emergence of some power laws and their universality (with a scaling exponent equal to about 1.1), driving the scale effects in the range from 5 Å to 60 Å. The more complex case deals with a nonlinear matrix: it is now very difficult to find exact results by means of the

Characterization of atomistic size-effects in the elastic behavior of nano-inclusions: power laws and scaling exponents

The constitutive force field beyond the Eshelby theory results

elasticity theory and, therefore, the atomistic simulations becomes the most important tool to analyze the elastic behavior of the system. We have therefore investigated the elastic response of the inclusion (both elastically linear and nonlinear) for different kinds of nonlinearities describing the elasticity of the matrix.

Size-effects in nanocomposites elasticity

Finally, the constitutive force field approach has been applied to the effective elastic behavior of a dispersion of nonlinear inhomogeneities (Section 7.2). We have verified the onset of the same size-effects induced by the atomic structure in a single nano-inclusion. Consistently with such results, the size-dependence is present, at the nanoscale, when the inclusions are softer than the hosting matrix. On the other hand, when the inclusion is stiffer than the matrix, the continuum-based results on the composite nonlinear elasticity exhibit a surprising capability in predicting the effective properties of the complex medium also for high concentration of the inclusions, i.e. also far from the hypothesis of dilute dispersion involved in the theory.

The homogeneization procedure provides meaningful results also for the elasticity of a non dilute dispersion

Part IV

APPENDIX

A

ANALYTICAL DEVELOPMENTS

A.1 ANALYTICAL EXPRESSIONS OF THE ESHELBY TENSOR

We report, for the sake of completeness, the analytical expressions of the Eshelby tensor for different geometries of the inclusion.

Ellipsoid

Let start with an ellipsoidal shape with the three principal axes of lengths $a_1 > a_2 > a_3 > 0$. The reference frame is fixed do that the axes $x_1 = x$, $x_2 = y$, $x_3 = z$ are aligned with the ellipsoidal axes. We introduce also the so-called aspect ratios e and g, defining the shape of the ellipsoid, so that $0 < e = a_3/a_2 < 1$ e $0 < g = a_2/a_1 < 1$. We firstly report the depolarization factors [70]

$$I_3 = \frac{4\pi}{1-e^2} - \frac{4\pi e}{(1-e^2)\sqrt{1-e^2g^2}}\mathcal{E}(\nu, q) \tag{A.1}$$

$$I_2 = \frac{4\pi e\left(1-e^2g^2\right)}{(1-e^2)(1-g^2)\sqrt{1-e^2g^2}}\mathcal{E}(\nu, q) - \frac{4\pi eg^2}{(1-g^2)\sqrt{1-e^2g^2}}\mathcal{F}(\nu, q) - \frac{4\pi e^2}{1-e^2} \tag{A.2}$$

$$I_1 = \frac{4\pi eg^2}{(1-g^2)\sqrt{1-e^2g^2}}\left[\mathcal{F}(\nu, q) - \mathcal{E}(\nu, q)\right] \tag{A.3}$$

where

$$\nu = \arcsin\sqrt{1-e^2g^2} \tag{A.4}$$

$$q = \sqrt{\frac{1-g^2}{1-e^2g^2}} \tag{A.5}$$

while, the incomplete elliptical integrals of first and second kind are defined as [203, 204]

$$\mathcal{F}(\nu, q) = \int_0^{\nu} \frac{d\alpha}{\sqrt{1-q^2\sin^2\alpha}} = \int_0^{\sin\nu} \frac{dx}{\sqrt{(1-x^2)(1-q^2x^2)}} \tag{A.6}$$

$$\mathcal{E}(\nu, q) = \int_0^{\nu} \sqrt{1-q^2\sin^2\alpha}\,d\alpha = \int_0^{\sin\nu} \frac{\sqrt{1-q^2x^2}}{\sqrt{1-x^2}}dx \tag{A.7}$$

Moreover, we introduce the following parameters

$$
\begin{aligned}
I_{12} &= \frac{I_2 - I_1}{1 - g^2} \\
I_{13} &= \frac{I_3 - I_1}{1 - e^2 g^2} \\
I_{23} &= \frac{I_3 - I_2}{g^2 \left(1 - e^2\right)} \\
I_{11} &= \frac{1}{3} \frac{I_1 \left(e^2 g^4 - 2e^2 g^2 - 2g^2 + 3\right) + I_2 g^2 \left(e^2 g^2 - 1\right) + I_3 e^2 g^2 \left(g^2 - 1\right)}{\left(1 - g^2\right)\left(1 - e^2 g^2\right)} \\
I_{22} &= \frac{1}{3} \frac{I_1 \left(1 - e^2\right) + I_2 \left(2e^2 g^2 - 3g^2 + 2 - e^2\right) + I_3 e^2 \left(g^2 - 1\right)}{g^2 \left(1 - e^2\right)\left(1 - g^2\right)} \\
I_{33} &= \frac{1}{3} \frac{I_1 \left(1 - e^2\right) + I_2 \left(1 - e^2 g^2\right) + I_3 \left(1 - 2e^2 g^2 + 3e^4 g^2 - 2e^2\right)}{e^2 g^2 \left(1 - e^2\right)\left(1 - e^2 g^2\right)}
\end{aligned}
\tag{A.8}
$$

The Eshelby tensor, within the Voigt notation, can be expressed in the form

$$
\tilde{S} = \begin{bmatrix} M & 0 \\ 0 & N \end{bmatrix} \tag{A.9}
$$

The matrix M and O can be obtained by means of

$$
M = \begin{bmatrix}
\frac{3I_{11} + (1-2\nu) I_1}{8\pi(1-\nu)} & \frac{g^2 I_{12} - (1-2\nu) I_1}{8\pi(1-\nu)} & \frac{e^2 g^2 I_{13} - (1-2\nu) I_1}{8\pi(1-\nu)} \\
\frac{I_{12} - (1-2\nu) I_2}{8\pi(1-\nu)} & \frac{3g^2 I_{22} + (1-2\nu) I_2}{8\pi(1-\nu)} & \frac{e^2 g^2 I_{23} - (1-2\nu) I_2}{8\pi(1-\nu)} \\
\frac{I_{13} - (1-2\nu) I_3}{8\pi(1-\nu)} & \frac{g^2 I_{23} - (1-2\nu) I_3}{8\pi(1-\nu)} & \frac{3e^2 g^2 I_{33} + (1-2\nu) I_3}{8\pi(1-\nu)}
\end{bmatrix}
\tag{A.10}
$$

$$
N = \begin{bmatrix} N_{11} & 0 & 0 \\ 0 & N_{22} & 0 \\ 0 & 0 & N_{33} \end{bmatrix} \tag{A.11}
$$

where

$$
\begin{aligned}
N_{11} &= \frac{\left(1 + g^2\right) I_{12} + (1 - 2\nu)\left(I_1 + I_2\right)}{8\pi\left(1 - \nu\right)} \\
N_{22} &= \frac{g^2 \left(1 + e^2\right) I_{23} + (1 - 2\nu)\left(I_2 + I_3\right)}{8\pi\left(1 - \nu\right)} \\
N_{33} &= \frac{\left(1 + e^2 g^2\right) I_{13} + (1 - 2\nu)\left(I_1 + I_3\right)}{8\pi\left(1 - \nu\right)}
\end{aligned}
\tag{A.12}
$$

In the following, the expressions of the Eshelby tensors for the limiting cases of sphere, cylinders, flat elliptic inclusion, and for oblate and prolate spheroids are reported.

Sphere

$$\tilde{S} = \begin{bmatrix} \frac{1}{15}\frac{7-5\nu}{1-\nu} & \frac{1}{15}\frac{5\nu-1}{1-\nu} & \frac{1}{15}\frac{5\nu-1}{1-\nu} & 0 & 0 & 0 \\ \frac{1}{15}\frac{5\nu-1}{1-\nu} & \frac{1}{15}\frac{7-5\nu}{1-\nu} & \frac{1}{15}\frac{5\nu-1}{1-\nu} & 0 & 0 & 0 \\ \frac{1}{15}\frac{5\nu-1}{1-\nu} & \frac{1}{15}\frac{5\nu-1}{1-\nu} & \frac{1}{15}\frac{7-5\nu}{1-\nu} & 0 & 0 & 0 \\ 0 & 0 & 0 & \frac{2}{15}\frac{4-5\nu}{1-\nu} & 0 & 0 \\ 0 & 0 & 0 & 0 & \frac{2}{15}\frac{4-5\nu}{1-\nu} & 0 \\ 0 & 0 & 0 & 0 & 0 & \frac{2}{15}\frac{4-5\nu}{1-\nu} \end{bmatrix} \tag{A.13}$$

Cylinder

If the axis of the cylinder is aligned with $x_1 = x$, we find

$$\tilde{S} = \begin{bmatrix} 0 & 0 & 0 & 0 & 0 & 0 \\ \frac{1}{2}\frac{\nu}{1-\nu} & \frac{1}{8}\frac{5-4\nu}{1-\nu} & \frac{1}{8}\frac{4\nu-1}{1-\nu} & 0 & 0 & 0 \\ \frac{1}{2}\frac{\nu}{1-\nu} & \frac{1}{8}\frac{4\nu-1}{1-\nu} & \frac{1}{8}\frac{5-4\nu}{1-\nu} & 0 & 0 & 0 \\ 0 & 0 & 0 & \frac{1}{2} & 0 & 0 \\ 0 & 0 & 0 & 0 & \frac{1}{4}\frac{3-4\nu}{1-\nu} & 0 \\ 0 & 0 & 0 & 0 & 0 & \frac{1}{2} \end{bmatrix} \tag{A.14}$$

Elliptical cylinder

If the cylinder is aligned along the $x_1 = x$ axis and being e the aspect ratio of the base ellipse, we find, in the notation of Eq. (A.9) the following expressions for M ed N

$$M = \begin{bmatrix} 0 & 0 & 0 \\ \frac{e\nu}{(1+e)(1-\nu)} & \frac{1}{2(1-\nu)}\left[\frac{e^2+2e}{(1+e)^2} + \frac{e(1-2\nu)}{(1+e)}\right] & \frac{1}{2(1-\nu)}\left[\frac{e^2}{(1+e)^2} - \frac{e(1-2\nu)}{(1+e)}\right] \\ \frac{\nu}{(1+e)(1-\nu)} & \frac{1}{2(1-\nu)}\left[\frac{1}{(1+e)^2} - \frac{(1-2\nu)}{(1+e)}\right] & \frac{1}{2(1-\nu)}\left[\frac{1+2e}{(1+e)^2} + \frac{(1-2\nu)}{(1+e)}\right] \end{bmatrix} \tag{A.15}$$

$$N = \begin{bmatrix} \frac{e}{1+e} & 0 & 0 \\ 0 & \frac{1}{2(1-\nu)}\left[\frac{1+e^2}{(1+e)^2} + 1 - 2\nu\right] & 0 \\ 0 & 0 & \frac{1}{1+e} \end{bmatrix} \tag{A.16}$$

Elliptical flat (or penny-shaped) inclusion

If the ellipse is arranged on the (x_1, x_2) , we get

$$\tilde{S} = \begin{bmatrix} 0 & 0 & 0 & 0 & 0 & 0 \\ 0 & 0 & 0 & 0 & 0 & 0 \\ \frac{\nu}{1-\nu} & \frac{\nu}{1-\nu} & 1 & 0 & 0 & 0 \\ 0 & 0 & 0 & 0 & 0 & 0 \\ 0 & 0 & 0 & 0 & 1 & 0 \\ 0 & 0 & 0 & 0 & 0 & 1 \end{bmatrix} \tag{A.17}$$

Rotational ellipsoids

Assuming $x_3 = z$ as the rotation axis, we can express the Eshelby tensor in the following simplified form

$$\tilde{\mathcal{S}} = \begin{bmatrix} \mathcal{S}_{1111} & \mathcal{S}_{1122} & \mathcal{S}_{1133} & 0 & 0 & 0 \\ \mathcal{S}_{1122} & \mathcal{S}_{1111} & \mathcal{S}_{1133} & 0 & 0 & 0 \\ \mathcal{S}_{3311} & \mathcal{S}_{3311} & \mathcal{S}_{3333} & 0 & 0 & 0 \\ 0 & 0 & 0 & \mathcal{S}_{1111} - \mathcal{S}_{1122} & 0 & 0 \\ 0 & 0 & 0 & 0 & 2\mathcal{S}_{1313} & 0 \\ 0 & 0 & 0 & 0 & 0 & 2\mathcal{S}_{1313} \end{bmatrix} \tag{A.18}$$

The elements of this a tensor can be calculated by means of the depolarization factor

$$\mathcal{L} = \frac{e}{2} \int_0^{+\infty} \frac{d\xi}{(\xi+1)^2 \left(\xi+e^2\right)^{1/2}} \tag{A.19}$$

$$= \begin{cases} \frac{e}{4\left(\sqrt{e^2-1}\right)^3} \left[2e\sqrt{e^2-1} + \ln \frac{e-\sqrt{e^2-1}}{e+\sqrt{e^2-1}}\right] & \text{if} \quad e > 1 \\ \frac{e}{4\left(\sqrt{1-e^2}\right)^3} \left[\pi - 2e\sqrt{1-e^2} - 2\arctan \frac{e}{\sqrt{1-e^2}}\right] & \text{if} \quad e < 1 \end{cases}$$

The cases $e < 1$ and $e > 1$ correspond to the *oblate* ellipsoids (minor axis aligned along the rotation direction) and to the *prolate* ellipsoids (major axis aligned along the rotation direction), respectively. Finally, the components of $\hat{\mathcal{S}}$ are

$$\mathcal{S}_{1111} = \frac{1}{8} \frac{13\mathcal{L} - 3e^2 - 4e^2\mathcal{L} + 8\mathcal{L}\nu e^2 - 8\mathcal{L}\nu}{\left(1-e^2\right)(1-\nu)} \tag{A.20}$$

$$\mathcal{S}_{1122} = -\frac{1}{8} \frac{e^2 + \mathcal{L} - 4e^2\mathcal{L} + 8\mathcal{L}\nu e^2 - 8\mathcal{L}\nu}{\left(1-e^2\right)(1-\nu)} \tag{A.21}$$

$$\mathcal{S}_{1133} = -\frac{1}{2} \frac{2e^2\mathcal{L} - e^2 + \mathcal{L} + 2\mathcal{L}\nu e^2 - 2\mathcal{L}\nu}{\left(1-e^2\right)(1-\nu)} \tag{A.22}$$

$$\mathcal{S}_{3311} = \frac{1}{2} \frac{e^2 - \mathcal{L} - 2e^2\mathcal{L} - 2\nu e^2 + 2\nu + 4\mathcal{L}\nu e^2 - 4\mathcal{L}\nu}{\left(1-e^2\right)(1-\nu)} \tag{A.23}$$

$$\mathcal{S}_{3333} = \frac{1 - 2e^2 + 4e^2\mathcal{L} - \mathcal{L} + \nu e^2 - \nu - 2\mathcal{L}\nu e^2 + 2\mathcal{L}\nu}{\left(1-e^2\right)(1-\nu)} \tag{A.24}$$

$$\mathcal{S}_{1313} = -\frac{1}{4} \frac{e^2\mathcal{L} + 2\mathcal{L} - 1 + \mathcal{L}\nu e^2 - \mathcal{L}\nu - \nu e^2 + \nu}{\left(1-e^2\right)(1-\nu)} \tag{A.25}$$

A.2 SYMMETRY AND POSITIVE DEFINITENESS OF $\hat{\mathbf{q}}$

Here we derive the symmetry and positive definiteness of the tensor $\hat{\mathbf{q}} = \hat{\mathbb{C}}^{(1)} \left[\hat{\mathcal{S}}^{-1} - \hat{\mathbb{I}}\right]$ involved in Eq.2.91 concluding the proof of the existence and uniqueness of the nonlinear Eshelby solution in Eq.(2.89) (see Section 2.3.2). We briefly outline the concepts of inclusion and linear inhomogeneity in order to present the adopted notation and to recall the most important equations of the Eshelby theory [45, 8, 49].

Concept of inclusion. We suppose to consider an infinite medium with stiffness tensor $\hat{\mathbb{C}}^{(1)}$; moreover, we consider an embedded ellipsoidal inclusion V described by the constitutive equation $\hat{\mathbf{T}} = \hat{\mathbb{C}}^{(1)} \left(\hat{\boldsymbol{\varepsilon}} - \hat{\boldsymbol{\varepsilon}}^*\right)$.

The strain $\hat{\epsilon}^*$ is called eigenstrain (or stress-free strain). In these conditions the following relations describe the strain inside and outside the inclusion [45]

$$\hat{\epsilon}(\vec{x}) = \begin{cases} \hat{S}\hat{\epsilon}^* & \text{if } \vec{x} \in V \\ \hat{S}^\infty(\vec{x})\,\hat{\epsilon}^* & \text{if } \vec{x} \notin V \end{cases} \tag{A.26}$$

where $\hat{S}$ is the internal Eshelby tensor and $\hat{S}^\infty$ is the external Eshelby tensor.

Concept of inhomogeneity. We suppose now to consider an infinite medium with stiffness tensor $\hat{C}^{(1)}$ in $\mathfrak{R}^3 \setminus V$ (matrix) and $\hat{C}^{(2)}$ in the ellipsoidal region V (inhomogeneity). We remotely load the system with a uniform strain $\hat{\epsilon}^\infty$ or, equivalently, with the uniform stress $\hat{T}^\infty$. Of course we have $\hat{T}^\infty = \hat{C}^{(1)}\hat{\epsilon}^\infty$. This configuration can be analyzed by means of the Eshelby equivalence principle [8]. The system can be described by the superimposition of two simpler cases (see Fig.5) [45]. The first situation A concerns a medium with stiffness $\hat{C}^{(1)}$ (without inclusions or inhomogeneities) uniformly deformed by means of the remote loads $\hat{\epsilon}^\infty$ or T^∞. The second situation B is represented by an inclusion embedded in a medium, characterized everywhere by $\hat{C}^{(1)}$ and having an eigenstrain $\hat{\epsilon}^*$ in V. The situation B is without remote loads. The eigenstrain must be imposed searching for the equivalence between the original inhomogeneity problem and the superimposition $A + B$. The following relation hold on inside the region V (s means inside V)

$$\begin{aligned} \hat{\epsilon}^s &= \hat{\epsilon}^{A,s} + \hat{\epsilon}^{B,s} = \hat{\epsilon}^\infty + \hat{S}\hat{\epsilon}^* \\ \hat{T}^s &= \hat{T}^{A,s} + \hat{T}^{B,s} = \hat{C}^{(1)}\hat{\epsilon}^\infty + \hat{C}^{(1)}\left(\hat{\epsilon}^{B,s} - \hat{\epsilon}^*\right) \\ &= \hat{C}^{(1)}\hat{\epsilon}^\infty + \hat{C}^{(1)}\left(\hat{S}\hat{\epsilon}^* - \hat{\epsilon}^*\right) \end{aligned} \tag{A.27}$$

In the inhomogeneity we have $\hat{T}^s = \hat{C}^{(2)}\hat{\epsilon}^s$ and therefore

$$\underbrace{\hat{C}^{(1)}\hat{\epsilon}^\infty + \hat{C}^{(1)}\left(\hat{S}\hat{\epsilon}^* - \hat{\epsilon}^*\right)}_{T^s} = \hat{C}^{(2)}\underbrace{\left(\hat{\epsilon}^\infty + \hat{S}\hat{\epsilon}^*\right)}_{\hat{\epsilon}^s} \tag{A.28}$$

The following relations can be finally obtained for the eigenstrain and for the actual strain in V

$$\hat{\epsilon}^* = \left[\left(\hat{I} - \left(\hat{C}^{(1)}\right)^{-1}\hat{C}^{(2)}\right)^{-1} - \hat{S}\right]^{-1}\hat{\epsilon}^\infty \tag{A.29}$$

$$\hat{\epsilon}^s = \left(\hat{I} - \left(\hat{C}^{(1)}\right)^{-1}\hat{C}^{(2)}\right)^{-1}\hat{\epsilon}^* \tag{A.30}$$

$$\hat{\epsilon}^s = \left[\hat{I} - \hat{S}\left(\hat{I} - \left(\hat{C}^{(1)}\right)^{-1}\hat{C}^{(2)}\right)\right]^{-1}\hat{\epsilon}^\infty \tag{A.31}$$

If $\hat{C}^{(2)} = 0$ (void) we obtain

$$\hat{\epsilon}^* = \hat{\epsilon}^s = \left[\hat{I} - \hat{S}\right]^{-1}\hat{\epsilon}^\infty \tag{A.32}$$

Lemma: the tensor $\hat{C}^{(1)}\left[\hat{S}^{-1} - \hat{I}\right]$ is symmetric. We consider the same inclusion V with two different values for the eigenstrain $\hat{\epsilon}^*$ and $\hat{\epsilon}^{**}$ embedded in the material defined by $\hat{C}^{(1)}$. The symmetry of the tensor can be established by means of a revised version of the Betti's

reciprocal theorem [36]. We define $\hat{\mathbf{T}}^* = \hat{\mathcal{C}}^{(1)}\hat{\boldsymbol{\varepsilon}}^*$ and $\hat{\mathbf{T}}^{**} = \hat{\mathcal{C}}^{(1)}\hat{\boldsymbol{\varepsilon}}^{**}$. The first situation is described by the fields $\hat{\mathbf{T}}', \hat{\boldsymbol{\varepsilon}}', \vec{u}'$ and the second one by $\hat{\mathbf{T}}'', \hat{\boldsymbol{\varepsilon}}'', \vec{u}''$ everywhere in the space. The preliminary symmetry of the tensor $\hat{\mathcal{S}}\left[\hat{\mathcal{C}}^{(1)}\right]^{-1}$ is proved. We begin by considering the following relation (V is the inclusion volume , Σ its boundary and $\vec{n}$ its external normal unit vector)

$$\begin{aligned} V\hat{\mathbf{T}}^*\hat{\mathcal{S}}\left[\hat{\mathcal{C}}^{(1)}\right]^{-1}\hat{\mathbf{T}}^{**} &= V\hat{\mathbf{T}}^*\hat{\mathcal{S}}\hat{\boldsymbol{\varepsilon}}^{**} = V\hat{\mathbf{T}}^*\hat{\boldsymbol{\varepsilon}}'' \\ &= \hat{\mathbf{T}}^*\int_V \hat{\boldsymbol{\varepsilon}}''dv = \hat{\mathbf{T}}^*\int_V \frac{\partial \vec{u}''}{\partial \vec{x}}dv \\ &= \hat{\mathbf{T}}^*\int_\Sigma \vec{u}''\vec{n}dS = \hat{\mathcal{C}}^{(1)}\hat{\boldsymbol{\varepsilon}}^*\int_\Sigma \vec{u}''\vec{n}dS \end{aligned} \tag{A.33}$$

At the interface Σ we have $\hat{\mathbf{T}}'\vec{n}|_{\Sigma^-} = \hat{\mathbf{T}}'\vec{n}|_{\Sigma^+}$ (sign $+$ indicates the external side of Σ and sign $-$ indicates its internal side). Recalling the definition of inclusion we simply obtain $\hat{\mathcal{C}}^{(1)}\left(\hat{\boldsymbol{\varepsilon}}' - \hat{\boldsymbol{\varepsilon}}^*\right)\vec{n}|_{\Sigma^-} = \hat{\mathcal{C}}^{(1)}\hat{\boldsymbol{\varepsilon}}'\vec{n}|_{\Sigma^+}$ and finally we get $\hat{\mathcal{C}}^{(1)}\hat{\boldsymbol{\varepsilon}}'\vec{n}|_{\Sigma^-} - \hat{\mathcal{C}}^{(1)}\hat{\boldsymbol{\varepsilon}}'\vec{n}|_{\Sigma^+} = \hat{\mathcal{C}}^{(1)}\hat{\boldsymbol{\varepsilon}}^*\vec{n}$. We use it in Eq.(A.33), obtaining

$$V\hat{\mathbf{T}}^*\hat{\mathcal{S}}\left[\hat{\mathcal{C}}^{(1)}\right]^{-1}\hat{\mathbf{T}}^{**} = \int_\Sigma \left[\hat{\mathcal{C}}^{(1)}\hat{\boldsymbol{\varepsilon}}'\vec{n}|_{\Sigma^-} - \hat{\mathcal{C}}^{(1)}\hat{\boldsymbol{\varepsilon}}'\vec{n}|_{\Sigma^+}\right]\vec{u}''dS \tag{A.34}$$

On Σ^- we have $\hat{\mathbf{T}}' = \hat{\mathcal{C}}^{(1)}\left(\hat{\boldsymbol{\varepsilon}}' - \hat{\boldsymbol{\varepsilon}}^*\right)$ and on Σ^+ we have $\hat{\mathbf{T}}' = \hat{\mathcal{C}}^{(1)}\hat{\boldsymbol{\varepsilon}}'$, therefore

$$\begin{aligned} & V\hat{\mathbf{T}}^*\hat{\mathcal{S}}\left[\hat{\mathcal{C}}^{(1)}\right]^{-1}\hat{\mathbf{T}}^{**} \\ = & \int_{\Sigma^-}\left(\hat{\mathbf{T}}' + \hat{\mathbf{T}}^*\right)\vec{n}\vec{u}''dS - \int_{\Sigma^+}\hat{\mathbf{T}}'\vec{n}\vec{u}''dS \\ = & \int_V \frac{\partial}{\partial \vec{x}}\left[\left(\hat{\mathbf{T}}' + \hat{\mathbf{T}}^*\right)\vec{u}''\right]dv + \int_{\mathfrak{R}^3\setminus V}\frac{\partial}{\partial \vec{x}}\left[\hat{\mathbf{T}}'\vec{u}''\right]dv \\ = & \int_V \left(\hat{\mathbf{T}}' + \hat{\mathbf{T}}^*\right)\hat{\boldsymbol{\varepsilon}}''dv + \int_{\mathfrak{R}^3\setminus V}\hat{\mathbf{T}}'\hat{\boldsymbol{\varepsilon}}''dv \\ = & \int_V \left[\hat{\mathcal{C}}^{(1)}\left(\hat{\boldsymbol{\varepsilon}}' - \hat{\boldsymbol{\varepsilon}}^*\right) + \hat{\mathbf{T}}^*\right]\hat{\boldsymbol{\varepsilon}}''dv + \int_{\mathfrak{R}^3\setminus V}\hat{\mathbf{T}}'\hat{\boldsymbol{\varepsilon}}''dv \\ = & \int_V \hat{\boldsymbol{\varepsilon}}'\hat{\mathcal{C}}^{(1)}\hat{\boldsymbol{\varepsilon}}''dv + \int_{\mathfrak{R}^3\setminus V}\hat{\boldsymbol{\varepsilon}}'\hat{\mathcal{C}}^{(1)}\hat{\boldsymbol{\varepsilon}}''dv \\ = & \int_{\mathfrak{R}^3}\hat{\boldsymbol{\varepsilon}}'\hat{\mathcal{C}}^{(1)}\hat{\boldsymbol{\varepsilon}}''dv \end{aligned} \tag{A.35}$$

We have now obtained a symmetric form (since $\hat{\mathcal{C}}^{(1)}$ is symmetric). Therefore, the following dual relation is valid and it can be verified as above

$$V\hat{\mathbf{T}}^{**}\hat{\mathcal{S}}\left[\hat{\mathcal{C}}^{(1)}\right]^{-1}\hat{\mathbf{T}}^{*} = \int_{\mathfrak{R}^3}\hat{\boldsymbol{\varepsilon}}'\hat{\mathcal{C}}^{(1)}\hat{\boldsymbol{\varepsilon}}''dv \tag{A.36}$$

By comparison of Eqs.(A.35) and (A.36) we obtain

$$V\hat{\mathbf{T}}^*\hat{\mathcal{S}}\left[\hat{\mathcal{C}}^{(1)}\right]^{-1}\hat{\mathbf{T}}^{**} = V\hat{\mathbf{T}}^{**}\hat{\mathcal{S}}\left[\hat{\mathcal{C}}^{(1)}\right]^{-1}\hat{\mathbf{T}}^{*} \tag{A.37}$$

which establishes the symmetry of $\hat{\mathcal{S}}\left[\hat{\mathcal{C}}^{(1)}\right]^{-1}$. The inverse tensor $\left\{\hat{\mathcal{S}}\left[\hat{\mathcal{C}}^{(1)}\right]^{-1}\right\}^{-1} = \hat{\mathcal{C}}^{(1)}\hat{\mathcal{S}}^{-1}$ is again symmetric and, finally, the quantity $\hat{\mathcal{C}}^{(1)}\left[\hat{\mathcal{S}}^{-1} - \hat{\mathbf{I}}\right]$ is symmetric since it is a sum of symmetric tensors.

Lemma: the tensor $\hat{\mathbb{C}}^{(1)}\left[\hat{\mathbb{S}}^{-1}-\hat{\mathbb{I}}\right]$ is positive definite. We consider two similar situations as described in Fig.62. The first deals with an homogeneous medium with displacement prescribed on the boundary, while the second case considers the addition of an inhomogeneity without changing the fixed displacements on the external surface. No body forces are present in both schemes. We begin searching for the

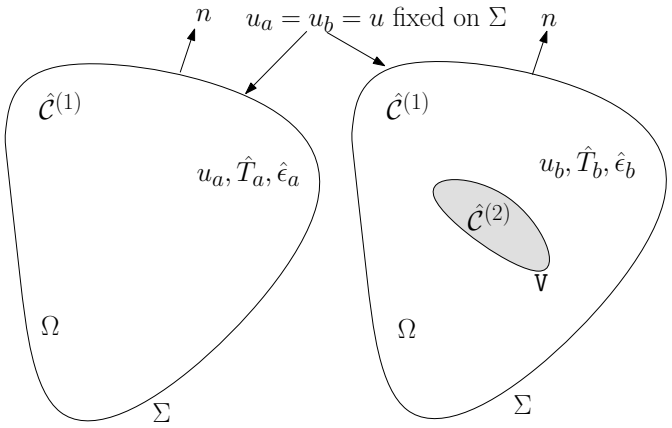

Figure 62: Schemes of an homogeneous region and an heterogeneous one with an inhomogeneity V. The boundary conditions prescribe the same displacement on the external surface.

difference between the elastic energy stored in the two cases

$$\Delta E = \frac{1}{2}\int_{\Omega}\left(\hat{\epsilon}_b\hat{T}_b - \hat{\epsilon}_a\hat{T}_a\right)dv \tag{A.38}$$

We simply verify that

$$\int_{\Omega}\hat{\epsilon}_a\hat{T}_a dv = \int_{\Omega}\hat{\epsilon}_b\hat{T}_a dv \tag{A.39}$$

$$\int_{\Omega}\hat{\epsilon}_a\hat{T}_b dv = \int_{\Omega}\hat{\epsilon}_b\hat{T}_b dv \tag{A.40}$$

In order to verify Eq.(A.39) we write the relation

$$\int_{\Omega}\left(\hat{\epsilon}_a - \hat{\epsilon}_b\right)\hat{T}_a dv = \int_{\Omega}\left(\frac{\partial\vec{u}_a}{\partial\vec{x}}\hat{T}_a - \frac{\partial\vec{u}_b}{\partial\vec{x}}\hat{T}_a\right)dv \tag{A.41}$$

where $\frac{\partial\vec{u}_a}{\partial\vec{x}}\hat{T}_a = \frac{\partial\vec{u}_a\hat{T}_a}{\partial\vec{x}}$ since $\frac{\partial\hat{T}_a}{\partial\vec{x}} = 0$ at equilibrium and similarly $\frac{\partial\vec{u}_b}{\partial\vec{x}}\hat{T}_a = \frac{\partial\vec{u}_b\hat{T}_a}{\partial\vec{x}}$. Therefore, we obtain

$$\begin{aligned}\int_{\Omega}\left(\hat{\epsilon}_a - \hat{\epsilon}_b\right)\hat{T}_a dv &= \int_{\Omega}\left(\frac{\partial\vec{u}_a\hat{T}_a}{\partial\vec{x}} - \frac{\partial\vec{u}_b\hat{T}_a}{\partial\vec{x}}\right)dv \\ &= \int_{\Sigma}\left(\vec{u}_a\hat{T}_a - \vec{u}_b\hat{T}_a\right)\vec{n}dS = 0\end{aligned} \tag{A.42}$$

since $\vec{u}_a = \vec{u}_b$ on Σ. The dual relation given in Eq.(A.40) can be verified with the same method.

By inserting Eqs.(A.39) and (A.40) into Eq.(A.38) we obtain

$$\begin{aligned}
\Delta E &= \frac{1}{2}\int_{\Omega}\left(\hat{\varepsilon}_b\hat{T}_b - \hat{\varepsilon}_a\hat{T}_a\right)dv \\
&= \frac{1}{2}\int_{\Omega}\left(\hat{\varepsilon}_a\hat{T}_b - \hat{\varepsilon}_b\hat{T}_a\right)dv \\
&= \frac{1}{2}\int_{\Omega\ v}\left(\hat{\varepsilon}_a\hat{T}_b - \hat{\varepsilon}_b\hat{T}_a\right)dv \\
&\quad +\frac{1}{2}\int_{v}\left(\hat{\varepsilon}_a\hat{T}_b - \hat{\varepsilon}_b\hat{T}_a\right)dv \\
&= \frac{1}{2}\int_{\Omega\ v}\left(\hat{\varepsilon}_a\hat{\mathcal{C}}^{(1)}\hat{\varepsilon}_b - \hat{\varepsilon}_b\hat{\mathcal{C}}^{(1)}\hat{\varepsilon}_a\right)dv \\
&\quad +\frac{1}{2}\int_{v}\left(\hat{\varepsilon}_a\hat{T}_b - \hat{\varepsilon}_b\hat{T}_a\right)dv
\end{aligned} \tag{A.43}$$

Since the stiffness tensor $\hat{\mathcal{C}}^{(1)}$ is symmetric, we obtain the following general expression for the energy difference

$$\Delta E = \frac{1}{2}\int_{v}\left(\hat{\varepsilon}_a\hat{T}_b - \hat{\varepsilon}_b\hat{T}_a\right)dv \tag{A.44}$$

We suppose now that the prescribed displacement on Σ imposes a uniform strain in the first case of Fig.62; therefore, the second situation can be described by the Eshelby solution. With this additional hypothesis the energy difference can be rearranged as follows

$$\begin{aligned}
\Delta E &= -\frac{1}{2}\int_{v}\left(\hat{T}_a\hat{\varepsilon}_b - \hat{\varepsilon}_a\hat{T}_b\right)dv \\
&= -\frac{1}{2}\int_{v}\left(\hat{T}_a\hat{\varepsilon}_b - \hat{T}_a\left(\hat{\mathcal{C}}^{(1)}\right)^{-1}\hat{\mathcal{C}}^{(2)}\hat{\varepsilon}_b\right)dv \\
&= -\frac{1}{2}\int_{v}\hat{T}_a\left(\hat{I} - \left(\hat{\mathcal{C}}^{(1)}\right)^{-1}\hat{\mathcal{C}}^{(2)}\right)\hat{\varepsilon}_b dv \\
&= -\frac{1}{2}\int_{v}\hat{T}_a\hat{\varepsilon}^* dv
\end{aligned} \tag{A.45}$$

having used Eq.(A.30). Utilizing Eq.(A.29) we obtain

$$\Delta E = -\frac{1}{2}\int_{v}\hat{\varepsilon}_a\hat{\mathcal{C}}^{(1)}\left[\left(\hat{I} - \left(\hat{\mathcal{C}}^{(1)}\right)^{-1}\hat{\mathcal{C}}^{(2)}\right)^{-1} - \hat{S}\right]^{-1}\hat{\varepsilon}_a dv \tag{A.46}$$

From now on we suppose that the embedded inhomogeneity is a void ($\hat{\mathcal{C}}^{(2)} = 0$) and, therefore, we obtain

$$\Delta E = E_b\left(\hat{\varepsilon}_b\right) - E_a\left(\hat{\varepsilon}_a\right) = -\frac{1}{2}\int_{v}\hat{\varepsilon}_a\hat{\mathcal{C}}^{(1)}\left[\hat{I} - \hat{S}\right]^{-1}\hat{\varepsilon}_a dv \tag{A.47}$$

We may now consider the variational formulation of the elasticity theory [36, 39]. If we take into account a body without body forces and with prescribed displacements on the whole external surface, then the variational formulation leads to the minimum potential energy principle. We may apply this principle to the second case of Fig.62 (with a void). If the fields $\vec{u}_b, \hat{\varepsilon}_b, \hat{T}_b$ correspond of the actual elastic fields in such a case, we have $E_b\left(\vec{u}_b, \hat{\varepsilon}_b, \hat{T}_b\right) \leqslant E_b\left(\vec{u}, \hat{\varepsilon}, \hat{T}\right)$ where the fields $\vec{u}, \hat{\varepsilon}, \hat{T}$ correspond to any displacement $\vec{u}$ matching the prescribed

boundary. In particular we have $E_b(\hat{e}_b) \leqslant E_b(\hat{e}_a)$, where $\hat{e}_a$ is the strain in the first case of Fig.62. Moreover, we may write

$$\begin{aligned} E_b(\hat{e}_a) &= \frac{1}{2}\int_{\Omega\, V} \hat{e}_a \hat{\mathcal{C}}^{(1)} \hat{e}_a dv + \frac{1}{2}\int_V \hat{e}_a \hat{\mathcal{C}}^{(2)} \hat{e}_a dv \\ &= \frac{1}{2}\int_{\Omega\, V} \hat{e}_a \hat{\mathcal{C}}^{(1)} \hat{e}_a dv \\ &= E_a(\hat{e}_a) - \frac{1}{2}\int_V \hat{e}_a \hat{\mathcal{C}}^{(1)} \hat{e}_a dv \end{aligned} \tag{A.48}$$

Summing up

$$\begin{aligned} E_b(\hat{e}_b) &\leqslant E_b(\hat{e}_a) \\ E_b(\hat{e}_b) &\leqslant E_a(\hat{e}_a) - \frac{1}{2}\int_V \hat{e}_a \hat{\mathcal{C}}^{(1)} \hat{e}_a dv \\ E_b(\hat{e}_b) - E_a(\hat{e}_a) &\leqslant -\frac{1}{2}\int_V \hat{e}_a \hat{\mathcal{C}}^{(1)} \hat{e}_a dv \end{aligned} \tag{A.49}$$

Since $\hat{e}_a$ is uniform, combining Eqs.(A.47) and (A.49), we obtain

$$\hat{e}_a \hat{\mathcal{C}}^{(1)} \left[\hat{I} - \hat{\mathcal{S}}\right]^{-1} \hat{e}_a - \hat{e}_a \hat{\mathcal{C}}^{(1)} \hat{e}_a \geqslant 0 \tag{A.50}$$

or

$$\hat{T}_a \left[\hat{I} - \hat{\mathcal{S}}\right]^{-1} \left[\hat{\mathcal{C}}^{(1)}\right]^{-1} \hat{T}_a - \hat{T}_a \left[\hat{\mathcal{C}}^{(1)}\right]^{-1} \hat{T}_a \geqslant 0 \tag{A.51}$$

So, the tensor $\left[\hat{I} - \hat{\mathcal{S}}\right]^{-1} \left[\hat{\mathcal{C}}^{(1)}\right]^{-1} - \left[\hat{\mathcal{C}}^{(1)}\right]^{-1}$ is positive definite.
For any tensor it is true that $[I - A]^{-1} = I + \left[A^{-1} - I\right]^{-1}$ and therefore we obtain

$$\begin{aligned} &\left[\hat{I} - \hat{\mathcal{S}}\right]^{-1} \left[\hat{\mathcal{C}}^{(1)}\right]^{-1} - \left[\hat{\mathcal{C}}^{(1)}\right]^{-1} \\ &\qquad = \left[\hat{\mathcal{S}}^{-1} - \hat{I}\right]^{-1} \left[\hat{\mathcal{C}}^{(1)}\right]^{-1} \end{aligned} \tag{A.52}$$

Finally, the tensor $\left[\hat{\mathcal{S}}^{-1} - \hat{I}\right]^{-1} \left[\hat{\mathcal{C}}^{(1)}\right]^{-1}$ and its inverse $\hat{\mathcal{C}}^{(1)} \left[\hat{\mathcal{S}}^{-1} - \hat{I}\right]$ are symmetric and positive definite.

It is interesting to observe that all the results given in Appendix A.2 and in Sections 2.3.2 and 2.3.2 exactly apply also for an anisotropic and homogeneous ellipsoidal inhomogeneity embedded in an anisotropic and homogeneous matrix. In this case, the Eshelby tensor $\hat{\mathcal{S}}$ depends on the geometry and on $\hat{\mathcal{C}}^{(1)}$ [45].

A.3 FIRST ORDER EXPANSIONS FOR A DISPERSION OF SPHERES

In this Appendix we present the first order expansions in the volume fraction of the effective nonlinear moduli A_{eff}, B_{eff}, C_{eff}, and D_{eff} for a dispersion of spheres. In particular we consider four different cases where only one nonlinear modulus of the spheres (A, B, C or D) is different from zero. These solutions are coherent with the scheme represented in Fig. 15. If $C \neq 0$ we obtain

$$\begin{cases} C^C_{eff} = \frac{(3K_1+4\mu_1)^3}{(4\mu_1+3K_2)^3} Cc + O\left(c^2\right) \\ \\ A^C_{eff} = B^C_{eff} = D^C_{eff} = 0 \end{cases} \tag{A.53}$$

If $B \neq 0$ we have

$$\begin{cases} B^B_{eff} &= 25\frac{{\mu_1}^2}{\left(6\mu_2K_1+12\mu_2\mu_1+9\mu_1K_1+8{\mu_1}^2\right)^2} \\ &\times \frac{\left(3K_1+4\mu_1\right)^3}{4\mu_1+3K_2}Bc+O\left(c^2\right) \\ C^B_{eff} &= \frac{6\mu_2K_1+12\mu_2\mu_1+9\mu_1K_1+28{\mu_1}^2+15K_2\mu_1}{\left(6\mu_2K_1+12\mu_2\mu_1+9\mu_1K_1+8{\mu_1}^2\right)^2} \\ &\times \frac{3\mu_1K_1-5K_2\mu_1+2\mu_2K_1+4\mu_2\mu_1-4{\mu_1}^2}{\left(4\mu_1+3K_2\right)^3} \\ &\times \left(3K_1+4\mu_1\right)^3Bc+O\left(c^2\right) \\ A^B_{eff} &= D^B_{eff}=0 \end{cases} \tag{A.54}$$

If $D \neq 0$ we obtain

$$\begin{cases} C^D_{eff} &= \frac{3\mu_1K_1-5K_2\mu_1+2\mu_2K_1+4\mu_2\mu_1-4{\mu_1}^2}{\left(9\mu_1K_1+8{\mu_1}^2+6\mu_2K_1+12\mu_2\mu_1\right)^2} \\ &\times \frac{6\mu_2K_1+12\mu_2\mu_1+28{\mu_1}^2+9\mu_1K_1+15K_2\mu_1}{\left(4\mu_1+3K_2\right)^3} \\ &\times \left(3K_1+4\mu_1\right)^3Dc+O\left(c^2\right) \\ D^D_{eff} &= 25\frac{{\mu_1}^2}{\left(9\mu_1K_1+8{\mu_1}^2+6\mu_2K_1+12\mu_2\mu_1\right)^2} \\ &\times \frac{\left(3K_1+4\mu_1\right)^3}{4\mu_1+3K_2}Dc+O\left(c^2\right) \\ A^D_{eff} &= B^D_{eff}=0 \end{cases} \tag{A.55}$$

Finally, if $A \neq 0$ all the effective nonlinear moduli are different from zero and they can be eventually written as

$$\begin{cases} A^A_{eff} &= \frac{125\left(3K_1+4\mu_1\right)^3{\mu_1}^3Ac}{\left(9K_1\mu_1+8{\mu_1}^2+6K_1\mu_2+12\mu_2\mu_1\right)^3}+O\left(c^2\right) \\ B^A_{eff} &= 25\frac{3K_1\mu_1-5K2\mu_1+2K1\mu_2+4\mu_2\mu_1-4{\mu_1}^2}{\left(9K1\mu_1+8{\mu_1}^2+6K_1\mu_2+12\mu_2\mu_1\right)^3} \\ &\times \frac{\left(3K_1+4\mu_1\right)^3{\mu_1}^2Ac}{4\mu_1+3K_2}+O\left(c^2\right) \\ C^A_{eff} &= 3\frac{\left(3K_1\mu_1-5K_2\mu_1+2K_1\mu_2+4\mu_2\mu_1-4{\mu_1}^2\right)^2}{\left(9K_1\mu_1+8{\mu_1}^2+6K_1\mu_2+12\mu_2\mu_1\right)^3} \\ &\times \frac{10K_2\mu_1+2K_1\mu_2+3K_1\mu_1+4\mu_2\mu_1+16{\mu_1}^2}{\left(4\mu_1+3K_2\right)^3} \\ &\times \left(3K_1+4\mu_1\right)^3Ac+O\left(c^2\right) \\ D^A_{eff} &= 50\frac{{\mu_1}^2}{\left(9K_1\mu_1+8{\mu_1}^2+6K_1\mu_2+12\mu_2\mu_1\right)^3} \\ &\times \frac{3K_1\mu_1-5K_2\mu_1+2K_1\mu_2+4\mu_2\mu_1-4{\mu_1}^2}{4\mu_1+3K_2} \\ &\times \left(3K_1+4\mu_1\right)^3Ac+O\left(c^2\right) \end{cases} \tag{A.56}$$

It is interesting to remark that the more complicated cases, with all the nonlinear moduli of the spheres different form zero, can be simply handled by means of the superimposition of the four cases above considered.

A.4 FIRST ORDER EXPANSIONS FOR A DISPERSION OF CYLINDERS

Here we present the first order expansions in the volume fraction of the effective nonlinear moduli A_{eff}, B_{eff}, C_{eff}, and D_{eff} for a dispersion of cylinders. In particular we consider four different cases where only one nonlinear modulus of the cylinders (A, B, C or D) is different from zero. If $C \neq 0$ we have

$$\begin{cases} C^C_{eff} &= \frac{(K_1+\mu_1)^3}{(K_2+\mu_1)^3} Cc + O\left(c^2\right) \\ \\ A^C_{eff} &= B^C_{eff} = D^C_{eff} = 0 \end{cases} \tag{A.57}$$

If $B \neq 0$ we obtain

$$\begin{cases} B^B_{eff} &= \frac{4(K_1+\mu_1)^3 {\mu_1}^2 B}{(K_2+\mu_1)(\mu_1 K_1+\mu_2 K_1+2\mu_2\mu_1)^2} c + O\left(c^2\right) \\ \\ C^B_{eff} &= \frac{1}{2}\frac{2K_2\mu_1+\mu_1 K_1+\mu_2 K_1+2\mu_2\mu_1+2\mu_1^2}{(\mu_1 K_1+\mu_2 K_1+2\mu_2\mu_1)^2} \\ &\times \frac{\mu_1 K_1-2K_2\mu_1+\mu_2 K_1+2\mu_2\mu_1-2\mu_1^2}{(K_2+\mu_1)^3} \\ &\times (K_1+\mu_1)^3 Bc + O\left(c^2\right) \\ \\ A^B_{eff} &= D^B_{eff} = 0 \end{cases} \tag{A.58}$$

If $D \neq 0$ we have

$$\begin{cases} C^D_{eff} &= \frac{1}{2}\frac{K_1\mu_1-2K_2\mu_1+K_1\mu_2+2\mu_2\mu_1-2\mu_1^2}{(K_1\mu_1+K_1\mu_2+2\mu_2\mu_1)^2} \\ &\times \frac{K_1\mu_2+K_1\mu_1+2\mu_2\mu_1+2K_2\mu_1+2\mu_1^2}{(K_2+\mu_1)^3} \\ &\times (K_1+\mu_1)^3 Dc + O\left(c^2\right) \\ \\ D^D_{eff} &= \frac{4(K_1+\mu_1)^3 {\mu_1}^2 Dc}{(K_2+\mu_1)(K_1\mu_1+K_1\mu_2+2\mu_2\mu_1)^2} + O\left(c^2\right) \\ \\ A^D_{eff} &= B^D_{eff} = 0 \end{cases} \tag{A.59}$$

Finally, if $A \neq 0$, as predicted by the scheme represented in Fig. 15, all the effective nonlinear moduli are different from zero and the final expressions are given below

$$\begin{cases} A^A_{eff} &= 8\frac{(K_1+\mu_1)^3{\mu_1}^3}{(K_1\mu_1+K_1\mu_2+2\mu_2\mu_1)^3}Ac + O\left(c^2\right) \\ B^A_{eff} &= 2\frac{{\mu_1}^2}{(K_1\mu_1+K_1\mu_2+2\mu_2\mu_1)^3} \\ &\times \frac{K_1\mu_1-2K_2\mu_1+K_1\mu_2+2\mu_2\mu_1-2\mu_1^2}{K_2+\mu_1} \\ &\times (K_1+\mu_1)^3 Ac + O\left(c^2\right) \\ C^A_{eff} &= \frac{1}{4}\frac{\left(K_1\mu_1-2K_2\mu_1+K_1\mu_2+2\mu_2\mu_1-2\mu_1^2\right)^2}{(K_1\mu_1+K_1\mu_2+2\mu_2\mu_1)^3} \\ &\times \frac{K_1\mu_2+2\mu_2\mu_1+K_1\mu_1+4K_2\mu_1+4\mu_1^2}{(K_2+\mu_1)^3} \\ &\times (K_1+\mu_1)^3 Ac + O\left(c^2\right) \\ D^A_{eff} &= 4\frac{{\mu_1}^2}{(K_1\mu_1+K_1\mu_2+2\mu_2\mu_1)^3} \\ &\times \frac{K_1\mu_1-2K_2\mu_1+K_1\mu_2+2\mu_2\mu_1-2\mu_1^2}{(K_2+\mu_1)} \\ &\times (K_1+\mu_1)^3 Ac + O\left(c^2\right) \end{cases} \tag{A.60}$$

BIBLIOGRAPHY

[1] B. Bhushan, editor. *Springer Handbook of Nanotechnology*. Springer Verlag, New York, 2004. (Cited on page 1.)

[2] M. Sahimil. *Heterogeneous Materials*. Springer-Verlag, New York, 2003. (Cited on pages 2 and 4.)

[3] J. C. Maxwell. *Philos. Trans. Soc. London.*, **157**:49, 1867. (Cited on page 2.)

[4] J. C. Maxwell. *A treatise on electricity and magnetism*. Clarendon Press, Oxford, 3rd. ed. edition, 1873. (Cited on page 2.)

[5] J. W. Rayleigh. *Phil. Mag.*, **32**:481–491, 1892. (Cited on page 2.)

[6] W. Voigt. *Wied. Ann.*, **38**:573–587, 1889. (Cited on page 2.)

[7] A. Reuss. *Z. angew. Math. Mech.*, **9**:49–58, 1929. (Cited on page 2.)

[8] J. D. Eshelby. *Proc. R. Soc. London, Ser. A*, **241**: 376–396, 1957. (Cited on pages 2, 33, 36, 61, 117, 172, and 173.)

[9] G.I. Taylor. *J. Inst. Metals*, **62**:307, 1938. (Cited on page 3.)

[10] J.F.W. Bishop and R. Hill. *Philos. Mag.*, **42**:414, 1951. (Cited on page 3.)

[11] J.F.W. Bishop and R. Hill. *Philos. Mag.*, **42**:1298, 1951. (Cited on page 3.)

[12] D.C. Drucker. *On minimum weight design and strength of non-homogeneous plastic bodies*. Non-homogeneity in Elasticity and Plasticity. Pergamon Press, New York, 1959. p. 139. (Cited on page 3.)

[13] T. Christman, A. Needleman, and S. Suresh. *Acta Metall. Mater.*, **37**:3029, 1989. (Cited on page 3.)

[14] V. Tvergaard. *Acta Metall. Mater.*, **38**:185, 1990. (Cited on page 3.)

[15] G. Bao, J.W. Hutchinson, and R. M. McMeeking. *Acta Metall. Mater.*, **39**:1871, 1991. (Cited on page 3.)

[16] J. Brockenborough, S. Suresh, and H.Wienecke. *Acta Metall. Mater.*, **39**:735, 1991. (Cited on page 3.)

[17] H. Moulinec and P. Suquet. *AFTT-based numerical method for computing the mechanical properties of composites from images of their microstructure*. Microstructure-Properly Interactions in Composite Materials. Kluwer, Netherlands, 1995. p. 235. (Cited on page 3.)

[18] P. Suquet. *C. R. Acad. Sci. Paris Ser. II*, **320**:563, 1995. (Cited on page 3.)

[19] P. Ponte Castañeda and P. Suquet. *Adv. Appl. Mech.*, **34**:172, 1998. (Cited on page 3.)

[20] W. K. Liu, E. G. Karpov, and H. S. Park. *Nano Mechanics and Materials: Theory, Multiscale Methods and Applications*. John Wiley & Sons, New York, 2006. (Cited on page 4.)

[21] M. Ortiz and R. Phillips. *Adv. Appl. Mech.*, **36**:1, 1999. (Cited on page 4.)

[22] R. Phillips. *Crystals, Defects, and Microstructures: Modeling across Scales*. Cambridge University Press, Cambridge, 2001. (Cited on page 4.)

[23] E. Clementi. *Philos. Trans. R. Soc. Lond. A*, **326**:445, 1988. (Cited on page 4.)

[24] L.A. Zepeda-Ruiz, D. Maroudas, and W.H. Weinberg. *J. Appl. Phys.*, **85**:3677, 1999. (Cited on page 5.)

[25] P. N. Keating. *Phys. Rev.*, **145**: 637, 1966. (Cited on page 5.)

[26] F. H. Stillinger and T. A. Weber. *Phys. Rev. B*, **31**:5262, 1985. (Cited on pages 7 and 90.)

[27] J. Tersoff. *Phys. Rev. B*, **39**:5566, 1989. (Cited on pages 7 and 91.)

[28] J. L. Synge and A. Schild. *Tensor Calculus*. Dover Publication Inc., New York, 1978. (Cited on pages 11, 21, and 22.)

[29] C. P. Chou and N. J. Pagano. *Elasticity. Tensor, Dyadic, and Engineering Approaches*. Dover Publication Inc., New York, 1992. (Cited on pages 11, 21, and 27.)

[30] J. E. Marsden and T. J. R. Hughes. *Mathematical Foundations of Elasticity*. Dover Publication Inc., New York, 1994. (Cited on pages 11 and 17.)

[31] R. J. Atkin and N. Fox. *An Introduction to the Theory of Elasticity*. Dover Publication Inc., New York, 1980. (Cited on pages 11, 12, 14, 15, 17, 19, 26, 41, 58, 59, 60, 118, 119, and 126.)

[32] A. E. Green and W. Zerna. *Theoretical Elasticity*. Clarendon Press, Oxford, 1954. (Cited on pages 11, 15, 16, 115, and 119.)

[33] V. V. Novozhilov. *Foundations of the Nonlinear Theory of Elasticity*. Dover Publication Inc., New York, 1999. (Cited on pages 11, 19, and 58.)

[34] Y. A. Amenzade. *Theory of Elasticity*. MIR Publisher, Moscow, 1979. (Cited on pages 11, 12, 13, 17, and 26.)

[35] I. N. Sneddon and D. S. Berry. *The Classical Theory of Elasticity*, volume VI of *Encyclopaedia of Physics*. Springer Verlag, Berlin, 1958. pp. 1-126. (Cited on pages 11, 17, and 26.)

[36] A. E. H. Love. *A Treatise on the Mathematical Theory of Elasticity*. Dover Publication Inc., New York, 1964. (Cited on pages 11, 12, 13, 14, 15, 17, 21, 26, 30, 60, 174, and 176.)

[37] V. Parton and P. Perline. *Méthodes de la Théorie Mathématique de l'Élasticité*, volume 1 et 2. Éditions MIR, Moscow, 1981. (Cited on page 11.)

[38] M. Ciarletta and D. Iesan. *Non-Classical Elastic Solids*. Longman Scientific and Technical, Harlow, 1993. (Cited on page 17.)

[39] L. Landau and E. Lifshitz. *Theory of Elasticity*. Pergamon Press, Oxford, 1959. (Cited on pages 19, 20, 31, 41, 60, and 176.)

[40] J. P. Den Hartog. *Advanced Strength of Materials*. Dover Publication Inc., New York, 1987. (Cited on page 19.)

[41] J. Lubliner. *Plasticity theory*. Macmillan Publishing Company, New York, 1990. (Cited on page 19.)

[42] C. Kittel. *Introduction to Solid State Physics*. John Wiley & Sons, New York, 7th edition edition, 1996. (Cited on page 20.)

[43] K. F. Graff. *Wave Motion in Elastic Solids*. Dover Publication Inc., New York, 1991. (Cited on page 26.)

[44] V. Rékatch. *Problèmes de la Théorie de l'Élasticité*. Éditions MIR, Moscow, 1980. (Cited on page 26.)

[45] T. Mura. *Micromechanics of Defects in Solids*. Kluwer Academic Publishers, Dordrecht, 2nd revised edition edition, 1987. (Cited on pages 26, 35, 36, 46, 47, 66, 75, 115, 120, 172, 173, and 177.)

[46] R. Lakes. *Science*, **235**: 1038, 1987. (Cited on pages 31 and 88.)

[47] N. R. Keskar and J. R. Chelikowsky. *Nature*, **358**: 222, 1992. (Cited on page 31.)

[48] A. Yeganeh-Haeri, D. J. Weidner, and J. B. Parise. *Science*, **357**: 650, 1992. (Cited on page 31.)

[49] J. D. Eshelby. *Proc. R. Soc. London, Ser. A*, **252**: 561–569, 1959. (Cited on pages 33, 36, 61, and 172.)

[50] J. D. Eshelby. *Elastic inclusions and inhomogeneities*, volume 2 (Ch. III) of *Progress in solid mechanics*. North-Holland, Amsterdam, 1973. (Cited on pages 33 and 34.)

[51] L. J. Walpole. *Proc. R. Soc. London, Ser. A*, **300**: 270–189, 1967. (Cited on page 33.)

[52] T. M. Michelitsch, H. Gao, and V. M. Levin. *Proc. R. Soc. London, Ser. A*, **459**: 863, 2003. (Cited on page 33.)

[53] Y. Mikata and S. Nemat-Nasser. *Journal of Applied Mechanics*, **57**: 845–849, 1990. (Cited on page 33.)

[54] Z. Q. Cheng and R. C. Batra. *Journal of Applied Mechanics*, **66**: 563–565, 1999. (Cited on page 33.)

[55] L. J. Walpole. *Proc. R. Soc. London, Ser. A*, **434**: 571–585, 1991. (Cited on pages 33 and 34.)

[56] L. J. Walpole. *Proc. R. Soc. London, Ser. A*, **433**: 179–207, 1991. (Cited on pages 33 and 34.)

[57] J. G. Berryman. *Phys. Rev. Lett.*, **79**: 1142–1145, 1997. (Cited on page 34.)

[58] L. Dormieux, D. Kondo, and F. J. Ulm. *Microporomechanics*. John Wiley & Sons, Ltd, England, 2006. (Cited on page 34.)

[59] J. H. Huang and J. S. Yu. *Composites Engineering*, **4**: 1169–1182, 1994. (Cited on page 34.)

[60] J. H. Huang, Y. H. Chiu, and H. K. Liu. *J. Appl. Phys.*, **83**: 5364–5370, 1998. (Cited on page 34.)

[61] S. Giordano and P. L. Palla. *J. Phys. A: Math.Theor.*, **41**: 415205, 2008. (Cited on page 34.)

[62] S. Giordano, P. L. Palla, and L. Colombo. *The Euro. Phys. J. B*, **66**: 29–35, 2008. (Cited on page 34.)

[63] G. Sendeckyj. *Int. J. Solids Struct.*, **6**: 1535–1543, 1970. (Cited on page 34.)

[64] Q. C. Ru and P. Schiavone. *Math. Mech. Solids*, **1**: 327–333, 1996. (Cited on page 34.)

[65] H. Kang and G. W. Milton. *Arch. Rat. Mech. Analysis*, **62**: 384–409, 1914. (Cited on page 34.)

[66] L. P. Liu. *Proc. R. Soc. A*, **464**: 573–594, 2008. (Cited on page 34.)

[67] L. K. H. Van Beek. *Dielectric behavior of heterogeneous systems*, volume 7 (pp. 71-114) of *Progress in Dielectric*. Heywood, London, 1967. (Cited on pages 35 and 64.)

[68] L. J. Walpole. *Advanced in Applied Mechanics*, **11**: 169–242, 1981. (Cited on pages 35, 46, 64, and 66.)

[69] Z. Hashin. *J. Appl. Mech.*, **50**: 481–505, 1983. (Cited on pages 35, 64, and 70.)

[70] K. Z. Markov. *Elementary micromechanics of heterogeneous media*. In: Heterogeneous Media: Micromechanics Modeling Methods and Simulations. Birkhauser, Boston, 2000. pp.1-162. (Cited on pages 35, 64, and 169.)

[71] T. Mori and K. Tanaka. *Acta Metallurgica*, **21**: 571–574, 1973. (Cited on page 35.)

[72] M. Avellaneda. *Communications on Pure and Applied Mathematics*, **40**: 527–554, 1987. (Cited on page 35.)

[73] R. McLaughlin. *Int. J. Eng. Sci.*, **15**: 237–244, 1977. (Cited on pages 35, 64, and 74.)

[74] S. Giordano. *European Journal of Mechanics A/Solids*, **22**: 885–902, 2003. (Cited on pages 35, 64, and 72.)

[75] R. Hill. *J. Mech. Phys. Solids*, **11**: 357–372, 1963. (Cited on page 35.)

[76] K. A. Snyder and E. J. Garboczi. *J. Appl. Phys.*, **72**: 5948–5955, 1992. (Cited on pages 35 and 77.)

[77] M. Kachanov and I. Sevostianov. *Int. J. Solids Struct.*, **42**: 309, 2005. (Cited on pages 35 and 64.)

[78] B. Budiansky and R. J. O'Connell. *Int. J. Solids Struct.*, **12**: 81–97, 1976. (Cited on page 35.)

[79] M. Kachanov. *Appl. Mech. Rev.*, **45**: 305–336, 1992. (Cited on page 35.)

[80] S. Giordano and L. Colombo. *Phys. Rev. Lett.*, **98**(055503): 055503, 2007. (Cited on pages 35 and 64.)

[81] J. R. Willis. *J. Mech. Phys. Solids*, **13**: 377–395, 1965. (Cited on page 42.)

[82] J. D. Eshelby. *Phil. Trans. R. Soc Lond. A*, **274**: 331–338, 1973. (Cited on page 42.)

[83] G. Kolosoff. *Doctoral dissertation*. Dorpat, Estonia, 1909. (Cited on pages 47 and 118.)

[84] G. Kolosoff. *Zeitschrift fur Math. und Physik*, **62**: 384–409, 1914. (Cited on pages 47 and 118.)

[85] G. Kolosoff. *Some basic problems in the mathematical theory of elasticity*. Noordhoff, Groningen, Holland, 1953. (Cited on page 47.)

[86] P. L. Palla, S. Giordano, and L. Colombo. *Phys. Rev. B*, **80**:054105, 2009. (Cited on pages 49, 111, 140, and 163.)

[87] S. Giordano, P.L. Palla, and L. Colombo. *Euro Physics Letters*, **83**: 66003, 2008. (Cited on pages 58, 70, 126, and 163.)

[88] T. K. Ballabh, M. Paul, T. R. Middya, and A. N. Basu. *Phys. Rev. B*, **45**: 2761, 1992. (Cited on pages 58 and 59.)

[89] S. S. Sekoyan. *Int. Appl. Mech.*, **10-11**: 1259, 1974. (Cited on page 59.)

[90] Y. Hiki. *Ann. Rev. Mater. Sci.*, **11**: 51, 1981. (Cited on page 59.)

[91] D. S. Hughes and J. L. Kelly. *Phys. Rev.*, **92**: 1145, 1953. (Cited on page 59.)

[92] T. Bateman, W. P. Mason, and H. J. McSkimin. *J. Appl. Phys.*, **32**: 928, 1961. (Cited on page 59.)

[93] T. Cagin and J. R. Ray. *Phys. Rev. B*, **38**: 7940, 1988. (Cited on page 59.)

[94] J. Zhao, J. M. Winey, and Y. M. Gupta. *Phys. Rev. B*, **75**: 094105, 2007. (Cited on pages 59, 107, and 109.)

[95] I. Sevostianov and A. Vakulenko. *Int. J. Fracture*, **107**: L9, 2000. (Cited on page 61.)

[96] I. Yu. Tsvelodub. *J. Appl. Mech. Tech. Phys.*, **41**: 734, 2000. (Cited on page 61.)

[97] I. Yu. Tsvelodub. *J. Appl. Mech. Tech. Phys.*, **45**: 69, 2004. (Cited on page 61.)

[98] S. Torquato. *Phys. Rev. Lett.*, **79**: 681, 1997. (Cited on pages 63 and 103.)

[99] Z. Hashin and S. Shtrikman. *J. Appl. Phys.*, **33**: 3125, 1962. (Cited on pages 63 and 156.)

[100] Z. Hashin and S. Shtrikman. *J. Mech. Phys. Solids*, **10**: 335, 1962. (Cited on pages 63, 73, and 156.)

[101] W. F. Brown. *J. Chem. Phys.*, **23**:1514, 1955. (Cited on page 63.)

[102] S. Torquato. *J. Mech. Phys. Solids*, **45**: 1421, 1997. (Cited on page 63.)

[103] S. Torquato. *J. Mech. Phys. Solids*, **46**: 1411, 1998. (Cited on page 63.)

[104] J. C. Maxwell. *A treatise on electricity and magnetism*. Oxford, clarendon edition, 1881. (Cited on page 63.)

[105] D. A. G. Bruggeman. *Ann. Phys. (Leipzig)*, **24**: 636, 1935. (Cited on page 64.)

[106] A. V. Goncharenko, V. V. Popelnukh, and E. F. Venger. **35**: 1833, 2002. (Cited on page 64.)

[107] A. Lakhtakia and T. G. Mackay. *AEU Int. J. Electron. Commun.*, **58**: 1, 2004. (Cited on page 64.)

[108] T. G. Mackay. *Proc. SPIE*, **5509**, 2004. (Cited on page 64.)

[109] A. A. Zharov, I. V. Shadrivov, and Y. S. Kivshar. *Phys. Rev. Lett.*, **91**: 3740, 2003. (Cited on page 64.)

[110] S. Giordano and W. Rocchia. *J. Appl. Phys.*, **98**:104101, 2005. (Cited on page 64.)

[111] R. M. Christensen. *Mechanics of composite materials*. Dover Publication Inc., New York, 2005. (Cited on pages 64, 73, and 125.)

[112] N. Norris. *Mech. of Mat.*, **4**:1, 1985. (Cited on page 64.)

[113] M. Kachanov. *Appl. Mech. Rev.*, **45**:305, 1992. (Cited on page 64.)

[114] S. Giordano and L. Colombo. *Eng. Frac. Mech.*, **74**:1983, 2007. (Cited on page 64.)

[115] P. Gilormini and F. Montheillet. *J. Mech. Phys. Solids*, **34**:97, 1986. (Cited on page 64.)

[116] P. Ponte Casta neda. *J. Mech. Phys. Solids*, **39**:45, 1991. (Cited on page 64.)

[117] P. Suquet. *J. Mech. Phys. Solids*, **41**:981, 1993. (Cited on page 64.)

[118] S. Catheline, J.-L. Gennisson, and M. Fink. *J. Acoust. Soc. Am.*, **114**:3087, 2003. (Cited on page 64.)

[119] S. Catheline, J. L. Gennisson, M. Tanter, and M. Fink. *Phys. Rev. Lett.*, **91**:164301, 2003. (Cited on page 64.)

[120] M. J. Buehler, F. F. Abraham, and H. Gao. *Nature*, **426**:141, 2003. (Cited on pages 64, 126, and 133.)

[121] M. J. Buehler and H. Gao. *Nature*, **439**:307, 2006. (Cited on pages 64, 126, and 133.)

[122] V. Holỳ, G. Springholz, M. Pinczolits, and G. Bauer. *Phys. Rev. Lett.*, **83**:356, 1999. (Cited on pages 64 and 111.)

[123] M. Schmidbauer, Sh. Seydmohamadi, D. Grigoriev, Zh. M. Wang, Yu. I. Mazur, P. Schäfer, M. Hanke, R. Köhler, and G. J. Salamo. *Phys. Rev. Lett.*, **96**:066108, 2006. (Cited on pages 64 and 111.)

[124] A. Mattoni, L. Colombo, and F. Cleri. *Phys. Rev. B*, **70**:094108, 2004. (Cited on page 64.)

[125] S. Giordano, P. Palla, and L. Colombo. *Eur. Phys. J. B*, **68**:89–101, 2009. (Cited on pages 64, 70, 126, and 163.)

[126] R. M. Christensen. *Proc. R. Soc. London, Ser. A*, **440**: 461, 1993. (Cited on page 72.)

[127] M. F. Thorpe and P. N. Sen. *J. Acoust. Soc. Am.*, **77**:1674, 1985. (Cited on pages 74, 75, and 78.)

[128] R. Hill. *J. Mech. Phys. Solids*, **12**:199, 1964. (Cited on page 74.)

[129] R. Hill. *J. Mech. Phys. Solids*, **12**:213, 1964. (Cited on page 74.)

[130] R. Hill. *J. Mech. Phys. Solids*, **13**:189, 1965. (Cited on page 74.)

[131] I. Todhunter. *A History of the Theory of Elasticity and of the Strength of Materials from Galilei to the Present Time*. Cambridge University Press, 1893. (Cited on page 83.)

[132] P. L. Palla, M. Ippolito, S. Giordano, A. Mattoni, and L. Colombo. *Atomistic approach to nanomechanics: Concepts, methods, and (some) applications*. The Nanomechanics in Italy. Research Signpost, Kerala, 2007. (Cited on pages 83 and 164.)

[133] N. W. Ashcroft and N. D. Mermin. *Solid state Physics*. Saunders College Publishing, Orlando, 1976. (Cited on page 85.)

[134] J. W. Martin. *J. Phys. C: Solid State Phys.*, **8**:2837, 1975. (Cited on page 88.)

[135] M. Catti. *Acta Cryst.*, **A41**:494, 1985. (Cited on page 88.)

[136] R. Pasianot, D. Farkas, and E. J. Savino. *Phys. Rev. B*, **43**:6952, 1991. (Cited on page 88.)

[137] R. Pasianot, D. Farkas, and E. J. Savino. *Phys. Rev. B*, **47**:4149, 1993. (Cited on page 88.)

[138] R. Pasianot and E. J. Savino. *Phys. Rev. B*, **45**:12704, 1992. (Cited on page 88.)

[139] R. Pasianot and E. J. Savino. *Phys. Stat. Sol. (b)*, **176**:327, 1993. (Cited on page 88.)

[140] M. C. Rechtsman, F. H. Stillinger, and S. Torquato. *Phys. Rev. Lett.*, **101**:085501, 2008. (Cited on page 88.)

[141] J. E. Lennard-Jones. *Proceedings of the Physical Society*, **43**:461, 1931. (Cited on page 89.)

[142] T. H. K. Barron and C. Domb. *Proceedings of the Royal Society of London. Series A, Mathematical and Physical Sciences*, **227**:447, 1955. (Cited on page 90.)

[143] C. Krzeminski, Q. Brulin, V. Cuny, E. Lecat, E. Lampin, and F. Cleri. *J. Appl. Phys.*, **101**:123506, 2007. (Cited on page 90.)

[144] D. Holland and M. Marder. *Adv. Mater.*, **11**:783, 1999. (Cited on page 90.)

[145] J. F. Justo, M. Z. Bazant, E. Kaxiras, V. V Bulatov, and Sidney Yip. *Phys. Rev. B*, **58**:2539, 1998. (Cited on page 90.)

[146] M. Z. Bazant, E. Kaxiras, and J. F. Justo. *Phys. Rev. B*, **56**:8542, 1997. (Cited on pages 90 and 91.)

[147] M. Z. Bazant and E. Kaxiras. *Phys. Rev. Lett.*, **77**:4370, 1996. (Cited on pages 90 and 91.)

[148] G. C. Abell. *Phys. Rev. B*, **31**:6184, 1985. (Cited on page 91.)

[149] J. H. Roseand, J. R. Smith, F. Guinea, and J. Ferrante. *Phys. Rev. B*, **29**:2963, 1984. (Cited on page 91.)

[150] D. W. Brenner. *Phys. Rev. B*, **42**:9458, 1990. (Cited on page 92.)

[151] D. W. Brenner, O. A. Shenderova, J. A. Harrison, S. J. Stuart, B. Ni, and S. B. Sinnott. *J. Phys.: Condens. Matter*, **14**:783, 2002. (Cited on page 92.)

[152] A. K. Subramaniyan and C.T. Sun. *International Journal of Solids and Structures*, **45**:4340, 2008. (Cited on pages 95 and 99.)

[153] M. Ippolito, G. Fugallo, A. Mattoni, and L. Colombo. *Strength, Fracture and Complexity*, **3**:89, 2005. (Cited on page 96.)

[154] A. G. McLellan. *Am. J. Phys.*, **42**:239, 1974. (Cited on page 98.)

[155] R. J. Swenson. *Am. J. Phys.*, **51**:940, 1983. (Cited on page 98.)

[156] R. Clausius. *Phil. Mag.*, **40**:122, 1870. (Cited on page 98.)

[157] J. C. Maxwell. *Transactions of the Royal Society of Edinburg*, **XXVI**:1, 1870. (Cited on page 98.)

[158] M. Zhou. *Proc. R. Soc. Lond. A*, **459**:2347, 2003. (Cited on page 98.)

[159] J. H. Irving and J. G. Kirkwood. *The Journal of Chemical Physics*, **18**:817, 1950. (Cited on page 98.)

[160] P. C. Andia, F. Costanzo, and G. L. Gray. *Modelling and Simulation in Materials Science and Engineering*, **14**:741, 2006. (Cited on page 98.)

[161] P. C. Andia, F. Costanzo, and G. L. Gray. *International Journal of Solids and Structures*, **42**:6409, 2005. (Cited on page 98.)

[162] J. Gao and J. H. Weiner. *Macromolecules*, **20**:2520, 1987. (Cited on page 99.)

[163] S. Torquato and M. D. Rintoul. *Phys. Rev. Lett.*, **75**:4067, 1995. (Cited on page 103.)

[164] Y. Benveniste and G. W. Milton. *J. Mech. Phys. Solids.*, **51**:1773, 2003. (Cited on page 103.)

[165] Y. Benveniste. *J. Mech. Phys. Solids.*, **54**:708, 2006. (Cited on page 103.)

[166] Y. Benveniste. *J. Mech. Phys. Solids.*, **55**:666, 2007. (Cited on page 103.)

[167] K. Bertoldi, D. Bigoni, and W. J. Drugan. *J. Mech. Phys. Solids.*, **55**:1, 2007. (Cited on pages 103 and 111.)

[168] K. Bertoldi, D. Bigoni, and W. J. Drugan. *J. Mech. Phys. Solids.*, **55**:35, 2007. (Cited on pages 103 and 111.)

[169] L.Colombo, M. Ippolito, A. Mattoni, and F. Cleri. volume 83 of *In: Advances in Contact Mechanics: Implications for Materials Science, Engineering and Biology*. Transworld Research network, Kerala, 2006. (Cited on page 103.)

[170] F. Djurabekova and K. Nordlund. *Phys. Rev. B*, **77**:115325, 2008. (Cited on page 103.)

[171] B. Luan and M. O. Robbins. *Phys. Rev. E*, **74**:026111, 2006. (Cited on page 103.)

[172] A. Mattoni, M. Ippolito, and L. Colombo. *Phys. Rev. B*, **76**:224103, 2007. (Cited on page 103.)

[173] M. Ippolito, A. Mattoni, and L. Colombo. *Phys. Rev. B*, **73**:104111, 2006. (Cited on page 103.)

[174] P. L. Palla, S. Giordano, and L. Colombo. *Phys. Rev. B*, **78**:012105, 2008. (Cited on pages 104 and 163.)

[175] M. D. Kluge and J.R.Ray. *Phys. Rev. B*, **37**:4132, 1988. (Cited on pages 107 and 109.)

[176] K.H. Hellwege, editor. *Crystal and Solid State Physics*. Landolt-BornStein. Springer, Berlin, 1979. (Cited on pages 107 and 109.)

[177] P. Sharma and S. Ganti. *Phys. Status Solidi B*, **234**: R10–R12, 2002. (Cited on pages 111 and 125.)

[178] M. Yang, J. C. Sturm, and J. Prevost. *Phys. Rev. B*, **56**:1973, 1997. (Cited on pages 111 and 125.)

[179] X. Zhang and P. Sharma. *Phys. Rev. B*, **72**: 195345, 2005. (Cited on pages 111 and 125.)

[180] J. Singh. *Physics of Semiconductors and Their Heterostructures*. McGraw-Hill Higher Education, New York, 1992. (Cited on pages 111 and 163.)

[181] R. Maranganti and P. Sharma. *A Review of Strain Field Calculations in Embedded Quantum Dots and Wires*. In: Handbook of Theoretical and Computational Nanotechnology. American Scientific Publishers, CA United States, 2006. (Cited on page 111.)

[182] R. Timm, H. Eisele, A. Lenz, L. Ivanova, G.Balakrishnan, D. L. Huffaker, and M. Dähne. *Phys. Rev. Lett.*, **101**: 256101, 2008. (Cited on page 111.)

[183] P. Harrison. *Quantum Wells, Wires and Dots: Theoretical and Computational Physics of Semiconductor Nanostructures*. John Wiley and Sons Ltd, Chichester, 2005. (Cited on page 111.)

[184] P. Sharma and S. Ganti. *J. Appl. Mech.*, **71**: 663–671, 2004. (Cited on page 111.)

[185] P. Sharma, S. Ganti, and N. Bhate. *Appl. Phys. Lett.*, **82**: 535–537, 2003. (Cited on page 111.)

[186] A. Mattoni and L. Colombo. *Phys. Rev. B*, **78**:075408, 2008. (Cited on page 111.)

[187] A. Mattoni and L. Colombo. *Phys. Rev. Lett.*, **99**:205501, 2007. (Cited on page 111.)

[188] S. Pizzini, M. Acciarri, S. Binetti, D. Cavalcoli, A. Cavallini, D. Chrastina, L. Colombo, E. Grilli, G. Isella, M. Lancin, A. Le Donne, A. Mattoni, K. Peter, B. Pichaud, E. Poliani, M. Rossi, S. Sanguinetti, M. Texier, and H. von Känel. *Mater. Sci. Eng. B*, **134**:118, 2006. (Cited on page 111.)

[189] J. Tersoff. *Phys. Rev. B*, **37**:6991, 1988. (Cited on page 112.)

[190] F. Cleri, P. Keblinski, L. Colombo, S. R. Phillpot, and D. Wolf. *Phys. Rev. B*, **57**:6247, 1998. (Cited on page 114.)

[191] F. Cleri, P. Keblinski, L. Colombo, D. Wolf, and S. R. Phillpot. *Europhys. Lett.*, **46**:671, 1999. (Cited on page 114.)

[192] H. C. Yang and Y. T. Chou. *J. Appl. Mech.*, **98**:424, 1976. (Cited on page 115.)

[193] N. I. Muskhelishvili. *Some Basic Problems in the Mathematical Theory of Elasticity*. Noordhoff, Groningen, 1953. (Cited on pages 118 and 119.)

[194] J. N. Israelachvili. *Intermolecular and surface forces*. Academic Press, San Diego, 1992. (Cited on page 125.)

[195] D. Leckband and J. N. Israelachvili. *Quart. Rev. Biophys*, **34**:105–267, 2001. (Cited on page 125.)

[196] H. Y. Hwangi. *Science*, **313**:1895, 2006. (Cited on page 126.)

[197] Z. Erdelyi, M. Sladecek, L.M. Stadler, I. Zizak, G. A. Langer, M. Kis-Varga, D. L. Beke, and B. Sepiol. *Science*, **306**:1913, 2004. (Cited on page 126.)

[198] S. Suresh. *Science*, **292**:2447, 2001. (Cited on page 126.)

[199] J. F. Nye. *Physical properties of crystals*. Oxford, oxford university press edition, 1985. (Cited on pages 129 and 136.)

[200] H. B. Huntington. *The elastic constants of crystals*. New York, academic press edition, 1958. (Cited on page 130.)

[201] E. Cadelano, P. L. Palla, S. Giordano, and L. Colombo. *Phys. Rev. Lett.*, **102**:235502, 2009. (Cited on page 130.)

[202] S. Torquato. *Phys. Rev. E*, **51**:03170, 1995. (Cited on page 152.)

[203] M. Abramowitz and I.A.Stegun. *Handbook of mathematical function*. Dover Publication Inc., New York, 1965. (Cited on page 169.)

[204] I. S. Gradshteyn and I.M. Ryzhik. *Table of integrals, series and products*. Academic Press, San Diego, 1965. (Cited on page 169.)

ACKNOWLEDGMENTS

I am grateful to my advisor, Prof. Luciano Colombo, for his guidance, support and encouragement and also for providing me the opportunity to work in a very stimulating research environment. His guidance has been fundamental for improving my scientific and professional growth.

I would like to thank my friend (and tutor) Stefano Giordano: his genuine and trustworthy friendship, as much as his crucial scientific collaboration, meant a great deal to me. Certainly, working with him has been my most amazing and formative scientific experience.

I wish to extend my worm thanks to Alessandro Mattoni for his support in improve my skills in coding softwares and for his encouragement during my whole PhD work.

I thanks all the research group of my advisor, particularly Emiliano Cadelano, for providing me a friendly and inspiring fellowship inside as outside the working environment.

I further acknowledge Matteo Dessalvi and the CASPUR (Rome, Italy) staff, particularly Luca Ferraro, for their patient computational support.

A special thank to my partner Loredana Braccini for her patience and for having shared with me this adventure. Finally, I would like to express my gratefulness to all my friends from the incredible land of Sardinia.